Interaction of endocytic vacuoles with autophagic pathways and actin cytoskeleton in pancreatic acinar cells

Francesca De Faveri

Thesis submitted in accordance with the requirements of the University of Liverpool for the degree of Doctor of Philosophy

September 2018

Acknowledgments

I wish to primarily thank my supervisor Professor Alexei Tepikin, who has guided and supported me throughout my PhD. I am very grateful to Doctor Svetlana Voronina and Doctor Michael Chvanov, for sharing all their knowledge and always being keen to help me. I would also like to thank Doctor David Criddle, for all his great advice. I have extremely enjoyed my time in Blue Block which has become a sort of family for me, and I will always remember it with affection.

I wish to thank my co-supervisors Doctor Lee Haynes and Doctor John Quayle for their help and guidance. I am very grateful to Doctor Muhammad Awais, Ms Diane Latawiec, Professor Robert Sutton, Doctor David Mason, Doctor Tomoko Tamishima, Professor Ian Prior, Miss Alison Beckett, Doctor Tobias Zech, Professor Judy Coulson and Doctor Caroline Dart, for their technical and advisory support. I would also like to thank the staff of the Biomedical Services Unit.

I have been very lucky to meet lovely friends in the Department, they have been a fantastic company and a valuable moral support. Thanks to Shiquan, Louise, Charlotte, Jack, Zohra, Fiona, Alistair, Rick, Hannah, Nordine, Steve. A huge thank you to Helen, for being a best friend and a perfect companion in the lab, it would have not been the same without you.

I have awesome friends in Italy (and Paris), who have been always present despite the distance. Thanks to Maria Chiara, Stefania, Alessandra, Gioia, Elena, Roberta, Anna. Thanks to Lara for being there for me every time I needed you and for being the best travel companion, other than my best friend.

Thanks to Kieran for making my evenings and weekends so enjoyable and for taking me places. Thank you so much for your patience and moral support, particularly in this last year.

Thanks to my family, for all their love and for putting up with me being far away. I am sorry that I cannot see you more often. Grazie mamma, papá, Jo, Ale, Maddi, nonne, zie e zii, cugini e cugine. I love you.

Finally and most importantly, I would like to thank the Wellcome Trust for funding me and the research presented in this study.

Declaration

This dissertation is the result of my own work, carried out at the University of Liverpool between October 2015 and September 2018.

Francesca De Faveri

September 2018

Abstract

Interaction of endocytic vacuoles with autophagic pathways and actin cytoskeleton in pancreatic acinar cells

Francesca De Faveri, University of Liverpool, 2018

Pancreatic acinar cells are polarised secretory epithelial cells responsible for calcium-dependent exocytosis of zymogen granules, containing digestive enzymes and proenzymes. Large endocytic vacuoles are formed as a mechanism of compensatory membrane retrieval. In conditions of supramaximal stimulation, trypsinogen is activated within endocytic vacuoles; this represents one of the early events in the pathogenesis of acute pancreatitis.

Macroautophagy refers to the molecular pathway responsible for targeting several types of cargo for lysosomal degradation. This involves specific selection of cargo and its subsequent sequestration into a membrane bound autophagosomal compartment. A hallmark of acute pancreatitis is upregulation of macroautophagy and disruption of cargo flux through this pathway. One aim of this study was to investigate whether the autophagic machinery interacted with endocytic vacuoles. Confocal microscopy of isolated primary pancreatic acinar cells was performed following stimulation with calcium-releasing agonists. GFP-LC3 transgenic mice were utilised to monitor autophagy, and cell impermeable fluorescent indicators were utilised to label endocytic vacuoles. A proportion of endocytic vacuoles were coated by the autophagosome marker GFP-LC3. Application of inhibitors of the autophagic pathway revealed that the process of GFP-LC3 coating was independent of ULK1 and PI(3)K complexes, but was inhibited by agents disrupting acidification of cellular organelles. Correlative light and electron microscopy showed that these organelles have a single lipid membrane. Correlative immunofluorescence staining showed that they co-localised with Atg16L1. Collectively, these results suggest that the LC3 lipidation on endocytic vacuoles occurs by a non-canonical autophagy pathway.

Zymogen granules fused to the plasma membrane are coated by actin filaments; endocytic vacuoles originate from post-exocytic structures. A second aim of this study was to investigate whether actin filaments interact with endocytic vacuoles. A cell permeable fluorescent indicator or a reporter construct inserted into an adenoviral vector were utilised to label endogenous actin filaments. A proportion of endocytic vacuoles were coated by F-actin. Experiments utilising inhibitors of actin polymerisation indicated that actin coating depended on both formins and the Arp2/3 complex, and was regulated by GTPases Rho and Cdc42. Correlative immunofluorescence staining suggested co-localisation of mDia1, Arp2/3 and N-WASP with endocytic vacuoles.

I extended my investigation to study the relationships between actination and autophagy of endocytic vacuoles. LC3 and actin coating of endocytic vacuoles were simultaneously monitored. LC3 and actin were not present on the same endocytic vacuoles, suggesting that these processes might occur sequentially in the lifetime of these organelles. Combinations of pH sensitive and insensitive cell impermeant fluorescent indicators were used to measure the pH inside endocytic vacuoles, actin-coated endocytic vacuoles or LC3-coated endocytic vacuoles. The results suggested that there was no pH difference between these populations of organelles.

Collectively, the data presented in this study characterises two new phenomena: LC3 lipidation and actination of endocytic vacuoles. Future work will be directed at further describing the dynamics and function of these unique organelles in the context of acinar cell physiology and acute pancreatitis pathophysiology.

Table of contents

Acknowledgments 1

Declaration 2

Abstract 3

Abbreviations 7

1 Introduction 11

1.1 Overview 12

1.2 The pancreas 13

1.2.1 Pancreatic exocrine secretion 14

1.3 The pancreatic acinar cell 17

1.3.1 Secretagogue-induced calcium signalling 18

1.3.2 Exocytosis and endocytosis in pancreatic acinar cells 25

1.4 The actin cytoskeleton 29

1.4.1 Actin nucleators 29

1.4.2 Actin filaments in pancreatic acinar cells 34

1.5 Autophagic pathways 35

1.5.1 LC3 and monitoring autophagy 42

1.5.2 Autophagy in pancreatic acinar cells 43

1.6 Acute pancreatitis 44

1.6.1 Experimental pancreatitis 44

1.6.2 Intra-acinar trypsinogen activation 47

1.6.3 Autophagy in pancreatitis 49

1.6.4 Endocytic vacuoles are the site of trypsinogen activation 50

1.7 Aims 52

2 Material and Methods 53

2.1 Materials 54

2.1.1 Reagents and suppliers 54

2.1.2 Solutions 55

2.2 Animals 56

2.2.1 Conditional inducible knock-out of *Atg5* 58
2.3 Primary pancreatic acinar cell isolation 60
2.4 Labelling endocytic vacuoles 61
2.4.1 pH measurements in endocytic vacuoles 61
2.5 Adenoviral transfection 63
2.6 Staining the actin cytoskeleton 63
2.7 Disruption of the autophagic pathway 64
2.8 Disruption of the actin cytoskeleton 65
2.9 Immunofluorescence 66
2.10 Confocal microscopy 67
2.11 Correlative Light and Electron Microscopy 68
2.11.1 Transmission electron microscopy 68
2.12 Western blotting 71
2.13 Image processing and data analysis 73

3 Investigating autophagy of endocytic vacuoles 77

3.1 Introduction 78
3.2 Results 83
3.2.1 LC3-coating of endocytic vacuoles 83
3.2.2 Regulators of LC3-coating of endocytic vacuoles 96
3.2.3 Structural properties of the LC3-coated endocytic vacuoles 103
3.2.4 LC3 lipidation machinery on endocytic vacuoles 110
3.3 Discussion 117

4 Investigating the interaction of endocytic vacuoles and actin ... 136

4.1 Introduction 137
4.2 Results 141
4.2.1 Actin filaments coat endocytic vacuoles 141
4.2.2 Regulators of actin-coating of endocytic vacuoles 152
4.2.3 Phosphoinositides and actin-coating of endocytic vacuoles 168
4.3 Discussion 171

5 Investigating the relationship between actination, autophagy and pH of endocytic vacuoles 182

5.1 Introduction 183

5.2 Results 186

5.2.1 Relationship between LC3 and actin on endocytic vacuoles.....186

5.2.2 pH of endocytic vacuoles 192

5.3 Discussion.....198

6 Concluding remarks 206

6.1 Summary and interpretation of the findings 207

6.2 Actin cytoskeleton and stabilisation of endocytic vacuoles 210

6.3 Non-canonical LC3 lipidation on endocytic vacuoles.....212

6.4 Relevance to acute pancreatitis.....213

6.5 Future perspectives.....215

Bibliography 217

Abbreviations

ACh	acetylcholine
AMDE1	autophagy modulator with dual effect-1
ANOVA	one-way analysis of variance
AP	acute pancreatitis
Arp	actin related protein
ATG	autophagy related
AV	autophagic vacuole
AWERB	Animal Welfare and Ethical Review Body
BCA	bicinchoninic acid
BSA	bovine serum albumin
BSU	Biomedical Services Unit
cADPR	cyclic ADP ribose
CCK	cholecystokinin
CDE	choline-deficient ethionine-supplemented
CICR	calcium-induced calcium release
CIE	clathrin-independent endocytosis
CLC	chloride channel
CLEM	correlative light and electron microscopy
CMA	chaperone-mediated autophagy
CME	clathrin-mediated endocytosis
CP	chronic pancreatitis
CRAC	calcium release-activated channel
CV	condensing vacuole
DAMP	damage-associated molecular pattern
ddH_2O	double deionised water
DFCP1	double FYVE domain-containing protein
DMSO	dimethyl sulfoxide
ECL	enhanced chemiluminescence
EE	early endosome
EM	electron microscopy

ER	endoplasmic reticulum
ESCRT	endosomal sorting complexes required for transport
EV	endocytic vacuole
FAEE	fatty acid ethyl ester
FBD	FIP200-binding domain
FcγR	Fc receptor for IgG
FH	formin homology
FITC	fluorescein isothiocyanate
GABARAP	gamma-aminobutyric acid receptor-associated protein
GAP	GTPase-activating protein
GATE-16	Golgi-associated ATPase enhancer of 16 kDa
GEF	guanine nucleotide exchange factor
GPCR	G-protein coupled receptor
HRP	horseradish peroxidase
HRS	hepatocyte growth factor–regulated tyrosine kinase substrate
ICG	intra-cisternal granule
IP_3	inositol triphosphate receptor
IP_3R	IP_3 receptor
IQR	inter-quartile range
JMY	junction-mediating and regulatory protein
KO	knock-out
LAP	LC3-associated phagocytosis
LDS	LIR docking site
LE	late endosome
LIR	LC3-interacting region
LSM	laser scanning microscope
LY	lucifer yellow
MAPLC3	microtubule associated protein 1 light chain 3
MCU	mitochondrial calcium uniporter
MPTP	mitochondrial permeability transition pore
mTORC1	mammalian target of rapamycin complex 1
MW	molecular weight

N-WASP	neuronal WASP
NA	numerical aperture
NAADP	nicotinic acid adenine dinucleotide phosphate
NAD	nicotinamide adenine dinucleotide
NF-κB	nuclear factor kappa-light-chain-enhancer of activated B cells
NOX2	NADPH oxidase 2
NPF	nucleation promoting factor
NSF	N-ethylmaleimide-sensitive factor
PAC	pancreatic acinar cell
PAS	pre-autophagosomal structure
PBS	phosphate buffered saline
PDC	pancreatic ductal cell
PLC	phospholipase C
PE	phosphatidylethanolamine
PFA	paraformaldehyde
PI	phosphoinositide
PI(3)K	phosphatidylinositol-3-kinase
PIKfyve	phosphoinositide kinase, FYVE-type zinc finger containing
PIP	phosphatidylinositol phosphate
PLL	poly-L-lysine
PMCA	plasma membrane calcium ATPase
POA	palmitoleic acid
POAEE	palmitoleic acid ethyl-ester
PSC	pancreatic stellate cell
RER	rough ER
RhoGDI	Rho GDP-dissociation inhibitor
ROS	reactive oxygen species
RT	room temperature
RYR	ryanodine receptor
SDS	sodium dodecyl sulphate
SEM	standard error of the mean
SERCA	sarco/endoplasmic reticulum calcium ATPase

SG	secretory granule
SNAP	synaptosome-associated protein
SNARE	soluble NSF attachment protein receptor
SOCE	store-operated calcium entry
SPF	specific-pathogen-free
STIM1	stromal interaction module 1
STX	syntaxin
TCH	thiocarbohydrazide
TGN	trans-Golgi network
TEM	transmission electron microscopy
TLC-S	taurocholic acid-3-sulfate
TLR	Toll-like receptor
TMD	transmembrane domain
TPC	two-pore channel
TRD	Texas Red dextran
TRPC	transient receptor potential channel
V-ATPase	vacuolar-type H^+-ATPase
VMP1	vacuolar membrane protein 1
WASH	WASP and SCAR homologue
WASP	Wiskott–Aldrich Syndrome protein
WAVE	WASP-family verprolin-homologous protein
WHAMM	WASP homolog associated with actin, membranes and microtubules
WIPI	WD-repeat protein interacting with phosphoinositides
WT	wild type
ZG	zymogen granule

1 Introduction

1.1 Overview

The pancreatic acinar cells are responsible for stimulated exocrine secretion of digestive enzymes and precursors of digestive enzymes. Acute pancreatitis is an inflammatory disease of the pancreas associated with premature activation of trypsin within the pancreatic acinar cells (reviewed in (Singh & Garg, 2016; Gukovskaya *et al.*, 2017; Gerasimenko *et al.*, 2018)). Studies from our laboratory have identified endocytic vacuoles (EVs) formed in pathological conditions as the site of intracellular trypsinogen conversion to trypsin (Sherwood *et al.*, 2007). Rupture of these organelles may represent the escape route of active trypsin from a membrane enclosed compartment to the cytosol (Chvanov *et al.*, 2018).

This thesis explored the intracellular processing of EVs, in both physiological and pathological conditions, utilising primary pancreatic acinar cells as an experimental model. Early in the project two novel phenomena were discovered: the interaction of EVs with the actin cytoskeleton and with the autophagic marker LC3. The characterisation of these processes became the focus of the investigation. This chapter provides background information and justification for the study.

1.2 The pancreas

The pancreas is a glandular organ present in vertebrates. In humans, it is located in the abdominal cavity behind the stomach. It has a head, a body and a tail; two additional parts are sometimes described: the neck and the pyramidal process. The head of the pancreas is located by the loop of the duodenum; the tail is located towards the spleen (**Figure 1.1** A) (reviewed in (Go, 1993)). Three parts can be identified in the mouse pancreas: the duodenal lobe (homologous to the head of the human pancreas), the splenic lobe (homologous to body and tail) and the gastric lobe (homologous to the pyramidal process) (**Figure 1.1** B). Each lobe is divided into smaller lobules. The human pancreas is ~15 cm long, the mouse pancreas is approximately 10 times smaller (Dolensek *et al.*, 2015). The blood supply to the pancreas derives from the celiac and the superior mesenteric arteries, branches of the abdominal aorta. The blood is drained from the pancreas via the splenic and the superior mesenteric veins, into the portal vein. The pancreas is a mixed – both exocrine and endocrine – gland. The exocrine component constitutes ~85% of the pancreatic mass and includes acinar and ductal cells. The exocrine pancreas has a digestive function, secreting digestive enzymes, fluid and bicarbonate in response to food ingestion. The pancreatic exocrine secretory products are released into the duodenum through the pancreatic duct and the common bile duct (Pandol, 2010). The endocrine component, representing ~2% of the pancreatic mass, is constituted by the islets of Langerhans, consisting of five cell subtypes: α, β, δ, ε, and PP cells. The endocrine pancreas controls blood sugar levels by regulating energy metabolism through release of hormones (insulin, glucagon, amylin, somatostatin and pancreatic polypeptide) directly into the blood stream (reviewed in (Korc, 1993)). The remaining

pancreatic mass comprises of stellate cells (Bachem *et al.*, 1998; Masamune & Shimosegawa, 2013), connective tissue and blood vessels.

1.2.1 Pancreatic exocrine secretion

The exocrine secretory cells are pancreatic acinar cells (PACs) and pancreatic ductal cells (PDCs). PACs mainly secrete digestive enzymes and fluid. The main digestive enzymes classes are endo- and exo-proteases, lipases, glycosidases, and nucleases. The pancreatic digestive enzymes are amylase, carboxyl ester hydrolase, ribonuclease, and deoxy ribonuclease I. Other digestive enzymes, and particularly proteases, are synthesised as inactive precursors, called zymogens. The pancreatic zymogens are trypsinogen, chymotrypsinogen, proelastase 2, procarboxypeptidase A, procarboxypeptidase B, proprotease 2, kallikreinogen, prophospholipase A, and procolipase. In the duodenum, trypsinogen is cleaved by enteropeptidase and becomes active trypsin, which cleaves and activates trypsinogen and the other zymogens (reviewed in (Go, 1993)). PDCs mainly secrete chloride-rich fluid and bicarbonate (Hollander & Birnbaum, 1952). Digestive enzymes and bicarbonate released in the duodenum are responsible for catabolism of partially digested food and neutralisation of the acidic gastric chyme.

Pancreatic exocrine secretion is regulated via both stimulatory and inhibitory signals elicited by food intake through three phases of meal response: cephalic, gastric, intestinal (reviewed in (Pandol, 2010)). Secretion from the cephalic phase is rich in digestive enzymes and low in bicarbonate, and it primarily involves the acinar cells. Stimulation occurs via the vagus nerve, transmitting the sensory inputs initiated by

food anticipation. The main neurotransmitter regulating the cephalic phase is acetylcholine (ACh). The gastric phase accounts for ~10% of the pancreatic exocrine secretion and also primarily involves the acinar cells and vagal stimulation. The intestinal phase accounts for up to ~80% of the pancreatic exocrine secretion, stimulating both acinar and ductal cells. The acidity of the gastric chyme induces release of the hormone secretin from S cells (Konturek *et al.*, 1969). Secretin stimulates ductal cells to secrete bicarbonate (Bayliss & Starling, 1902). The hormone cholecystokinin (CCK) is released from I cells of the duodenum (Liddle, 1997) following induction by fatty acids, proteins and proteolytic degradation products including peptides and free amino acids. CCK stimulates secretion of digestive enzymes from the acinar cells (Owyang, 1996; Liang *et al.*, 2017). The secretory response is amplified by cholinergic stimulation via the enteropancreatic reflex (Singer & Niebergall-Roth, 2009). Regulation of pancreatic secretion occurs via a feedback mechanism, mediated by protease concentration in the duodenum: active proteases inhibit secretion, whereas reduced protease activity stimulates it. This occurs via regulation of CCK releasing factor, which is inactivated by active proteases, thus preventing CCK release, whereas in the absence of proteases it can promote CCK release (Liddle, 1995; Spannagel *et al.*, 1996). Secretion is positively regulated by monitor peptide, released by the acinar cells once pancreatic secretion has been triggered, and is responsible for stimulating CCK release thus amplifying the pancreatic response (Bouras *et al.*, 1992; Liddle *et al.*, 1992). CCK receptors are also present on the pancreatic stellate cells (PSCs) where they stimulate ACh release which stimulates the acinar cells, via another pathway of CCK-induced pancreatic secretion (Phillips *et al.*, 2010).

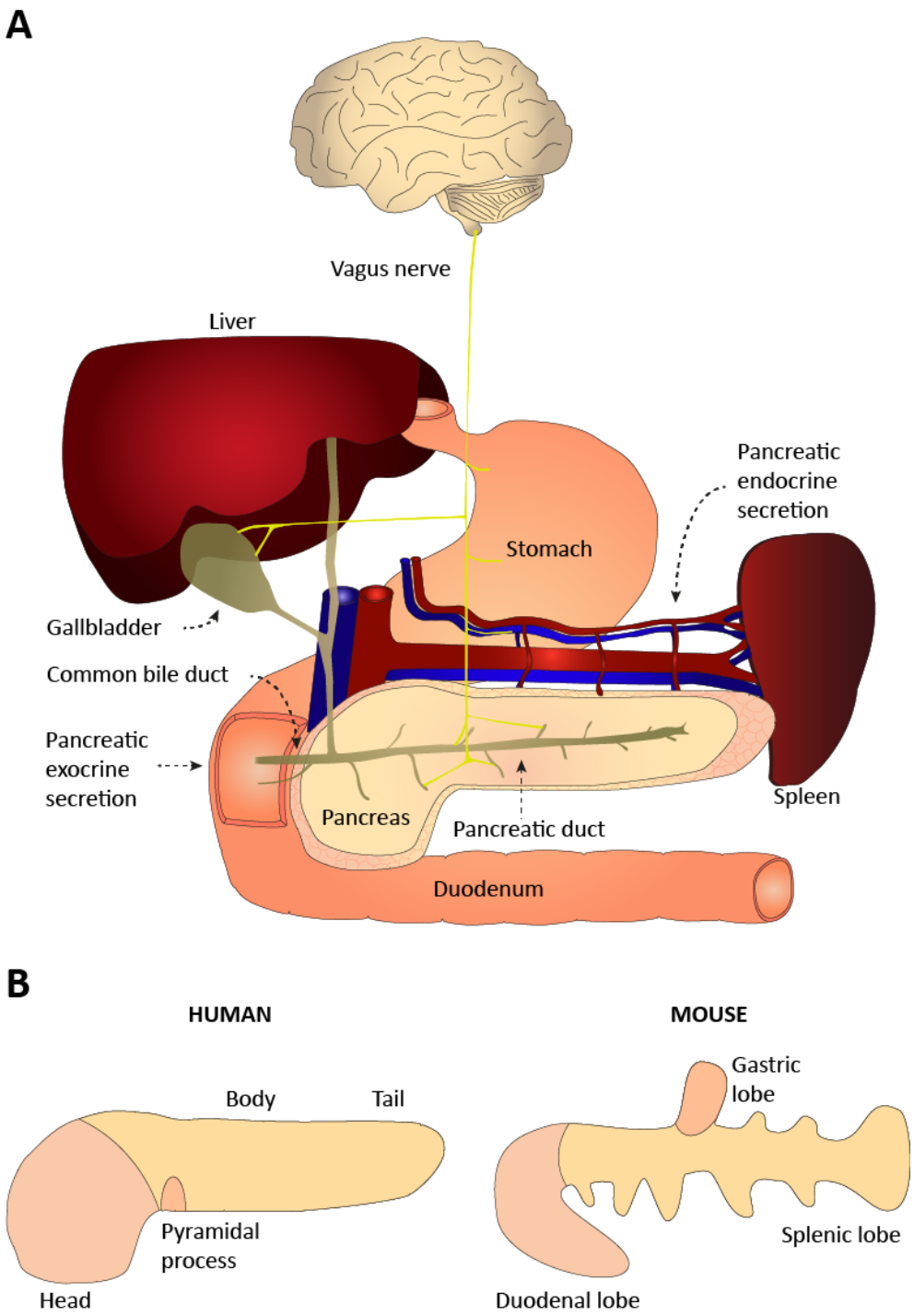

Figure 1.1 The pancreas. A) In humans, the pancreas is located below the stomach, the head towards the duodenum, the tail towards the spleen. The products of pancreatic exocrine secretion are released via the pancreatic duct and the common bile duct into the duodenum. The products of pancreatic endocrine secretion are released into the blood stream. The pancreas receives afferent innervation from the vagus nerve, which contributes to stimulating pancreatic exocrine secretion. **B)** Comparison of structures of human and murine pancreas. Illustration was created using Adobe Illustrator utilising information adapted from (Go, 1993; Pandol, 2010; Dolensek *et al.*, 2015).

1.3 The pancreatic acinar cell

PACs are organised in spherical or tubular clusters called acini (**Figure 1.2**), with centrally located terminal ducts that join interlobular ducts, thus merging to form the main pancreatic duct. PACs are polarised epithelial cells; the apical membrane, responsible for secretion, is located towards the lumen of the duct. Secretory granules (SGs) contain digestive enzymes and zymogens, and are thus referred to as zymogen granules (ZGs), which are about 1 µm in diameter and constitute ~6% of the total cell volume (Bolender, 1974). Approximately 100 ZGs per cell are concentrated in the apical area of the cell, where they are surrounded by a mitochondrial belt. Mitochondria are also located below the basolateral plasma membrane. Tight junctions (Rahner *et al.*, 2001) separate the apical from the basolateral membrane and act as a barrier around the apical area preventing the passage of digestive enzymes. Communication between cells in the acinus is permitted by gap junctions on the lateral membrane (Stauffer *et al.*, 1993). A highly developed rough endoplasmic reticulum (RER), accounting for ~22% of the cell volume and ~60% of the total membrane surface area (Bolender, 1974), is responsible for protein synthesis by the associated ribosomes. ~90% of the synthesised proteins are directed for secretion (Scheele *et al.*, 1978). The site of protein sorting towards secretory or lysosomal pathways is the trans-Golgi network (TGN) (Griffiths & Simons, 1986). The TGN is an acidified compartment; progressive acidification through the TGN leads to protein interaction and assembly of membrane microdomains rich in glycolipids. The membrane microdomains rich in GP2 (the main glycoprotein in ZG membranes) are retained within acidic condensing vacuoles (CVs) that pinch off the TGN. (Sesso *et al.*, 1980; Orci *et al.*, 1987a; Orci *et al.*, 1987b). Within the CVs, the secretory products

undergo progressive pH-dependent condensation until they form mature ZGs (Jamieson & Palade, 1967, 1971; Kraehenbuhl *et al.*, 1977; Bendayan *et al.*, 1980; Freedman & Scheele, 1993; Leblond *et al.*, 1993; Dartsch *et al.*, 1998).

Several secretory pathways exist: constitutive, constitutive-like, minor regulated, and regulated. The constitutive, constitutive-like and minor regulated pathways are responsible for basal secretion, they occur in other exocrine cells like parotid acinar cells (Huang *et al.*, 2001). The regulated secretory pathway, described in the previous paragraph, is stimulated by secretagogues (Bieger *et al.*, 1976a; Bieger *et al.*, 1976b) and it is the most relevant to PAC function. Receptors for secretagogues are located on the basal plasma membrane. The main trigger of regulated secretion from PACs is rise in intracellular calcium, induced by ACh and CCK (and bombesin (Deschodt-Lanckman *et al.*, 1976)). However, cAMP can also contribute to potentiation of secretion, through pathways activated by secretin and vasoactive intestinal peptide (Meuth-Metzinger *et al.*, 2005) and by high CCK concentrations. For the purpose of this study, the next section will focus on the main secretagogues ACh and CCK and how they regulate calcium signalling.

1.3.1 Secretagogue-induced calcium signalling

ACh released from the vagus nerve binds to muscarinic G-protein coupled receptors (GPCRs) with seven transmembrane domains (TMDs). There are five types of muscarinic receptors; in PACs, M1 and M3 expressed on the basolateral membrane are involved in exocrine secretion (Gautam *et al.*, 2005). CCK, released by I cells in the duodenum, exists in different molecular forms deriving from endopeptidase

cleavage of CCK-58. CCK-8, the smallest active peptide, and CCK-58 have the same function (Criddle *et al.*, 2009). CCK receptors are GPCRs. CCK1R is selective for CCK, CCK2R binds both CCK and gastrin and is also referred to as gastrin receptor (Dufresne *et al.*, 2006). CCK1R is considered the mediator of CCK-induced pancreatic secretion, despite conflicting views about its expression/function in human PACs (Ji *et al.*, 2002; Murphy *et al.*, 2008; Liang *et al.*, 2017). CCK binding provokes a conformational change that promotes coupling of the receptor with heterotrimeric G proteins, triggering dissociation of α subunits which bind to GTP and activate downstream signalling pathways (reviewed in (Williams, 2001)).

The main pathway responsible for calcium-dependent stimulation of secretion by secretagogues involves $G_{\alpha q}$-mediated activation of phospholipase C (PLC) (**Figure 1.3**). PLC hydrolyses phosphatidylinositol-4,5-biphosphate ($PI(4,5)P_2$) generating membrane bound diacylglycerol (a protein kinase C activator) and soluble inositol 1,4,5-triphosphate (IP_3). IP_3 induces calcium release from the ER via binding to IP_3 receptors (IP_3Rs) which are ligand-gated calcium channels. PACs express all three types of IP_3Rs, located below the apical and lateral membrane (Fujino *et al.*, 1995; Yule *et al.*, 1997). IP_3Rs are biphasically regulated by calcium: potentiated by low and inhibited by high calcium concentrations (Bezprozvanny *et al.*, 1991). Their activity is also decreased by phosphorylation by protein kinase A, activated by CCK but not ACh signalling (Straub *et al.*, 2002). Calcium release from IP_3R activates a second class of ER-localised ligand-gated calcium release channels, the ryanodine receptors (RYRs), through a process termed calcium-induced calcium release (CICR). PACs express all sub-types of RYRs, which are widely distributed throughout the cell (Fitzsimmons *et*

al., 2000). RYR activity is modulated by cyclic ADP ribose (cADPR), produced by ADP-rybosyl cyclase, activated by both CCK and ACh (Gerasimenko *et al.*, 2006). Additionally, CCK but not ACh promotes nicotinic acid adenine dinucleotide phosphate (NAADP) production (Cancela *et al.*, 2000; Yamasaki *et al.*, 2005), responsible for a small calcium elevation sufficient to sensitise IP_3Rs and RYRs (Menteyne *et al.*, 2006). The two-pore channels (TPCs) located on lysosomes have been proposed as mediator of the NAADP response (Cancela *et al.*, 1999; Yamasaki *et al.*, 2004; Williams, 2010), however direct proof of the NAADP receptor on lysosomes is still lacking.

The resting intracellular calcium concentration in PACs is 50-200 nM. Extensive studies with fluorometric calcium indicators have characterised the acinar cell responses to stimulation. Calcium signals are initiated in the apical region of the cell (Kasai *et al.*, 1993; Thorn *et al.*, 1993), where they trigger exocytosis of the ZGs and activation of chloride channels, important for fluid secretion (Park *et al.*, 2001). Apically initiated calcium signals propagate globally (Kasai & Augustine, 1990; Toescu *et al.*, 1992; Straub *et al.*, 2000) and spread across gap junctions to adjacent cells (Stauffer *et al.*, 1993; Yule *et al.*, 1996). Physiological concentrations of secretagogues determine intracellular calcium oscillations (Stuenkel *et al.*, 1989; Yule *et al.*, 1991). Oscillations are guaranteed by the sarco/endoplasmic reticulum calcium-ATPase (SERCA) pump that replenishes the ER store. Differently, maximal concentrations of CCK and ACh determine a peak and plateau response (**Figure 1.4**). Whilst the peak is determined by release from intracellular stores, the plateau requires calcium entry from the extracellular medium, since it is attenuated when

experiments are performed in calcium-free medium (reviewed in (Petersen & Tepikin, 2008)). Sustained calcium oscillations are also prevented by absence of extracellular calcium. In fact, when ER stores are depleted, store-operated calcium entry (SOCE) pathways are activated that determine calcium entry from the extracellular medium to refill the ER. The protein machinery that regulates SOCE is constituted by the ER calcium sensor stromal interaction molecule 1 (STIM1). Following ER calcium depletion, STIM1 aggregates at ER-plasma membrane contact sites, where it interacts with channels responsible for calcium entry (Williams, 2010). These can be members of the calcium release-activated channel (CRAC) family (e.g. ORAI1) or transient receptor potential channels (TRPCs). Both STIM1 and ORAI1 are expressed in PACs (Lur *et al.*, 2009); TRPC3 channels might also be involved in PAC SOCE (Kim *et al.*, 2009). Calcium extrusion was observed when monitoring extracellular calcium following secretagogue stimulation (Tepikin *et al.*, 1992; Tepikin *et al.*, 1994). Calcium extrusion occurs via the plasma membrane calcium ATPase (PMCA), localised on the apical and lateral plasma membrane. This process guarantees that intracellular calcium levels can be tightly regulated. The cytosolic calcium concentration is also regulated through calcium uptake by the mitochondria, which are located in the perigranular belt, and occurs via a mitochondrial calcium uniporter (MCU). Mitochondrial calcium uptake is associated with nicotinamide adenine dinucleotide (NAD) to NADH conversion and increased ATP production (Voronina *et al.*, 2002b; Voronina *et al.*, 2010). Calcium and ATP levels are importantly interlinked, since calcium regulates ATP production and ATP is required for activity of calcium pumps and activation of IP_3Rs (Barrow *et al.*, 2008; Park *et al.*, 2008).

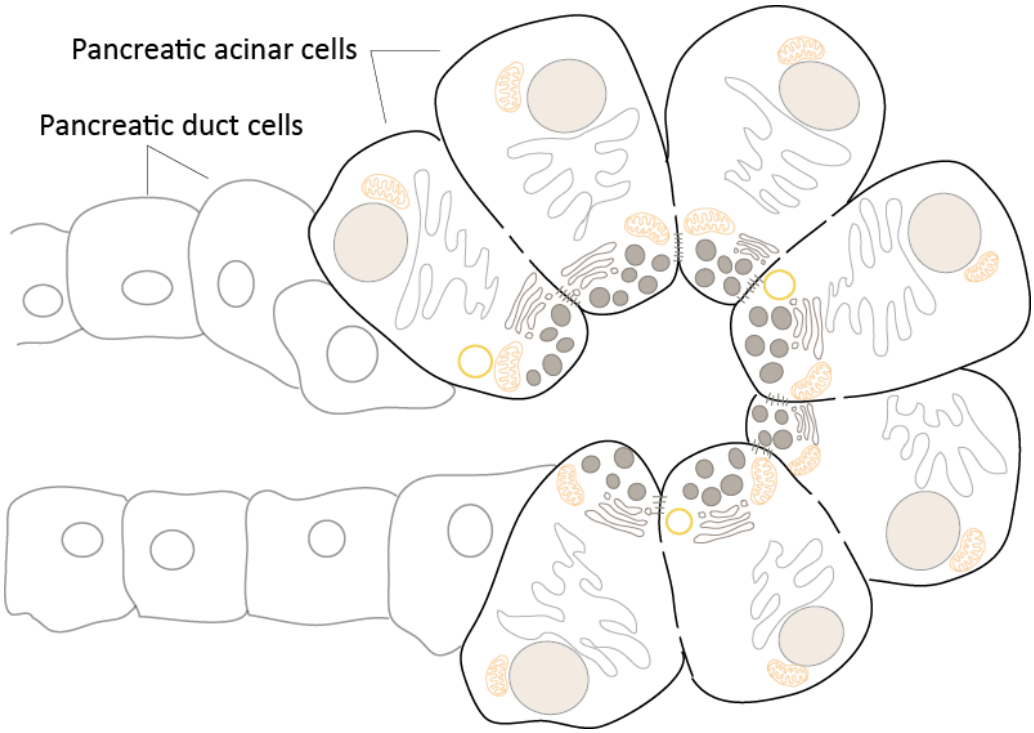

Figure 1.2 Pancreatic acinus. PACs are organised in acini, flanked by PDCs. The apical, secretory part of PACs is located toward the acinar lumen and presents ZGs, mitochondria, the Golgi complex and acidic stores. The RER is located in the infra- and para-nuclear region of the cell. Tight junctions are localised close to the luminal membrane, gap junctions are located on the lateral membrane. The structural properties of the acinar cells are described in (Kern, 1993).

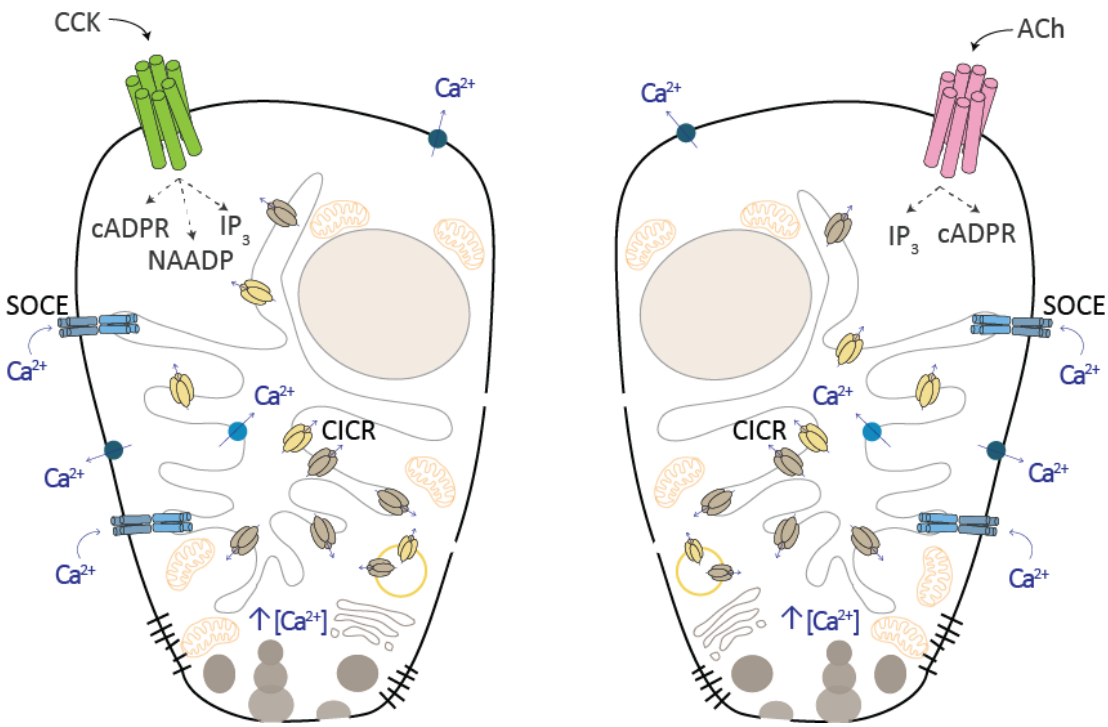

Figure 1.3 Calcium signalling in pancreatic acinar cells. The secretagogues CCK and ACh bind to their receptors on the basolateral plasma membrane and induce second messenger signalling cascades. IP_3, cADPR and NAADP trigger calcium release from intracellular stores (ER and acidic stores). When stores are depleted, SOCE allows for calcium entry from the extracellular medium. Intracellular calcium concentrations are regulated by active pumps located on the ER and the plasma membrane. Increase in intracellular calcium concentration triggers compound exocytosis of ZGs at the apical plasma membrane Illustration was created using Adobe Illustrator utilising information adapted from (Yule, 2015).

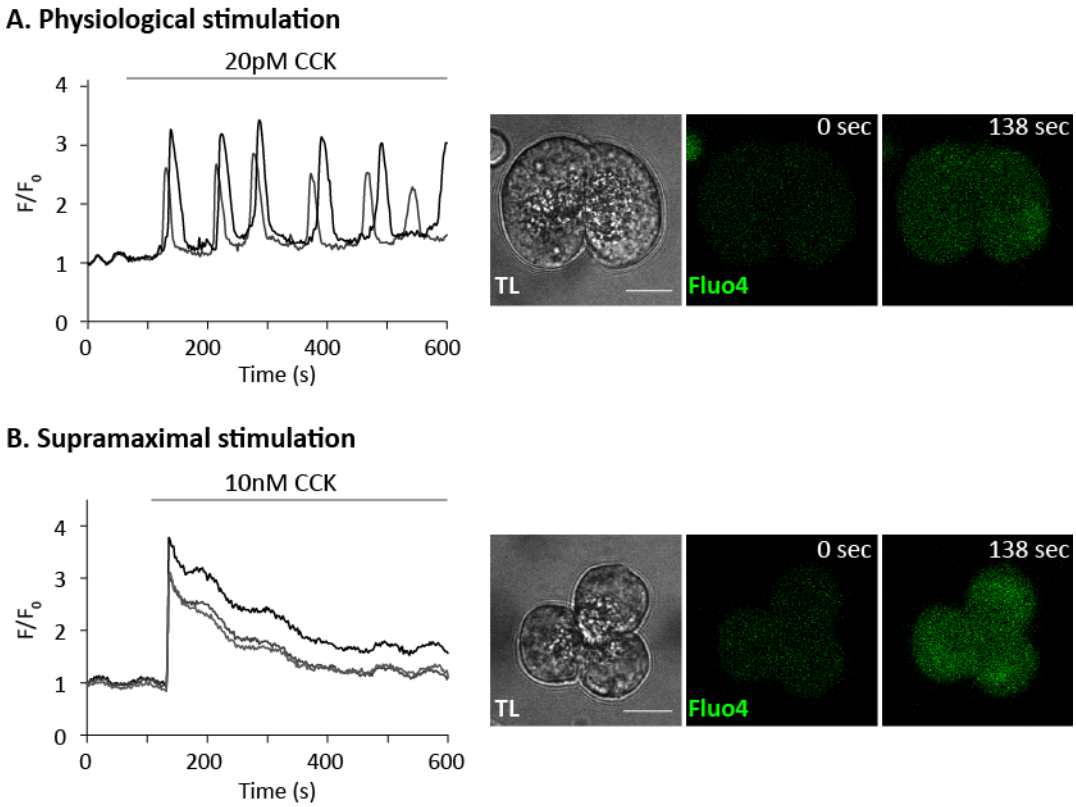

Figure 1.4 Calcium responses to physiological and supramaximal CCK concentrations. Calcium concentration rises are revealed by increase in Fluo4 fluorescence intensity. Transmitted light (TL) images (grey) and Fluo4 images (green) before and during stimulation (0 and 138 seconds). **A)** Physiological CCK stimulation induces oscillations. 20 pM CCK was added after 60 seconds. **B)** Supramaximal CCK stimulation induces a peak/plateau response. 10 nM CCK was added after 120 seconds. Scale bars = 10 µm. This figure was generated from data I obtained before the start of the study; similar results are well documented in the field (Stuenkel *et al.*, 1989; Yule *et al.*, 1991; Criddle *et al.*, 2009).

1.3.2 Exocytosis and endocytosis in pancreatic acinar cells

Secretagogue-stimulated exocytosis of ZGs is elicited by elevations of intracellular calcium concentration. In PACs, synaptotagmin 1 acts as calcium sensor and final trigger of ZG exocytosis (Falkowski *et al.*, 2011). Proteomic analysis of the protein composition of isolated ZGs enabled the identification of digestive enzymes, ZG matrix proteins, vesicular trafficking proteins, pumps, channels and transporters (Chen *et al.*, 2006; Rindler *et al.*, 2007; Chen *et al.*, 2008). ZGs express both chloride and potassium channels; these, under the chemiosmotic hypothesis of exocytosis, facilitate release of the contents via osmotic swelling (Thevenod, 2002). Membrane fusion events are mediated by soluble N-ethylmaleimide-sensitive factor (NSF) attachment protein receptor (SNARE) protein machinery. There are three families of SNAREs: syntaxin (STX), synaptosome-associated protein (SNAP) and vesicle associated membrane protein (VAMP). They are functionally classified as v-SNAREs (VAMPs) located on the vesicle membrane and t-SNAREs (STXs and SNAPs) located on the target membrane. The SNARE machinery is also involved in ZG fusion in PACs, where SNARE complexes are stabilised by the accessory protein complexin-2 (Falkowski *et al.*, 2010). Exocytosis of ZGs occurs via compound exocytosis, involving primary fusion of ZGs to the apical plasma membrane, followed by secondary fusion of ZGs to the primary fused ones (Nemoto *et al.*, 2001; Pickett *et al.*, 2005). The SNARE machinery that controls primary or secondary fusion events is specific (Pickett *et al.*, 2007; Behrendorff *et al.*, 2011; Thorn & Gaisano, 2012). As schematised in **Figure 1.5** A, STX2, VAMP2, SNAP23 and Munc18b mediate primary fusion, whereas STX3, VAMP8, SNAP23 and Munc18b mediate secondary fusion. **Figure 1.5** B schematises basolateral exocytosis, occurring via STX4, VAMP8, SNAP23 and

Munc18c. This process was first revealed in pathological conditions (Cosen-Binker *et al.*, 2008). Whereas VAMP2 mediates an early phase of secretion, VAMP2 and VAMP8 mediate a prolonged phase of secretion (Messenger *et al.*, 2014a). VAMP8-mediated secretion is also associated with endosomal trafficking, being dependent on the constitutive-like secretory pathway (Messenger *et al.*, 2013; Messenger *et al.*, 2014b; Messenger *et al.*, 2015). ZG trafficking, fusion and exocytosis are also regulated by Rab proteins, which are Ras-related small GTPases involved in membrane trafficking events in many cell types (Zerial & McBride, 2001; Stenmark, 2009). In PACs, Rab3D (Valentijn *et al.*, 1996; Chen *et al.*, 2002; Riedel *et al.*, 2002) and Rab27B (Chen *et al.*, 2004b; Hou *et al.*, 2016) ae implicated in ZG maturation and exocytosis. Rap1 is implicated in exocytosis triggered by CCK, ACh and cAMP (Sabbatini *et al.*, 2008), whereas Rab27A is involved in secretion occurring via the endolysosomal pathway (Hou *et al.*, 2015). On the contrary, Rab4 negatively regulates ZG exocytosis (Ohnishi *et al.*, 1999).

Furthermore, actin cytoskeleton reorganisation is required for ZG fusion to the plasma membrane and exocytosis (Muallem *et al.*, 1995). Actin filaments coat the ZGs after these fuse to the plasma membrane (Valentijn *et al.*, 2000; Nemoto *et al.*, 2004; Turvey & Thorn, 2004; Jang *et al.*, 2012) and play an important role in regulation of secretion and fusion pore dynamics (Valentijn *et al.*, 1999b; Larina *et al.*, 2007). The actin coat was suggested to stabilise the membrane-fused ZGs, also termed Ω-shapes. No lipid interchange was observed between the ZG and plasma membrane, possibly facilitating the recycling of the granule membrane (Thorn *et al.*, 2004).

Exocytosis requires a compensatory membrane retrieval mechanism, to reuptake and recycle the membrane of the fused vesicle/granule. In neurons, synaptic vesicle membrane is recycled via clathrin-mediated endocytosis (CME) (Jung & Haucke, 2007). Membrane retrieval in PACs was also attributed to a clathrin-dependent process and suggested that recycled membranes fused to the Golgi (Herzog & Farquhar, 1977; Herzog & Reggio, 1980). Clathrin, AP-2 and caveolin were detected at the apical membrane (Valentijn *et al.*, 1999a; Valentijn *et al.*, 1999b), and actin dynamics were suggested to contribute to membrane retrieval (Valentijn *et al.*, 1999b). Direct monitoring of exocytosis revealed that endocytic recycling does not involve uptake of intact granules; rather, the granule membrane is recycled in small pieces whilst the granule is still fused to the plasma membrane (Thorn *et al.*, 2004). Supra-physiological stimulation determines an expansion of the Ω-shapes and appearance of large vacuoles (Nemoto *et al.*, 2004), the post-exocytic Ω-shapes are disconnected from the apical membrane in the form of large EVs (Sherwood *et al.*, 2007). EVs do not present early endosome antigen 1 (EEA1), a marker of early endosomes (EE). In PACs, Rab5 co-localises with D52 and EEA1 at EE (Messenger *et al.*, 2017). Rab5 regulates homotypic fusion of EE to form late endosomes (LE), whilst Rab11a mediates conversion of EE to recycling endosomes, a process implicated in the constitutive-like pathway of secretion (Messenger *et al.*, 2015). These studies did not enquire on the origin of the endosomes, which may or may not originate from fused ZGs. Despite evidence on different stages of compensatory membrane retrieval mechanisms, the complete process of ZG membrane reuptake/recycling in PACs is still undetermined. The intracellular processing of the EVs originating from post-exocytic ZGs will be the focus of this thesis.

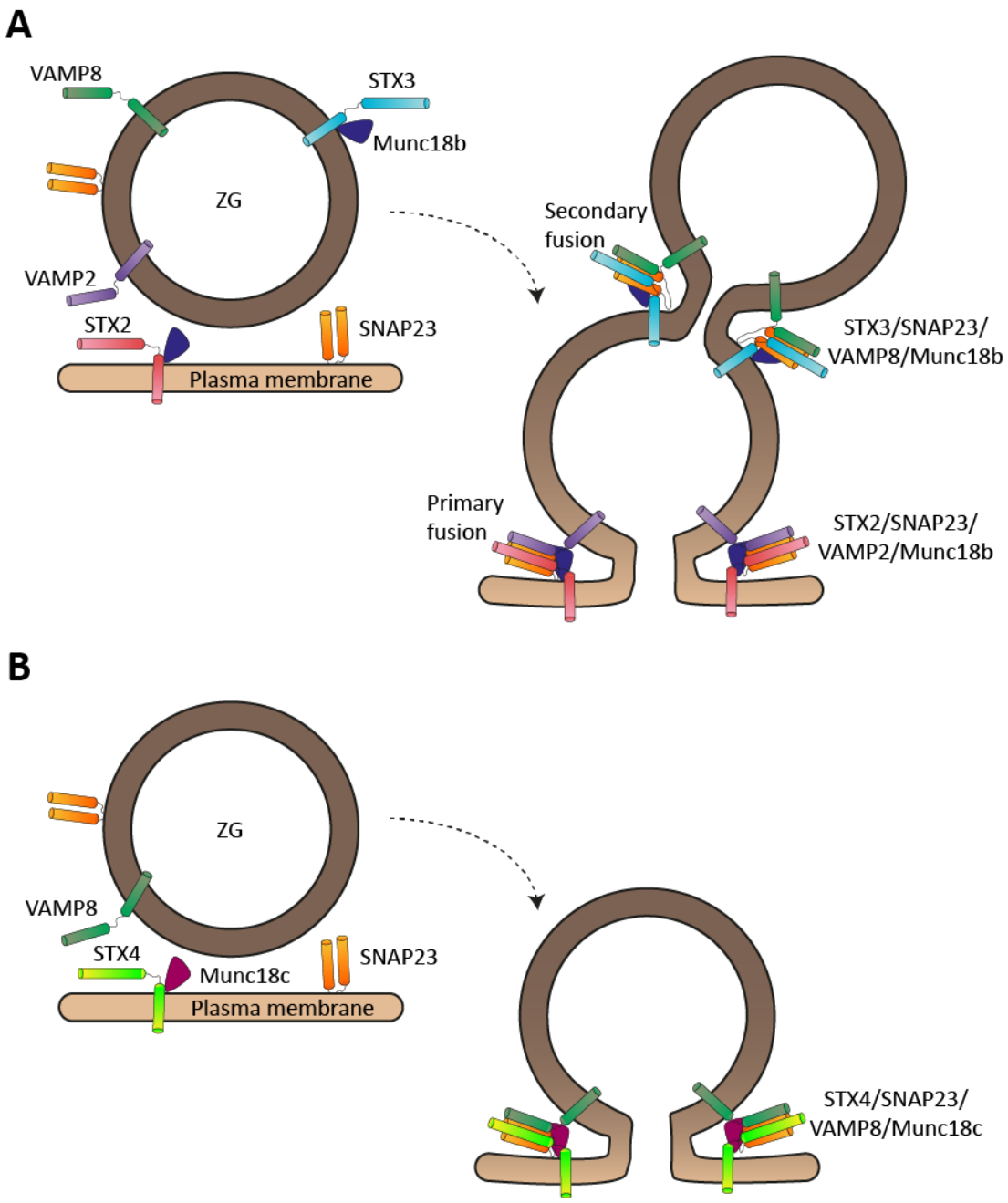

Figure 1.5 Membrane fusion machinery in apical and basolateral exocytosis of zymogen granules. A) Compound exocytosis of ZGs at the apical plasma membrane involves STX2/SNAP23/VAMP2/Mucn18b for primary fusion of ZG to the plasma membrane, and STX3/SNAP23/VAMP8/Munc18b for secondary fusion of a ZG to a plasma membrane-fused ZG. **B)** Basolateral exocytosis of ZGs requires STX4/SNAP23/VAMP8/Munc18c. Illustration was created using Adobe Illustrator utilising information adapted from (Cosen-Binker *et al.*, 2008; Behrendorff *et al.*, 2011; Dolai *et al.*, 2012; Thorn & Gaisano, 2012; Messenger *et al.*, 2014a; Messenger *et al.*, 2014b).

1.4 The actin cytoskeleton

As explained before, a functional actin cytoskeleton is essential to aid PAC secretory function (Muallem *et al.*, 1995; Nemoto *et al.*, 2004; Larina *et al.*, 2007; Jang *et al.*, 2012). Hence, this section will provide a brief introduction to the structural and dynamic properties of actin filaments, and their specific function in PACs. In non-muscle cells, the actin cytoskeleton is constituted by β-actin (ACTB) and γ-actin (ACTG). Actin is a 42 kDa ATPase. It exists in monomeric globular (G-actin) and polymeric filamentous (F-actin) forms. Actin filaments (~6 nm in diameter) are double helix filaments with a polarity: ATP-bound G-actin is incorporated at (+) barbed ends, whereas ADP-bound G-actin is dissociated from (-) pointed ends (**Figure 1.6**). Actin filament dynamics depend on the relative rates of polymerisation and depolymerisation. Several actin nucleators and actin binding proteins exist and they facilitate polymerisation, depolymerisation or stabilisation. Actin filaments play fundamental roles in cell structure, migration, exocytosis and endocytosis. The roles of the actin cytoskeleton in endocytosis will be described in Chapter 4.

1.4.1 Actin nucleators

Actin nucleators promote actin polymerisation. A major actin nucleator is the actin related protein 2/3 (Arp2/3) complex, a seven-subunit 220 kDa complex that determines the branching of actin filaments, by promoting the assembly of a new filament at a 70° angle of an existing one (Goley & Welch, 2006). The process requires ATP and the engagement of nucleation-promoting factors (NPFs), activating Arp2/3 through WCA domains (**Figure 1.7** A). Five groups of class I NPFs (presenting C-terminal WCA domains) exist: Wiskott-Aldrich syndrome protein (WASP) and neural

WASP (N-WASP), WASP-family verprolin homologue (WAVE), WASP and SCAR homologue (WASH), WASP homologue associated with actin, membrane and microtubules (WHAMM) and junction-mediating protein (JMY) (Campellone & Welch, 2010). These groups differ in regulation and function. Formins are another class of actin nucleators, responsible for filament elongation (**Figure 1.7** B). They possess formin homology (FH) domains FH1 and FH2, and are classified based on the sequence of the FH2 domain. Formins are active as dimers and interact with profilin to promote F-actin polymerisation at barbed ends (Campellone & Welch, 2010).

Actin nucleators are regulated upstream by the small GTPases of the Rho family: Rho, Rac and Cdc42 (reviewed in (Sit & Manser, 2011; Hanna & El-Sibai, 2013; Haga & Ridley, 2016)). RhoA activates the formin mDia, Rac1 activates WAVE and Cdc42 activates N-WASP, resulting in activation of the Arp2/3 complex. RhoA also activates ROCK which controls actomyosin contractility (**Figure 1.8**). Rho GTPases, like other families of GTPases, are active when bound to GTP, inactive when bound to GDP (Jaffe & Hall, 2005). They are positively regulated by guanine nucleotide exchange factors (GEFs), facilitating exchange of GDP for GTP. They are negatively regulated by GTPase activating proteins (GAPs), promoting GTP hydrolysis, and by Rho GDP-dissociation inhibitor (RhoGDI) proteins, inhibiting exchange of GDI for GTP (Rossman *et al.*, 2005; Bos *et al.*, 2007).

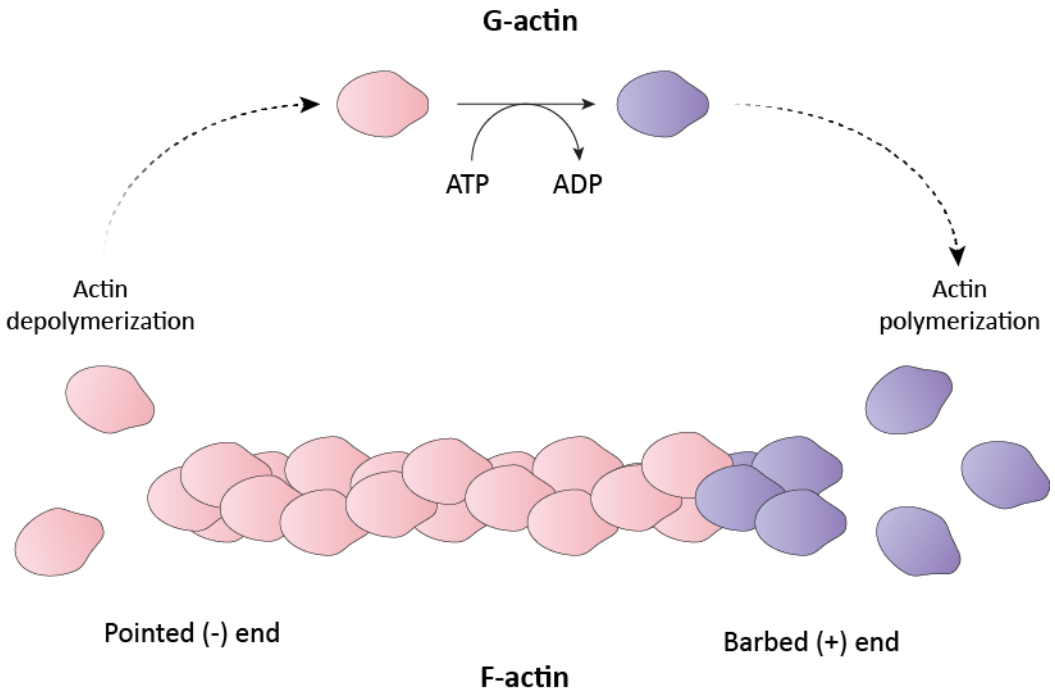

Figure 1.6 Actin dynamics. Actin filaments polymerise at barbed ends by addition of ATP-bound actin monomers, and depolymerise at pointed ends releasing ADP-bound actin monomers. Filaments are highly dynamic: the overall polymerisation/depolymerisation depends on the relative rates of polymerisation at barbed ends and depolymerisation at pointed ends. Illustration was created using Adobe Illustrator utilising information adapted from (Monastyrska *et al.*, 2009).

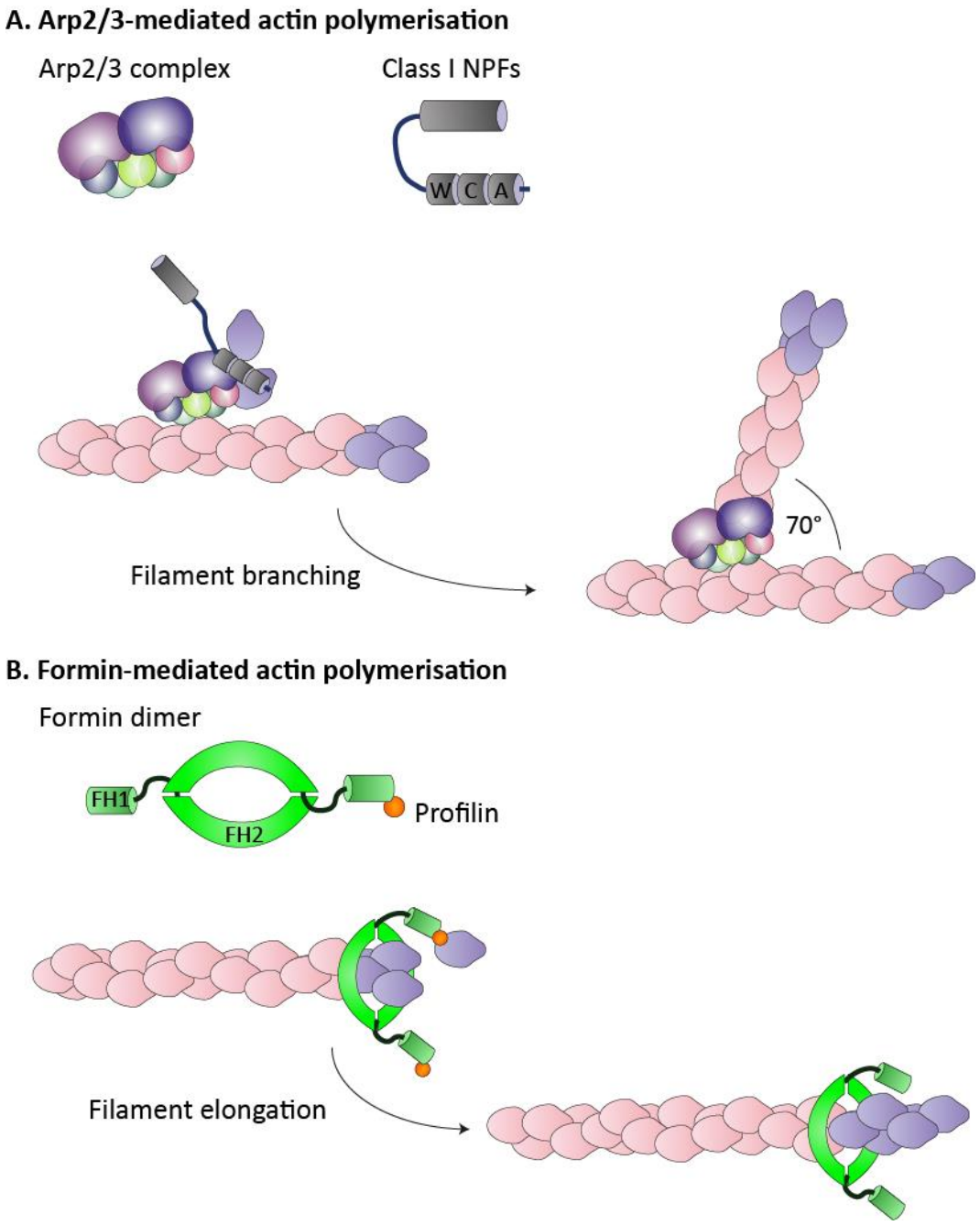

Figure 1.7 Arp2/3 and formin mediated actin polymerisation. A) NPF-activated Arp2/3 complex mediates actin branching promoting filament polymerisation at 70° angles. **B)** Active formin dimers interact with profilin and trigger actin filament elongation by promoting polymerisation at barbed ends. Illustration was created using Adobe Illustrator utilising information adapted from (Campellone & Welch, 2010).

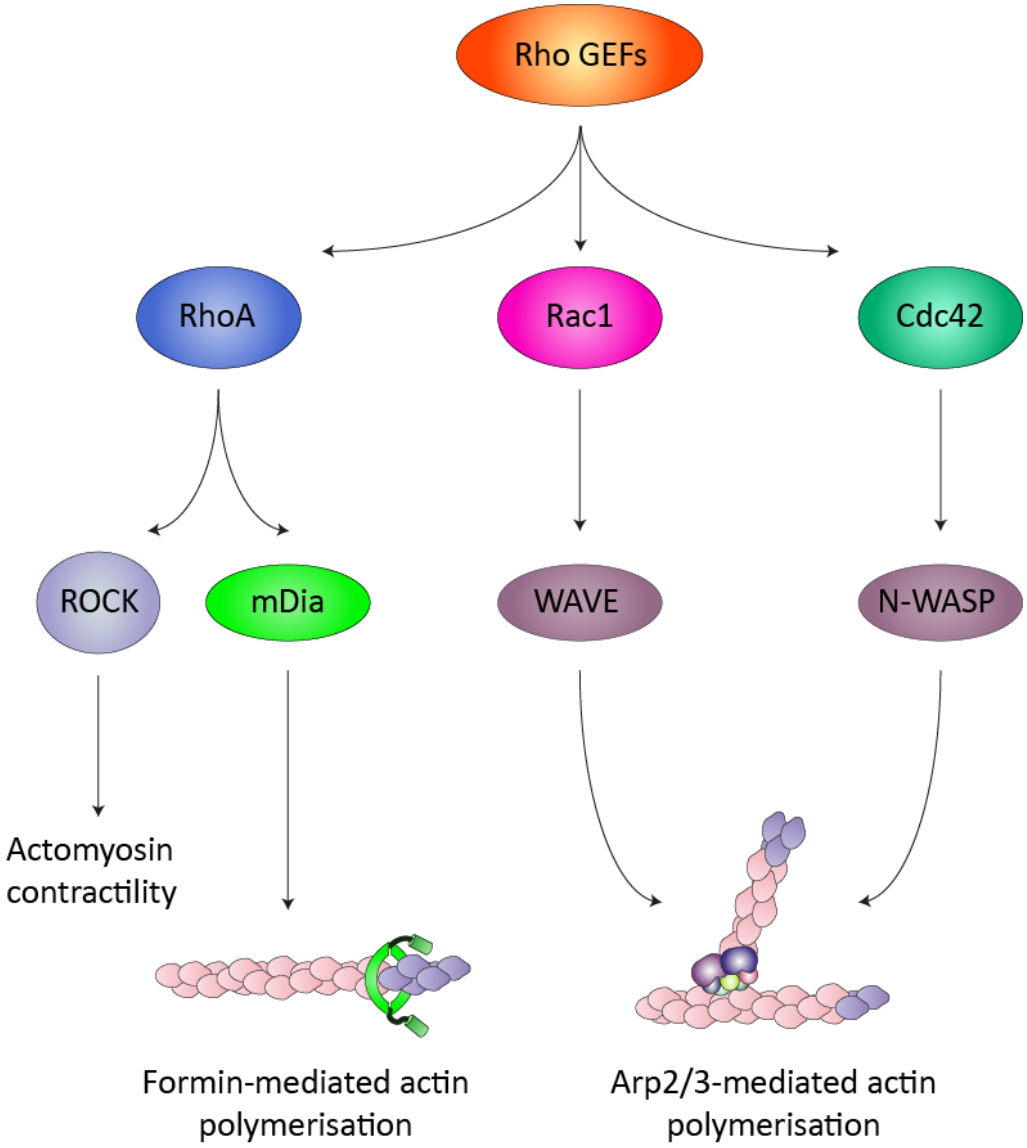

Figure 1.8 Rho GTPases regulate actin dynamics. Rho-GTPases are active when bound to GTP, a process faciliated by Rho GEFs. RhoA activates ROCK, responsible for actomyosin contractility, and mDia, responsible for actin filament elongation. Rac1 activates WAVE, Cdc42 activates N-WASP. WAVE and N-WASP activate the Arp2/3 complex, responsible for actin filament branching. Illustration was created using Adobe Illustrator utilising information adapted from (Auer *et al.*, 2011; Draber *et al.*, 2012; Prudnikova *et al.*, 2015).

1.4.2 Actin filaments in pancreatic acinar cells

Actin filaments in PACs are concentrated in the terminal web (also called the cortical actin network) below the apical plasma membrane, where they play an essential role in ZG exocytosis (Muallem *et al.*, 1995; Nemoto *et al.*, 2004; Larina *et al.*, 2007; Jang *et al.*, 2012). The cortical actin network is also located along the basolateral plasma membrane. Supramaximal stimulation is associated with reorganization of the actin cytoskeleton and the appearance of basolateral membrane protrusions (blebs) (Burnham & Williams, 1982). Additionally, a ring of actin filaments located at the adherens junctions encircles each acinar cell. Actin cables perpendicular to the apical membrane have also been identified (Geron *et al.*, 2013).

F-actin dynamics during secretion are regulated by RhoA and Rac1 (Bi *et al.*, 2005; Bi & Williams, 2005). CCK triggers RhoA pathway activation through CCK1R coupling with $G_{\alpha 13}$, and Rac1 activation through $G_{\alpha 13}$ and $G_{\alpha q}$ (Sabbatini *et al.*, 2010). The RhoGEF Vav-2 is associated with CCK-induced RhoA signalling (Kim *et al.*, 2006), and the p115 RhoGEF is implicated in CCK-induced RhoA and Rac1 activation (Sabbatini *et al.*, 2010). p50 RhoGAP and p190 RhoGAP-B are responsible for RhoA inactivation (Williams *et al.*, 2009); RhoGDI1 and RhoGDI3 interact with both RhoA and Rac1 (Sabbatini & Williams, 2013).

1.5 Autophagic pathways

PAC damage in acute pancreatitis, which will be described later in this chapter, is associated with disruption of autophagy (reviewed in (Gukovsky *et al.*, 2012; Gukovskaya *et al.*, 2017)). Autophagic pathways might also be relevant to the processing of EVs, the main focus of this thesis. Hence, this section will provide an overview of autophagy and its roles in PACs. Autophagy - meaning self-eating - is a conserved cellular process. There are different types of autophagy: macroautophagy, chaperone-mediated autophagy (CMA) and microautophagy (Mizushima *et al.*, 2011; Yu *et al.*, 2018). Macroautophagy is involved in the degradation of cytoplasmic contents such as proteins and organelles via engulfment in double-membrane autophagosomes which then fuse with lysosomes. CMA involves the recognition of a marker peptide present on cytosolic proteins, which are then transported into the lysosomes. Microautophagy consists of the direct engulfment of cytosolic components by the lysosomal membranes. Macroautophagy, hereafter referred to as (canonical) autophagy, is an essential cellular process, occurring in both basal and stressed conditions. Protective autophagy mediates the degradation of damaged components (e.g. organelles) and regenerative autophagy allows for recycling of material in conditions of starvation (i.e. degradation of long-lived proteins to get amino acids). Specific names refer to selective autophagy processes (Galluzzi *et al.*, 2017). Mitophagy, pexophagy, reticulophagy (or ERphagy), ribophagy, lysophagy and proteophagy refer to autophagy of mitochondria, peroxisomes, ER, ribosomes, lysosomes and proteasomes, respectively. Aggrephagy refers to autophagy of protein aggregates, lipophagy of lipid droplets. Xenophagy indicates autophagy of pathogens that have escaped the phagocytic pathway.

In mammalian cells, autophagy initiation triggers the formation of a phagophore isolation membrane (also called pre-autophagosomal structure, PAS) engulfing a portion of the cytoplasm. Nascent phagophores originate from membrane structures called omegasomes. Omegasomes form at ER-mitochondria contact sites (Axe *et al.*, 2008), at the Golgi-endosomal system or at the plasma membrane (Ravikumar *et al.*, 2010; Orsi *et al.*, 2012; Puri *et al.*, 2013). During the elongation phase, the PAS matures into a double-membrane autophagosome that later fuses with lysosomes, forming an autolysosome. Autophagosome-lysosome fusion is mediated by Rab7A (Gutierrez *et al.*, 2004) and by the SNARE complex STX17-SNAP29-VAMP8 (Itakura *et al.*, 2012). STX17 is also involved in autophagosome closure (Tsuboyama *et al.*, 2016). In autolysosomes, acidic pH permits activity of lysosomal hydrolases which degrade the cargo and also the inner autophagosomal membrane (**Figure 1.9**).

The processes of autophagosome formation are regulated by autophagy related (ATG) protein machinery, which was initially identified in yeast and is conserved in mammals (Mizushima *et al.*, 2011). In starvation conditions, mammalian target of rapamycin complex 1 (mTORC1) inhibition relieves the inhibitory phosphorylation of ULK1 and ATG13, which form a complex with FIP200 and ATG101. Thereafter, ULK1 phosphorylates ATG13, FIP200 and itself, activating the complex. The ULK1 complex phosphorylates ATG9 (Orsi *et al.*, 2012), required for the formation of phagophore precursors (Mizushima *et al.*, 2011; Yu *et al.*, 2018). The active ULK1 complex interacts with the phosphatidylinositol-3-kinase (PI(3)K) class III complex, constituted by the PI(3)K class III Vps34 and by Vps15, Beclin1, ATG14 and Ambra1. ULK1 and PI(3)K class III complexes accumulate at ATG9-positive membranes. Here, Vps34

generates phosphatidylinositol-3-phosphate (PI(3)P). PI(3)P-binding proteins, such as WD-repeat protein interacting with phosphoinositides (WIPI2) or double FYVE domain-containing protein (DFCP1), are recruited at these sites. In parallel, two ubiquitin-like conjugation reactions occur (**Figure 1.10**). The first reaction involves the E1-like enzyme ATG7 and the E2-like enzyme ATG10 and determines the conjugation of ATG12 to ATG5. ATG12-ATG5 then form tetrameric complexes with ATG16L1. In the second reaction, the cytosolic protein LC3-I, which is cleaved from its precursor by ATG4, is conjugated to phosphatidylethanolamine (PE) via E1-like ATG7 and E2-like ATG3, forming LC3-II (Mizushima *et al.*, 2011). The ATG5-ATG12-ATG16L1 complex is responsible for targeting LC3-II to both sides of PI(3)P-positive isolation membranes (Fujita *et al.*, 2008). LC3 is an ubiquitin-like protein, recognised by LC3 interacting regions (LIR) of proteins which bind to the hydrophobic N-terminal LIR docking site (LDS) domain of LC3. After fusion with lysosomes, the LC3-II located on the luminal membrane is degraded by lysosomal hydrolases, whilst the LC3-II on the cytoplasmic membrane is de-lipidated by ATG4 and recycled.

In the last ten years, several processes differing from (canonical) autophagy in mechanistic, structural and functional characteristics have been described. Thus, the concept of non-canonical autophagy has been introduced (**Figure 1.11**). On a mechanistic level, non-canonical autophagic pathways are independent from one or multiple of the upstream regulators of autophagosome biogenesis. For instance, processes independent from ULK1 (Florey *et al.*, 2015), PI(3)K (Niso-Santano *et al.*, 2015; Jacquin *et al.*, 2017) or ATG5/ATG7 (Nishida *et al.*, 2009) have been reported. Non-canonical autophagy can be activated by NADPH oxidase 2 (NOX2), by Toll-like

receptor (TLR) or by Fc receptor for IgG (FcγR) (Sanjuan *et al.*, 2007; Huang *et al.*, 2009; Henault *et al.*, 2012; Martinez *et al.*, 2015). The non-canonical PI(3)K class III complex is different from the canonical one, being constituted by UVRAG and not by ATG14 or Ambra1, and being positively regulated by Rubicon (Martinez *et al.*, 2015). In non-canonical autophagy, ATG16L1-mediated LC3-II targeting to membranes depends on a different domain (the C-terminal WD40 domain) than the FIP200-binding domain (FBD) involved in interaction with WIPI2 and FIP200 in canonical autophagy (Dooley *et al.*, 2014; Fletcher *et al.*, 2018). On a structural level, in non-canonical autophagy LC3-positive organelles have a single membrane (Florey *et al.*, 2011), differently from the double-membrane autophagosomes described in canonical autophagy. On a functional level, non-canonical autophagy usually deals with extracellular "threats" (e.g. pathogens), differently from canonical autophagy dealing with intracellular ones (e.g. damaged organelles or protein aggregates) – with the exception of xenophagy. Examples of non-canonical autophagy are LC3-associated phagocytosis (LAP) (Sanjuan *et al.*, 2007; Martinez *et al.*, 2011; Gluschko *et al.*, 2018), macropinocytosis and entosis (Florey *et al.*, 2011; Martinez *et al.*, 2011), all targeting cargo of extracellular origin. A recent review recommended against using the terms canonical and non-canonical autophagy, based on the number of variants of the latter (Galluzzi *et al.*, 2017). In this thesis, I will nonetheless adopt the term non-canonical autophagy, to refer to any process independent from at least one of the complexes essential for canonical autophagy, and involving the lipidation of LC3 on single membrane organelles.

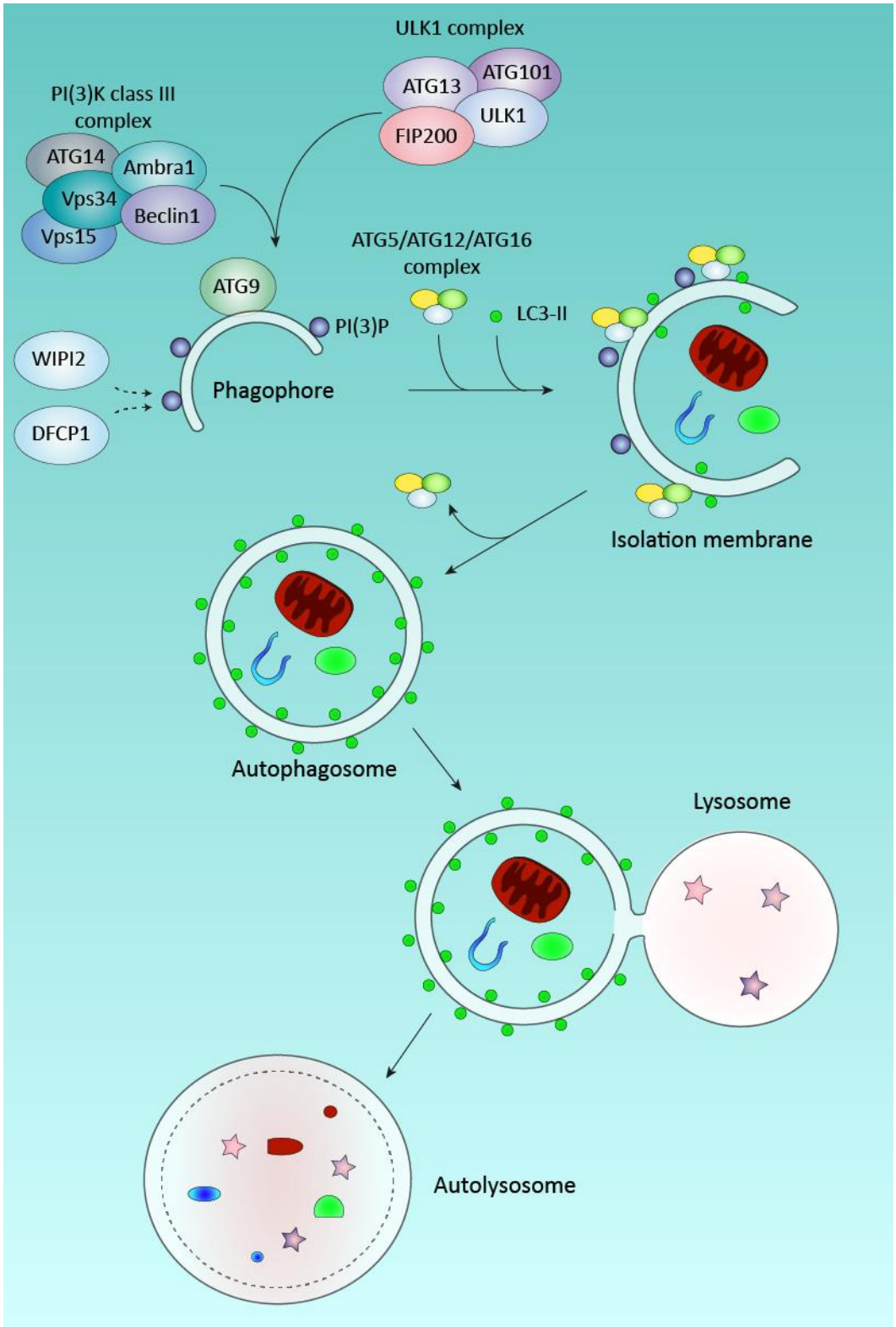

Figure 1.9 (Canonical) autophagy. The ULK1 complex activates and associates with the PI(3)K class III complex, at ATG9-labelled membranes. Here, PI(3)P formation recruits WIPI2 or DFCP1; these recruit the ATG5/ATG12/ATG16L1 complex. LC3 is lipidated on double membrane nascent autophagosomes, which will fuse with lysosomes forming autolysosomes. Illustration was created using Adobe Illustrator utilising information adapted from (Rubinsztein *et al.*, 2007; Feng *et al.*, 2014; Parzych & Klionsky, 2014).

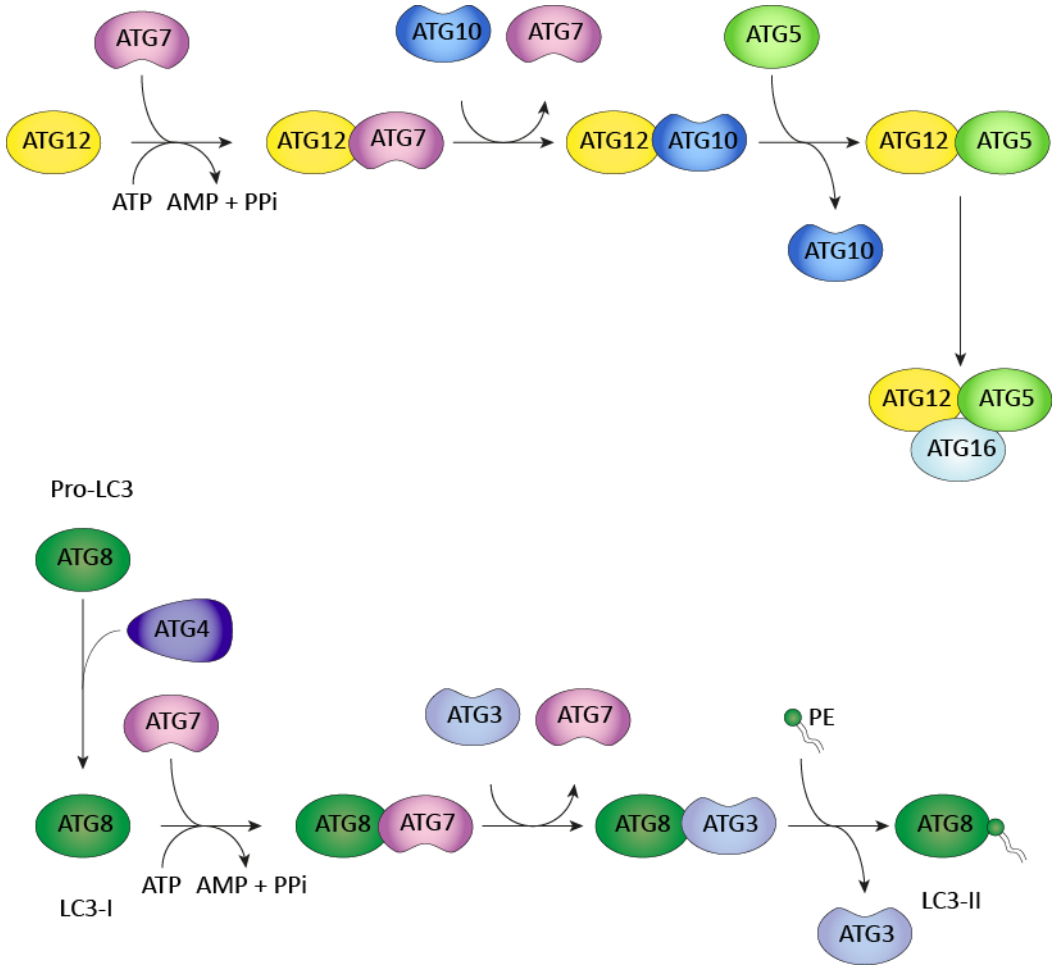

Figure 1.10 LC3 conjugation machinery (involved in canonical autophagy). In the first ubiquitin-like conjugation reaction, ATG7 and ATG10 conjugate ATG12 to ATG5. ATG12-ATG5 will then form complexes with ATG16L1. In the second ubiquitin-like conjugation reaction, LC3 – cleaved from Pro-LC3 by ATG4 – is conjugated to PE by ATG7 and ATG3. Illustration was created using Adobe Illustrator utilising information adapted from (Geng & Klionsky, 2008; Chen & Klionsky, 2011).

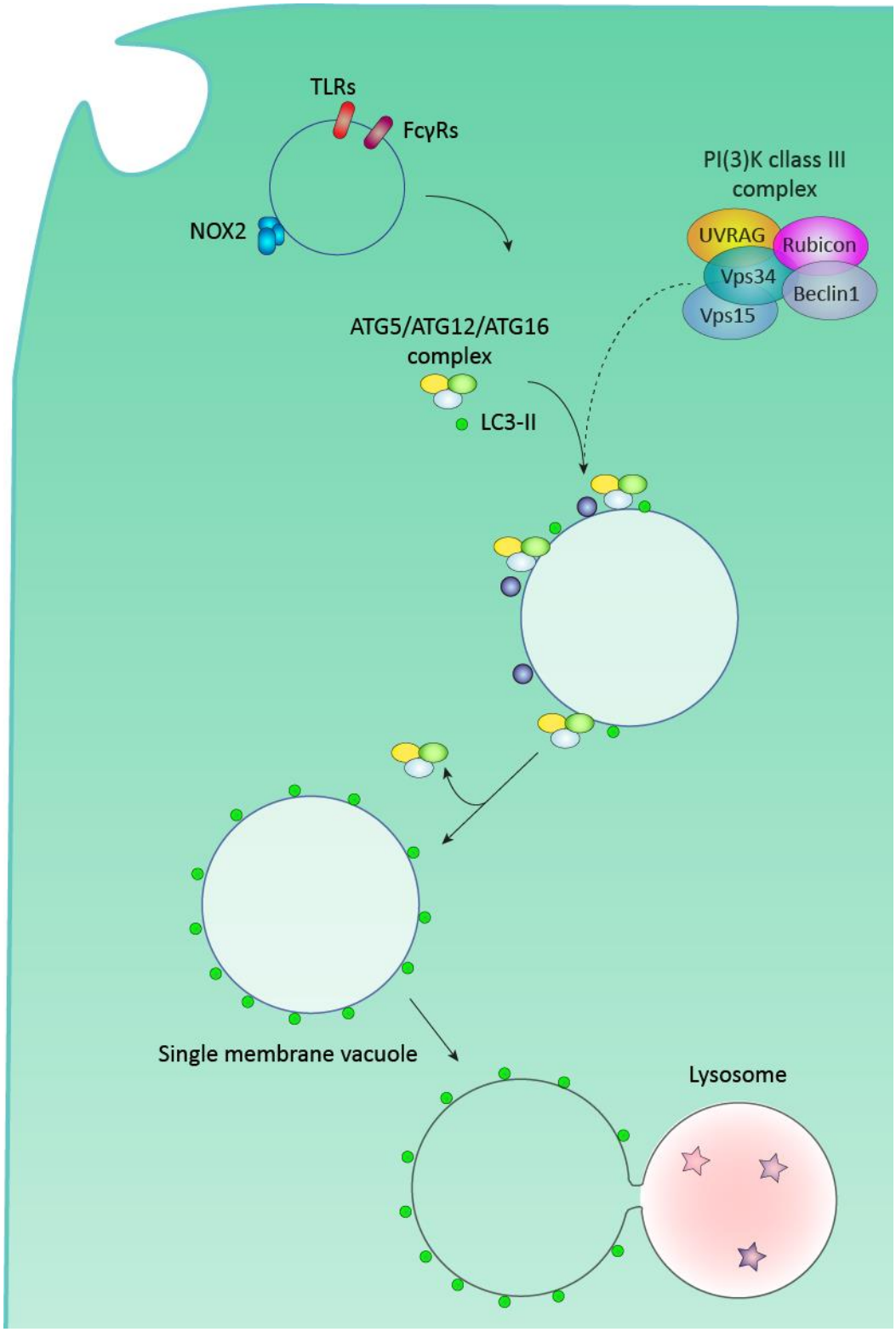

Figure 1.11 Non-canonical autophagy. Upstream signals trigger PI(3)K class III activation and PI(3)P generation, recruiting the ATG5/ATG12/ATG16L1 complex. LC3 is lipidated on single-membrane vacuoles, which will then fuse with lysosomes. Illustration was created using Adobe Illustrator utilising information adapted from (Florey & Overholtzer, 2012; Boyle & Randow, 2015).

1.5.1 LC3 and monitoring autophagy

In mammals the *ATG8* gene family consists of microtubule associated protein 1 light chain 3 (*MAPLC3*, hereafter referred to as *LC3*), γ-aminobutyric acid type A receptor associated protein (*GABARAP*) and Golgi-associated ATPase enhancer of 16 kDa (*GATE-16*). The *LC3* subfamily encodes five protein variants: LC3Av1, LC3Av2, LC3B, LC3B2 and LC3C. The *GABARAP* subfamily encodes four protein variants: GABARAP, GABARAPL1, GABARAPL2/GATE16 and GABARAPL3. Both LC3 and GABARAP proteins also have roles independent from autophagy (Schaaf *et al.*, 2016). The LC3 splice variants undergo different post-translational modifications (He *et al.*, 2003; Tanida *et al.*, 2004) and present different subcellular localisation (Koukourakis *et al.*, 2015) and different tissue distribution. Differences between isoforms also vary when comparing human, mouse and rat (Wu *et al.*, 2006; Zois *et al.*, 2011; Schaaf *et al.*, 2016).

"Guidelines for the use and interpretation of assays for monitoring autophagy" (Klionsky *et al.*, 2016) provides an extensive, periodically updated review of methods and considerations to be undertaken when evaluating autophagy. It is fundamental to appreciate that autophagy is a flux; in its evolution, autophagosomes undergo initiation, elongation and fusion phases. Disruption of the autophagic flux is therefore extensively utilised to study autophagy. The most common readout of autophagy activation is the LC3 status, which can be measured in terms of LC3-II/LC3-I ratio via Western blotting, or by detecting hotspots of LC3 reporter construct fluorescence. The GFP-LC3 transgenic mice provide a powerful tool to monitor autophagy in live primary cells (Mizushima *et al.*, 2004) and so are utilised in this thesis.

1.5.2 Autophagy in pancreatic acinar cells

PACs are a fundamental source of exocytosed proteins, involved in digestion. Such proteins are synthesised in the highly developed RER of these cells. The PAC secretory activity thus requires active processes to maintain protein homeostasis (proteostasis), protecting the cell from misfolding and aggregation. A recent study has identified cell-cycle progression gene 1 (CCPG1) as a receptor for autophagy of the RER (Smith *et al.*, 2018). CCPG1 interacts with LC3 and GABARAP through a LIR motif, and with FIP200 through the N-terminal domain (Lahiri & Klionsky, 2018). CCPG1 deficient mice presented ER stress and defective proteostasis (Smith *et al.*, 2018). The CCPG1 deficient phenotype is less severe compared to mouse models deficient for ATG5 (Diakopoulos *et al.*, 2015) or ATG7 (Antonucci *et al.*, 2015), where all autophagic pathways are disrupted, including mitophagy and aggrephagy. It is therefore clear that autophagy plays an important role in PAC homeostasis, at both the ER and other organelles.

1.6 Acute pancreatitis

Acute pancreatitis (AP) is a disease of the pancreas with 5% mortality rate (Banks *et al.*, 2006). The diagnosis is associated with abdominal pain and more than three-fold increased levels of serum amylase and/or lipase (Tenner *et al.*, 2013). The main features of AP are pancreatic inflammation, oedema and necrosis; the disease can involve inflammation and injury of other organs. AP requires hospitalisation and multiple episodes can provoke chronic pancreatitis (CP). CP is associated with an increased risk of developing pancreatic cancer. Although most cases of AP are mild to moderate, when the disease is severe it has a 30% probability of death. Severe pancreatitis is associated with systemic inflammation and multi-organ failure. The pathogenesis of AP is not well understood. The first phase of the pathophysiology of AP is the intra-acinar activation of trypsin (reviewed in (Singh & Garg, 2016; Gukovskaya *et al.*, 2017; Gerasimenko *et al.*, 2018)). This is followed by intra- and extra-pancreatic inflammation. The aetiology of AP is mainly associated with bile acids reflux due to gallstones and alcohol abuse (reviewed in (Pandol *et al.*, 2007)). In addition, genetic factors such as mutations in the cationic trypsinogen gene can contribute to pancreatitis (Whitcomb *et al.*, 1996). Recently a novel factor has been identified, asparaginase, a drug currently used in the treatment of acute lymphoblastic leukaemia (ALL) (Gerasimenko *et al.*, 2018).

1.6.1 Experimental pancreatitis

Historically, AP has been described as “autodigestion” of the pancreas. This is associated with the premature conversion of trypsinogen to trypsin in acinar cells. Further research has shown that the disease depends of both acinar cell injury and

inflammatory response. Animal models of pancreatitis have been developed with the aim to investigate its pathophysiology and develop therapies. The classical *in vivo* models of AP involve administration of secretagogues (CCK or its analogue caerulein) (Lampel & Kern, 1977), bile acids (taurocholic acid-3-sulfate (TLC-S) or Na-taurocholate) (Laukkarinen *et al.*, 2007) or fatty acid ethyl esters (FAEE) (Huang *et al.*, 2014). Other models include arginine administration (Tani *et al.*, 1990), choline-deficient ethionine-supplemented (CDE) diet (Lombardi *et al.*, 1975) and duct obstruction-ligation (Senninger *et al.*, 1986). Both histological (oedema, inflammation, necrosis) and biochemical (serum amylase, markers of inflammation, pancreatic trypsin) parameters are evaluated when characterising experimental pancreatitis in *in vivo* models.

In order to understand the cellular mechanism of AP pathophysiology, cellular *ex vivo* models are also extensively used. Acinar cells/clusters can be isolated by collagenase digestion, lobules can be isolated by micro-dissection. Isolated PACs can be maintained for short term culture, although they progressively lose their polarised phenotype and secretory capability. Hence, freshly isolated PACs are generally used, and they are used in this thesis. Alternatively, the rat acinar cell line AR42J can be used (Christophe, 1994), although it does not resemble all the PAC properties. In cellular *ex vivo* models of AP, PACs are exposed to supramaximal CCK stimulation (Williams *et al.*, 1978; Leach *et al.*, 1991; Saluja *et al.*, 1997), to TLC-S (Voronina *et al.*, 2002a) or to FAEE (Criddle *et al.*, 2004; Criddle *et al.*, 2006; Wu *et al.*, 2008; Dolai *et al.*, 2012). Calcium signalling, zymogen activation, mitochondrial dysfunction and cell

death (by necrosis and apoptosis) are monitored when characterising experimental pancreatitis in cellular *ex vivo* models.

Supramaximal stimulation, non-oxidative alcohol metabolites and bile acids empty the intracellular stores and activate SOCE pathways, provoking aberrant calcium signalling (Gerasimenko *et al.*, 2009; Huang *et al.*, 2014; Gerasimenko *et al.*, 2018). Calcium overload inhibits mitochondrial ATP production. ATP depletion affects calcium pumps, further exacerbating the cytosolic calcium overload. Calcium overload and PMCA inhibition provoked by oxidative stress are associated with mitochondrial depolarisation and mitochondrial permeability transition pore (MPTP) opening (Bruce & Elliott, 2007; Baggaley *et al.*, 2008). Mitochondrial dysfunction, mediated by the MPTP component cyclophilin D, induces ER stress and impairs autophagy (Biczo *et al.*, 2018).

In light of the role of aberrant calcium signalling in PAC injury, inhibitors of IP_3Rs (Huang *et al.*, 2017), SOCE (Gerasimenko *et al.*, 2013; Wen *et al.*, 2015) and MPTP opening (Mukherjee *et al.*, 2016; Javed *et al.*, 2018) have been tested and they reduced the severity of experimental pancreatitis. Other studies have identified a role for metabolism in PAC injury provoked by experimental pancreatitis. Interestingly, a switch to glycolytic metabolism induced by insulin resulted in protection of PACs from ATP depletion, calcium overload and necrosis (Mankad *et al.*, 2012; Samad *et al.*, 2014). Glycolytic ATP production was capable of supplying the PMCA, thus counteracting calcium overload.

Cytosolic and mitochondrial calcium overload also trigger vacuolisation, intracellular zymogen activation, oxidative stress, necrosis and apoptosis (although apoptosis is inhibited when ATP is depleted). In pancreatitis, apoptosis is considered protective compared to necrosis. Cell death by necrosis causes the release of nuclear proteins, DNA and ATP, which act as damage-associated molecular patterns (DAMPs) (Kang *et al.*, 2014; Yu *et al.*, 2014). Cell injury also triggers activation of the nuclear factor kappa-light-chain-enhancer of activated B cells (NF-κB) pathway (Gukovsky *et al.*, 1998) and release cytokines and chemokines by PACs (Gukovskaya *et al.*, 1997; Blinman *et al.*, 2000). Together, these signals trigger the innate immune response, inducing monocyte and neutrophil infiltration (Singh & Garg, 2016). Accumulating evidence highlight the role of inflammation in AP pathophysiology and severity (Aghdassi *et al.*, 2018; Sendler *et al.*, 2018). Another important factor is PDC damage, determining a defect in fluid and electrolyte secretion and an acidification of the luminal pH (Hegyi *et al.*, 2011). Recent studies have also proposed calcium-induced nitric oxide production by PSCs as a mediator of PAC damage in pathological conditions (Gryshchenko *et al.*, 2016; Gryshchenko *et al.*, 2018). However, for the purpose of this thesis, focus will be on the intra-acinar events of AP pathogenesis, in particular trypsinogen activation, autophagy disruption and vacuolisation.

1.6.2 Intra-acinar trypsinogen activation

The premature activation of trypsinogen occurs within the PACs (Hofbauer *et al.*, 1998; Luthen *et al.*, 1998). The auto-activation hypothesis suggests that zymogen accumulation in acidic vacuoles determines the auto-activation of trypsinogen and its conversion to trypsin. The co-localisation hypothesis states that trypsinogen

activation depends on the co-localisation of zymogens with lysosomal hydrolases (i.e. cathepsin B) (van Acker *et al.*, 2006; Van Acker *et al.*, 2007). This theory was supported by the observed shift of lysosomal hydrolases to the ZG-enriched subcellular fraction. Cathepsin B deficient mice injected with caerulein present less intracellular trypsinogen activation (Halangk *et al.*, 2000); CI-MPR/IGFII deficient mice, where sorting of cathepsin B to the lysosomal compartment is inhibited, present enhanced trypsinogen activation following induction of experimental pancreatitis (Meister *et al.*, 2010). However, cathepsin B missorting was not sufficient to trigger trypsinogen activation in the absence of stimulation. The co-localising vacuoles where cathepsin B activates trypsinogen would then become fragile and rupture, releasing their content (i.e. active trypsin and cathepsin B) into the cytosol (van Acker *et al.*, 2006; Talukdar *et al.*, 2016). Cathepsin B-mediated trypsinogen activation was responsible for induction of apoptosis via caspase 3 (Sendler *et al.*, 2016).

Controversially, in a recent study cathepsin B staining was increased in caerulein-treated mice compared to controls, and it localised at autophagosomes and autolysosomes rather than in ZGs (Zhang *et al.*, 2014). Differently, cathepsin D staining was decreased in caerulein-treated mice, and was found in autophagosomes but not autolysosomes. Also, whereas immunoblotting showed an increase in cathepsin B mature form, cathepsin D mature form was reduced in caerulein-treated mice. The cathepsin missorting theory has thus been challenged and replaced by the concept of maturation impairment and consequent dysfunction (Gukovsky *et al.*, 2012).

1.6.3 Autophagy in pancreatitis

An alternative theory for trypsinogen activation is the autophagy theory (Ohmuraya & Yamamura, 2008). Autophagy is activated in PACs following supramaximal stimulation with calcium-releasing agonists (Hashimoto *et al.*, 2008; Mareninova *et al.*, 2009). Induction of pancreatitis determines formation of larger vacuoles and prolonged LC3-II accumulation compared to starvation. Experimental AP is accompanied by autophagic flux disruption due to defective lysosomal degradation (Hashimoto *et al.*, 2008; Mareninova *et al.*, 2009). AP stimuli do not prevent autophagosome-lysosome fusion, but affect lysosomal function causing inefficient degradation of long-lived proteins. Lysosomal dysfunction is associated with improper maturation/activity of lysosomal hydrolases and targeting/function of LAMP proteins. Indeed, cathepsin processing is impaired and LAMP1 and LAMP2 levels are decreased in experimental pancreatitis (Gukovsky *et al.*, 2012; Zhang *et al.*, 2014). Moreover, *Lamp2* knock-out (KO) mice present pancreatic injury and accumulate large autophagic vacuoles, developing spontaneous pancreatitis (Mareninova *et al.*, 2015). These results demonstrate that lysosomal dysfunction is associated with pancreatitis pathophysiology. Controversially, previous studies reported that inhibiting autophagy activation (genetically or pharmacologically) reduced the severity of experimental pancreatitis (Gukovsky *et al.*, 2012). Nevertheless, defective autophagy produced by *Atg5* or *Atg7* KO provokes spontaneous pancreatitis (Diakopoulos *et al.*, 2015; Zhou *et al.*, 2017). These results indicate that autophagy is required for PAC homeostasis, but it becomes activated and its function disrupted in pancreatitis.

A selective autophagic pathway has also been detected in PACs, called zymophagy. Zymophagy is mediated by vacuolar membrane protein 1 (VMP1), a transmembrane protein that determines the ubiquitination and labelling for autophagy of ZGs (Ropolo *et al.*, 2007). This process could represent a protective mechanism that mediates the degradation of pathologically activated zymogens. 70% of VMP1-positive autophagosomes contained ZGs in caerulein-treated *ElaI-VMP1* mice, against 20% in controls (Grasso *et al.*, 2011; Vaccaro, 2012). However, activation of VMP1 had longer kinetics than vacuole formation and trypsinogen activation (Sherwood *et al.*, 2007; Vaccaro, 2012), so it cannot constitute a protection from these early events.

1.6.4 Endocytic vacuoles are the site of trypsinogen activation

Cytoplasmic vacuoles are a common feature of experimental pancreatitis (Niederau & Grendell, 1988; Raraty *et al.*, 2000) and exist in two populations, endocytic and non-endocytic vacuoles (Voronina *et al.*, 2007). Calcium-releasing agonists (CCK and TLC-S) induce vacuole formation and trypsin activation, and this is sustained by SOCE for refilling intracellular calcium stores and mediate the calcium plateau (Voronina *et al.*, 2015). A study from our laboratory showed that intracellular trypsinogen activation occurred within the EVs (Sherwood *et al.*, 2007). The acidic pH inside EVs is appropriate to permit activation of trypsinogen (via auto-activation or by co-localising lysosomal hydrolases). Alternatively, EVs could uptake active trypsin from the acinar lumen, thus mediating activation of inactive trypsinogen. In a more recent study, our laboratory reported that EVs could rupture and leak their contents into

the cytosol (Chvanov *et al.*, 2018). This means that active trypsin could also be released from these organelles, thus triggering cell damage.

1.7 Aims

Transgenic mice conditionally expressing endogenously activated trypsinogen in PACs develop AP (Gaiser *et al.*, 2011). Trypsinogen activation is thus an early pathogenic event in AP. EVs are the activating site of trypsinogen in cellular models of experimental pancreatitis (Sherwood *et al.*, 2007). Active trypsin might leak from ruptured EVs into the cytosol (Chvanov *et al.*, 2018), thus provoking PAC damage. Currently, the cellular mechanisms of EV processing are largely unknown. This became the focus of our study. Early in the project I observed the presence of F-actin and autophagy marker LC3 on some EVs. These observations formed the foundation of my study and helped to specify its aim and objectives.

The overarching aim of this study is to characterise the cellular processing of the EVs and how this might be disrupted in pathological conditions. Specific objectives of the study are:

1) To determine the cellular mechanisms of interaction between EVs and autophagic pathways.

2) To characterise the mechanisms involved in F-actin appearance on the surface of EVs (i.e. the mechanisms of EV actination).

3) To elucidate the relationships between autophagy and actination of EVs.

4) To characterise the pH properties of EVs at different stages of their development.

2 Material and Methods

2.1 Materials

2.1.1 Reagents and suppliers

The suppliers of reagents and equipment will be indicated throughout this chapter; when omitted, chemicals were purchased from Sigma-Aldrich. Suppliers' locations are alphabetically listed in Table 2.1:

Table 2.1 Suppliers used in this study

Supplier	Location
Abcam	Cambridge, UK
Agar Scientific	Stansted, Essex, UK
Atlas Antibodies	Bromma, Sweden
Aurion	Wageningen, The Netherlands
Becton, Dickinson and Company (BD)	Franklin Lakes, New Jersey, USA
Bio-Rad Laboratories	Hercules, California, USA
Bio-Techne	Minneapolis, Minnesota, USA
Cayman Chemical Company	Ann Arbor, Michigan, USA
Charles River	Margate, Kent, UK
Cyandye LLC	Sunny Isles Beach, Florida, USA
FEI	Hillsboro, Oregon, USA
Ibidi	Martinsried, Germany
Jackson Laboratory	Bar Harbor, Maine, USA
Leica Microsystems	Wetzlar, Germany
MatTek Corporation	Ashland, Massachusetts, USA
MBL International Corporation	Woburn, Massachusetts, USA
Merck	Darmstadt, Germany
Riken	Tokyo, Japan
Sigma-Aldrich	St Louis, Missouri, USA
Spirochrome	Stein and Rhein, Switzerland
Stratech	Newmarket, UK
TAAB	Reading, UK
Ted Pella Inc.	Redding, California, USA
Thermo Fisher Scientific	Waltham, Massachusetts, USA
Vector Biolabs	Malvern, Pennsylvania, USA
Zeiss	Oberkochen, Germany

2.1.2 Solutions

All solutions were freshly prepared with double deionised water (ddH_2O).

Table 2.2 Solutions used in this study

Extracellular solution 140 mM NaCl, 4.7 mM KCl, 1.13 mM $MgCl_2$, 10 mM 4-(2-hydroxyethyl)-1-piperazineethanesulfonic acid (HEPES), 10 mM D-glucose, 1.2 mM $CaCl_2$, pH 7.3
PAC culture media 130 mM NaCl, 4.7 mM KCl, 1.13 mM $MgCl_2$, 10 mM HEPES, 10 mM D-glucose, 1 mM $CaCl_2$, 1 mM Na_3PO_4, 2 mM pyruvate, Penicillin-Streptomycin-Glutamine 1X (Thermo Fisher Scientific), Minimum Essential Medium (MEM) amino acids 1X (Thermo Fisher Scientific), 1 µM trypsin inhibitor from *Glycine max* (soybean), pH 7.4
Phosphate buffered saline (PBS) 137 mM NaCl, 2.7 mM KCl, 10 mM NaH_2PO_4, pH 7.4
Phosphate buffered saline-Tween (PBST) PBS, 0.05% (v/v) Tween-20 (Thermo Fisher Scientific)
Blocking buffer for immunofluorescence staining PBS, 10% (v/v) goat serum, 1% (w/v) bovine serum albumin (BSA)
Primary antibody solution buffer for immunofluorescence staining PBS, 5% (v/v) goat serum, 0.1% (v/v) acetylated BSA (Aurion)
Reduced osmium staining for electron microscopy 2% (v/v) OsO_4, 1.5% (v/v) potassium ferrocyanide in ddH_2O
Walton's Lead Aspartate 0.02 M lead nitrate, 0.03 M aspartic acid, pH 5.5
Cell lysis buffer RIPA buffer, 2 mM EDTA, Protease Inhibitor Cocktail (1.04 mM AEBSF, 800 nM Aprotinin, 40 µM Bestatin, 14 µM E-64, 20 µM Leupeptin and 15 µM Pepstatin A)
Sodium dodecyl sulphate (SDS) loading buffer (4X) 250 mM Tris-HCl (pH 6.8), 8% (w/v) SDS, 0.2% (w/v) bromophenol blue, 40% (v/v) glycerol, 20% (v/v) β-mercaptoethanol
Transfer buffer for Western blot 25 mM Tris-HCl (pH 8.3), 192 mM glycine, 20% (v/v) methanol
Blocking buffer for Western blot PBS-T, 5% (w/v) BSA

2.2 Animals

Animals were housed in the Biomedical Services Unit (BSU) at the University of Liverpool, which is a Specific-Pathogen-Free (SPF) unit. Animals had *ad libitum* access to food and water. Male CD1 mice, aged 5-8 weeks, were obtained from Charles River. *B6.Tg-(CAG-Map1lc3bEGFP)53* mice (hereafter referred to as GFP-LC3) were obtained from Riken (RBRC00806) and bred in the BSU. *Tg(Cela1-cre/ERT)1Lgdn* mice (hereafter referred to as *CelaCreERT*) were obtained from Jackson Laboratory (025736). *B6.129S-Atg5tmMyok* mice (hereafter referred to as $Atg5^{flox/flox}$) were obtained from Riken (RBRC02975). These two strains were interbred by the BSU staff to generate compound mutant $Atg5^{flox/flox}$;$CelaCreERT^{+/-}$ mice, while $Atg5^{flox/flox}$;$CelaCreERT^{-/-}$ mice were used as control for these experiments (**Figure 2.1**). E230 mice were provided by Professor Ulrike Mayer and Professor Thomas Wileman (University of East Anglia, UK). Both female and male mice of the listed transgenic strains were used. Animals were sacrificed by the Schedule 1 method of cervical dislocation, in accordance with the Animal (Scientific Procedures) Act 1986 (ASPA) and with approval by the University of Liverpool Animal Welfare Committee and Ethical Review Body (AWERB).

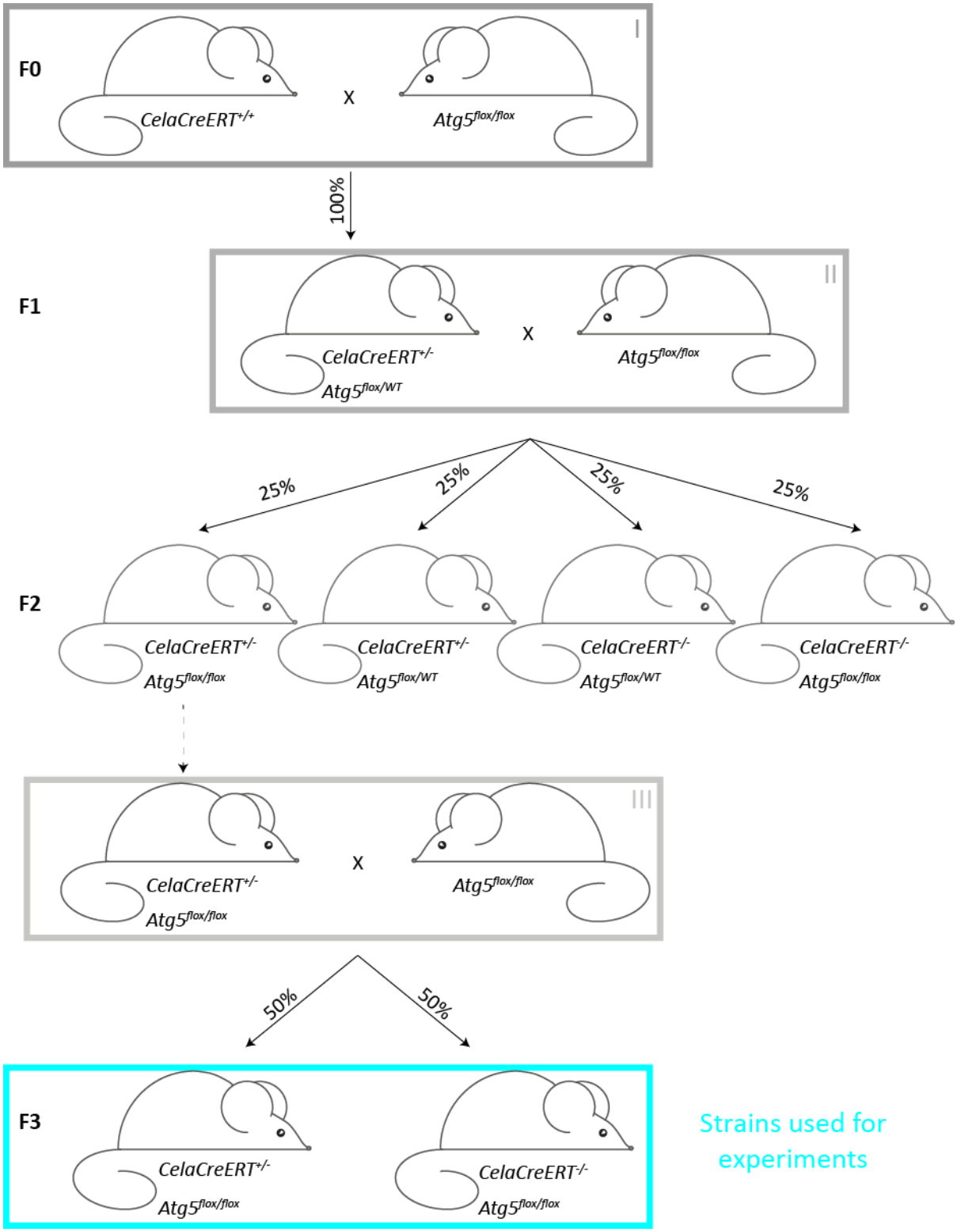

Figure 2.1 Breeding steps to generate compound mutant *Atg5$^{flox/flox}$;CelaCreERT$^{+/-}$* and *Atg5$^{flox/flox}$;CelaCreERT$^{-/-}$* mice.

2.2.1 Conditional inducible knock-out of *Atg5*

The Cre-Lox recombination technology is widely used for genetic manipulation. Briefly, it involves recognition of two 34 bp sequences, termed *loxP* sites, by the Cre enzyme, which recombines and splices out the sequence between the *loxP* sites (Sauer & Henderson, 1988). For KO purposes, the target gene is to be placed between two *loxP* sites. The so-called floxed gene will be excised by Cre recombinase. When the *Cre* gene is placed under a tissue-specific promoter, conditional KO of the target gene can be generated in a tissue of interest (Orban *et al.*, 1992). A further evolution of the technology involves ligand-dependent Cre enzymes, which have been modified to be inactive until bound to an activating ligand. This is the case of $CreER^T$, which is a fusion protein with mutated human estrogen receptor, sensitive to tamoxifen but not to endogenous estrogens (Feil *et al.*, 1996). This recombinase is only able to translocate to the nucleus and recombine floxed sequences when bound to 4-hydroxytamoxifen, the active metabolite of tamoxifen. Therefore, KO of the target gene can be induced at a desired time by administration of tamoxifen (**Figure 2.2** A). In this study, inducible KO of *Atg5* was carried out in $Atg5^{flox/flox}$;$CelaCreERT^{+/-}$ mice, while $Atg5^{flox/flox}$;$CelaCreERT^{-/-}$ mice were used as controls (**Figure 2.2** B,C). Because $CreER^T$ is located under the chymotrypsin-like elastase family, member 1 (*cela1*) promoter, it is expressed specifically in PACs. However, as explained above, $CreER^T$ only becomes active following tamoxifen administration. The protocol was optimised and performed by Doctor Michael Chvanov and consisted of 7 daily doses of a mixture of tamoxifen and hydroxytamoxifen (1 mg / 10 g body weight) by oral gavage.

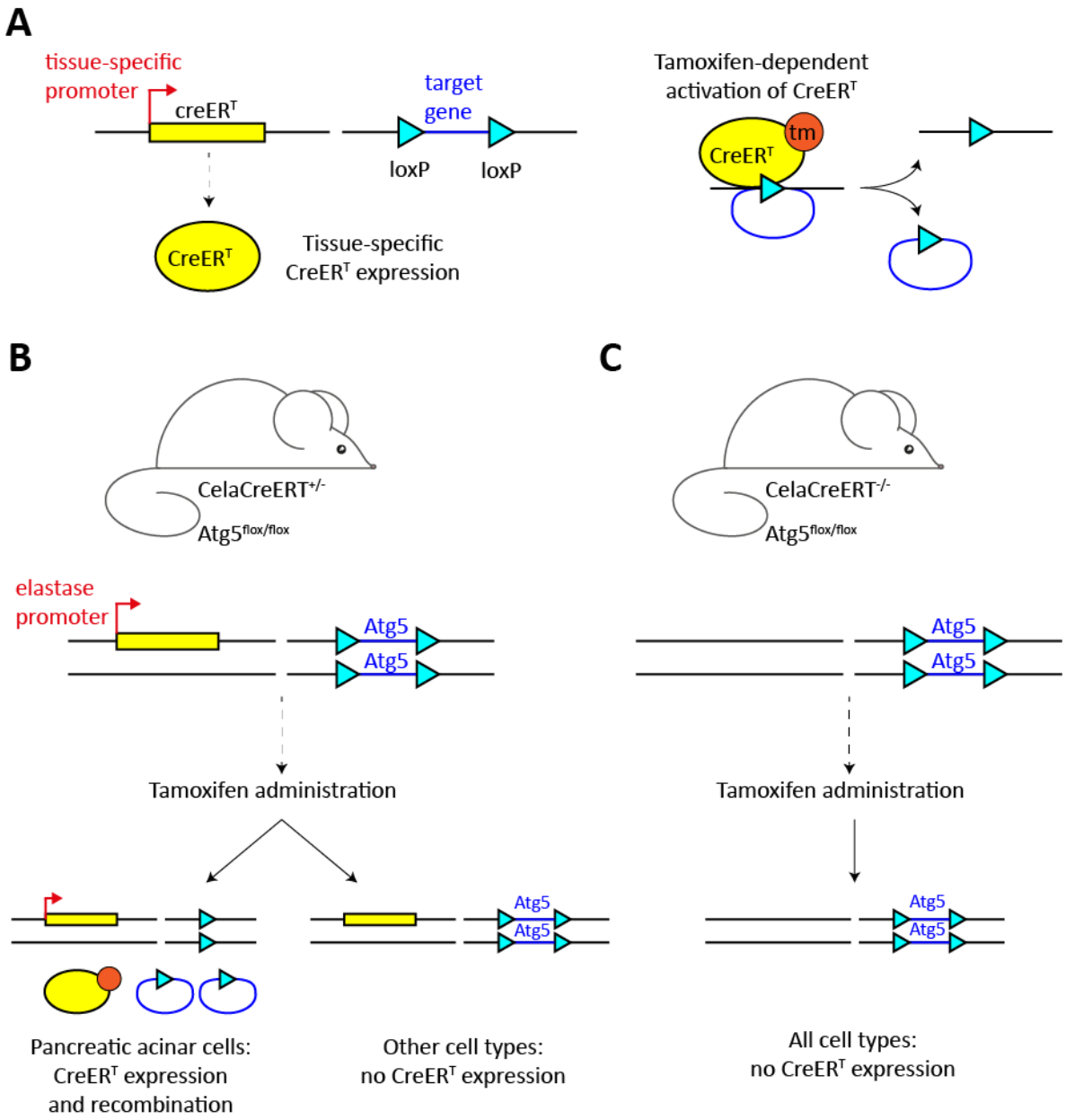

Figure 2.2 Mechanism of CreER^T-mediated recombination. A) CreER^T expressed under a tissue-specific promoter is activated by tamoxifen. **B)** In *Atg5$^{flox/flox}$;CelaCreERT$^{+/-}$* mice, CreER^T is expressed in PACs under the elastase promoter, and following tamoxifen administration, it recombines floxed *Atg5* in PACs. **C)** In *Atg5$^{flox/flox}$;CelaCreERT$^{-/-}$* mice, CreER^T is not expressed, therefore tamoxifen administration does not trigger *Atg5* recombination.

2.3 Primary pancreatic acinar cell isolation

Pancreata were excised from sacrificed animals by dissection and rinsed thoroughly in warm extracellular solution (Section 2.1.2) before injection with warm collagenase (0.14-0.16 mg/mL final concentration). The isolated tissue was then incubated at 36.5°C in a shaking water bath to facilitate digestion of the connective tissue. Incubation times varied from 18 to 25 minutes, to optimise the protocol for different batches of collagenase, and varying pancreas size (smaller in the transgenic mice utilised in this study, having C57BL/6J background). Collagenase activity was quenched by transferring the pancreatic tissue to a tube with extracellular solution. After discarding the excess solution, 2-3 mL of extracellular solution were added to the tube, which was shaken to release the cells. The solution containing released cells was transferred to a second tube. This process was repeated four times to ensure maximum recovery of cells. Released cells were centrifuged for 2 minutes at 500 rpm at room temperature (RT). The supernatant containing dead cells and debris was discarded, and the pellet was resuspended in 3-4 mL of extracellular solution. After pipetting to break down big clusters, the cell suspension was filtered through a 100 µm nylon mesh cell strainer (Thermo Fisher Scientific). The strained suspension was further centrifuged (2 minutes at 500 rpm at RT) and washed with extracellular solution for two more times. Isolated cells were kept in extracellular solution and, after approximately 30 minutes to allow for recovery from isolation, were used for up to 6 hours, unless cultured overnight (Section 2.5). For all experiments, cells were seeded on poly-L-Lysine (PLL) coated glass-bottom 35 mm dishes, with gridded coverslip for correlative experiments (MatTek Corporation). Dishes had previously been coated with PLL to facilitate the adhesion of the cells.

2.4 Labelling endocytic vacuoles

Secretion was stimulated with cholecystokinin fragment 26-33 (CCK-8, hereafter referred to as CCK) at 34.5°C, at concentrations indicated in the Results Chapters. In order to label EVs, cell impermeant fluorescent indicators were added to the extracellular solution at the time of stimulation of exocytosis. Because they are cell impermeant, these compounds will only enter the cell via endocytosis, which occurs as a mechanism of compensatory membrane retrieval, and will therefore be retained in endocytic organelles. Lucifer Yellow Lithium Salt (LY, Thermo Fisher Scientific) and disulfo-Cy5 carboxylic acid (Cy5, Cyandye LLC) have similar molecular weight (MW) of approximately 0.5 kDa. LY was added at a final concentration of 1 mM, Cy5 was added at a final concentration of 0.5 mM. Dextrans are polysaccharides of glucose (termed glucans) with cell impermeable property. Thermo Fisher Scientific offer a wide range of dextrans of different MW, conjugated to different fluorescent indicators. The number of dye moieties per dextran molecule is 0.5 to 1 in the 3 kDa range, 1 to 2 in the 10 kDa range. Table 2.3 summarises the dextran conjugates utilised in the study, specifying the final concentration of dextran and the estimated concentration of dye. The choice of different indicators was made in order to allow their use in combination with other fluorescent probes and/or with GFP-LC3, based on their excitation (Ex) and emission (Em) spectra.

2.4.1 pH measurements in endocytic vacuoles

For pH measurements in EVs, a combination of a pH sensitive and a pH insensitive dextran was used. Fluorescein isothiocyanate (FITC) decreases its fluorescence upon acidification. pHrodo™ Red increases its fluorescence upon acidification. Texas Red

and Alexa Fluor™ 647 are considered stable at different pH. CD1 PACs were stimulated with CCK at 34.5°C in presence of FITC and Texas Red dextran (Table 2.3). SiR-Actin stained (Section 2.6) CD1 PACs were stimulated with CCK at 34.5°C in presence of FITC and Texas Red dextran (Table 2.3). GFP-LC3 PACs were stimulated with CCK at 34.5°C in presence of pHrodo™ Red and Alexa Fluor™ 647 dextran (Table 2.3). At the end of each experiment, the extracellular solution was perfused with 10 µM nigericin solutions which had been adjusted at pH 7.1 and 5.5 with KOH. The same EVs were imaged at both pH 7.1 and 5.5 to obtain calibration values (Section 2.13).

Table 2.3 Fluorescently-labelled dextrans (Thermo Fisher Scientific)

Dextran conjugate	**MW (kDa)**	**Ex/Em (nm)**	**Final concentration of dextran**	**Estimated minimum concentration of indicator**
Dextran, Texas Red™, Neutral (D3329)	3	595/615	333 µM	167 µM
Dextran, Texas Red™, Lysine Fixable (D3328)	3	595/615	333 µM	167 µM
Dextran, Alexa Fluor™ 647, Anionic, Fixable (D22914)	10	650/668	50 µM	50 µM
Dextran, Lucifer Yellow, Anionic, Lysine Fixable (D1825)	10	425/528	250 µM	250 µM
Dextran, Fluorescein, Anionic (D1821)	10	494/521	250 µM	250 µM
Dextran, Fluorescein, Anionic, Lysine Fixable (D1820)	10	494/521	250 µM	250 µM
pHrodo™ Red Dextran (P10361)	10	560/585	250 µM	250 µM

2.5 Adenoviral transfection

Under sterile conditions, cells were seeded on PLL-coated glass-bottom 35 mm dishes, and transferred into sterile-filtered culture medium (Section 2.1.2). Adenoviral vectors were added at indicated concentrations (Table 2.4) and incubated at 35°C for 12-16 hours. After this time, the adenoviral vectors and culture medium were washed off and cells were bathed in extracellular solution (Section 2.1.2) to perform experiments.

Table 2.4 Adenoviral vectors

Vector	Supplier	Ex/Em (of expressed protein)	Final concentration
LifeAct-tagRFP	Ibidi	555/584	1 x 10^7 PFU/ml
LC3A-mCherry	Vector Biolabs	587/610	4 x 10^7 PFU/ml
LC3A-eYFP	Vector Biolabs	513/527	4 x 10^7 PFU/ml

2.6 Staining the actin cytoskeleton

To label actin filaments, PACs were incubated for 1 hour at 34.5°C in the presence of 1 µM SiR-Actin and 10 µM verapamil (Spirochrome). Cells were then washed with extracellular solution and utilised for experiments. SiR-Actin is a jasplakinolide analogue that binds actin filaments. The use of verapamil is advised by the supplier to enhance staining efficiency by inhibiting efflux pumps. Being aware that verapamil is also a calcium-channel inhibitor, we verified that this concentration did not cause side effects in our experiments.

2.7 Disruption of the autophagic pathway

GFP-LC3 PACs or E230 PACs transfected with *LC3A-mCherry* or *LC3A-eYFP* adenoviral vectors were utilised to investigate the interaction of autophagic proteins with EVs. Table 2.5 summarises the autophagy inhibitors applied for indicated pre-incubation times at indicated concentrations and compared to appropriate vehicle control (specified in the Results Chapter). The conditions (concentration and pre-incubation) were based on the literature for established inhibitors, or optimised for PACs with preliminary experiments.

Table 2.5 Drugs to disrupt the autophagic pathway

Drug	Supplier	Concentration	Pre-incubation
Bafilomycin A1	Bio-Techne	100 nM	30 min
Concanamycin A	Bio-Techne	100 nM	30 min
Monensin	Bio-Techne	10 µM	60 min
Chloroquine	Sigma-Aldrich	1 mM	60 min
Nigericin	Sigma-Aldrich	1 µM	30 min
MRT67307	Bio-Techne	10 µM	60 min
MRT68921	Stratech	1 µM	60 min
SAR405	Cayman Chemical	1 µM	30 min
LY294002	Bio-Techne	20 µM	30 min
Wortmannin	Bio-Techne	20 µM	30 min
YM201636	Stratech	100 nM	30 min

2.8 Disruption of the actin cytoskeleton

SiR-Actin-stained PACs or *LifeAct-tagRFP* transfected PACs were utilised to study the interaction of actin filaments and EVs. Table 2.6 summarises the actin disruptors applied for indicated pre-incubation times at indicated concentrations and compared to appropriate vehicle control (specified in the Results Chapter). The conditions (concentration and pre-incubation) were based on the literature for established inhibitors, or optimised for PACs with preliminary experiments.

Table 2.6 Drugs to disrupt the actin cytoskeleton

Drug	Supplier	Concentration	Pre-incubation
Latrunculin A	Abcam	10 µM	30 min
Latrunculin B	Abcam	10 µM	30 min
Jasplakinolide	Bio-Techne	1 µM	30 min
CK-666	Merck	500 µM	60 min
CK-869	Bio-Techne	250 µM	60 min
SMIFH2	Merck	50 µM	60 min
Rhosin	Merck	30 µM	60 min
Y27632	Bio-Techne	50 µM	60 min
GSK429286	Bio-Techne	10 µM	60 min
(-)Blebbistatin	Bio-Techne	50 µM	60 min
Aza1	Bio-Techne	60 µM	60 min
ML141	Bio-Techne	10 µM	30 min
Rac1 Inhibitor II	Merck	100 µM	30 min

2.9 Immunofluorescence

PACs were fixed in 4% paraformaldehyde (PFA, Agar Scientific) for 10-15 minutes at RT or 1.8% PFA for 48 hours at 4°C. Cells were then washed three times for 3 minutes in PBS and permeabilised in 0.2% Triton-X 100 for 5 minutes at RT. After two 3 minute washes in PBS, blocking solution (Section 2.1.2) was added for 1 hour at RT. Cells were then incubated in primary antibody dissolved in primary antibody solution (Section 2.1.2) at indicated concentrations (Table 2.7) for 1 hour at RT. After further three 3 minute PBS washing steps, secondary antibody (indicated dilutions in Table 2.8) was added for 30 minutes at RT. After three washes in PBS for 3 minutes, samples were stored at 4°C in 0.02% sodium azide.

Table 2.7 Primary antibodies used in immunofluorescence

Antigen (host)	Supplier (catalogue number)	Dilution
ATP6V0A1 (rabbit)	Abcam (ab176858)	1:100
LAMP1 (mouse)	Cayman Chemical (10011443)	1:400
P34-ARC/ARPC2 (rabbit)	Merck (07-227)	1:200
WASH1 (rabbit)	Atlas Antibodies (HPA002689)	1:100
N-WASP (rabbit)	Abcam (ab126626)	1:200
FMNL2 (rabbit)	Sigma-Aldrich (SAB2100828)	1:100
mDia1 (mouse)	BD (610848)	1:100
ATG5 (rabbit)	Abcam (ab108327)	1:100
ATG16L1 (rabbit)	MBL International Corporation (PM040)	1:100

Table 2.8 Secondary antibodies used in immunofluorescence

Antigen (host)	Supplier (catalogue number)	Dilution
Mouse IgG (H+L)–Alexa Fluor™ 647 (goat)	Thermo Fisher Scientific (A-21235)	1:500
Rabbit IgG (H+L)–Alexa Fluor™ 647 (goat)	Thermo Fisher Scientific (A-21244)	1:500

2.10 Confocal microscopy

Confocal microscopy was performed on the following setups: TCS SL and SP2 AOBS (Leica Microsystems), LSM 510 and LSM 710 (Zeiss). The following objectives were used: 63X 1.4 numerical aperture (NA) oil-immersion (Leica TCS SL, Leica SP2 AOBS, Zeiss LSM 710) and 63X 1.4 NA water-immersion (Zeiss LSM 510). Live cell imaging experiments on Leica TCS SL and Zeiss LSM 710 were performed at 34.5°C, as these systems are equipped with temperature control units. Z-stack images were acquired with a 1 µm distance between slices. The pinhole was 1.8 airy units. Table 2.9 summarises the laser lines used for excitation and the detection ranges used for emission for the fluorescent indicators/proteins used in this study. When fluorophores had partially overlapping spectra, images were acquired sequentially. Laser power, detector gain and other settings (zoom, averaging) were maintained constant throughout experiments of the same type.

Table 2.9 Settings for excitation of fluorescence and detection of emission

Fluorescent indicator/protein	**Laser line for Ex (nm)**	**Detection range for Em (nm)**
LY	458	500-565
GFP	488	500-530
FITC	488	500-560
eYFP	488	500-560
pHrodo™ Red	514	550-600
RFP	543	550-600
Texas Red	543	560-630
mCherry	543	550-600
Cy5	633	650-750
Alexa Fluor™ 647	633	650-750
SiR-Actin	633	650-750

2.11 Correlative Light and Electron Microscopy

GFP-LC3 PACs were seeded on PLL-coated gridded dishes and stimulated with 500 pM CCK in presence of Texas Red dextran at 34.5°C. After washing CCK and dextran with extracellular solution, cells were imaged on Leica TCS SL at 34.5°C. Z-stack images were acquired as described (see Section 2.10). The position of cell clusters on the grid was manually annotated. The samples were then processed for transmission electron microscopy (TEM).

2.11.1 Transmission electron microscopy

Samples were washed two times in 0.1 M PBS pH 7.4. Fixation of aldehyde groups in 2.5% glutaraldehyde was performed with 60 seconds on - 60 seconds off - 60 seconds on vacuum cycles in a Pelco BioWave® Pro (Ted Pella Inc.). Samples were then washed in 0.1 M PBS three times for 5 minutes. The same BioWave® protocol, consisting of 20 seconds on - 20 seconds off -20 seconds on - 20 seconds off vacuum cycles, was adopted for all the following staining steps. All the staining solutions were used immediately after preparation and filtered directly onto the Petri dish with 0.22 µm filters to avoid precipitates. The reduced osmium staining (Section 2.1.2), facilitating fixation of lipids, was followed by five 3 minute washes in ddH_2O. Samples were forward processed to mordant staining (1% (w/v) thiocarbohydrazide (TCH)), followed by five 3 minute washes in ddH_2O. At this point, a second osmium staining (2% (v/v) OsO_4 in ddH_2O) was performed, followed by three 5 minute washes in ddH_2O. Utilising a standard double contrast method, samples were stained with 1% (v/v) uranyl acetate, followed by three 5 minute washes in ddH_2O, and with Walton's Lead Aspartate (Section 2.1.2), also followed by three 5 minute washes in ddH_2O. The

samples were then dehydrated in ethanol gradient (30, 50, 70, 90% (v/v)) for 5 minutes each and two times for 3 minutes in 100% ethanol, on ice. Samples were then infiltrated in hard resin (TAAB): 1:1 resin:EtOH for 30 minutes and 100% resin two times for 30 minutes. Samples were embedded in 2.5 mL of resin at 60°C for 16 hours. For TEM, 70-74 nm serial sections were cut on a microtome (Leica Microsystems) and transferred onto Butvar (0.25% (v/v) in chloroform, TAAB) plastic-covered Gilder 200 hexagonal copper grids (GG017/C, TAAB). Images were acquired on a 120 kV Tecnai G2 Spirit BioTWIN (FEI). Images were then compared to the z-stacks confocal images for correlation (**Figure 2.3**).

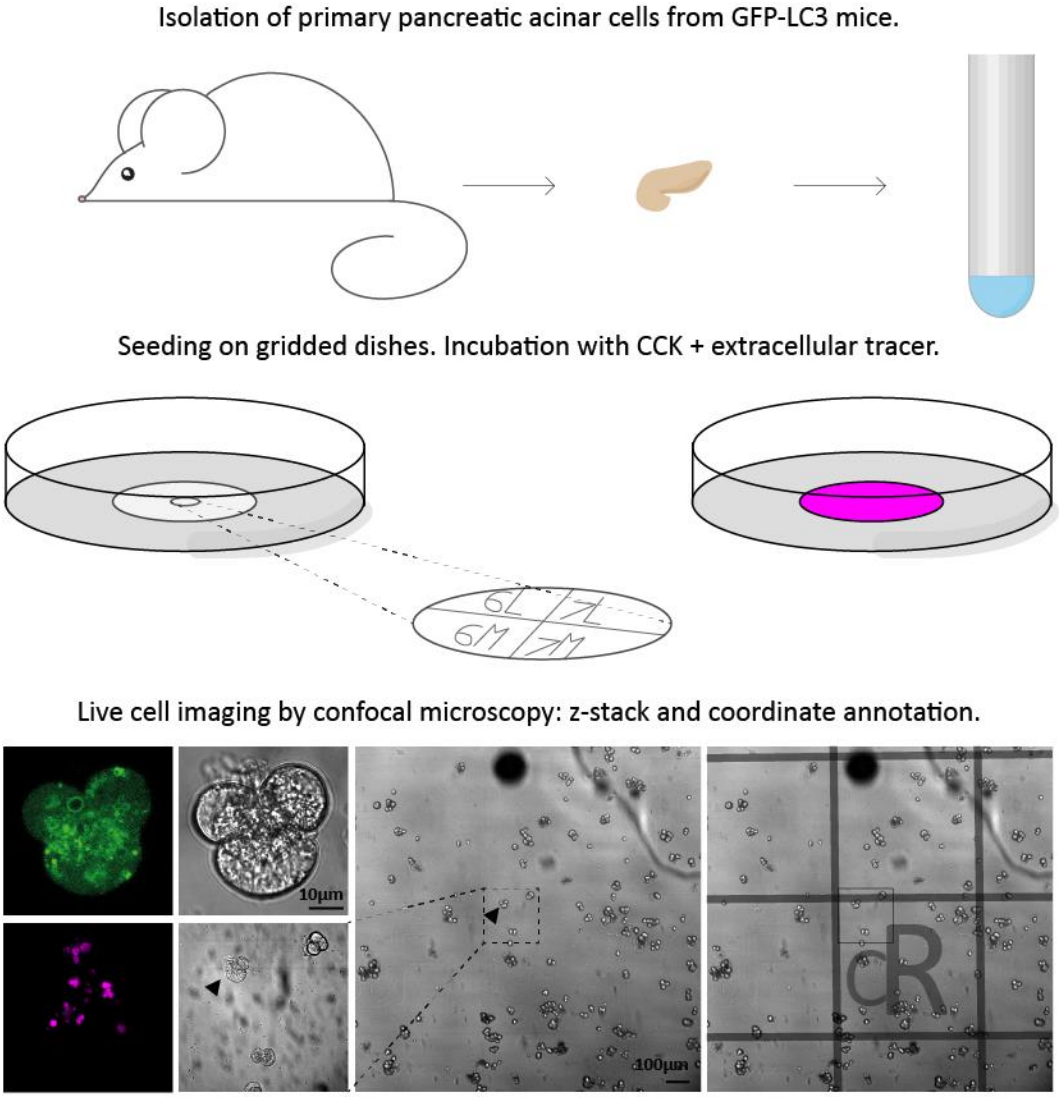

Figure 2.3 Correlative light and electron microscopy workflow.

2.12 Western blotting

Pancreata were homogenised and lysed in lysis buffer (Section 2.1.2) for 30 min at 4°C, then centrifuged for 10 min at 13000 g at 4°C. The supernatants were collected and stored at -80°C. Protein concentration was determined by Pierce bicinchoninic acid (BCA) protein assay (Thermo Fisher Scientific), using BSA standards of known concentration to obtain a calibration curve. 100 µg of protein per lane were separated by SDS-PAGE in 4-12% Bis-Tris gradient gels (Thermo Fisher Scientific), with SeeBlue™ Plus2 Pre-stained Protein Standard (Thermo Fisher Scientific), in MOPS running buffer (Thermo Fisher Scientific) at 160 V for approximately 70 minutes. Proteins were transferred to 0.45 µm nitrocellulose membrane (Thermo Fisher Scientific) in transfer buffer (Section 2.1.2) at 100 V for 1 hour. Membranes were blocked in blocking solution (Section 2.1.2) for 1 hour at RT with agitation, and then incubated with primary antibody diluted at indicated concentration (Table 2.10) in blocking solution overnight at 4°C with agitation. The membrane was then washed with PBST for 5 minutes and two times with PBS for 5 minutes at RT. It was then incubated with secondary antibody diluted at indicated concentrations (Table 2.11) in blocking solution for 1 hour at RT with agitation. The same washing steps were then repeated. At this point, equal volumes of enhanced chemiluminescence (ECL) A and ECL B solutions (Thermo Fisher Scientific) were added to cover the membrane and incubated for 2-3 minutes. Chemiluminescent signals were detected on a ChemiDoc XRS+ imaging system (Bio-Rad Laboratories).

Table 2.10 Primary antibodies used in western blot analysis

Antigen (host)	Supplier (catalog number)	Dilution
ATG5 (rabbit)	Bio-Techne (NB110-53818)	1:500
Calnexin (rabbit)	Abcam (ab22595)	1:1000

Table 2.11 Secondary antibody used in western blot analysis

Antigen (host)	Supplier (catalog number)	Dilution
Rabbit IgG (whole molecule) Peroxidase antibody (goat)	Sigma-Aldrich (A6154)	1:1000

2.13 Image processing and data analysis

Images were processed on the following software packages: Leica AF Lite, LSM Image Browser, Zen Lite, and ImageJ. For presentation purposes, linear adjustments of brightness and contrast were performed in ImageJ. Full size images with appropriate scale bars are shown, cropped fragments are clearly stated. Quantitative analysis was carried out on raw, unprocessed images. EVs (Section 2.4) were manually counted. Densitometry analysis of unsaturated Western blot images (Section 2.12) was carried out in ImageJ. Ratiometric pH measurement analysis (Section 2.4.1) was carried out in Leica AF Lite software. Regions of interest were drawn around each EV. Here, the ratio of the maximum fluorescence intensity of pH sensitive dextran (FITC or pHrodo Red) by pH insensitive dextran (Texas Red or Alexa Fluor™ 647) was calculated. The values obtained for EVs imaged at pH 7.1 and pH 5.5 were used to generate a calibration curve. The pH in EVs was calculated interpolating the dextran fluorescence intensity ratios to the calibration curve. As advised by Doctor David Mason, a macro was created for ImageJ to allow for semi-automated processing of GFP-LC3 fluorescence hotspots. The cytoplasm area was calculated by the pixels highlighted by a mask obtained by Huang method of thresholding (Huang & Wang, 1995). The area occupied by GFP-LC3 fluorescence hotspots was determined by the pixels highlighted by a mask obtained by Maximum Entropy thresholding, followed by a particle restriction limit of 10-Infinity pixels. The percentage of the area occupied by hotspots divided by the cytoplasm area was calculated (**Figure 2.4**).

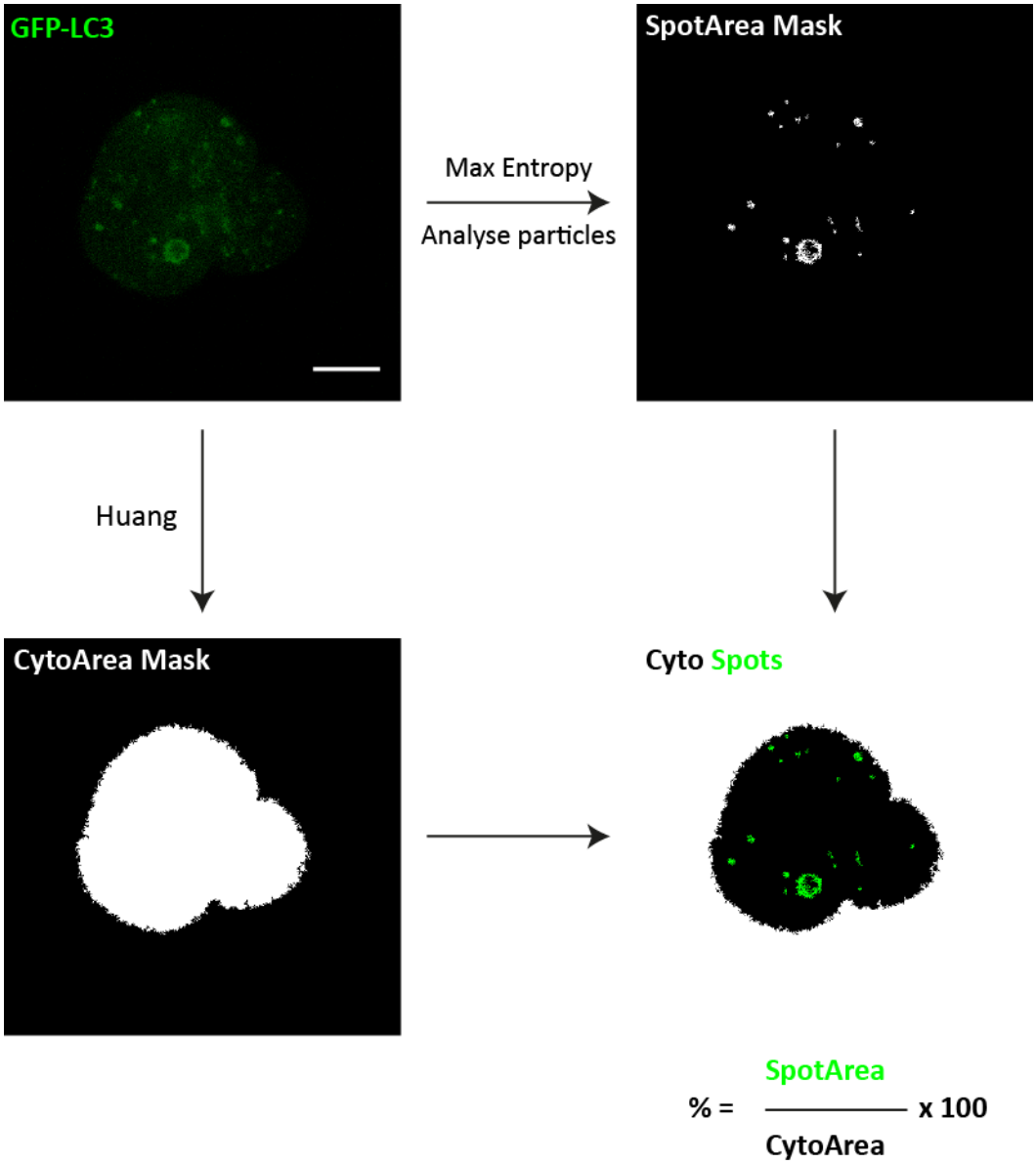

Figure 2.4 Semi-automated analysis of GFP-LC3 hotspots. The raw image (top left panel) is processed with the Huang method of thresholding to obtain a footprint of the cells (CytoArea Mask, bottom left panel). The raw image is also processed with the Maximum Entropy method of thresholding to highlight GFP-LC3 fluorescence hotspots (SpotArea Mask, top right panel). The percentage of the area occupied by the SpotArea to the CytoArea indicates the percentage of the cytoplasm occupied by GFP-LC3 fluorescence hotspots.

Experiments were repeated in N biological replicates (i.e. mice), each including n cells; N and n values are indicated throughout the Results Chapters. Since we were interested in intracellular events, individual cells (n) rather than animals (N) were considered the subject of statistics. Statistical analysis and graph generation were performed in R (http://www.r-project.org/). Firstly, data were tested for normality with Shapiro-Wilk test. Normal data are presented as bar graphs, where error bars represent standard error of the mean (SEM). Unpaired or paired t tests were used to compare two groups of independent or dependent observations, respectively. One-way analysis of variance (ANOVA) test was used to compare multiple groups of independent observations. When ANOVA was significant, *post-hoc* analysis was carried out to determine which groups differed. Depending on the assumptions of the experiment, Dunnett's test was used to compare individual groups to control, whilst Tukey's test was used for pairwise multiple comparisons. Data not following normal distribution are presented as box and whisker plots. The ends of the box represent first and third quartiles, the thick line represents the median. The top whisker represents the highest value equal or below the third quartile plus 1.5 times the inter-quartile range (IQR). Likewise, the bottom whisker represents the lowest value equal or above the first quartile minus 1.5 times the IQR. When data distribution was extremely skewed, meaning that whiskers, quartiles and median would fall on the same value, data are presented as dot plots. This format allows clear visualisation of the raw data and I feel that it represents the best way to present my data. Non parametric statistics were used for non-normal data. The Wilcoxon-Mann-Whitney test was used to compare two groups of independent observations. The Kruskal-Wallis rank sum test was used to compare multiple groups of

independent observations. Data was forward processed to a Dunn test for *post-hoc* analysis, to compare individual groups to control, with p-values adjusted with the Bonferroni method.

3 Investigating autophagy of endocytic vacuoles

3.1 Introduction

This chapter will address the interaction between EVs and autophagy in PACs. EVs are induced by AP stimuli and represent the acidified compartment where premature trypsinogen activation occurs (Sherwood *et al.*, 2007). AP stimuli also trigger upregulation of autophagy, and formation of autophagic vacuoles (AVs) is a hallmark of both *ex vivo* and *in vivo* models of AP (Hashimoto *et al.*, 2008; Mareninova *et al.*, 2009). In electron microscopy (EM) sections, PACs presented two types of AVs: initial (referred to as AVi), containing sequestered material, and late degradative (referred to as AVd), containing partially degraded cargo (Mareninova *et al.*, 2009). Some of these vacuoles contained ZGs. The authors reported co-localisation of LC3 with amylase in a ZG-enriched subcellular fraction. This result further supported the evidence that AVs can engulf ZGs. It was suggested that the presence of ZGs in AVs is the consequence of a selective autophagic pathway, referred to as zymophagy, acting as a protective mechanism of clearance of ZGs containing active digestive enzymes (Vaccaro, 2012). Since EVs originate following compound exocytosis of ZGs, it is possible that they are also targeted by selective autophagy. Interaction of endocytic and autophagic pathways in the exocrine pancreas has been previously reported (Tooze *et al.*, 1990). This study focused on intracisternal granules (ICGs) that form in guinea pig PACs. ICGs represent aggregates of digestive enzymes and proenzymes, developing in the RER lumen, and they are processed by autophagy. The study reports three classes of autophagic organelles, which they refer to as phagophores, Type I AVs and Type II AVs, based on EM analysis and histochemical markers. Type I and Type II AVs also contained endocytosed material (having incubated the pancreatic lobules with horseradish peroxidase (HRP)).

The endocytic and autophagic pathways converge in different processes and cell types, as schematised in Figure 3.1. Double-membrane autophagosomes and single-membrane endosomes can fuse forming single-membrane amphisomes (Gordon & Seglen, 1988), a phenomenon originally characterised in rat hepatocytes (Liou *et al.*, 1997; Berg *et al.*, 1998). Endocytosed tracer co-localised with AVs, which were classified into three categories: initial (AVi), intermediate (AVi/d) and degradative (AVd); the percentage of endocytosed tracer localised in AVd (rather than AVi) increased with time (Liou *et al.*, 1997). Both vesicular endosomes and multivesicular endosomes could fuse to AVs at all stages, with a preference for AVi and AVi/d. Autophagy machinery and endosomes are also associated with secretory pathways, playing an important role in the intestine, both in goblet cells (secreting mucus) and Paneth cells (secreting antimicrobial peptides and lysozyme) (Patel *et al.*, 2013; Bel *et al.*, 2017). Furthermore, autophagy can interact with phagocytosis (Brooks *et al.*, 2015): autophagosomes can engulf phagosomes, or alternatively LC3 is directly lipidated on nascent phagosomes, via a non-canonical autophagic process referred to as LC3-associated phagocytosis (LAP) (Sanjuan *et al.*, 2007). Non-canonical LC3 lipidation occurs on other endocytic compartments such as macropinosomes and entotic vacuoles (Florey *et al.*, 2011; Florey *et al.*, 2015) and it is also involved in antigen presentation (Ma *et al.*, 2012). In intestinal epithelial cells, mechanical stress induces formation of large vacuoles containing extracellular contents and these organelles are also processed by non-canonical autophagy (Kim *et al.*, 2017). Thus, endosomes, phagosomes, macropinosomes and entotic vacuoles can directly fuse with lysosomes, or converge to (canonical or non-canonical) autophagic pathways (Figure 3.1).

These pathways (described in Section 1.5) can be easily distinguished pharmacologically: the V-ATPase inhibitor bafilomycin A1 facilitates LC3-II accumulation in canonical autophagy, whilst it prevents LC3-II formation in non-canonical autophagy (Florey *et al.*, 2015; Jacquin *et al.*, 2017). Canonical autophagy is triggered by the ULK1-FIP200-ATG13-ATG101 complex, which activates the Vps34-Beclin1-Vps15-Ambra1 PI(3)K class III complex. Vps34 generates PI(3)P, recruiting WIPI2 and DFCP1 proteins which interact with the ATG5-ATG12-ATG16L1 lipidation machinery. Non-canonical autophagy is independent from ULK1, however it can be Vps34-dependent (Florey *et al.*, 2011; Martinez *et al.*, 2015) or Vps34-independent (Florey *et al.*, 2015; Jacquin *et al.*, 2017). Recently, a novel distinction between canonical and non-canonical autophagy has been identified: whereas both processes depend on the ATG5-ATG12-ATG16L1 complex for LC3 lipidation, it appears that the ATG16L1 domains involved in membrane recognition are different; the central FIP200 and WIPI2b binding domain is involved in canonical autophagy (Gammoh *et al.*, 2013; Dooley *et al.*, 2014), whilst the C-terminal WD40 domain is required for non-canonical autophagy (Fletcher *et al.*, 2018). Importantly, the two processes can also be distinguished structurally: while classical autophagosomes have a double membrane, non-canonical LC3-lipidated vacuoles have a single membrane (Florey *et al.*, 2011). Both classical autophagosomes and non-canonical LC3-positive vacuoles eventually fuse with lysosomes for degradation of their cargo.

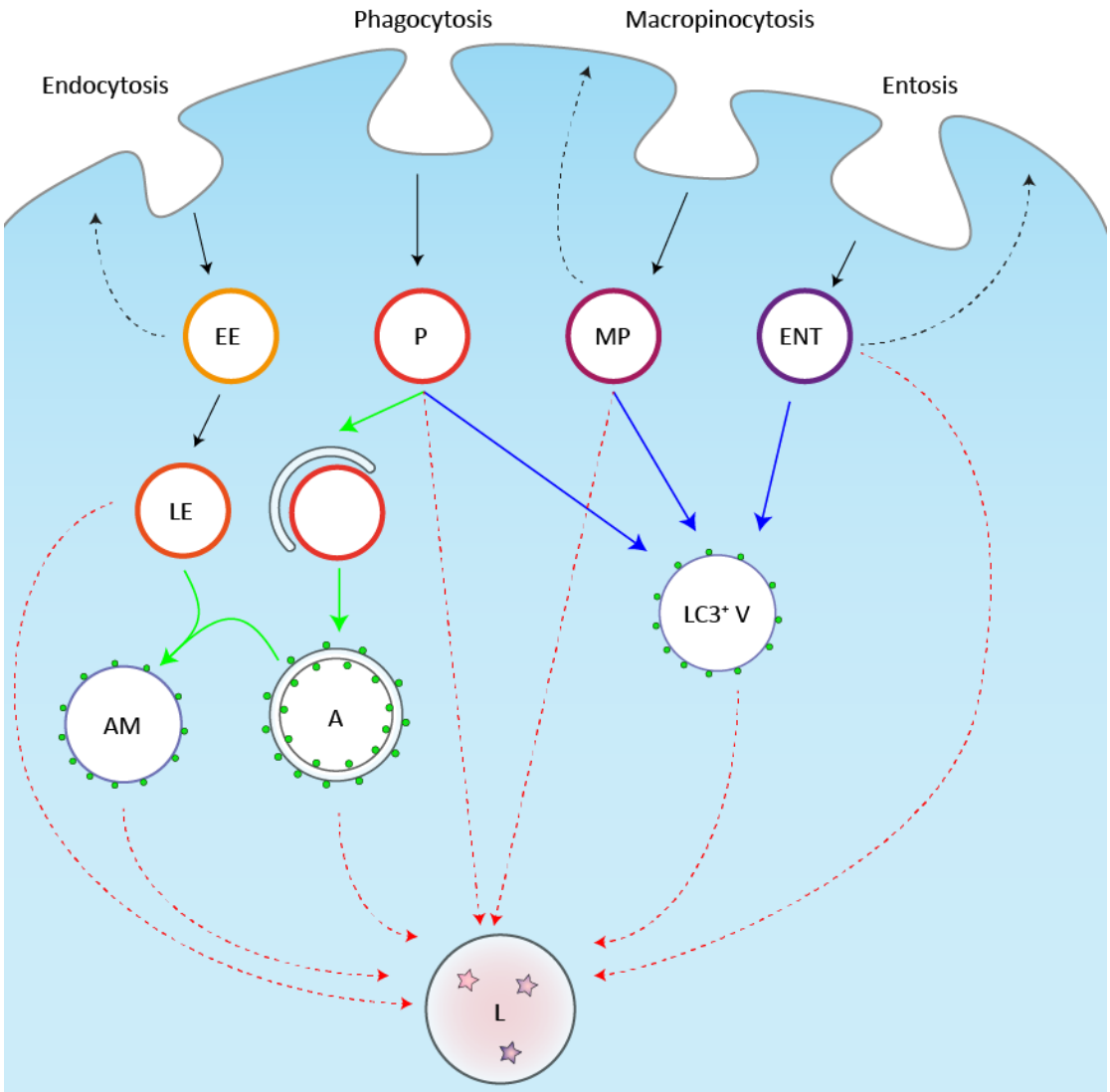

Figure 3.1 Interaction between endocytic and autophagic pathways. Black arrows indicate internalisation (endocytosis, phagocytosis, macropinocytosis, and entosis) pathways. Green arrows indicate canonical autophagy. Blue arrows indicate non-canonical autophagy. Early endosomes (EE), macropinosomes (MP) and entotic vacuoles (ENT) can be recycled to the plasma membrane (black dashed arrows). Late endosomes (LE), phagosomes (P), MP and ENT can directly fuse with lysosomes (red dashed arrows). LE can fuse to autophagosomes (A) forming amphisomes (AM). P can be engulfed by phagophores and enter the autophagic pathway through A. P, MP and ENT can be targeted by non-canonical LC3 lipidation and form single membrane vacuoles ($LC3^+$ V). A, AM and $LC3^+$ V fuse with lysosomes (red dashed arrows).

The EVs originated from post-exocytic structures in PACs can be up to 10 µm in size and have acidic luminal pH (Sherwood *et al.*, 2007). The same calcium-releasing agonists that trigger EV formation also trigger autophagy activation. This project therefore asked whether endocytic and autophagic vacuoles would interact in PACs exposed to inducers of AP. To address this question, I took advantage of GFP-LC3 mice to monitor autophagy (Mizushima *et al.*, 2004), and used cell impermeable fluorescent dextrans to label EVs. PACs were stimulated with the calcium-releasing agonists CCK and TLC-S and monitored by live cell imaging to investigate the interaction between the two populations of organelles. Protein complexes implicated in autophagic pathways were targeted pharmacologically to characterise whether the process occurring in PACs was canonical or non-canonical. Finally, immunofluorescence staining and EM analysis were performed to further characterise the membrane properties of these organelles.

3.2 Results

3.2.1 LC3-coating of endocytic vacuoles

The aim of this part of the study was to assess the potential role of the autophagic pathway in the clearance of the EVs in pathophysiological conditions of AP. In cellular *ex vivo* models of AP, PACs are exposed to supramaximal concentrations of secretagogues or bile acids, associated with aberrant calcium signalling. Therefore, this project primarily sought to determine whether calcium-releasing agonists (which are known to cause EV formation) would trigger activation of autophagy. GFP-LC3 PACs were incubated at RT or 35°C w/o calcium-releasing agonist, then fixed and imaged, to quantify the percentage of the cytosol occupied by GFP-LC3 fluorescence hotspots (as described in Section 2.13). It was found that temperature control induced an increase in the hotspots area compared to unstimulated cells kept at RT (Figure 3.2). Supramaximal (10 nM) CCK provoked a significant increase compared to 35°C control. A physiological (10 pM) CCK-induced increase in GFP-LC3 hotspot area was not significantly different from 35°C control. Likewise, a 200 µM TLC-S-induced increase in GFP-LC3 hotspot area was not significantly different from 35°C control.

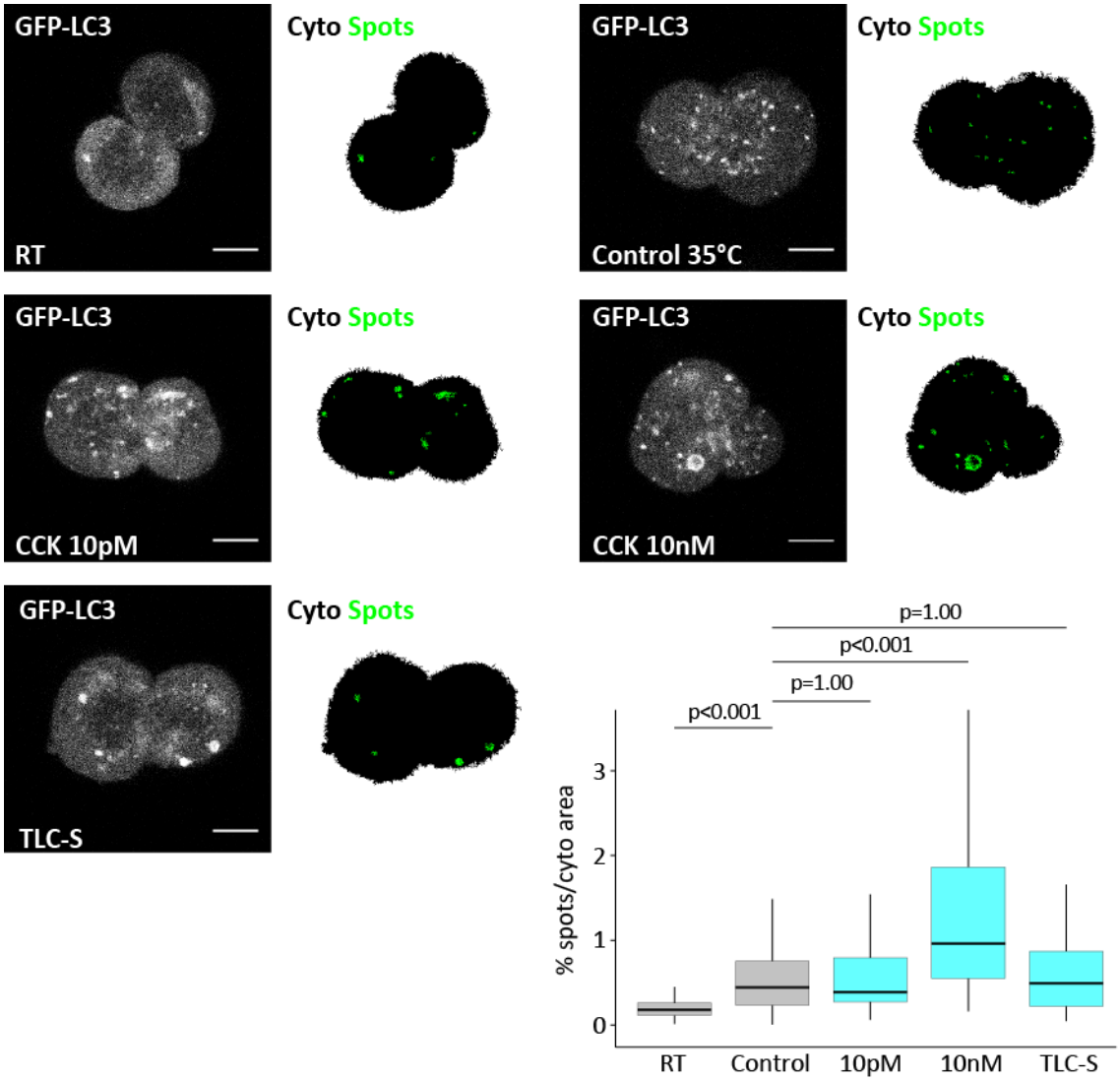

Figure 3.2 Increase in GFP-LC3 hotspots by CCK and TLC-S. GFP-LC3 PACs were incubated at RT (n=53) or 35°C (Control, n=66), with 10 pM CCK (n=84), 10 nM CCK (n=80) or 200 µM TLC-S (n=73); N=4 for each condition. Representative images of GFP-LC3 fluorescence (grey) and masks obtained as described in Section 2.13 (CytoArea=black, SpotsArea=green). The area of the cytoplasm occupied by GFP-LC3 hotspots was calculated as described in **Figure 2.4** and is shown in the box and whisker plot. Data were compared by Kruskal-Wallis rank sum test and individual P values adjusted for multiple comparisons against "Control" group are reported.

This study next sought to determine whether autophagic (i.e. LC3-positive) organelles interacted with dextran-labelled EVs (as described in Section 2.4). In GFP-LC3 PACs stimulated with CCK (Figure 3.3) or TLC-S (Figure 3.4), it was observed that some EVs were coated by GFP-LC3, whereas others were not. To further characterise this phenomenon, the total number of EVs and the percentage of LC3-coated EVs in stimulated cells were quantified (Figure 3.5). Supra-physiological (i.e. > 10 pM) CCK concentrations caused a strong increase in the total number of EVs per cell. In 10 pM CCK, 11.4% of 728 analysed EVs were coated by LC3. In 100 pM CCK, 7.6% of 1381 analysed EVs were coated by LC3. In 500 pM CCK, 8.9% of 1330 analysed EVs were coated by LC3. In 10 nM CCK, 6.1% of 1205 analysed EVs were coated by LC3. In 200 µM TLC-S, 2.2% of 1646 analysed EVs were coated by LC3.

The dynamics of LC3 association with EVs was explored by performing time-lapse imaging of GFP-LC3 PACs stimulated with CCK in the presence of the extracellular tracer TRD (Figure 3.6). To avoid photobleaching of fluorophores and undue cellular stress induced by continuous scanning, z-stack images were acquired every 5 minutes. LC3 lipidation was observed to occur on previously-formed (i.e. dextran-positive) EVs. On average, LC3-coating was detectable 15.0 ± 4.1 minutes or 16.9 ± 7.0 minutes after the appearance of an EV, in 100 pM or 500 pM CCK stimulated cells respectively.

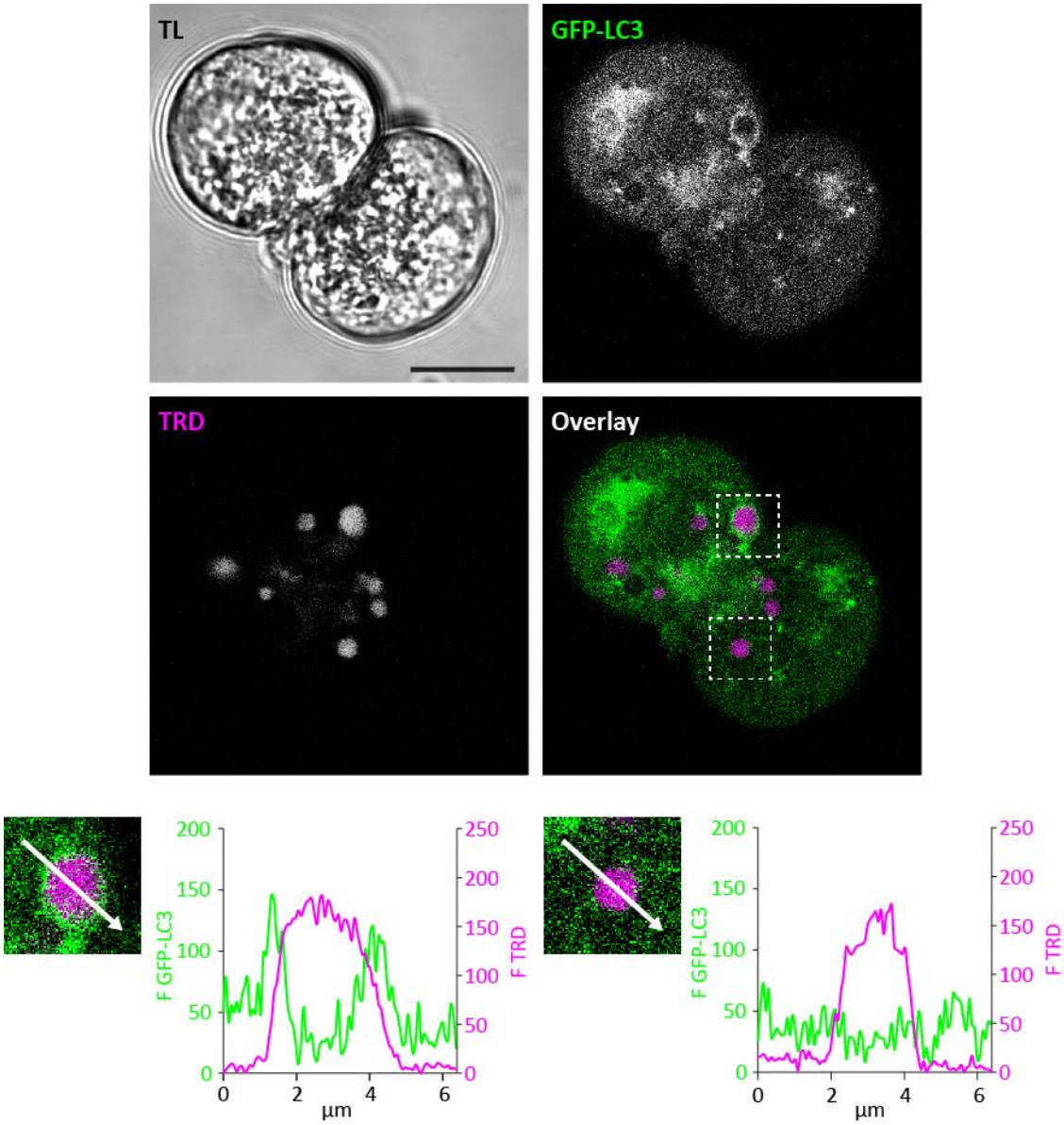

Figure 3.3 LC3-coated and uncoated endocytic vacuoles in CCK-stimulated pancreatic acinar cells. Representative images of GFP-LC3 (green) PACs stimulated with 500 pM CCK for 30 min at 34.5°C in presence of TRD (magenta). Lower panels show selected LC3-coated (left) and uncoated (right) EVs in an expanded scale and fluorescence intensity profiles plotted along the arrows. Scale bar = 10 µm.

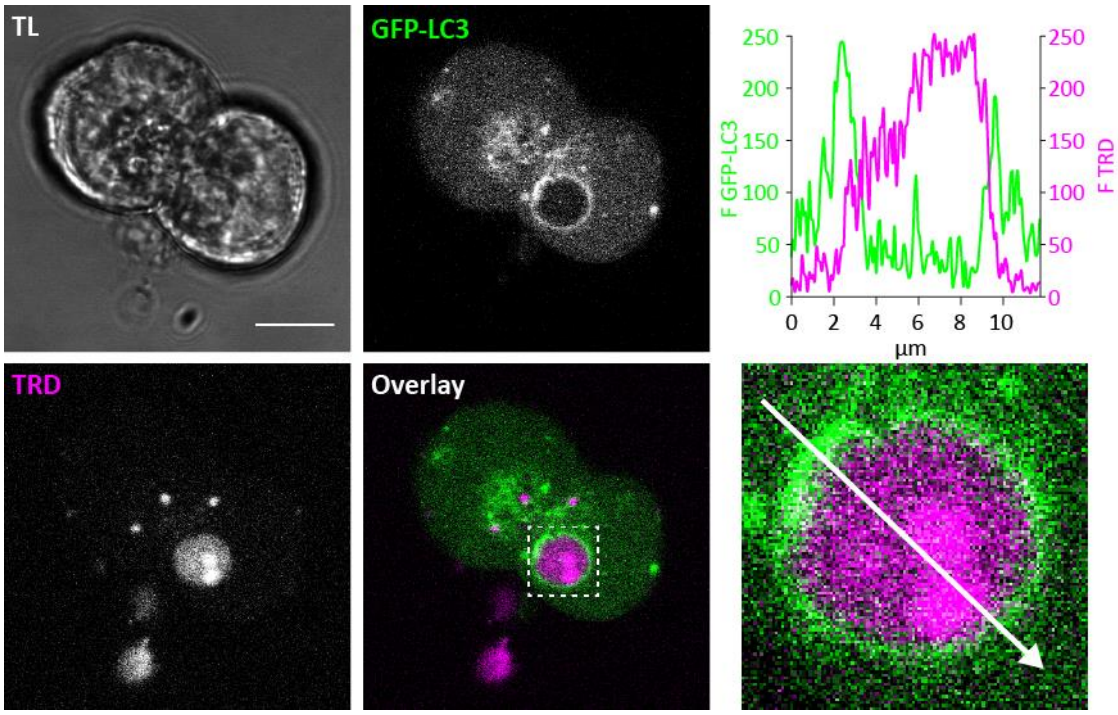

Figure 3.4 LC3-coated endocytic vacuoles in TLC-S-stimulated pancreatic acinar cells. Representative images of GFP-LC3 (green) PACs stimulated with 200 µM TLC-S for 20 min at 34.5°C in presence of TRD (magenta). The right panel shows a selected LC3-coated EV (highlighted by dashed square) in an expanded scale and fluorescence intensity profile plotted along the arrow. Scale bar = 10 µm.

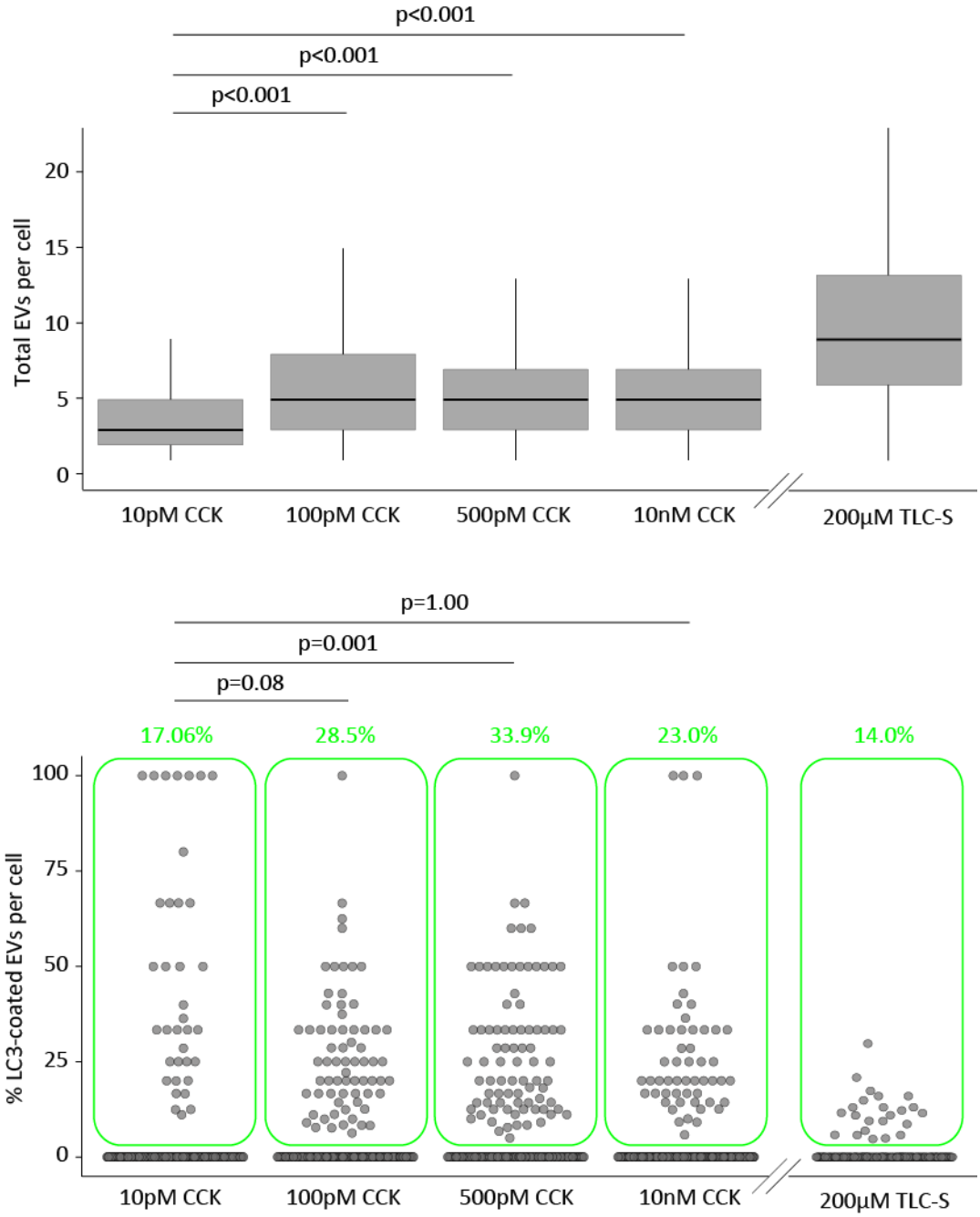

Figure 3.5 Total and LC3-coated endocytic vacuoles in PACs stimulated by CCK and TLC-S. The box and whisker plot (top) shows total number of EVs per cell, the dot plot (bottom) shows percentage of LC3-coated EVs per cell. In the dot plot, green boxes highlight cells with percentage of LC3-coated EVs above 0, the percentage of such cells is indicated above. GFP-LC3 PACs were stimulated for 30 min at 34.5°C with 10 pM (n=211), 100 pM (n=239), 500 pM (n=245) or 10 nM CCK (n=235); N=6 for all conditions. GFP-LC3 PACs were stimulated for 20 min at 34.5°C with 200 µM TLC-S (n=164); N=3. Data were compared by Kruskal-Wallis rank sum test and individual P values adjusted for multiple comparisons against "10 pM" group are reported.

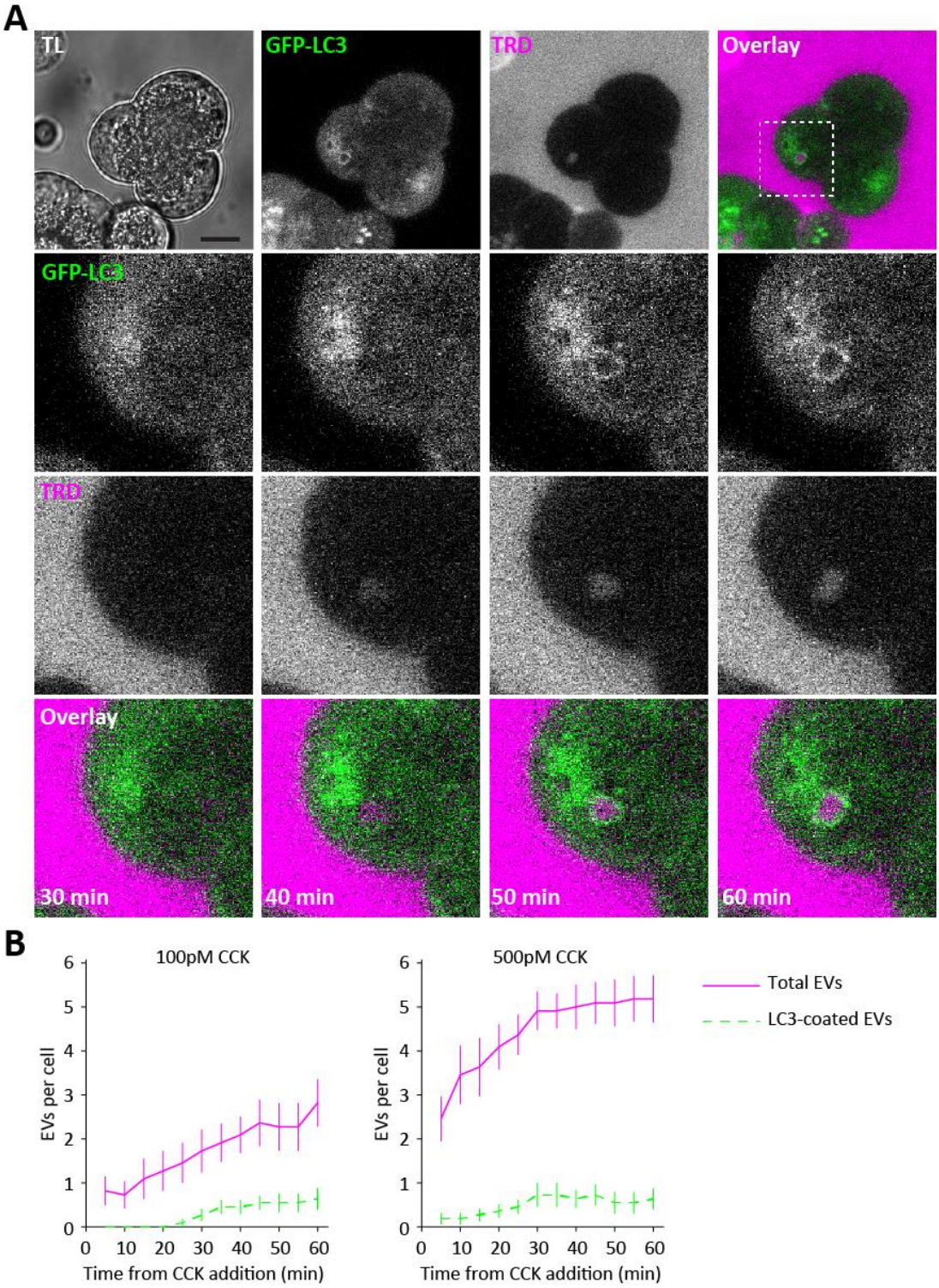

Figure 3.6 Dynamics of LC3-coating of endocytic vacuoles. A) GFP-LC3 (green) PACs were stimulated with 100 pM CCK in presence of TRD (magenta). Top panels show images at 60 min. Scale bar = 10 µm. Panels below show fragment (dashed square) in an expanded scale at indicated times. **B)** Time graphs displaying mean ± SEM number of EVs (magenta) and LC3-coated EVs (green) in PACs stimulated with 100 pM (left) or 500 pM (right) CCK. N=5, n=11 for each condition.

LC3-coating only occurred in a small proportion of EVs, rendering this phenomenon problematic to study. To circumvent this issue, accumulation of autophagic (i.e. LC3-positive) organelles was induced by application of bafilomycin A1 (hereafter referred to as bafilomycin), an inhibitor of the V-ATPase (Yoshimori *et al.*, 1991), which prevents lysosomal degradation of LC3-II. It was initially verified that pre-treatment with bafilomycin followed by CCK stimulation (in continuous presence of bafilomycin) caused an increase in the GFP-LC3 hotspot area compared to CCK control (Figure 3.7).

Having determined that V-ATPase inhibition elicited an accumulation of LC3-positive organelles, bafilomycin and concanamycin A (hereafter referred to as concanamycin), another V-ATPase inhibitor, were subsequently employed in the study of the LC3-coating of EVs. Unexpectedly, it was found that pre-treatment with V-ATPase inhibitors strongly (completely, in the case of bafilomycin) prevented the appearance of LC3-coated EVs (Figure 3.8). Additionally, bafilomycin, but not concanamycin, slightly reduced the total number of EVs.

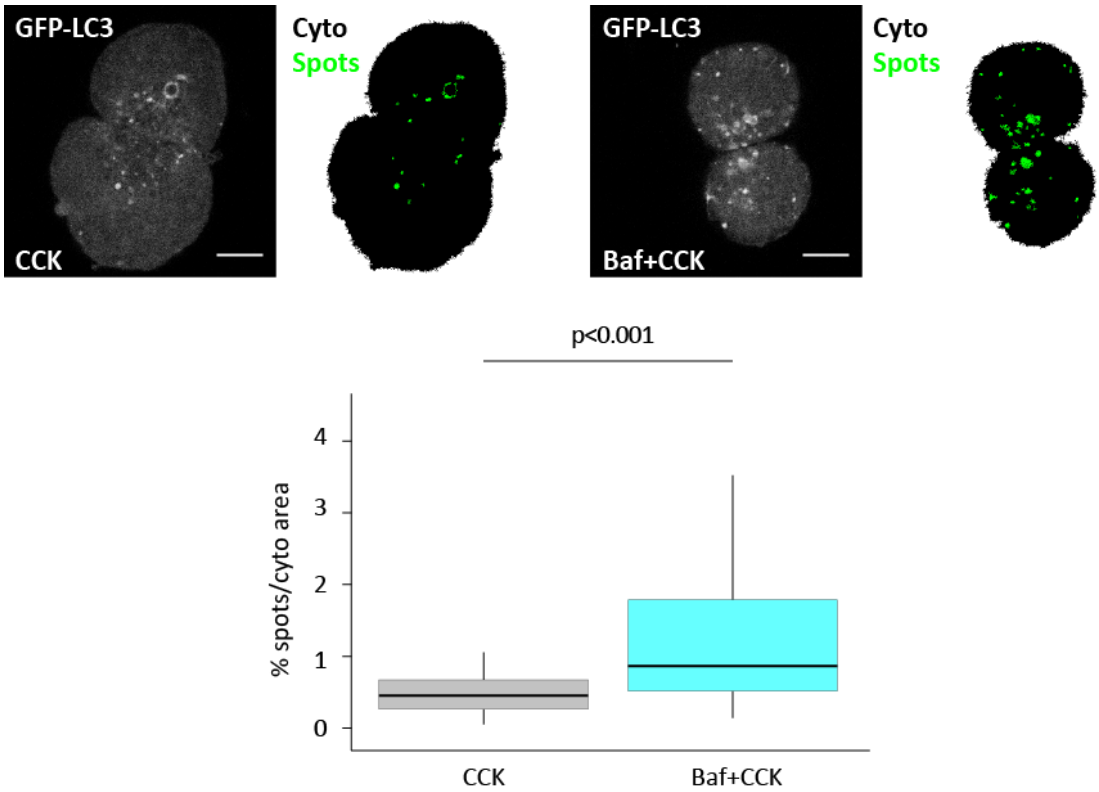

Figure 3.7 Accumulation of GFP-LC3 hotspots by bafilomycin. GFP-LC3 PACs were incubated with 100 pM CCK for 30 min, after 30 min pre-incubation and in continuous presence of 0.1% DMSO (CCK, n=83) or 100 nM bafilomycin (Baf+CCK, n=76); N=4 for both conditions. Representative images of GFP-LC3 fluorescence (grey) and masks obtained as described in Section 2.13 (CytoArea=black, SpotsArea=green). The area of the cytoplasm occupied by GFP-LC3 hotspots was calculated as described in **Figure 2.4**, shown in the box plot. Data were compared by Wilcoxon-Mann-Whitney test.

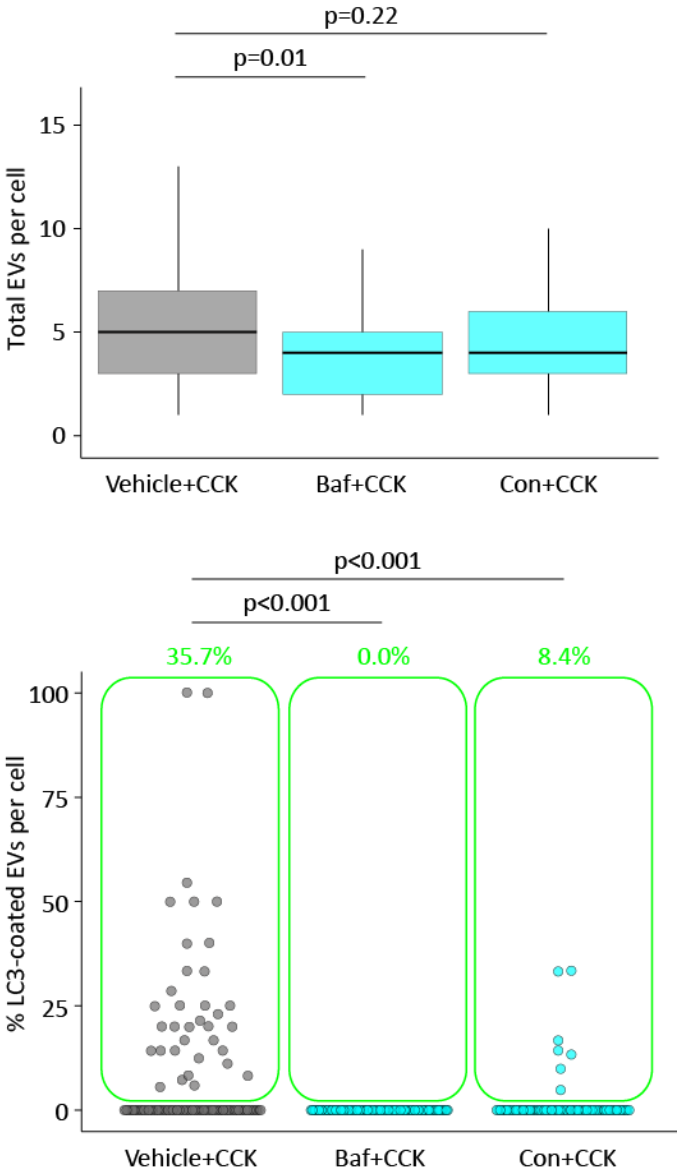

Figure 3.8 V-ATPase inhibitors reduce the LC3-coating of endocytic vacuoles. The box and whisker plot (top) shows total number of EVs per cell, the dot plot (bottom) shows percentage of LC3-coated EVs per cell. In the dot plot, green boxes highlight cells with percentage of LC3-coated EVs above 0, the percentage of such cells is indicated above. GFP-LC3 PACs were stimulated with 100 pM CCK for 30 min, after 30 minutes pre-incubation and in continuous presence of 0.1% DMSO (Vehicle, n=98), 100 nM bafilomycin (Baf, n=105) or 100 nM concanamycin (Con, n=83); N=3 for all conditions. Data were compared by Kruskal-Wallis rank sum test and individual P values adjusted for multiple comparisons against "Vehicle+CCK" group are reported.

The function of the V-ATPase is to pump protons into the lumen of an organelle in an ATP-dependent manner (Harvey, 1992). The dependence of LC3-coating of EVs on acidic intra-organellar pH was therefore tested. To this end, the ionophores nigericin and monensin were employed to disrupt the acidic pH in EVs. Both compounds reduced both the total number of EVs and importantly the percentage of LC3-coated EVs (Figure 3.9).

Chloroquine, a weak base that accumulates in acidic organelles and induces luminal alkalinisation was observed to have the same effect, decreasing both total number of EVs and the percentage of LC3-coated EVs (Figure 3.10). Thus, it was concluded that an acidic pH is required for the LC3 lipidation on EVs. A focused investigation of the pH of these organelles was carried out and will be presented in Chapter 5.

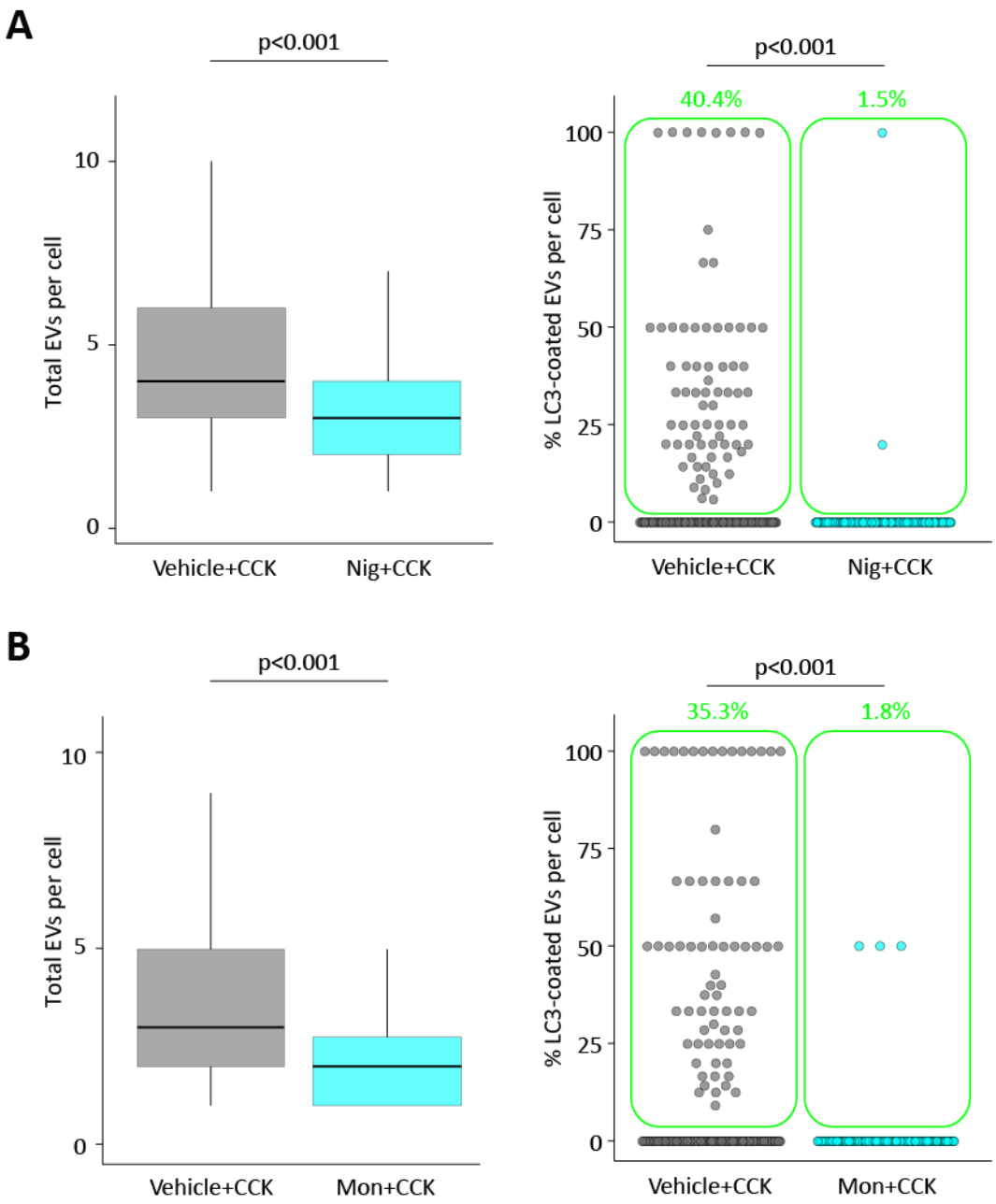

Figure 3.9 Ionophores nigericin and monensin inhibit the LC3-coating of endocytic vacuoles. The box and whisker plots (left) show total number of EVs per cell, the dot plots (right) show percentage of LC3-coated EVs per cell. In the dot plots, green boxes highlight cells with percentage of LC3-coated EVs above 0, the percentage of such cells is indicated above. **A)** GFP-LC3 PACs were stimulated with 100 pM CCK for 30 min, after 30 minutes pre-incubation and in continuous presence of 0.2% ethanol (Vehicle, n=178) or 1 µM nigericin (Nig, n=133); N=3 for both conditions. **B)** GFP-LC3 PACs were stimulated with 100 pM CCK for 30 min, after 60 minutes pre-incubation and in continuous presence of 0.1% ethanol (Vehicle, n=201) or 10 µM monensin (Mon, n=170); N=3 for both conditions.

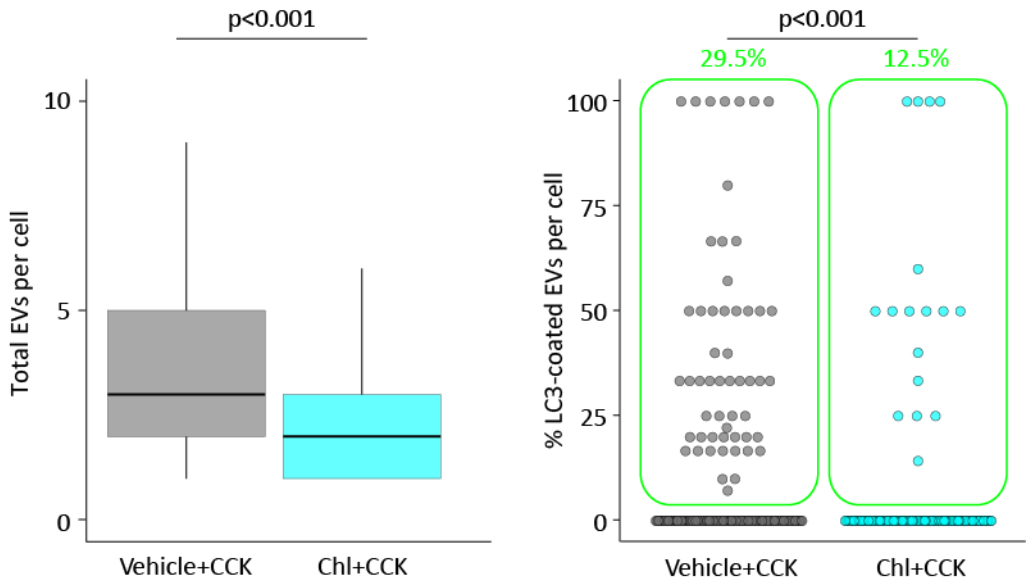

Figure 3.10 Lysomotropic agent chloroquine inhibits the LC3-coating of endocytic vacuoles. The box and whisker plot (left) shows total number of EVs per cell, the dot plot (right) shows percentage of LC3-coated EVs per cell. In the dot plot, green boxes highlight cells with percentage of LC3-coated EVs above 0, the percentage of such cells is indicated above. GFP-LC3 PACs were stimulated with 100 pM CCK for 30 min, after 60 minutes pre-incubation and in continuous presence of 0.1% ethanol (Vehicle, n=183) or 1 mM chloroquine (Chl, n=136); N=3 for both conditions. Data were compared by Wilcoxon-Mann-Whitney test.

3.2.2 Regulators of LC3-coating of endocytic vacuoles

Based on the unexpected effect of the V-ATPase inhibitors, it was hypothesised that the LC3 lipidation on EVs might not represent a canonical autophagic pathway. As described in Section 3.1, non-canonical LC3-lipidation is independent of the ULK1 complex and can be independent from the PI(3)K class III complex (Florey *et al.*, 2011; Florey *et al.*, 2015; Jacquin *et al.*, 2017). Therefore, inhibitors of these complexes were utilised and the percentage of LC3-coated EVs per cell evaluated. The ULK1/2 inhibitors MRT68921 and MRT67307 (Petherick *et al.*, 2015) had no effect on the total number of EVs or the percentage of LC3-coated EVs (Figure 3.11) suggesting that the LC3 lipidation on EVs does not depend on the ULK1 complex.

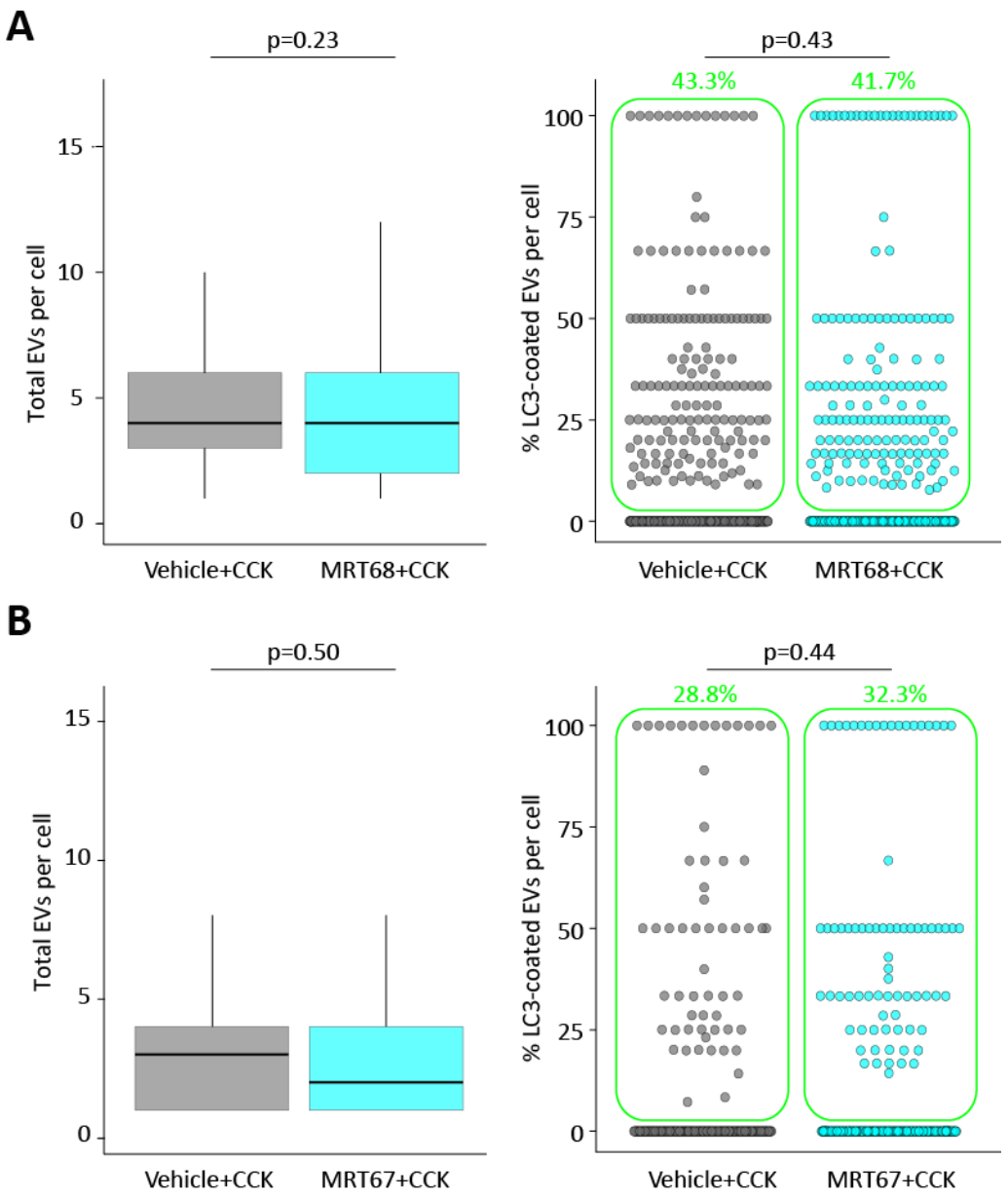

Figure 3.11 ULK1 inhibitors do not affect the LC3-coating of endocytic vacuoles. The box and whisker plots (left) show total number of EVs per cell, the dot plots (right) show percentage of LC3-coated EVs per cell. In the dot plots, green boxes highlight cells with percentage of LC3-coated EVs above 0, the percentage of such cells is indicated above. **A)** GFP-LC3 PACs were stimulated with 100 pM CCK for 30 min, after 60 minutes pre-incubation and in continuous presence of 0.1% DMSO (Vehicle, n=360) or 1 µM MRT68921 (n=367); N=5 for both conditions. **B)** GFP-LC3 PACs were stimulated with 100 pM CCK for 30 min, after 60 minutes pre-incubation and in continuous presence of 0.1% DMSO (Vehicle, n=205) or 10 µM MRT67307 (n=238); N=6 for both conditions. Data were compared by Wilcoxon-Mann-Whitney test.

The PI(3)K inhibitors LY294002 and wortmannin moderately increased and decreased the total number of EVs, respectively; however, they did not affect the percentage of LC3-coated EVs (Figure 3.12). A selective PI(3)K class III inhibitor, SAR405 (Ronan *et al.*, 2014) was therefore tested. SAR405 had no effect on the total number of EVs or the percentage of LC3-coated EVs (Figure 3.13). Collectively, these results suggest that the LC3 lipidation on EVs does not depend on *de novo* PI(3)P formation by the PI(3)K class III complex.

It has been reported that, in conditions of PI(3)P depletion, PI(5)P can promote autophagosome formation (Vicinanza *et al.*, 2015). In order to test this possibility, the effect of YM201636, an inhibitor of PIKfyve, the enzyme responsible for PI(5)P production from PI (Sbrissa *et al.*, 2002), was examined. YM201636 had no effect on the total number of EVs or on the percentage of LC3-coated EVs when applied alone (Figure 3.13). However, when YM201636 was applied in combination with SAR405 (Figure 3.13), with LY294002 (Figure 3.14) or with wortmannin (Figure 3.15), it provoked a significant, although not complete, decrease in the percentage of LC3-coated EVs. These results suggest that depleting PI(5)P in parallel to PI(3)P might affect this LC3 lipidation mechanism.

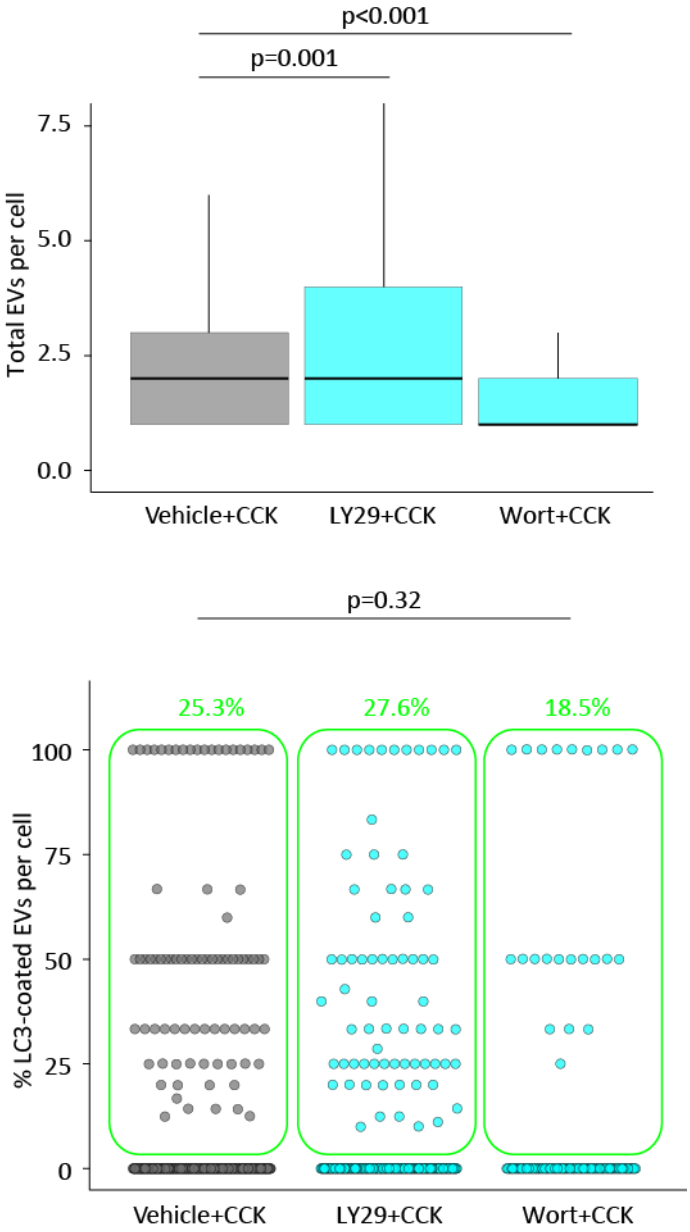

Figure 3.12 PI(3)K inhibitors do not affect the LC3-coating of endocytic vacuoles. The box and whisker plot (top) shows total number of EVs per cell, the dot plot (bottom) shows percentage of LC3-coated EVs per cell. In the dot plot, green boxes highlight cells with percentage of LC3-coated EVs above 0, the percentage of such cells is indicated above. GFP-LC3 PACs were stimulated with 100 pM CCK for 30 min, after 30 minutes pre-incubation and in continuous presence of 1% DMSO (Vehicle, n=328), 20 µM LY294002 (LY29, n=254) or 20 µM wortmannin (Wort, n=130); N=6 for all conditions. Data were compared by Kruskal-Wallis rank sum test and, when this was significant, individual P values adjusted for multiple comparisons against "Vehicle+CCK" group are reported.

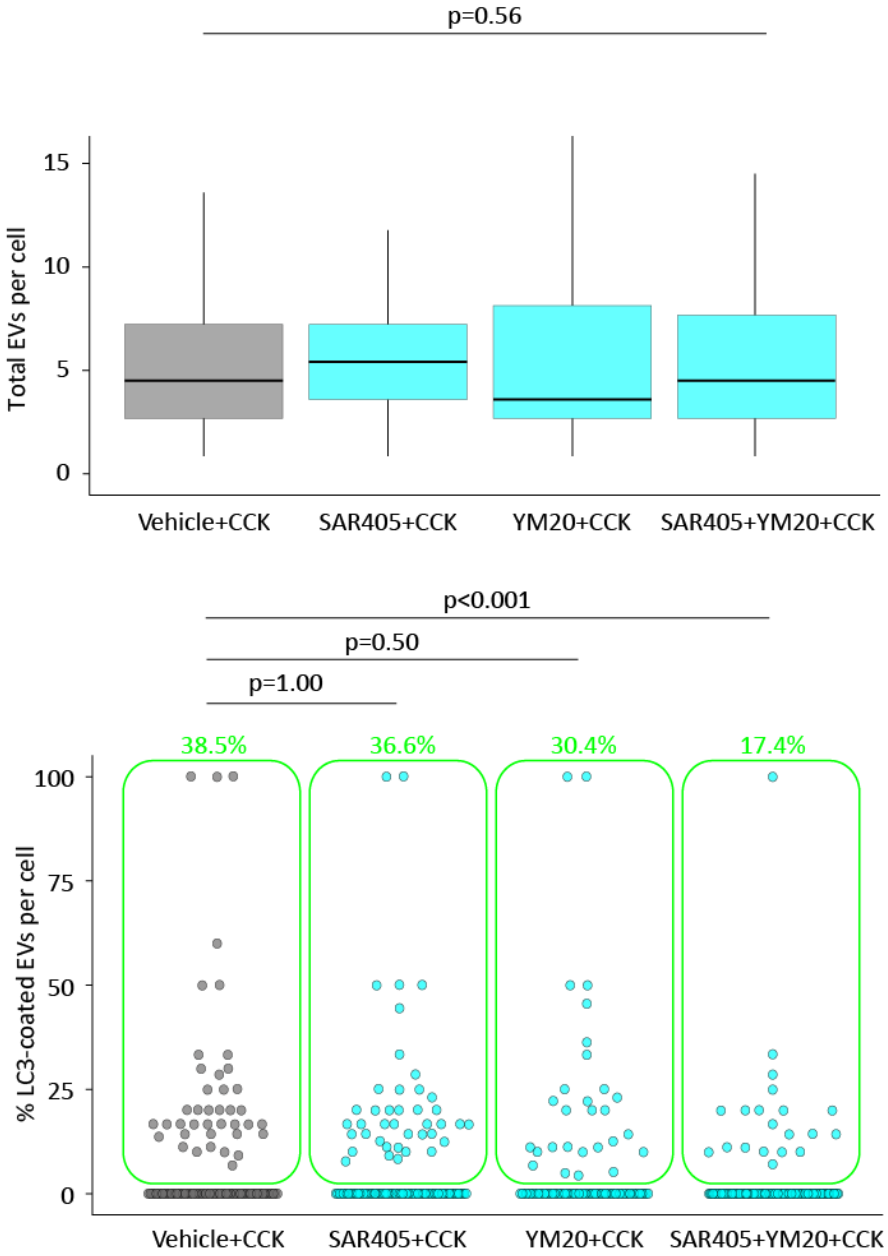

Figure 3.13 PI(3)K class III inhibitor SAR405 or PIKfyve inhibitor YM201636 do not affect the LC3-coating of endocytic vacuoles, but simultaneous application does. The box and whisker plot (top) shows total number of EVs per cell, the dot plot (bottom) shows percentage of LC3-coated EVs per cell. In the dot plot, green boxes highlight cells with percentage of LC3-coated EVs above 0, the percentage of such cells is indicated above. GFP-LC3 PACs were stimulated with 100 pM CCK for 30 min, after 30 minutes pre-incubation and in continuous presence of 0.1% DMSO (Vehicle, n=104), 1 µM SAR405 (n=112), 100 nM YM201636 (YM20, n=92) or 1 µM SAR405 + 100 nM YM20 (SAR405+YM20n=115); N=3 for all conditions. Data were compared by Kruskal-Wallis rank sum test and, when this was significant, individual P values adjusted for multiple comparisons against "Vehicle+CCK" group are reported.

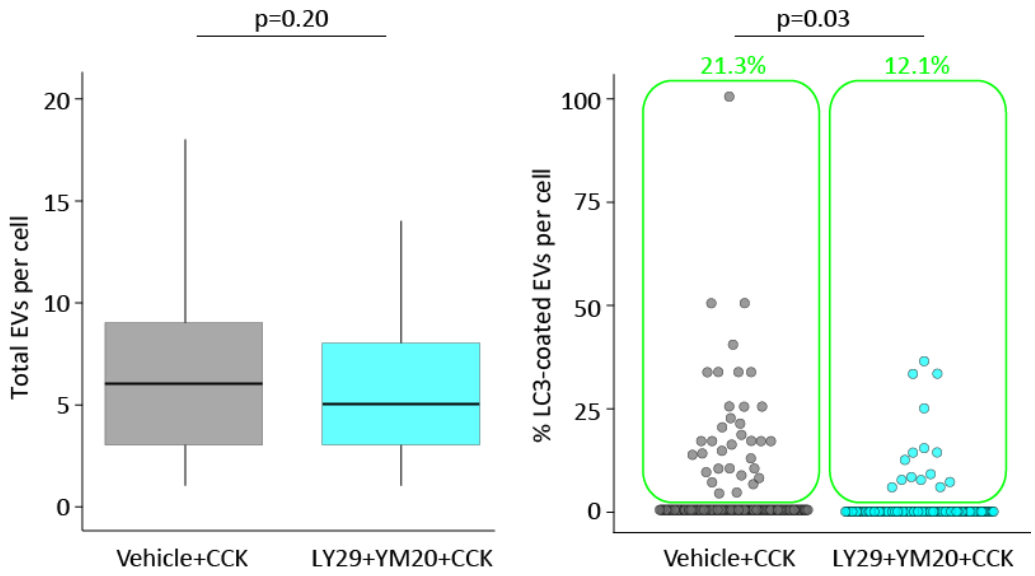

Figure 3.14 Combination of PI(3)K inhibitor LY294002 and PIKfyve inhibitor YM2016363 reduces the LC3-coating of endocytic vacuoles. The box and whisker plot (left) shows total number of EVs per cell, the dot plot (right) shows percentage of LC3-coated EVs per cell. In the dot plot, green boxes highlight cells with percentage of LC3-coated EVs above 0, the percentage of such cells is indicated above. GFP-LC3 PACs were stimulated with 100 pM CCK for 30 min, after 30 minutes pre-incubation and in continuous presence of 0.2% DMSO (Vehicle, n=164), or 20 µM LY294002 + 100 nM YM201636 (LY29+YM20 n=124); N=6 for both conditions. Data were compared by Wilcoxon-Mann-Whitney test.

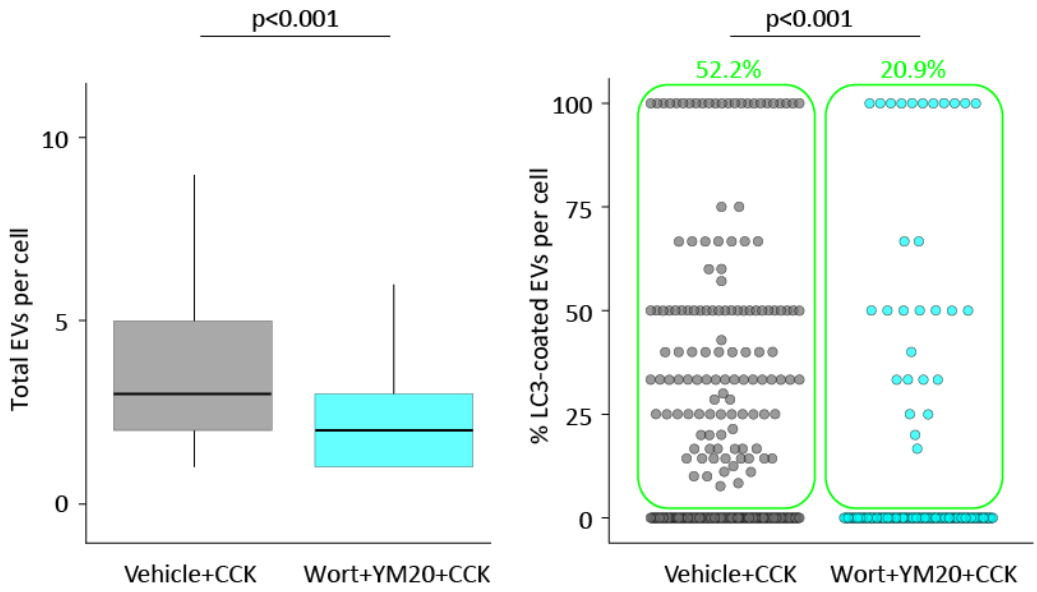

Figure 3.15 Combination of PI(3)K inhibitor wortmannin and PIKfyve inhibitor YM201636 reduces the LC3-coating of endocytic vacuoles. The box and whisker plot (left) shows total number of EVs per cell, the dot plot (right) shows percentage of LC3-coated EVs per cell. In the dot plot, green boxes highlight cells with percentage of LC3-coated EVs above 0, the percentage of such cells is indicated above. GFP-LC3 PACs were stimulated with 100 pM CCK for 30 min, after 30 minutes pre-incubation and in continuous presence of 1% DMSO (Vehicle, n=245) or 10 µM wortmannin + 100 nM YM201636 (Wort+YM20 n=139); N=5 for both conditions. Data were compared by Wilcoxon-Mann-Whitney test.

3.2.3 Structural properties of the LC3-coated endocytic vacuoles

Hypothesising that the LC3 lipidation on EVs occurs by non-canonical autophagy, the membrane properties of these organelles were examined by EM. In order to compare and distinguish classical autophagosomes, LC3-coated and uncoated EVs, correlative light and electron microscopy (CLEM) was performed. Live GFP-LC3 PACs, seeded on gridded dishes, were stimulated with 500 pM CCK in presence of TRD and imaged to find cells with LC3-coated EVs. The positions of these cells on the grid were noted. Cells were then fixed, stained and embedded in EM resin as described in Section 2.11.1, and the same cells as located on the grid processed for TEM. Single membranes were observed in all CLEM experiments with LC3-coated EVs (n=8 cells from N=4 mice) (Figure 3.16). This observation is consistent with a non-canonical autophagic pathway.

In all samples, it was also possible to clearly identify double-membrane bounded organelles (Figure 3.17). 6 double-membrane organelles were analysed and found to have an intermembrane space of 24.4 ± 1.2 nm. These double membrane structures suggest that it is feasible to resolve non-canonical (LC3-coated EVs) autophagic organelles from classical autophagosomes using CLEM.

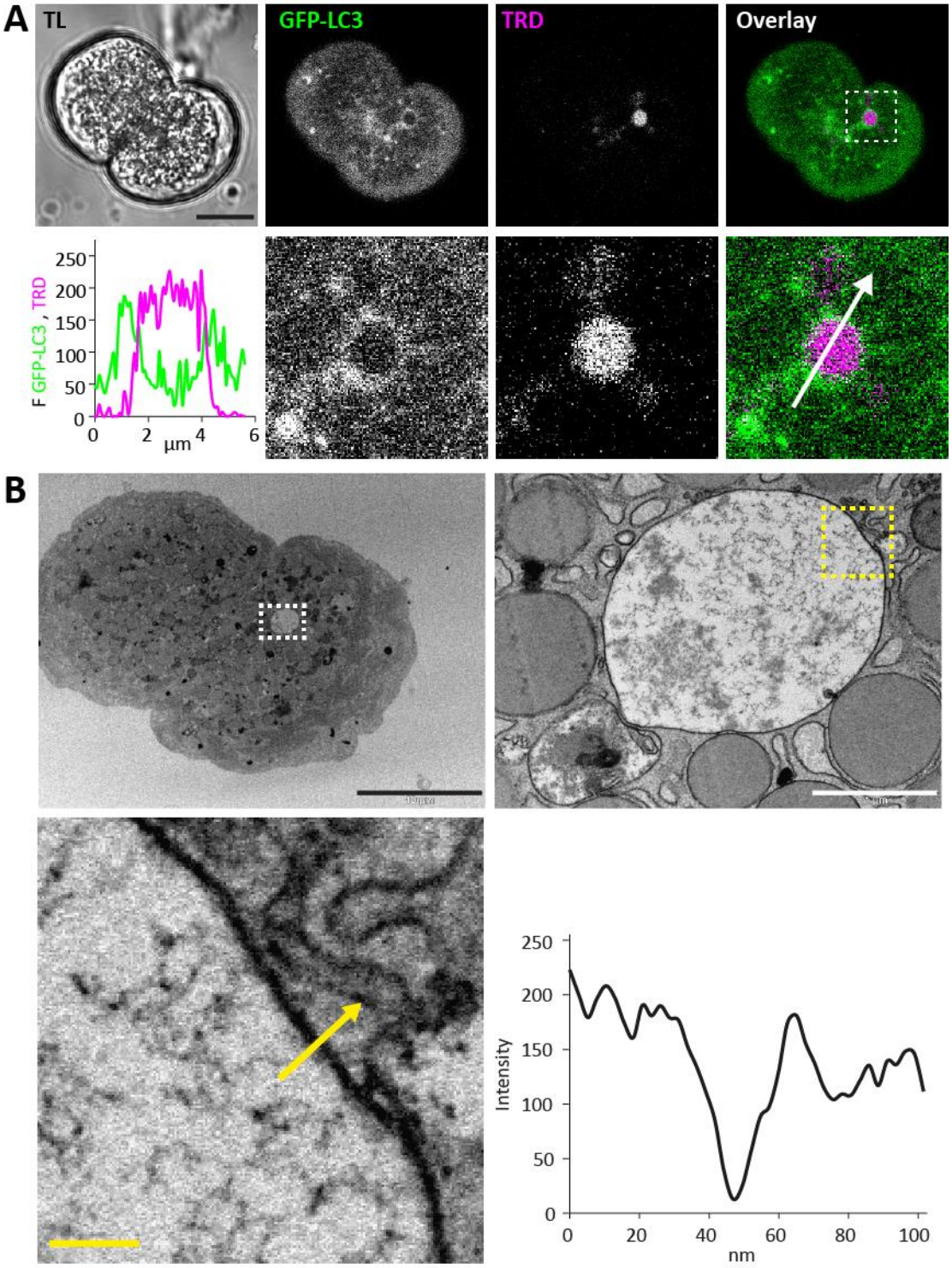

Figure 3.16 LC3-coated endocytic vacuoles have a single membrane. GFP-LC3 (green) PACs were stimulated with 500 pM CCK in presence of TRD (magenta). **A)** Live cell images, scale bar = 10 µm. The intensity profile along the white arrow is shown. **B)** TEM images of the same cell and EV. Black scale bar = 10 µm, white scale bar = 1 µm, yellow scale bar = 100 nm. The intensity profile along the yellow arrow is shown.

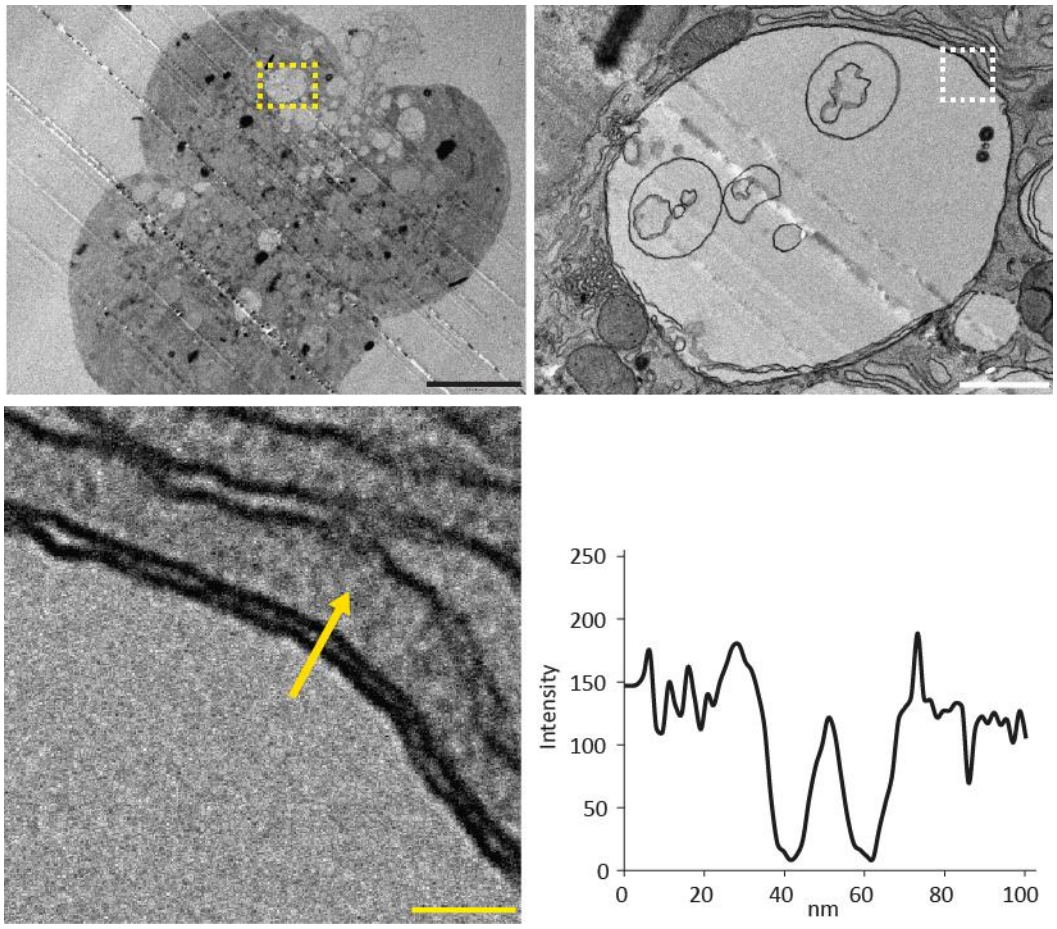

Figure 3.17 Example of organelle with double membrane. Representative TEM images showing a double-membrane organelle. Black scale bar = 10 µm, white scale bar = 1 µm, yellow scale bar = 100 nm. The intensity profile along the arrow is shown.

Having found that LC3-coated EVs have single membrane, it was next investigated whether this was due to fusion with lysosomes (and consequent degradation of the inner autophagosomal membrane). To achieve this aim, correlative immunofluorescence experiments were performed, where live GFP-LC3 PACs stimulated with 500 pM CCK in presence of TRD were imaged to find LC3-coated EVs. Cells were then fixed and processed for immunofluorescence staining as described in Section 2.9. Cells identified as having LC3-coated EVs were then located on the grids for analysis. 42 LC3-coated EVs were correlated in this way (in n=42 cells from N=3 mice), however, only 6 of these organelles had positive LAMP1 staining (Figure 3.18). From these experiments, it was concluded that, although the LC3-coated EVs can fuse with lysosomes, the majority of these organelles do not harbour lysosomal markers and therefore likely represent a pre-lysosomal compartment. In these experiments, partial co-localisation of LAMP1 was also found with non-endocytic GFP-LC3 hotspots, indicating expected fusion of classical autophagosomes with lysosomes (not shown).

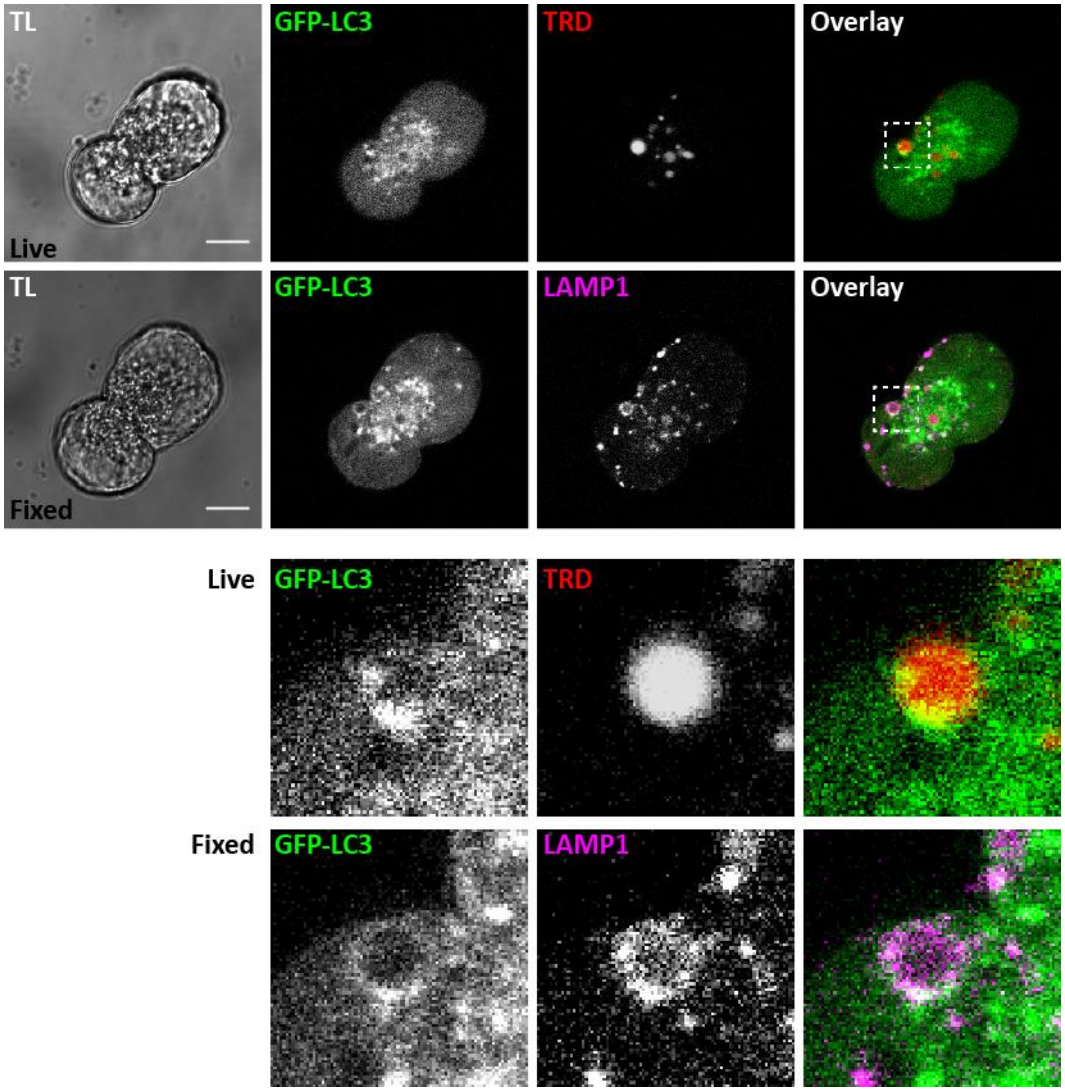

Figure 3.18 Correlative immunofluorescence for LAMP1 on LC3-coated endocytic vacuoles. GFP-LC3 (green) PACs were stimulated with 500 pM CCK for 30 min at 34.5°C in presence of TRD (red) and imaged live on gridded dishes. They were then fixed for 48 hours in 1.8% PFA at 4°C. Immunofluorescence staining for LAMP1 (magenta) was performed as described in Section 2.9. A correlative image of the same cell live and fixed is shown, with an LC3-coated EV in an expanded scale. Scale bars = 10 µm.

Having found that inhibition of V-ATPase and disruption of acidification prevented the LC3-coating of EVs, the presence of the V-ATPase on these organelles was examined. To this end, correlative immunofluorescence experiments were employed, where live GFP-LC3 PACs stimulated with 500 pM CCK in presence of TRD were imaged to find LC3-coated EVs. Cells were subsequently fixed, immunofluorescence staining was performed as described in Section 2.9, and the same cells as annotated on the grid were identified. 20 LC3-coated EVs were correlated (in n=20 cells from N=3 mice), with co-localisation with the V-ATPase subunit V0a1 staining observed in only 2 of these organelles (Figure 3.19). In these experiments, there was no noticeable co-localisation of V-ATPase with non-endocytic GFP-LC3 hotspots.

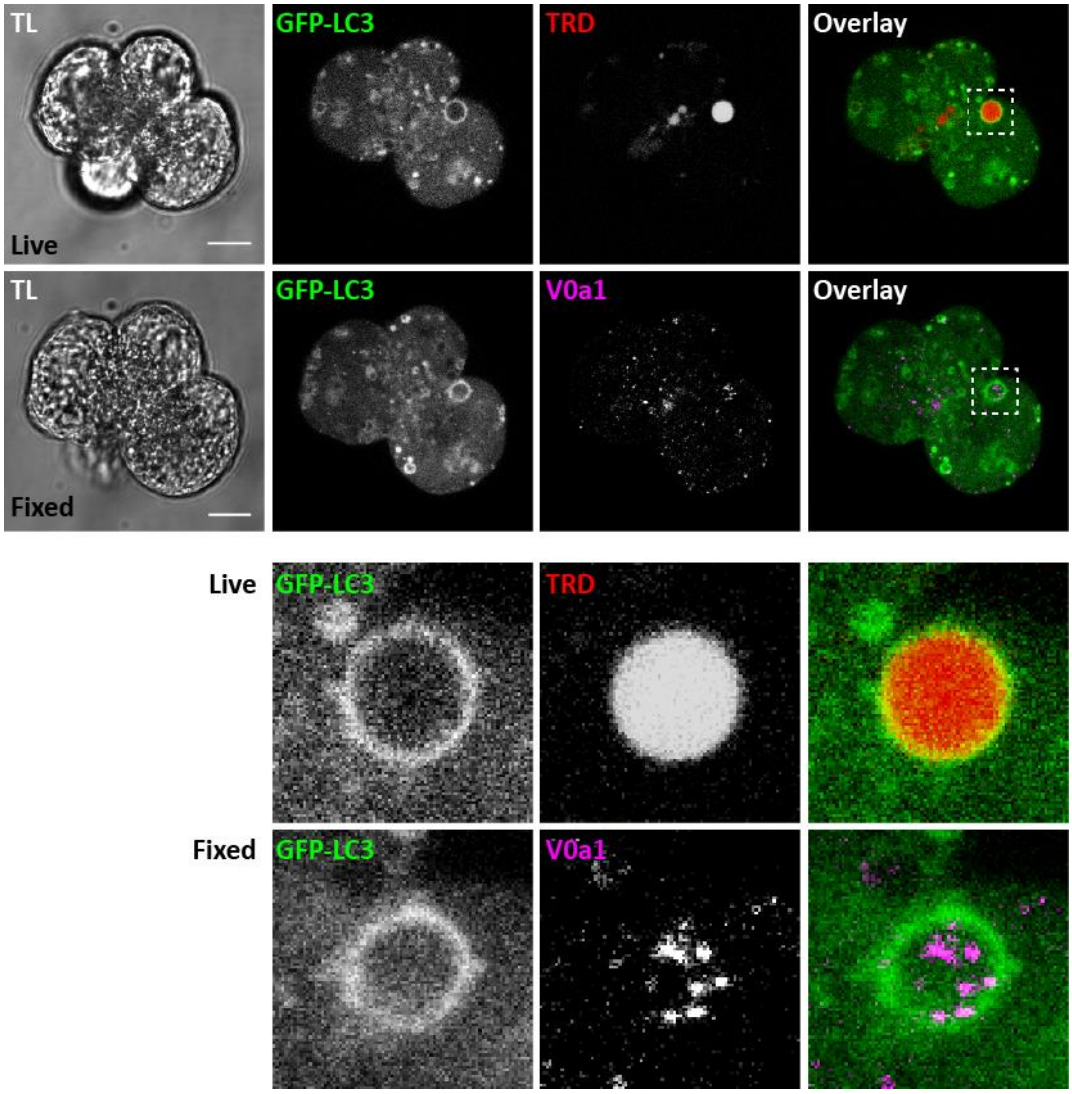

Figure 3.19 Correlative immunofluorescence for V-ATPase on LC3-coated endocytic vacuoles. GFP-LC3 (green) PACs were stimulated with 500 pM CCK for 30 min at 34.5°C in presence of TRD (red) and imaged live on gridded dishes. They were then fixed for 48 hours in 1.8% PFA at 4°C. Immunofluorescence staining for V-ATPase subunit V0a1 (magenta) was performed as described in Section 2.9. A correlative image of the same cell live and fixed is shown, with an LC3-coated EV in an expanded scale. Scale bars = 10 µm.

3.2.4 LC3 lipidation machinery on endocytic vacuoles

In both canonical and non-canonical autophagy, the last step of LC3 lipidation and membrane targeting is mediated by the ATG5-ATG12-ATG16L1 complex (Gammoh *et al.*, 2013; Dooley *et al.*, 2014; Fletcher *et al.*, 2018). However, ATG5 (and ATG7) independent autophagy also exists (Nishida *et al.*, 2009). In order to investigate the role of the ATG5-ATG12-ATG16L1 complex in the LC3 lipidation on EVs, correlative immunofluorescence for ATG5 and ATG16L1 was performed**,** where live GFP-LC3 PACs stimulated with 500 pM CCK in presence of TRD were imaged to find LC3-coated EVs. Cells were fixed and processed for immunofluorescence staining as described in Section 2.9, and the same cells as annotated on the grid were identified. 20 LC3-coated EVs were correlated (in n=20 cells from N=3 mice), with co-localisation with ATG5 staining observed in only 3 of these organelles (Figure 3.20). In these experiments there was no detectable co-localisation of ATG5 with non-endocytic GFP-LC3 hotspots (not shown). For ATG16L1 analyses, 47 LC3-coated EVs were correlated (in n=47 cells from N=3 mice), and co-localisation with ATG16L1 was observed in 45 of these organelles (Figure 3.21). In these experiments, there was an associated noticeable correlation of ATG16L1 with non-endocytic GFP-LC3 hotspots. Conversely, I did not find clear indication of ATG16L1 presence on EVs not coated by LC3. The bottom panel of Figure 3.21 is a clear example of these three populations of organelles: the top organelle (yellow asterisk) is an LC3-positive (classical) autophagosome (positive for ATG16L1, negative for TRD), the middle organelle (yellow arrowhead) is an LC3-coated EV (positive for ATG16L1, positive for TRD), the bottom organelle (yellow dot) is an uncoated EV (negative for ATG16L1, positive for TRD).

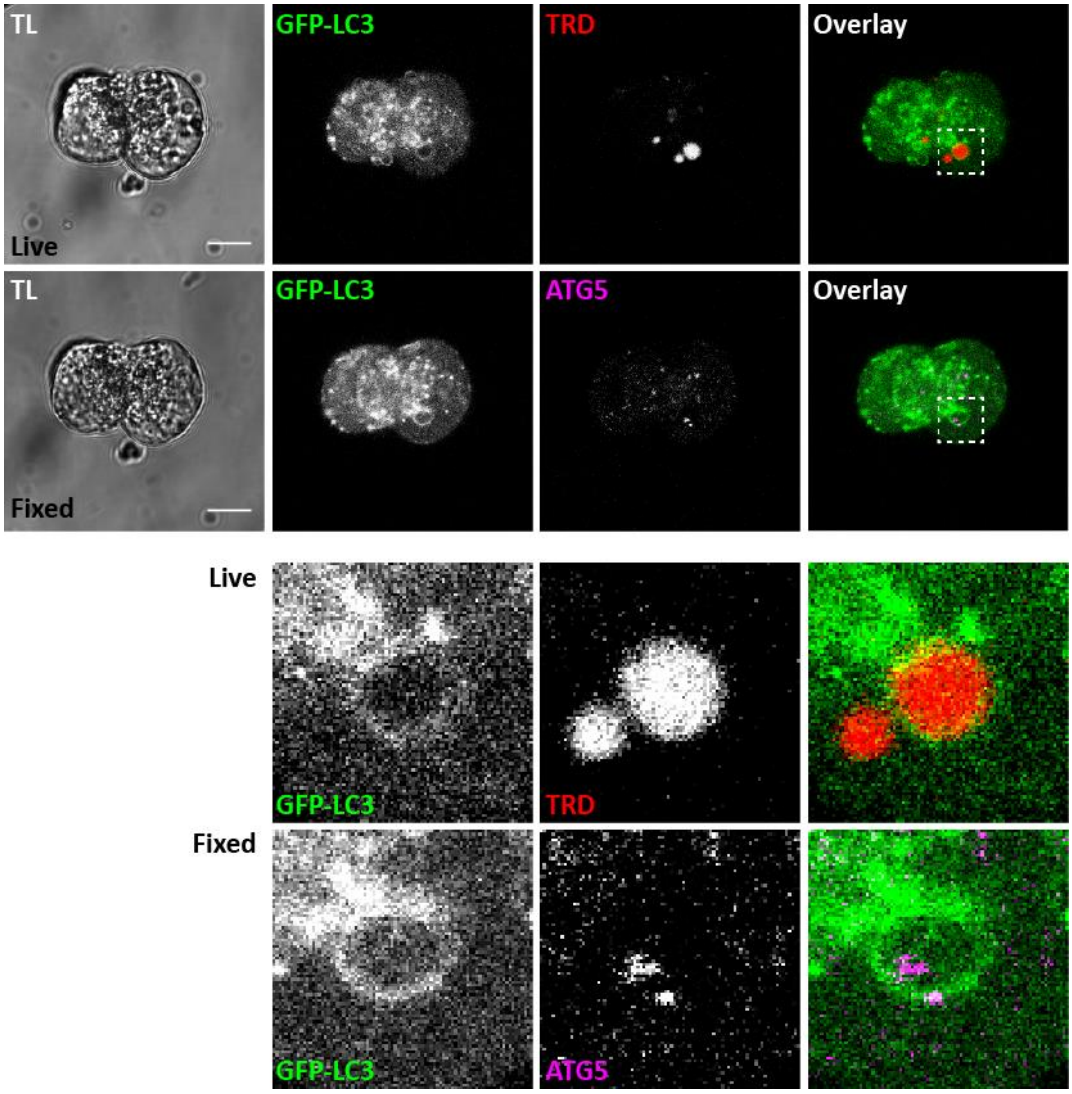

Figure 3.20 Correlative immunofluorescence for ATG5 on LC3-coated endocytic vacuoles. GFP-LC3 (green) PACs were stimulated with 500 pM CCK for 30 min at 34.5°C in presence of TRD (red) and imaged live on gridded dishes. They were then fixed for 48 hours in 1.8% PFA at 4°C. Immunofluorescence staining for ATG5 (magenta) was performed as described in Section 2.9. A correlative image of the same cell live and fixed is shown, with an LC3-coated EV in an expanded scale. Scale bars = 10 µm.

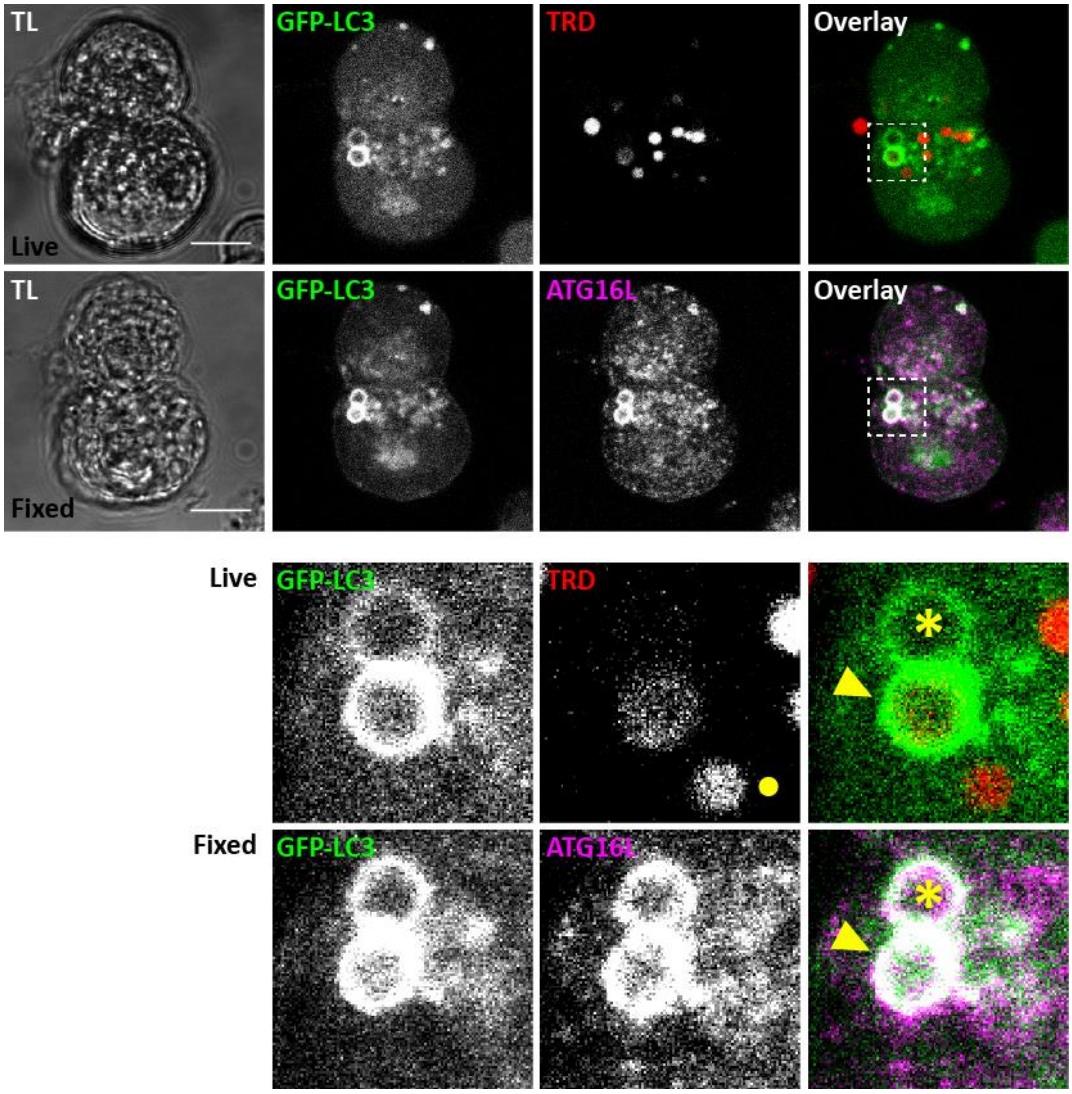

Figure 3.21 Correlative immunofluorescence for ATG16L1 on LC3-coated endocytic vacuoles. GFP-LC3 (green) PACs were stimulated with 500 pM CCK for 30 min at 34.5°C in presence of TRD (red) and imaged live on gridded dishes. They were then fixed for 10 min in 4% PFA at RT. Immunofluorescence staining for ATG16L1 (magenta) was performed as described in Section 2.9. A correlative image of the same cell live and fixed is shown, with an LC3-coated EV in an expanded scale (yellow arrowhead). Yellow asterisk refers to LC3-positive, dextran-negative organelle, yellow dot refers to LC3-negative, dextran-positive organelle, Scale bars = 10 µm.

The presence of ATG16L1 on LC3-coated EVs suggests the involvement of the ATG5-ATG12-ATG16L1 complex in the LC3 lipidation process. I wanted to verify this result by testing the LC3-coating of EVs in the absence of ATG5. For this work, an inducible conditional *Atg5* KO mouse model was employed. As explained in Section 2.2.1, activation of CreER^{T} recombinase, expressed in PACs under the *Cela1* promoter, was induced by tamoxifen administration. It was observed that some of the pancreata from *Atg5$^{flox/flox}$;CelaCreERT$^{+/-}$* mice that had been treated with tamoxifen were smaller, and this phenomenon correlated with the "success" of the KO, verified by Western blot analysis (Figure 3.22 A). In *Atg5$^{flox/flox}$;CelaCreERT$^{+/-}$* mice with normal pancreas morphology and size (referred to as 'Normal') the ATG5/calnexin ratio was not significantly lower (82%) than *Atg5$^{flox/flox}$;CelaCreERT$^{-/-}$* (Control) mice. Conversely, in *Atg5$^{flox/flox}$;CelaCreERT$^{+/-}$* mice with small pancreas (referred to as 'Small') the ATG5/calnexin ratio was significantly lower (38%) than Control (Figure 3.22 B). The wet weight of the pancreas was also significantly lower in *Atg5$^{flox/flox}$;CelaCreERT$^{+/-}$* mice (Small) where KO was successful rather than *Atg5$^{flox/flox}$;CelaCreERT$^{+/-}$* mice (Normal) where KO was not satisfactory (Figure 3.22 C). As a control, N=2 *Atg5$^{flox/flox}$;CelaCreERT$^{-/-}$* and N=2 *Atg5$^{flox/flox}$;CelaCreERT$^{+/-}$* were sacrificed prior tamoxifen treatment and no difference was found in pancreas size, weight, or ATG5/calnexin ratio, showing that the phenotype observed in some of the *Atg5$^{flox/flox}$;CelaCreERT$^{+/-}$* mice was triggered by tamoxifen (triggering Cre-mediated recombination). When attempts were made to isolate PACs to perform experiments, it was not possible to obtain viable cells from *Atg5$^{flox/flox}$;CelaCreERT$^{+/-}$* mice with small pancreata (i.e. successful KO animals). It was therefore not possible to assess whether LC3 lipidation on EVs can occur in absence of ATG5.

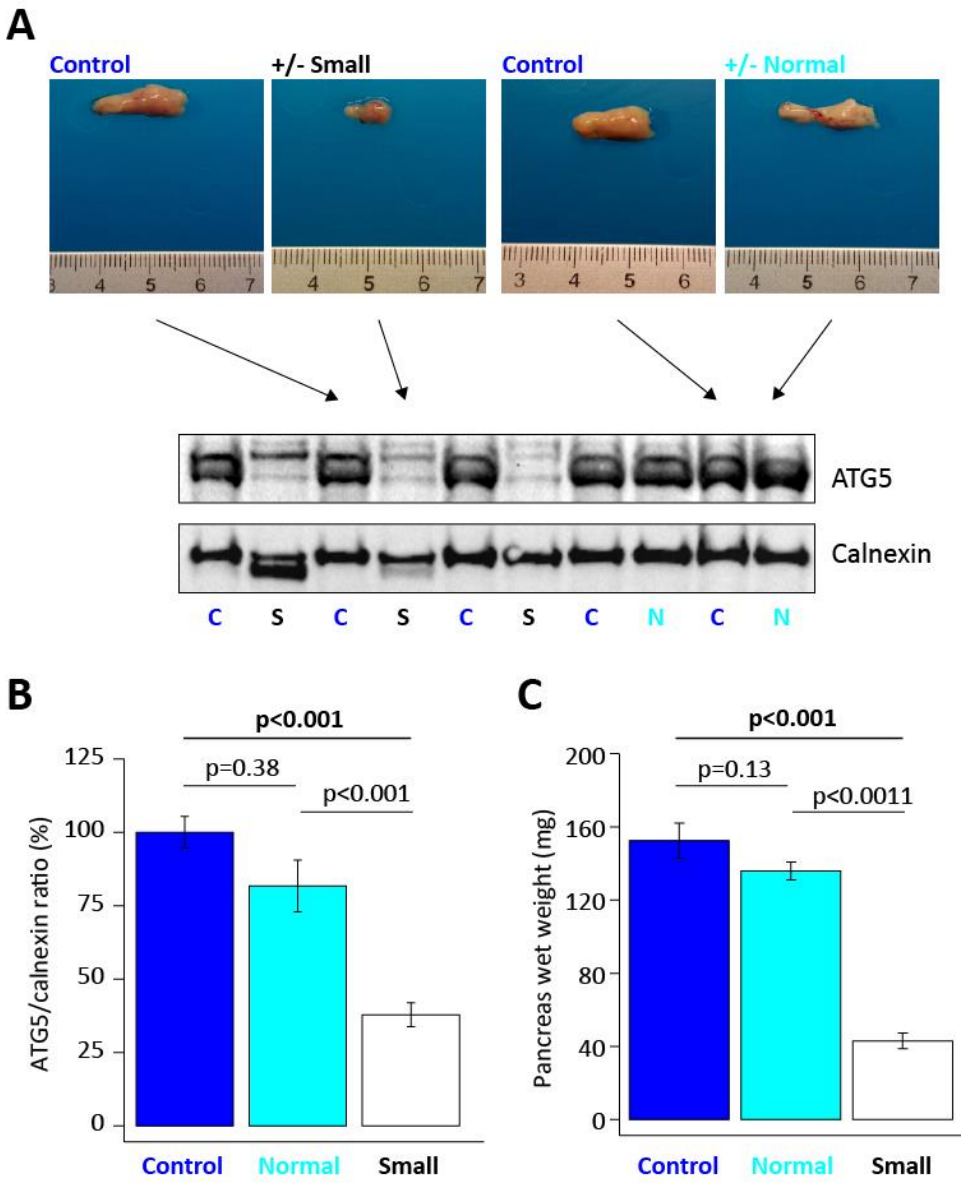

Figure 3.22 Inducing conditional knock-out of *Atg5*. *Atg5$^{flox/flox}$;CelaCreERT$^{+/-}$* and *Atg5$^{flox/flox}$;CelaCreERT$^{-/-}$* were treated with tamoxifen by Doctor Michael Chvanov as described in Section 2.2.1. **A)** Example photographs of pancreata excised from *Atg5$^{flox/flox}$;CelaCreERT$^{+/-}$* and *Atg5$^{flox/flox}$;CelaCreERT$^{-/-}$* (Control) mice, and corresponding lanes in Western blot analysis. **B)** The bar graph represents mean ± SEM for ATG5/calnexin ratio obtained by densitometry analysis. Control N=11, Normal N=6, Small N=5. **C)** The bar graph represents mean ± SEM for the wet weight of pancreata excised from *Atg5$^{flox/flox}$;CelaCreERT$^{+/-}$* and *Atg5$^{flox/flox}$;CelaCreERT$^{-/-}$* (Control) mice. Control N=10, Normal N=6, Small N=4.

Having failed to obtain functional evidence for the ATG5-dependence of LC3 lipidation on EVs, alternative evidence was generated to verify the hypothesis that this process represents a non-canonical autophagic mechanism. To this end, the E230 mouse model, which specifically lacks non-canonical autophagy but which exhibits competent canonical autophagy (Fletcher *et al.*, 2018), was used. Experiments were performed to determine whether E230 mice, deficient for non-canonical autophagy, would present LC3-coating of EVs. PACs were isolated from WT and E230 mice, infected with *LC3A-mCherry* (or *LC3A-eYFP*) adenoviral vectors (as described in Section 2.5), then stimulated with 100 pM CCK in the presence of LY (or Cy5). No significant difference in the total number of EVs was observed, however a strong, statistically significant (although not complete) reduction in the percentage of LC3-coated EVs in E230 mice was revealed (Figure 3.23).

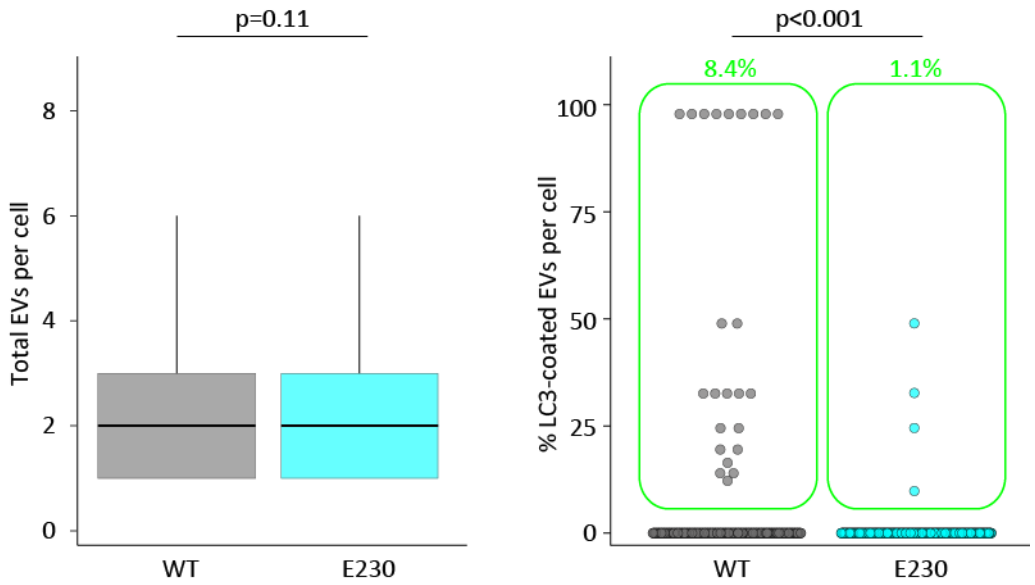

Figure 3.23 Mice defective for non-canonical autophagy have reduced percentage of LC3-coated endocytic vacuoles. The box and whisker plot (left) shows total number of EVs per cell, the dot plot (right) shows percentage of LC3-coated EVs per cell. In the dot plot, green boxes highlight cells with percentage of LC3-coated EVs above 0, the percentage of such cells is indicated above. *LC3A-mCherry* or *LC3A-eYFP* transfected PACs were stimulated with 100 pM CCK for 30 min at 35°C. WT N=9 mice n=285 cells, E230 N=11 mice n=361 cells. Data were compared by Wilcoxon-Mann-Whitney test.

3.3 Discussion

In this chapter the interaction of EVs with AVs in PACs has been examined in detail by taking advantage of the transgenic GFP-LC3 mouse model. 17-34% of cells present EVs coated by LC3 following stimulation by physiological to supramaximal CCK concentrations. Approximately 14% of cells present EVs coated by LC3 following stimulation by TLC-S. LC3-coating of EVs was prevented by V-ATPase inhibitors bafilomycin and concanamycin. Likewise, this phenomenon was inhibited by agents disrupting the maintenance of acidic pH: the ionophores monensin and nigericin and the lysomotropic weak base chloroquine. It was hypothesised that the LC3-coating of EVs might represent a non-canonical autophagic pathway (**Figure 3.24**). Thus, the ULK1 inhibitors MRT68921 and MRT67307 and PI(3)K inhibitors LY294002, wortmannin and SAR405 were tested and found to have no effect on the percentage of LC3-coated EVs. Interestingly, it was revealed that the combination of PIKfyve inhibitor YM201636 and PI(3)K inhibitors reduced - although not completely - the percentage of LC3-coated EVs. LC3-coated EVs were discovered to have a single membrane in ultrastructural studies, consistent with the hypothesis of a non-canonical autophagy mechanism. Partial co-localisation with the lysosomal marker LAMP1 was observed, and almost complete co-localisation with ATG16L1, indicating that the ATG5-ATG12-ATG16L1 complex is likely involved in this LC3 lipidation process. Finally, a reduction - although not complete- in the percentage of LC3-coated EVs in E230 mice, defective for non-canonical but competent for canonical autophagy, was discovered, which is also consistent with non-canonical autophagy.

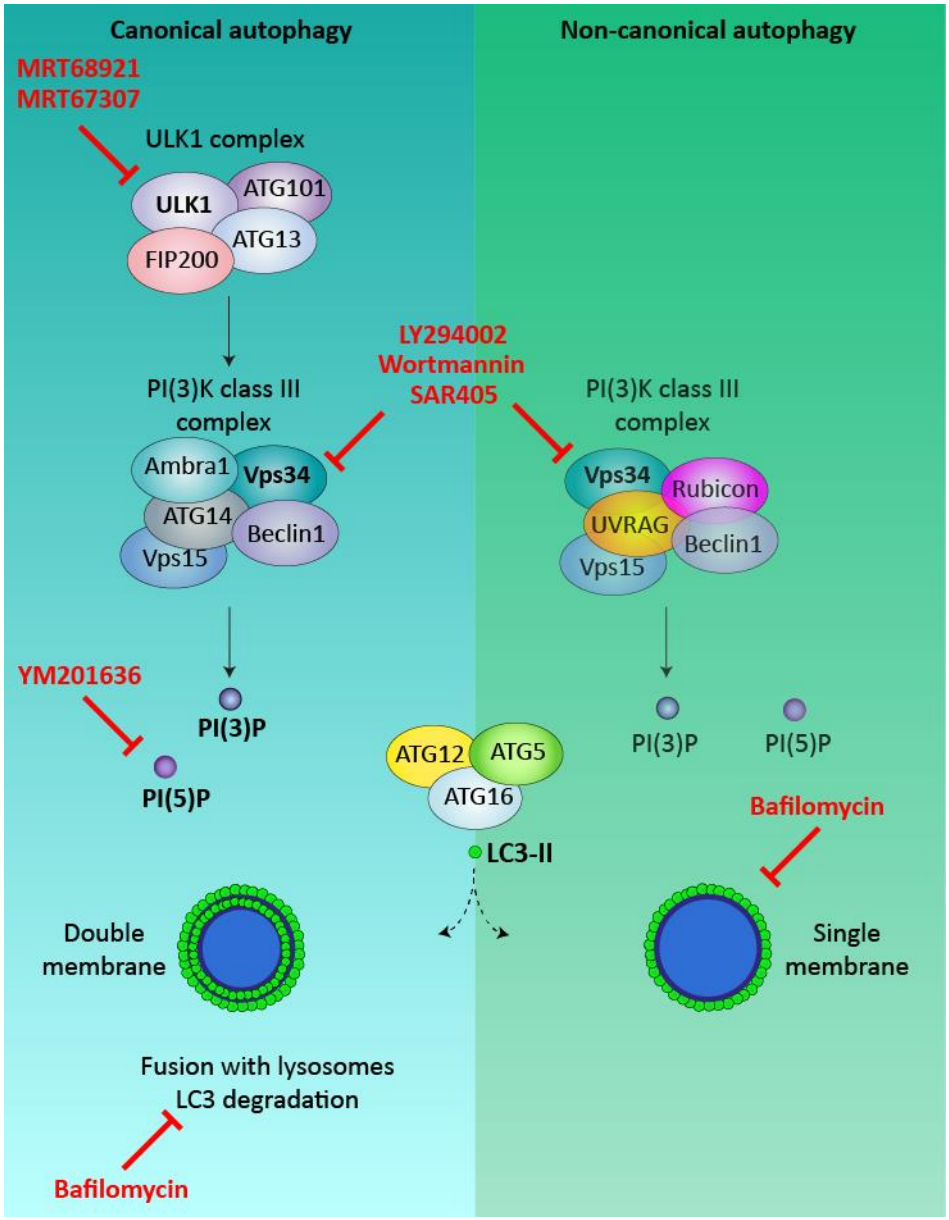

Figure 3.24 Summary of pharmacological characterisation of autophagic pathways. The schematic depicts the main complexes involved in canonical and non-canonical autophagy, and indicates the inhibitors utilised in this study.

PACs require basal autophagy as a protective mechanism to maintain their function of high-rate protein synthesis (Antonucci *et al.*, 2015; Smith *et al.*, 2018). It was firstly verified that calcium-releasing agonists drive upregulation of autophagy in PACs, as quantified by GFP-LC3 fluorescence. Supramaximal (10 nM) but not physiological (10 pM) CCK concentrations caused a significant increase in the area occupied by GFP-LC3 hotspots. Previous studies have reported autophagy activation following AP stimuli, revealed by Western blot analysis of LC3-II/LC3-I, GFP-LC3 fluorescence hotspots, or LC3 immunostaining (Hashimoto *et al.*, 2008; Mareninova *et al.*, 2009).

Calcium-releasing agonists also determine formation of EVs (Sherwood *et al.*, 2007). Early in this project, it was observed that a small proportion of EVs induced by CCK and TLC-S are coated by LC3. The interaction of EVs and AVs in PACs has been suggested before (Tooze *et al.*, 1990). The literature in the pancreatitis field accounts for activation/disruption of autophagy, reporting accumulation of AVs, increased expression of VMP1 and co-localisation of VMP1 with Beclin1 and LC3, alongside increased localisation to autophagosomes and/or autolysosomes of VMP1, LC3, Beclin1, LAMP2 and cathepsins B and D (Ropolo *et al.*, 2007; Zhang *et al.*, 2014; Mareninova *et al.*, 2015). Autophagic flux disruption and impairment of lysosomal function are associated with zymogen activation (Hashimoto *et al.*, 2008; Mareninova *et al.*, 2009; Gukovsky *et al.*, 2012; Mareninova *et al.*, 2015), which occurs in EVs (Sherwood *et al.*, 2007). Nevertheless, direct investigation of the interaction of autophagic pathways and EVs has not been carried out before. Previous studies in our field have performed subcellular fractionation followed by immunoassays to identify the presence of LC3 in specific compartments (Mareninova

et al., 2009; Zhang *et al.*, 2014). For the first time, the data presented in this thesis highlights a direct interaction between the autophagic marker LC3 and EVs in live cells.

The V-ATPase inhibitor bafilomycin is commonly used to disrupt autophagic flux and elicit accumulation of LC3-II and LC3-positive compartments (Klionsky *et al.*, 2016). Bafilomycin also allows discrimination between canonical and non-canonical autophagy: it causes LC3-II accumulation in the former, it prevents it in the latter (Florey *et al.*, 2015). The work presented in this chapter shows that bafilomycin pre-treatment increased the GFP-LC3 hotspots induced by CCK, consistent with activation of canonical autophagy. Unexpectedly, it was found that the LC3-coating of EVs was inhibited by bafilomycin and concanamycin. A similar observation was made in the study of non-canonical LC3 lipidation on phagosomes and entotic vacuoles; these processes were also sensitive to bafilomycin (Florey *et al.*, 2015). Thus, it was hypothesised that the phenomenon of EV coating with LC3 is also a non-canonical process.

Chloroquine and monensin induced the formation of phagosomes in macrophages and entotic vacuoles in MCF10a cells, these organelles became coated by LC3 (Florey *et al.*, 2015). Conversely, my experiments showed that disruption of acidification with chloroquine, monensin or nigericin had inhibitory effects on the LC3-coating of the EVs. A recent study reported a role for lysomotropic agents and ionophores in induction of bafilomycin-sensitive non-canonical autophagy (Jacquin *et al.*, 2017). The authors also tested the protonophore CCCP and the lysomotropic agent (and L-type calcium channel antagonist) amiodarone, and found that these compounds

induced both canonical and non-canonical autophagy. Another study found that Autophagy Modulator with Dual Effect-1 (AMDE-1) triggered both canonical and non-canonical autophagy (Gao *et al.*, 2016). Chloroquine, monensin and nigericin and other ionophores (valinomycin, gramidicin A, ionomycin and A23187) had no effect on AMDE-1 induced non-canonical autophagy (Gao *et al.*, 2016). Collectively, these examples of drug-induced non-canonical autophagy (which were not disrupted by lysomotropic agents) suggest an acidification-independent role of the V-ATPase in LC3-lipidation. Conversely, my experiments demonstrate that the LC3-coating of EVs is not only V-ATPase-dependent (i.e. sensitive to bafilomycin and concanamycin) but also acidification-dependent (i.e. sensitive to nigericin, monensin and chloroquine).

It is worthy to point out that the actual effects of the different drugs used to disrupt acidification are debated. As indicated above, bafilomycin is used to disrupt autophagic flux, without specifying at what level (e.g. autophagosome-lysosome fusion or autolysosome function). A study found that bafilomycin prevented autolysosome acidification via V-ATPase inhibition, whereas it prevented autophagosome-lysosome fusion via SERCA inhibition (Mauvezin *et al.*, 2015). Controversially, another research group reported that neither bafilomycin, nor nigericin affected phagosome-lysosome fusion (Kissing *et al.*, 2015). It would thus appear that neither acidity nor V-ATPase activity are required for fusion with lysosomes (but they are required for function of lysosomal hydrolases). A recent study reported that chloroquine prevented autophagosome-lysosome fusion, rather than disrupting lysosomal acidity or activity (Mauthe *et al.*, 2018). In the work presented here, it has been demonstrated that the V-ATPase inhibitors, chloroquine,

monensin and nigericin had similar effects in reducing the LC3-coating of EVs. The mechanism of this inhibition is unknown, however it can be speculated that it is primarily associated with acidification. Nevertheless, bafilomycin had a much stronger effect than chloroquine and this might suggest a direct role for the V-ATPase itself in this process. Indeed, the inhibitory effect of bafilomycin on non-canonical autophagy was associated to the V-ATPase directly (Florey *et al.*, 2015). Interestingly, the authors reported that LC3 was only lipidated on acidic vacuoles (Florey *et al.*, 2015). The results of investigating the pH properties of PAC EVs will be addressed in Chapter 5.

In the experiments described in this chapter, bafilomycin, nigericin, monensin and chloroquine all caused a moderate decrease in the total number of EVs. It was previously reported that bafilomycin increased CCK-induced secretion (Messenger *et al.*, 2015). An earlier study reported that V-ATPase inhibitors lobatomide B and salicyhalamide A inhibited caerulein-induced zymogen activation, but had no effect on amylase secretion (Kolodecik *et al.*, 2009). The same research group had also previously reported that V-ATPase inhibition with bafilomycin and pH modulation with chloroquine or monensin reduced intracellular trypsinogen activation induced by caerulein, however they did not examine the effect on secretion (Waterford *et al.*, 2005). Conversely, previous studies showed that chloroquine and monensin slightly increased CCK-stimulated amylase release (De Lisle & Williams, 1987). In other cell types, monensin is known to disrupt secretion (reviewed in (Tartakoff, 1983)). Indeed, ionophores will also affect the TGN, where acidic pH plays an important role in protein sorting through the regulated secretory pathway (discussed in Chapter 1).

Overall, it cannot be concluded that inhibiting intra-organellar acidification impairs secretion in PACs, although it seems to affect EV formation.

The previously reported examples of non-canonical autophagy were found to occur in *FIP200*, *ULK1* or *ATG13* KO cells, indicating independence from the ULK1 complex. These mechanisms of LC3 lipidation occurred in presence of LY294002, wortmannin or 3-methyladenine, indicating independence from the PI(3)K complex (Florey *et al.*, 2015; Gao *et al.*, 2016; Jacquin *et al.*, 2017). Similarly, in this work, it has been found that ULK1 or PI(3)K inhibition did not affect LC3 lipidation on EVs, strengthening the hypothesis of a non-canonical mechanism. No direct evidence for a role of ULK1-mediated autophagy in AP could be found in the literature. Conversely, PI(3)K inhibition with 3-methyladenine has been reported to reduce vacuole formation and trypsinogen activation (Mareninova *et al.*, 2009), indicating a role for PI(3)K in AP-induced autophagy.

In experiments examining the PI(3)K inhibitors LY294002 and wortmannin there was a moderate and opposite effect on the total number of EVs, which was increased by LY294002 and reduced by wortmannin. Previous studies showed that both wortmannin and LY294002 inhibited CCK-stimulated secretion (Nozu *et al.*, 2000; Ikeda & Fukuoka, 2003), and that wortmannin had an inhibitory effect on supramaximal ACh-stimulated secretion (Campos-Toimil *et al.*, 2002). Another study revealed that both wortmannin and LY294002 reduced trypsinogen activation in caerulein-stimulated cells, but whilst wortmannin had no effect on secretion, LY294002 inhibited secretion (Singh *et al.*, 2001). Another research group found no effect by LY294002 or wortmannin on CCK-stimulated secretion (Messenger *et al.*,

2015). The role of these PI(3)K inhibitors in secretion (and consequent EV formation) is therefore not clear. Interestingly, in the experiments discussed here, the PI(3)K class III inhibitor SAR405 had no effect on the total number of EVs, suggesting that LY294002 and wortmannin might be acting through a different pathway (i.e. another class of PI(3)K). The literature reports that both wortmannin and LY294002 regulate calcium responses to CCK and TLC-S by inhibiting SERCA (Fischer *et al.*, 2004; Fischer *et al.*, 2007). The direct role of calcium signalling in the LC3-coating of EVs has not been addressed in this thesis and this might represent an interesting future development for the project, in light of the debated role of calcium in regulating autophagy (Bootman *et al.*, 2018) and organelle dynamics (Kiselyov *et al.*, 2012) and the pathogenic role of aberrant calcium signalling in AP (reviewed in (Gerasimenko *et al.*, 2018)).

Interestingly, a significant reduction in the LC3-coating of EVs was observed when PI(3)K and PIKfyve inhibitors were simultaneously applied, suggesting that PI(5)P depletion, when PI(3)P is also depleted, prevents LC3 lipidation. PI(5)P is involved in glucose starvation autophagy when PI(3)P is depleted, e.g. in Vps34 deficient cells (Vicinanza *et al.*, 2015). PI(5)P is generated from PI by class III PI(5)K PIKfyve; this enzyme also produces PI(3,5)P_2 from PI(3)P. Vicinanza *et al* showed a biphasic effect of PIKfyve inhibitor YM201636: whilst low concentrations inhibited the production of PI(5)P from PI, high concentrations accumulated PI(3)P preventing its conversion to PI(3,5)P_2 (Vicinanza *et al.*, 2015). With this in mind, the same low concentration of YM201636 (100 nM) in combination with PI(3)K inhibitors has been employed here, to deplete PI(5)P (and PI(3)P) without replenishing PI(3)P. However, using this

approach it was found that the reduction in LC3-coated EVs was not complete. Interestingly, also in the cited study the effect of wortmannin and YM201636 on reducing autophagosome numbers was not complete (Vicinanza *et al.*, 2015). Recent evidence presented further functions of PIKfyve in organelle trafficking. Targeting either Vps34 or PIKfyve caused aberrant vacuolation, which was rescued by bafilomycin but not by chloroquine, suggesting a pH-independent function of the V-ATPase in the formation of these vacuoles (Compton *et al.*, 2016). Another work revealed that PIKfyve is involved in the maturation of entotic vacuoles, phagosomes and macropinosomes upstream fusion to lysosomes (Krishna *et al.*, 2016). They found that PIKfyve acts through the lysosomal cation channel TRPML1, and highlighted a role for NAADP-dependent calcium signalling in the redistribution of lysosome digested material. These findings indicate that PIKfyve inhibition might affect organelle maturation at multiple stages, not just related to LC3 lipidation. Nonetheless, here YM201636 had no effect on the total number of EVs, indicating that the low concentration used did not affect the steps leading to EV formation. Accordingly, a previous study reported that, while high dose of YM201636 increased basal and stimulated secretion, the low concentration that was used in this work (100 nM) had no effect on secretion (Messenger *et al.*, 2015). Interestingly, the authors found that YM201636 pre-treatment followed by CCK stimulation reduced the number of AVs in PACs (Messenger *et al.*, 2015). The aforementioned works (Messenger *et al.*, 2015; Krishna *et al.*, 2016) utilised both YM201636 and apilimod, an alternative PIKfyve inhibitor, which could also be employed in an extension to the studies presented here to corroborate the experimental findings.

PI(3)P interacts with proteins containing PX, FYVE or WD40 domains, such as WIPI2 (containing a WD domain) and DFCP1 (containing two FYVE domains). It has previously been demonstrated that PI(5)P acts through the same effectors as PI(3)P (Vicinanza *et al.*, 2015). Correlative immunofluorescence experiments for WIPI2 (and PI(3)P) were attempted but did not indicate co-localisation with GFP-LC3 (not shown). Since recruitment of a 2xFYVE domain during non-canonical LC3 lipidation was not observed (Florey *et al.*, 2015), and considering the PI(3)K-independence of the phenomenon described in this chapter, this was not pursued further. Nevertheless, in light of the essential role of PIs in membrane dynamics (Schink *et al.*, 2016), a detailed characterisation of the PI composition of the EVs is desirable. The use of reporter constructs for PI-binding domains might represent a potential tool for such investigations.

Rab GTPases are also essential for membrane trafficking (Stenmark, 2009). Rab3D, Rab4 and Rab27 have been implicated in ZG secretion in PACs (Ohnishi *et al.*, 1999; Chen *et al.*, 2002; Riedel *et al.*, 2002; Hou *et al.*, 2015; Hou *et al.*, 2016). In a recent study, Rab7 was found to have a role in both starvation and pancreatitis-induced autophagy in PACs (Takahashi *et al.*, 2017). The pancreas-specific Rab7 deletion impaired both autophagic flux and the endocytic pathway. Furthermore, Rab5 and Rab11a have been implicated in endosome maturation in PACs (Messenger *et al.*, 2015). It would therefore be interesting to address a potential role for Rab proteins in the maturation of EVs and their interaction with AVs.

The CLEM experiments presented in this chapter revealed that LC3-coated EVs have single membrane, consistent with the hypothesis that this process involves non-

canonical LC3 lipidation. In the cell samples it was possible to distinguish double-membrane organelles, indicating that also canonical autophagy is triggered by inducers of AP, and confirming that the experimental approach employed had the resolution capabilities to detect double-membrane bound organelles. It is plausible that the detection of single-membrane structures occurred because by the time the samples had been fixed, fusion with the lysosomes and degradation of the inner membrane had already occurred. Partial co-localisation of EVs and lysosomal marker LAMP1 has previously been reported (Sherwood *et al.*, 2007). In correlative immunofluorescence experiments, LAMP1 co-localisation was observed on ~7% of the examined LC3-coated EVs, indicating that only a small proportion of these organelles had already fused with lysosomes. The time elapsed before sample fixation is comparable between immunofluorescence and CLEM protocols. Hence, in the CLEM samples only a very small proportion of LC3-coated EVs would have been expected to have fused with lysosomes and lost their putative double membrane. Yet, single membranes were observed in all the LC3-coated EVs from CLEM experiments. Amphisomes, organelles deriving from the fusion of endosomes and autophagosomes, also have single membrane (Gordon & Seglen, 1988). However, it seems unlikely that the LC3-coated EVs reported here represent amphisomes, primarily because no effect of canonical autophagy inhibitors was observed on the formation of these organelles. In addition, amphisomes express endosomal markers such as EEA1 (Berg *et al.*, 1998), whilst such markers have not been found on EVs (Sherwood *et al.*, 2007).

Ultrastructural analysis of HRP-incorporating endocytic organelles fused to AVs in PACs had been performed previously (Tooze *et al.*, 1990), however, their EM sections provide no clear examples of double membranes. Resolution limits also preclude the appreciation of double membranes in other studies in the pancreatitis field (Hashimoto *et al.*, 2008; Mareninova *et al.*, 2009). The double membrane structures resolved here have an intermembrane space of 24.4 ± 1.2 nm. This is in line with the 20-50 nm range specified for the lamellar spacing (i.e. the distance between lipid bilayers) in phagophores, isolation membranes, mature autophagosomes (Nguyen *et al.*, 2017). Researchers in the field stress the importance in distinguishing lipid bilayers from intermembrane space in EM images, dictated by resolution limits (Eskelinen & Kovacs, 2011). Whilst a lipid bilayer appears as a single membrane at low resolution, at higher resolution it will appear as a double laminar structure. Conversely, what appears as a double membrane at low resolution, will appear as two bilaminar structures. The thickness of each bilayer (6-7 nm) in a double-membrane autophagosome is lower than the single lysosomal bilayer (9-10 nm) (Eskelinen & Kovacs, 2011). A distance of approximately 25 nm measured in my experimental samples studies is likely to represent intermembrane space rather than a bilayer, and this provides confidence in the classification of single- and double-membrane organelles.

Only limited co-localisation of V-ATPase and GFP-LC3 was observed. Calcium-releasing agonists (caerulein, carbachol and thapsigargin) induce translocation of V-ATPase E subunit (part of the V1 domain) to membranes, suggesting activation of V-ATPase (Waterford *et al.*, 2005). In this thesis, an antibody for the a1 subunit of the

V0 domain, which is transmembrane and therefore does not depend on activation/assembly with the V1 domain (Gorelick *et al.*, 2006), was used. Of note, bafilomycin and concanamycin bind to the c subunit of the V0 domain (Gorelick *et al.*, 2006). Relevant examples of immunofluorescence staining for this enzyme in PACs are lacking and therefore it is currently not possible to compare the distribution observed here with a reference sample. The experiments presented in this chapter indicate that the role of V-ATPase in the LC3-coating of EVs is related to its catalytic activity, because disrupting acidic pH prevents this process. As mentioned, in other non-canonical autophagy processes the V-ATPase appears to have an acidification-independent function, rather related to recruiting LC3 to membranes (Florey *et al.*, 2015; Gao *et al.*, 2016; Jacquin *et al.*, 2017). V-ATPase-dependent LC3 lipidation on Golgi-derived membranes was demonstrated by the co-localisation of LC3 with Golgi network markers (Gao *et al.*, 2016). Classical (i.e. starvation-induced) autophagosomes generally form from the ER (Axe *et al.*, 2008). However, other membranes can originate autophagosomes (reviewed in (Mari *et al.*, 2011)). This thesis has not investigated co-localisation with Golgi, ER, or other membrane markers on EVs, which represents a logical development for the study.

ATG5 is recruited on macroendocytic vacuoles undergoing non-canonical LC3 lipidation (Florey *et al.*, 2015). In correlative immunofluorescence experiments, no clear co-localisation of ATG5 with GFP-LC3 was observed. Unfortunately, no examples in the literature could be found to compare with the staining pattern I generated for ATG5 in PACs. ATG5-ATG12 is essential for E3-like enzymatic activity (Hanada *et al.*, 2007), while ATG16L1 is essential for targeting the ATG5-ATG12-

ATG16L1 complex to membranes (Fujita *et al.*, 2008). Hence, the presence of ATG16L1 is sufficient to indicate that the ATG5-ATG12-ATG16L1 lipidation machinery is involved in LC3 lipidation. The ATG16L1 correlative immunofluorescence experiments provided clear indication of ATG16L1 co-localisation with GFP-LC3 organelles, both endocytic and non-endocytic. This result led to the conclusion that ATG16L1 is recruited at both endocytic and non-endocytic LC3-positive organelles in PACs. A recent study reports that STX2 depletion induced by experimental pancreatitis, or *STX2* KO, promote autophagy and trypsinogen activation (Dolai *et al.*, 2018). The authors found that STX2 interacts with ATG16L1, preventing its binding to clathrin heavy chain 1, an early step in the formation of pre-autophagosomal structures. Their results support a role for ATG16L1 in PAC responses to AP stimuli. Another study showed that a complex of VMP1-Beclin1-Vps34 favours the interaction of ATG16L1 and LC3 on autophagosomal membranes in PACs (Molejon *et al.*, 2013), again indicating that ATG16L1 is involved in AP-induced autophagy.

Atg5 KO mice have reduced autophagy and reduced trypsinogen activation in AP (Hashimoto *et al.*, 2008), and so do *Atg5* knock-down PACs (Mareninova *et al.*, 2009). This study attempted to perform inducible conditional KO of *Atg5*, but encountered two major difficulties: firstly, the tamoxifen administration protocol for $CreER^T$ activation only worked in ~45% of the attempts, and secondly, the successful KO of *Atg5* determined a reduction in pancreas size which precluded the isolation of PACs to perform experiments. Gukovskaya's group successfully obtained siRNA-mediated knock-down of *Atg5* in murine PACs (Mareninova *et al.*, 2009). However, because a single cell analysis of a "yes-or-no" phenomenon (i.e. LC3-coating or no LC3-coating)

is required for my experiments, the knock-down approach would require an extra step to verify ATG5 expression in each individual cell, which might preclude clear outcomes. Therefore, a KO approach is desirable. Yamamura's group exploited a conditional *Atg5* KO model, with Cre recombinase expressed under *elastase* promoter (*EL-Cre2*) and not requiring activation by tamoxifen (Hashimoto *et al.*, 2008). They did not report size anomalies in the pancreata of *Atg5*$^{flox/flox}$*;ELCre2* mice. Algul's group studied two models of *Atg5* KO: a conditional Cre^{ex1}-mediated KO under the *Ptf1* promoter (referred to as *A5*), and an inducible conditional CreER^{T}-mediated KO (similar to that attempted in this study) under the *elastase* promoter (referred to as *Ela-Cre;A5*) (Diakopoulos *et al.*, 2015). They found that the *A5* pancreata were oedematous and enlarged at 4 weeks, and became atrophic with age. These animals developed features of CP, with increased vacuolation and other histological parameters. Conversely, they found that *Atg5* KO induction in adult age in *Ela-Cre;A5* mice had less impact on vacuolation and inflammation. Diakopoulos *et al* did not find a reduction in size of the pancreas in tamoxifen-treated *Ela-Cre;A5* mice. In our *Atg5* KO mice, the ATG5/calnexin ratio was ~37% of control, indicating that recombination had occurred in approximately 63% of the cells, proving a similar yield as the ~70% previously reported (Diakopoulos *et al.*, 2015). I decided to quantify ATG5 expression normalised to a calnexin loading control. In fact, it was noticed that despite performing BCA assays in order to load the same amount of protein per each lane (as described in Section 2.12), the lysates from the mice with small pancreata presented lower calnexin expression. It is conceivable that this indicates loss of acinar cells (e.g. as a result of acinar-ductal metaplasia) in the *Atg5* KO mice. In fact, PACs have a highly developed RER and are thus expected to express more calnexin. I therefore

feel that calnexin represents an appropriate normalisation factor to represent the acinar component in my pancreatic tissue lysates. I intend to perform histological analyses of these samples to assess damage of the acinar cells in the small *Atg5* KO pancreata, comparing them to control and normal *Atg5* "unsuccessful KO" pancreata. Notably, a significant reduction in wet weight was reported for the pancreas of a newly developed model: *Atg5*$^{-/-}$*;NSE-Atg5* mice (*Atg5* KO mice expressing ATG5 in neurons, preventing neonatal lethality) (Yoshii *et al.*, 2016). However, the pancreas/body weight ratio was not significantly lower, since the *Atg5*$^{-/-}$*;NSE-Atg5* mice were smaller than controls. This mouse model might represent a suitable alternative for our experiments. Acinar (and islet) cell degeneration was also observed in another recently developed model, of *Atg5*-shRNA (Cassidy *et al.*, 2018). In these mice, *Atg5* knock-down is induced by doxycycline in all tissues but the brain. The authors mainly focused on the hepatic phenotype of the inducible knock-down, however this model might represent another interesting system to investigate the role of ATG5 in PAC function.

This study obtained pharmacological and structural evidence that LC3 lipidation of EVs occurs by a non-canonical autophagy mechanism. E230 mice provide a convenient tool to distinguish canonical from non-canonical autophagy. This strain carries a deletion in ATG16L1 at position E230, removing the C-terminal WD40 domain required for LC3 targeting to membranes in non-canonical, but not in canonical, autophagy (Dooley *et al.*, 2014; Fletcher *et al.*, 2018). A significant, but unexpectedly not complete, reduction of LC3-coated EVs was found in E230 mice. In line with my non-canonical autophagy hypothesis, I expected to find no LC3-coated

EVs in this model. If my hypothesis was wrong (i.e. this process depends on canonical autophagy), I would have predicted no difference from WT mice. It is conceivable that the mechanism is redundant, and depends on both a canonical and a non-canonical component. However, a canonical component is not consistent with finding that bafilomycin completely inhibited the LC3-lipidation on EVs. At this stage, I can only speculate that canonical autophagy might be involved in LC3-coating of EVs as a compensatory adaptation occurred in E230 mice, deficient for non-canonical autophagy. To test this hypothesis, I would need to perform further experiments on these animals, and assess whether autophagy inhibitors completely deplete the LC3-coated EVs in E230 mice.

I also take into account that, differently from the experiments performed in GFP-LC3 mice, where LC3B is tagged by GFP, in this set of experiments I used adenoviral vectors to overexpress LC3A (tagged by mCherry or eYFP). It is conceivable that LC3B and LC3A are involved in different processes, since LC3 family proteins can have different subcellular distributions and functions (Weidberg *et al.*, 2010; Koukourakis *et al.*, 2015; Schaaf *et al.*, 2016). Importantly, I am also aware that viruses and autophagy have a complex interaction: autophagy can act as a protective but also as a pro-viral mechanism, and viruses can induce or impair autophagy (Kudchodkar & Levine, 2009; Shoji-Kawata & Levine, 2009; Lennemann & Coyne, 2015). It is thus conceivable that autophagy is altered in adenoviral vector transfected cells. Accordingly, we have planned the breeding of GFP-LC3 with E230 mice to investigate this phenomenon further.

This project found that LC3 lipidation occurs on some, but not all, the EVs. This suggests that a selective targeting mechanism is involved. In zymophagy, ZGs are targeted for autophagy by VMP1 (Vaccaro, 2012). Since VMP1 acts through the PI(3)K complex (Ropolo *et al.*, 2007; Molejon *et al.*, 2013), it was speculated that this might not be the mechanism occurring in our non-canonical PI(3)K-independent LC3 lipidation; hence, the co-localisation of VMP1 with LC3-coated EVs was not examined in this thesis. SQSTM1/p62 is a marker for selective autophagy, recruiting LC3 to ubiquitinated substrates to facilitate their degradation through autophagy (Pankiv *et al.*, 2007). Indeed, p62 degradation is often quantified for monitoring autophagy (Klionsky *et al.*, 2016). In AP, p62 is accumulated, indicating defective degradation due to impaired autophagic flux (Mareninova *et al.*, 2015). This thesis did not examine the presence of p62 on EVs, based on evidence of no co-localisation between p62 and LC3-lipidated entotic vacuoles (Florey *et al.*, 2015), indicating that p62 is not involved in non-canonical autophagy.

Recent studies have reported autophagosome targeting via recognition of LGALS3/galectin-3 (Maejima *et al.*, 2013) or LGALS8/galectin-8 (Falcon *et al.*, 2018; Jia *et al.*, 2018). Galectins recognise glycans and glycoproteins on the extracellular leaflet of the plasma membrane and the luminal leaflet of intracellular organelles; they can therefore sense glycans on vesicles incorporating pathogens (Falcon *et al.*, 2018) and reveal access to luminal glycoproteins of damaged endo-lysosomal organelles (Maejima *et al.*, 2013). Our research group recently reported that EVs can undergo rupture (Chvanov *et al.*, 2018). It is therefore possible that these organelles are targeted for autophagy by a similar mechanism, and future work should therefore

investigate the co-localisation with galectins. So far galectins have not been implicated in non-canonical LC3 lipidation. In drug-induced non-canonical autophagy, no co-localisation between galectin-3 and LC3 was observed (Jacquin *et al.*, 2017). Galectin-8 interacts with the autophagy receptor protein CALCOCO2/NDP52 (Falcon *et al.*, 2018). In non-canonical autophagy, no co-localisation of NDP52 and LC3 was found on entotic vacuoles (Florey *et al.*, 2015).

In summary, the findings presented in this chapter indicate that EVs are coated by LC3 through an ULK1-independent, PI(3)K-independent, ATG5-ATG12-ATG16L1-dependent process. The LC3-coated EVs have single membrane and it was therefore concluded that this represents a non-canonical autophagic pathway. Thus, in addition to previous evidence that (canonical) autophagy activation/disruption is implicated in AP, this thesis revealed that a non-canonical autophagic pathway is involved in interaction with EVs. Notably, these are the organelles where premature zymogen activation occurs. Future work should be directed at elucidating the functional relevance of this LC3 lipidation process, in the context of trypsinogen activation, EV rupture and acinar cell damage in the early stages of AP.

4 Investigating the interaction of endocytic vacuoles and actin

4.1 Introduction

This chapter will investigate the interaction between EVs and F-actin in PACs. F-actin is essential for exocytosis, in many cell types including PACs (Muallem *et al.*, 1995). Furthermore, F-actin is involved in multiple endocytic pathways, such as clathrin-mediated endocytosis (CME), clathrin-independent endocytosis (CIE), phagocytosis, macropinocytosis, circular dorsal ruffles (Girao *et al.*, 2008; Mooren *et al.*, 2012). As described in Section 1.4, actin dynamics are mediated by nucleators (formins and the Arp2/3 complex) promoting filament elongation or branching (Campellone & Welch, 2010), and by interaction with motor proteins (myosins). Arp2/3 is activated by NPFs such as WASP/N-WASP, WAVE, WASH, WHAMM or JMY. Upstream, actin nucleation and actomyosin contractility are regulated by the small GTPases of the Rho family: RhoA, Rac1 and Cdc42 (Hanna & El-Sibai, 2013; Haga & Ridley, 2016).

Figure 4.1 depicts the regulators of F-actin dynamics in endocytic pathways. The role of F-actin in CME has been thoroughly characterised in yeast (Kubler & Riezman, 1993), where it requires the Arp2/3 complex (Moreau *et al.*, 1997), activated by the WASP homologue Las17 (Naqvi *et al.*, 1998). CME is conserved in mammals (Ferguson *et al.*, 2009), where it also involves Arp2/3 and N-WASP (Merrifield *et al.*, 2004), and relies on myosin VI or myosin II (Hasson, 2003; Samaniego *et al.*, 2007; Chandrasekar *et al.*, 2014). CIE processes, such as caveolae endocytosis (Parton *et al.*, 1994), also require F-actin. WASP and Arp2/3 dependent actin dynamics are essential for phagocytosis (Castellano *et al.*, 2001; May & Machesky, 2001). Complement receptor-mediated phagocytosis is also regulated by formins Dia1/2 (Chhabra & Higgs, 2007). N-WASP/WAVE and Arp2/3 mediated actin remodelling is required for

the formation of circular dorsal ruffles (Hoon *et al.*, 2012). Moreover, Rac1-dependent actin reorganization occurs in macropinocytosis, a process extensively documented in *Dictyostelium* (Lee & Knecht, 2002; Swanson, 2008). The actin cytoskeleton not only generates the force for membrane curvature required for the initiation of endocytic events, but it is also involved in endocytic organelle trafficking, maturation and recycling (Durrbach *et al.*, 1996; Merrifield *et al.*, 1999). Endosome movement is dependent on Rho-mediated activation of Dia-related formins (Gasman *et al.*, 2003; Fernandez-Borja *et al.*, 2005; Wallar *et al.*, 2007) and caveolae trafficking along stress fibres is also regulated by mDia1 and RhoA (Echarri & Del Pozo, 2015). In addition, WASH and Arp2/3 mediated actin remodelling is implicated in maturation and recycling of phagosomes and macropinosomes (Carnell *et al.*, 2011; Park *et al.*, 2013; Buckley *et al.*, 2016), in integrin recycling from endosomes to the plasma membrane (Zech *et al.*, 2011) and in endosome fission (Derivery *et al.*, 2009).

The role of F-actin in endocytosis is also shaped by phosphoinositides (PIs). Indeed, the actin cytoskeleton interacts with PIs in several processes. For example, PI(4,5)P_2 is a central regulator of the interaction between plasma membrane and actin cortex (Tsujita & Itoh, 2015). Not only do PIs interact with actin, they can also facilitate F-actin polymerisation/depolymerisation, through recruitment of actin-binding proteins (Takenawa & Itoh, 2001). Specific PI species characterise individual cellular compartments, and therefore processes like endocytosis require modification of PI composition (Posor *et al.*, 2015). Several PI binding proteins involved in endocytic pathways can shape actin dynamics (Schink *et al.*, 2016). For instance, PIs activate WASP proteins (Rohatgi *et al.*, 1999). An additional link between PIs and F-actin in

endocytosis is that PIs are regulated by Rho GTPases: Rac1 is known to increase PI(4,5)P_2 levels (Hartwig *et al.*, 1995), an initiating step for both CME and macropinocytosis (Croise *et al.*, 2014; Posor *et al.*, 2015). PI conversion during endocytosis involves class I PIP(5)Ks and class I PI(3)Ks; these enzymes are also activated by Rho GTPases (Araki *et al.*, 1996; Weernink *et al.*, 2004; Swanson, 2008; Fritsch *et al.*, 2013).

The involvement of F-actin in endocytosis in polarised epithelial cells has been reported and reviewed (Apodaca, 2001). In PACs, it was suggested that actin is involved in compensatory endocytosis following content release from fused ZGs (Valentijn *et al.*, 1999b). We know that ZGs are coated by F-actin after fusion to the plasma membrane, and that EVs are the result of compensatory membrane retrieval. It is therefore logical to enquire whether these organelles retain the actin coat present on ZGs. To address this question, endogenous F-actin was stained in live cells by means of *LifeAct-tagRFP* adenoviral vector or cell permeable probe SiR-Actin, and cell impermeant indicators were used to label EVs. PACs were stimulated with the calcium-releasing agonists CCK and TLC-S and monitored by live cell imaging to investigate the interaction between F-actin and EVs. Actin nucleators and their upstream activators were tested pharmacologically to characterise the mechanism responsible for F-actin dynamics. Immunofluorescence staining was performed to investigate the interaction of EVs with specific actin nucleators and NPFs. Finally, PI kinases were targeted to explore the role of PI-regulated actin dynamics in this process.

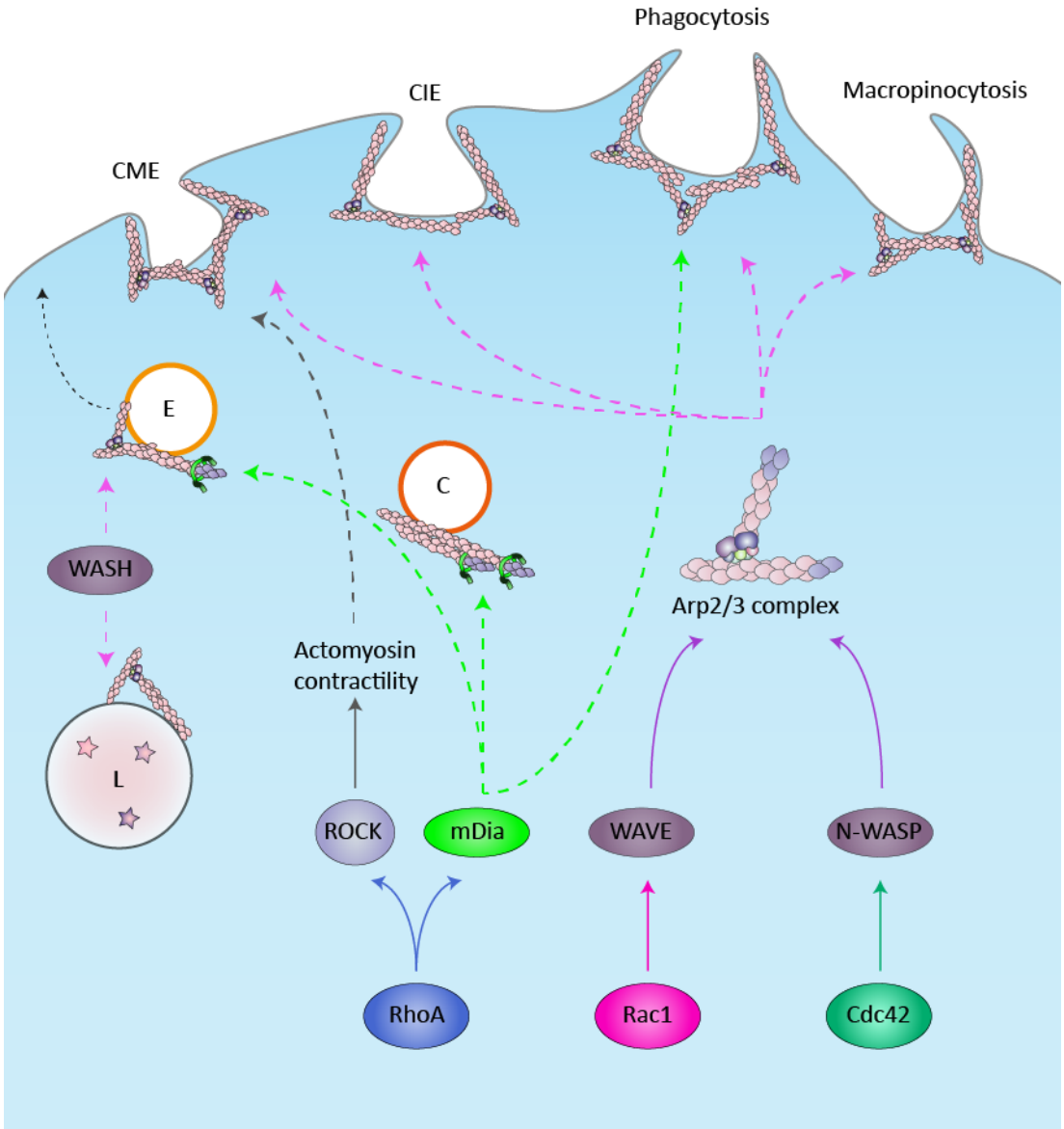

Figure 4.1 Regulation of actin dynamics in endocytic pathways. The schematic summarises F-actin polymerisation and remodelling required for attaining membrane curvature involved in clathrin-mediated endocytosis (CME), clathrin-independent endocytosis (CIE), phagocytosis and macropinocytosis. Filament elongation is mediated by formins (mDia), activated by RhoA. Filament branching is mediated by the Arp2/3 complex, activated by WASH, WAVE and N-WASP; WAVE and N-WASP are activated by Rac1 and Cdc42. RhoA-activated ROCK controls actomyosin contractility, implicated in CME. Formins are required for phagocytosis and for endosome (E) and caveolae (C) trafficking. WASH activity is required for recycling from E and lysosomes (L). Arp2/3 is implicated in CME, CIE, phagocytosis and macropinocytosis.

4.2 Results

4.2.1 Actin filaments coat endocytic vacuoles

The aim of this part of the study was to assess the potential interaction of F-actin and EVs. In *LifeAct-tagRFP* transfected PACs (Section 2.5) stimulated with CCK we found that some EVs were coated by F-Actin, whereas others were not (Figure 4.2). To verify that this result was not an artefact of adenovirus-mediated overexpression, and to bypass the need to culture cells overnight, endogenous F-actin was stained with SiR-Actin (Section 2.6). In SiR-Actin stained PACs stimulated by CCK (Figure 4.3) or TLC-S (Figure 4.4) only some EVs were coated by F-actin, similarly to the phenomenon observed in LifeAct-RFP expressing PACs.

To further characterise this phenomenon, the total number of EVs and the percentage of actin-coated EVs in CCK or TLC-S stimulated cells were evaluated (Figure 4.5). There was no significant difference in the percentage of actin-coated EVs at physiological (10 pM) and supramaximal (10 nM) CCK concentrations. This result indicates that F-actin coats EVs in both physiological and pathological conditions. In 10 pM CCK, 23.2% of 82 analysed EVs were coated by F-actin. In 10 nM CCK, 30.0% of 120 analysed EVs were coated by F-actin. In 200 µM TLC-S, 5.1% of 375 analysed EVs were coated by F-actin.

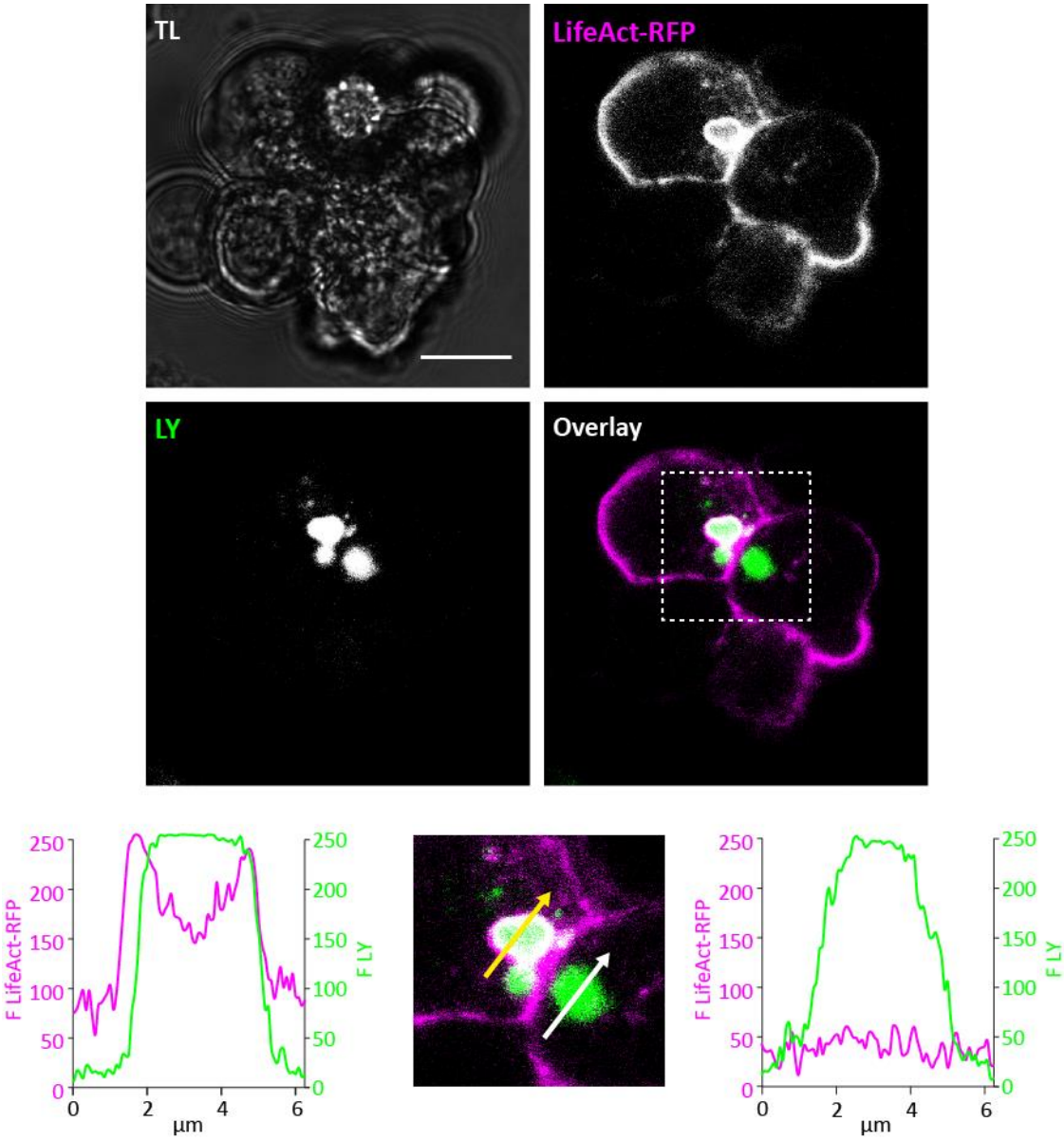

Figure 4.2 Actin-coated and uncoated endocytic vacuoles in CCK-stimulated pancreatic acinar cells. Representative images of LifeAct-RFP (magenta) expressing PACs stimulated with 10 nM CCK in presence of LY (green). The lower panel shows actin-coated and uncoated EVs in an expanded scale. The fluorescence intensity profile of an actin-coated EV, plotted along the yellow arrow, is shown on the left graph. The fluorescence intensity profile of an uncoated EV, plotted along the white arrow, is shown on the right graph. Scale bar = 10 µm.

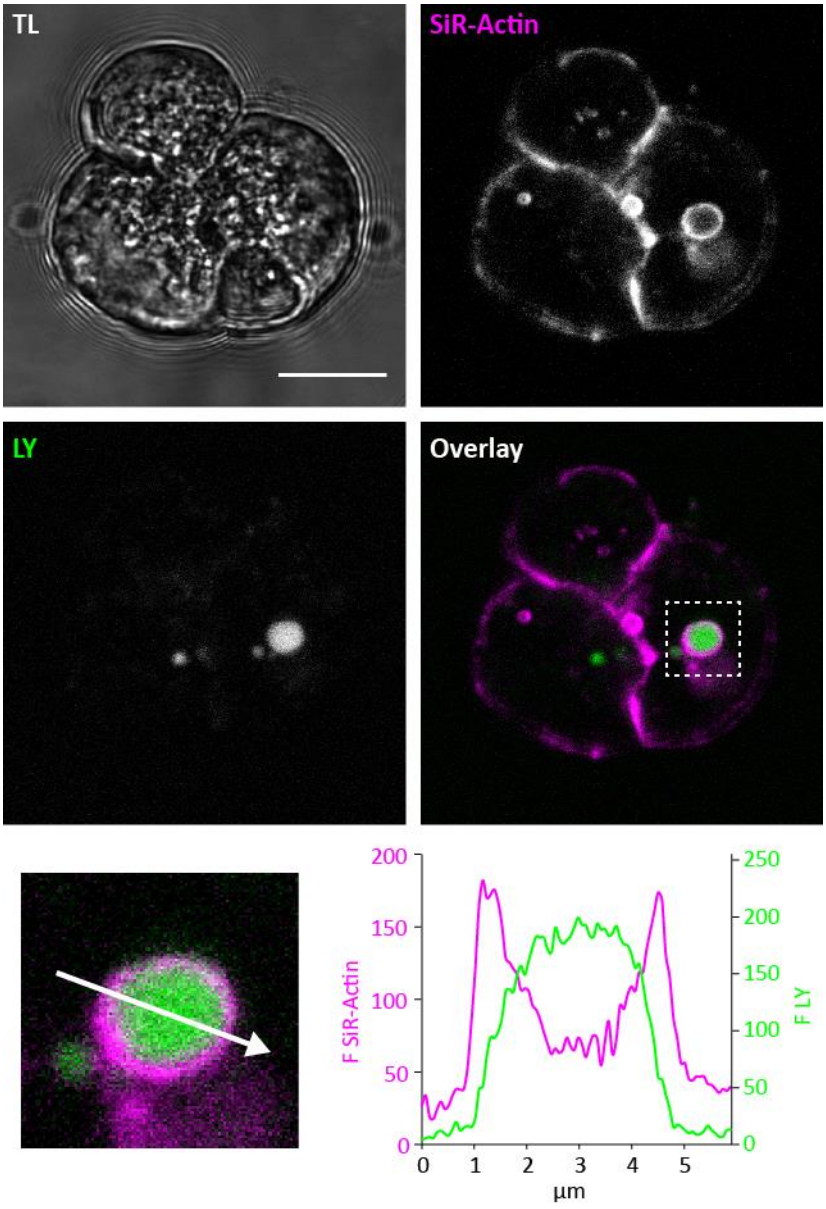

Figure 4.3 Actin-coated endocytic vacuoles in CCK-stimulated pancreatic acinar cells. Representative images of SiR-Actin (magenta) stained PACs stimulated with 10 nM CCK in presence of LY (green). The lower panels show an actin-coated EV in an expanded scale and fluorescence intensity profile plotted along the arrow. Scale bar = 10 µm.

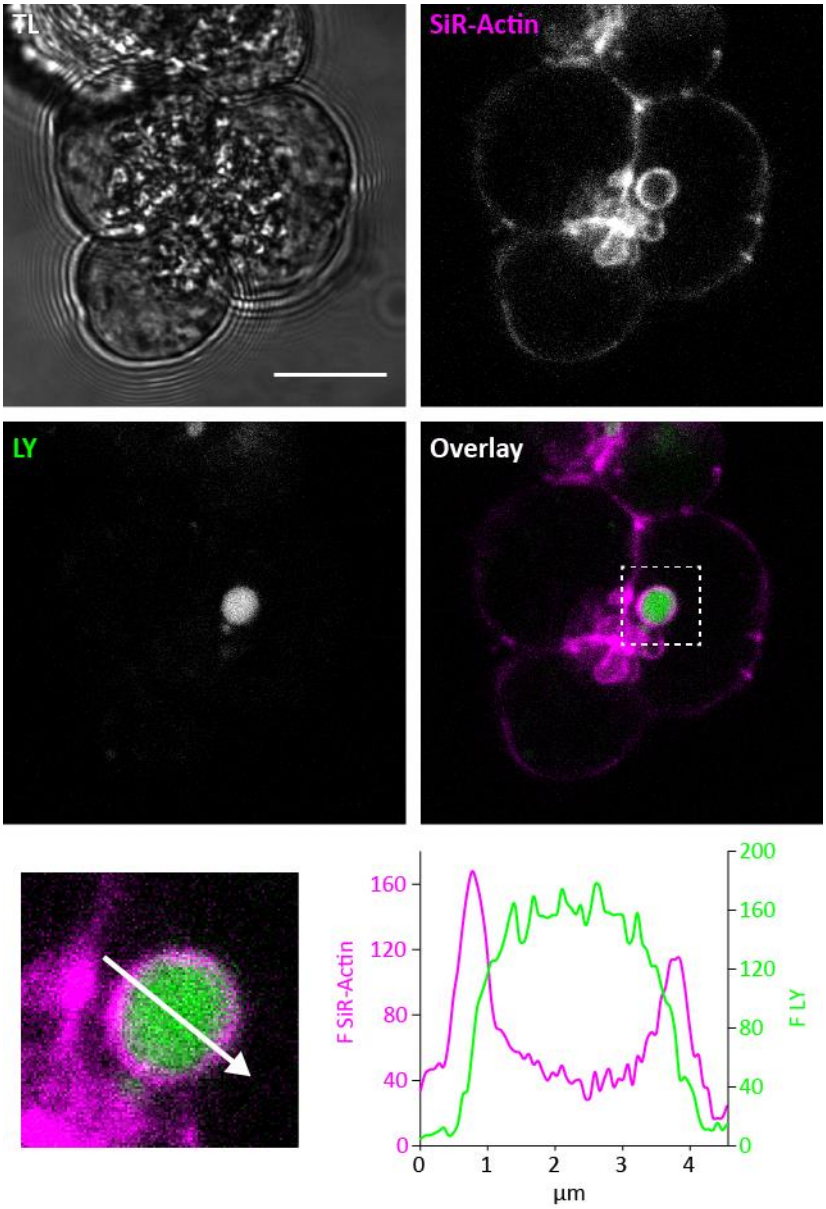

Figure 4.4 Actin-coated endocytic vacuoles in TLC-S-stimulated pancreatic acinar cells. Representative images of SiR-Actin (magenta) stained PACs stimulated with 200 µM TLC-S in presence of LY (green). The lower panels show an actin-coated EV in an expanded scale and fluorescence intensity profile plotted along the arrow. Scale bar = 10 µm.

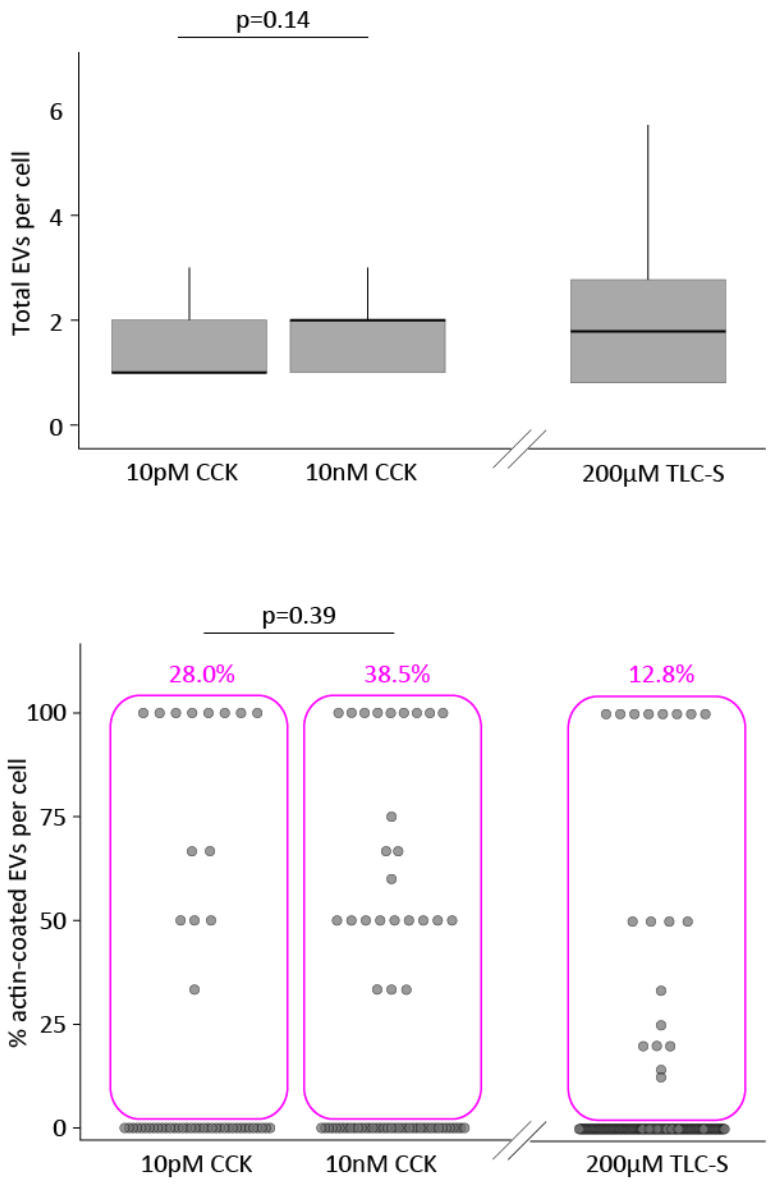

Figure 4.5 Actin-coated endocytic vacuoles in cells stimulated by CCK or TLC-S. The box and whisker plot (top) shows total number of EVs per cell, the dot plot (bottom) shows percentage of actin-coated EVs per cell. In the dot plot, magenta boxes highlight cells with percentage of actin-coated EVs above 0, the percentage of such cells is indicated above. SiR-Actin stained PACs were stimulated for 30 min at 34.5°C with 10 pM (n=50) or 10 nM CCK (n=65); N=3 for both conditions. SiR-Actin stained PACs were stimulated for 20 min at 34.5°C with 200 µM TLC-S (n=149); N=3. Data were compared by Wilcoxon-Mann-Whitney test.

SiR-Actin is structurally related to jasplakinolide, a compound determining stabilisation of F-actin (Bubb *et al.*, 2000). Thus, I decided to verify that the concentration of indicator used for labelling F-actin (1 µM) was not affecting the phenomenon investigated in this study. To this end, jasplakinolide pre-treated cells, then stimulated with CCK (in continuous presence of jasplakinolide), were compared to CCK control. To stain F-actin in these experiments, cells were transfected with *LifeAct-tagRFP*, since jasplakinolide would compete for the same binding sites as SiR-Actin. In 10 nM CCK stimulated PACs, 1 µM jasplakinolide had no effect on the total number of EVs nor on the percentage of actin-coated EVs (Figure 4.6). This result made me confident that 1 µM SiR-Actin would be a suitable tool for F-actin staining, without affecting the phenomenon I wanted to study.

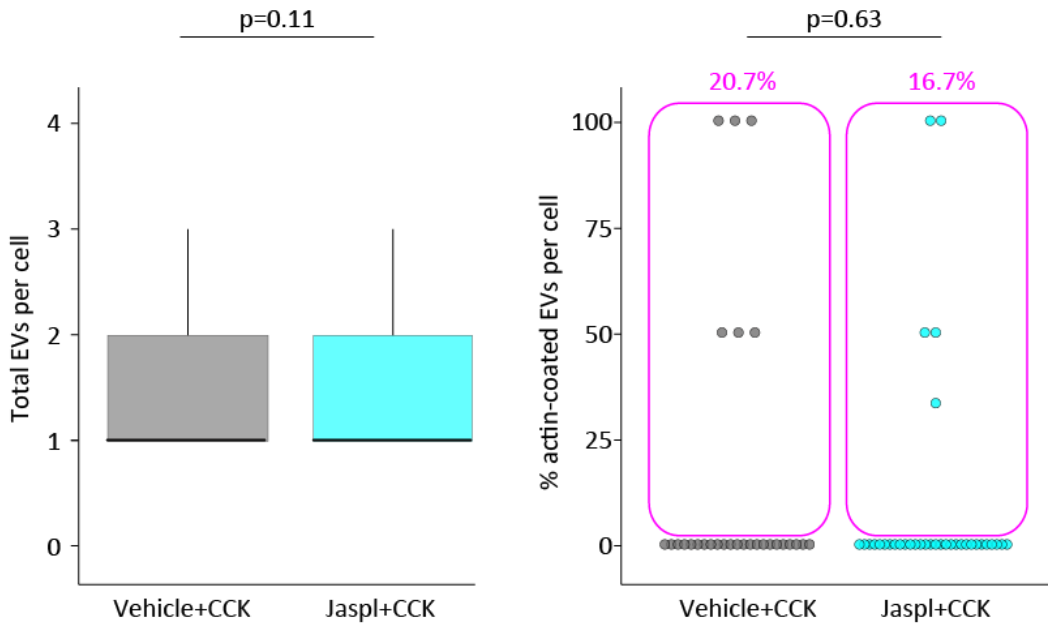

Figure 4.6 Effect of jasplakinolide on actin-coating of endocytic vacuoles. The box and whisker plot (left) shows total number of EVs per cell, the dot plot (right) shows percentage of actin-coated EVs per cell. In the dot plot, magenta boxes highlight cells with percentage of actin-coated EVs above 0, the percentage of such cells is indicated above. LifeAct-RFP transfected PACs were stimulated with 10 nM CCK for 30 min, after 30 min pre-incubation and in continuous presence of 0.1% DMSO (Vehicle, n=29) or 1 µM jasplakinolide (Jaspl, n=36); N=3 for both conditions. Data were compared by Wilcoxon-Mann-Whitney test.

Next, the investigation enquired on the dynamics of the F-actin interacting with EVs. Actin filaments undergo polymerisation and depolymerisation; the rates of these two processes determine the overall outcome. Latrunculin A shifts this equilibrium towards depolymerisation. PACs were pre-treated with latrunculin A, then stimulated with 10 nM CCK and in continuous presence of latrunculin A, and compared to CCK control. Latrunculin A did not affect the total number of EVs but caused a strong reduction in the percentage of actin-coated EVs (Figure 4.7). Latrunculin A sequesters actin monomers, thus preventing actin polymerisation, but it does not trigger depolymerisation of F-actin. Hence, these results indicate that actin polymerisation is required for actin-coating of EVs. In these experiments, it was noticeable that latrunculin A caused a strong reduction in F-actin staining, which particularly affected basolateral F-actin, whereas apical F-actin appeared to be more resistant (Figure 4.8).

F-actin dynamics also depend on interaction with motor proteins. When SiR-Actin stained PACs were pre-treated with myosin II inhibitor (-)blebbistatin (hereafter referred to as blebbistatin) (Straight *et al.*, 2003), there was no difference in the total number of EVs, but a significant reduction in the percentage of actin-coated EVs compared to CCK control (Figure 4.9). These results indicate that myosin II activity is required for F-actin interaction with EVs.

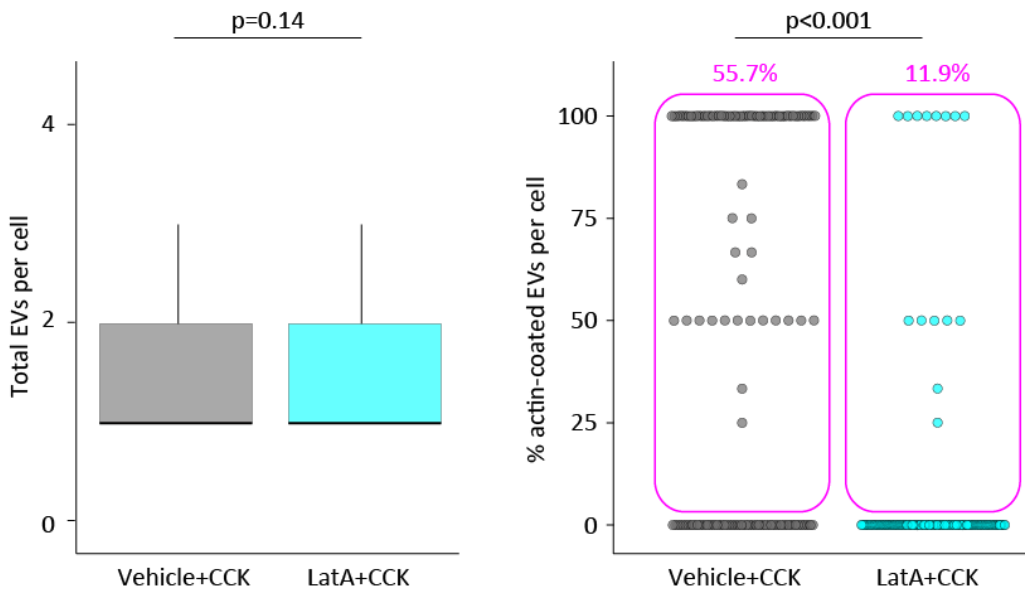

Figure 4.7 Preventing actin polymerisation reduces the actin-coating of endocytic vacuoles. The box and whisker plot (left) shows total number of EVs per cell, the dot plot (right) shows percentage of actin-coated EVs per cell. In the dot plot, magenta boxes highlight cells with percentage of actin-coated EVs above 0, the percentage of such cells is indicated above. LifeAct-RFP transfected PACs were stimulated with 10 nM CCK for 30 min, after 30 min pre-incubation and in continuous presence of 0.1% DMSO (Vehicle, n=131) or 10 µM latrunculin A (Lat A, n=126); N=3 for both conditions. Data were compared by Wilcoxon-Mann-Whitney test.

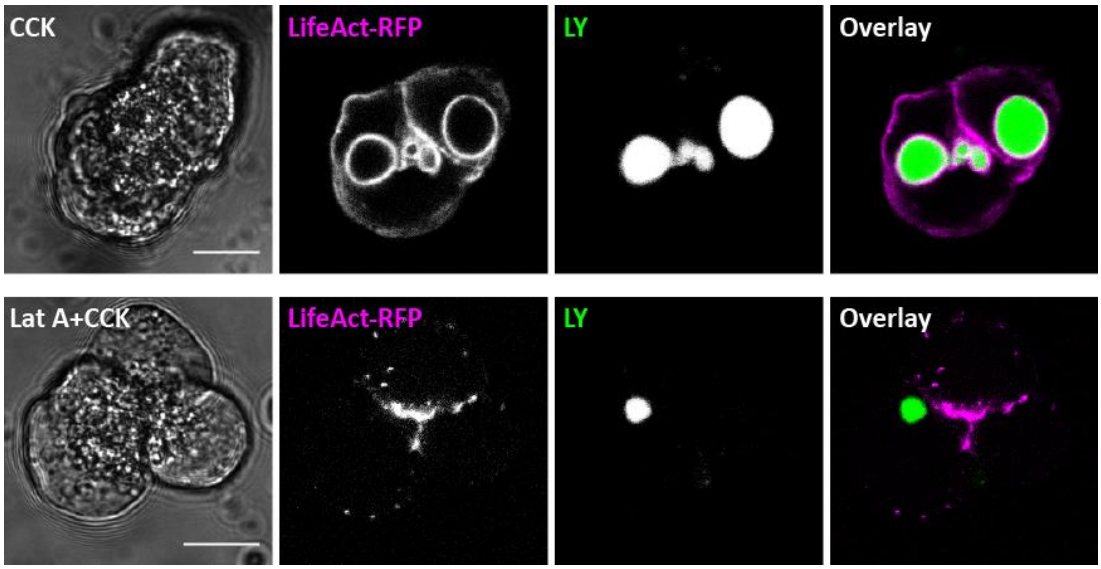

Figure 4.8 Latrunculin A disrupts F-actin. LifeAct-RFP (magenta) expressing PACs were stimulated with 10 nM CCK in presence of LY (green) and in continuous presence of 0.1% DMSO or 10 µM latrunculin A (Lat A). Top panels show control cells, bottom panels show 10 µM Lat A pre-treated cells. Scale bars = 10 µm.

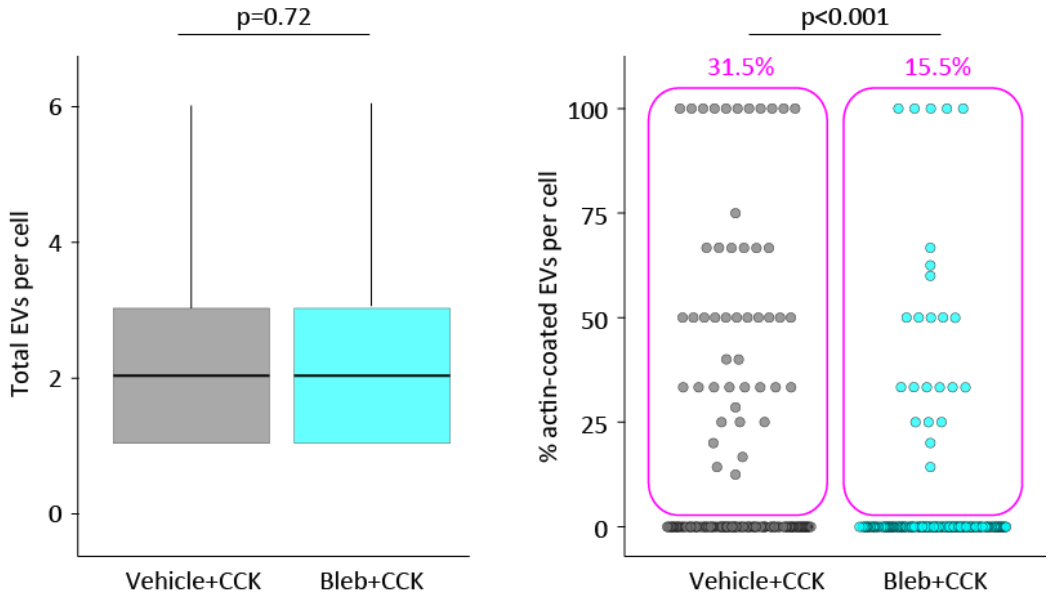

Figure 4.9 Myosin II inhibitor blebbistatin reduces the actin-coating of endocytic vacuoles. The box and whisker plot (left) shows total number of EVs per cell, the dot plot (right) shows percentage of actin-coated EVs per cell. In the dot plot, magenta boxes highlight cells with percentage of actin-coated EVs above 0, the percentage of such cells is indicated above. SiR-Actin stained PACs were stimulated with 10 nM CCK for 30 min, after 30 min pre-incubation and in continuous presence of 0.1% DMSO (Vehicle, n=149) or 30 µM blebbistatin (Bleb, n=155); N=3 for both conditions. Data were compared by Wilcoxon-Mann-Whitney test.

4.2.2 Regulators of actin-coating of endocytic vacuoles

Having established that a dynamic actin cytoskeleton is required for interaction with EVs, it was investigated if, and which, actin nucleators are involved. It was found that the formin inhibitor SMIFH2 (Rizvi *et al.*, 2009) caused a significant reduction in the percentage of actin-coated EVs, without affecting the total number of EVs (Figure 4.10). These results suggest that formins are implicated in actin-coating of EVs.

Correlative immunofluorescence experiments for mDia1 and FMNL2, two formins implicated in endocytic pathways (Fernandez-Borja *et al.*, 2005; Wang *et al.*, 2015) were thus performed. PACs stimulated with 10 nM CCK in presence of FITC dextran were imaged live to find EVs. The cells were then fixed and processed for immunofluorescence staining as described in Section 2.9, and the same cells were identified on the grid. 11 mDia1-coated organelles were correlated to EVs, in n=42 cells from N=2 mice. mDia1 staining appeared to localise along the cortical actin network, in particular at the basolateral membrane (Figure 4.11). Only 2 organelles presenting partial FMNL2 coating were correlated to EVs, in n=24 cells from N=2 mice. FMNL2 staining appeared to localise along the cortical actin network, in particular at the basolateral membrane (Figure 4.12).

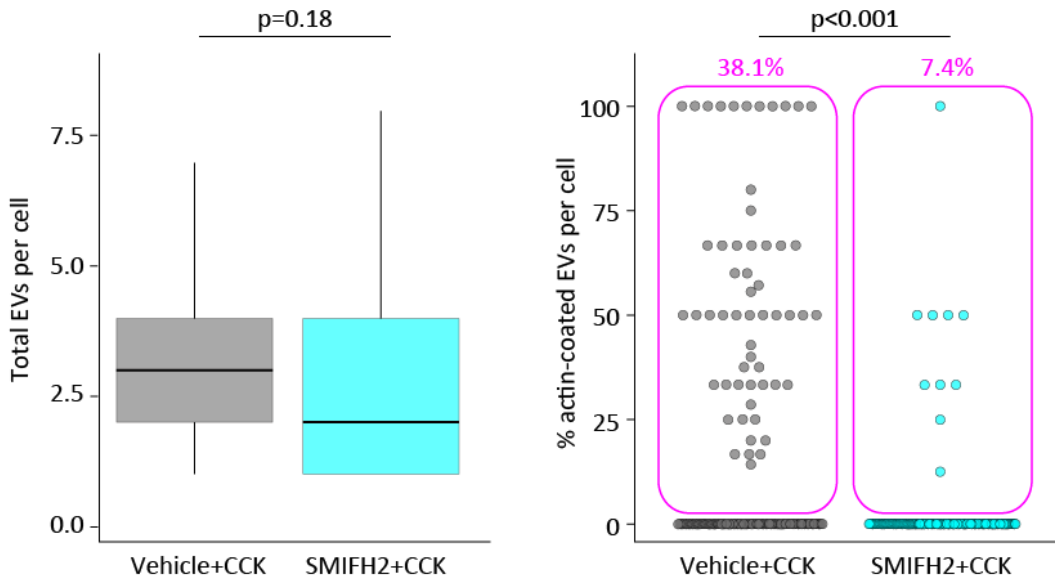

Figure 4.10 Formin inhibitor SMIFH2 reduces the actin-coating of endocytic vacuoles. The box and whisker plot (left) shows total number of EVs per cell, the dot plot (right) shows percentage of actin-coated EVs per cell. In the dot plot, magenta boxes highlight cells with percentage of actin-coated EVs above 0, the percentage of such cells is indicated above. SiR-Actin stained PACs were stimulated with 10 nM CCK for 30 min, after 60 min pre-incubation and in continuous presence of 0.5% DMSO (Vehicle, n=147) or 50 µM SMIFH2 (n=135); N=3 for both conditions. Data were compared by Wilcoxon-Mann-Whitney test.

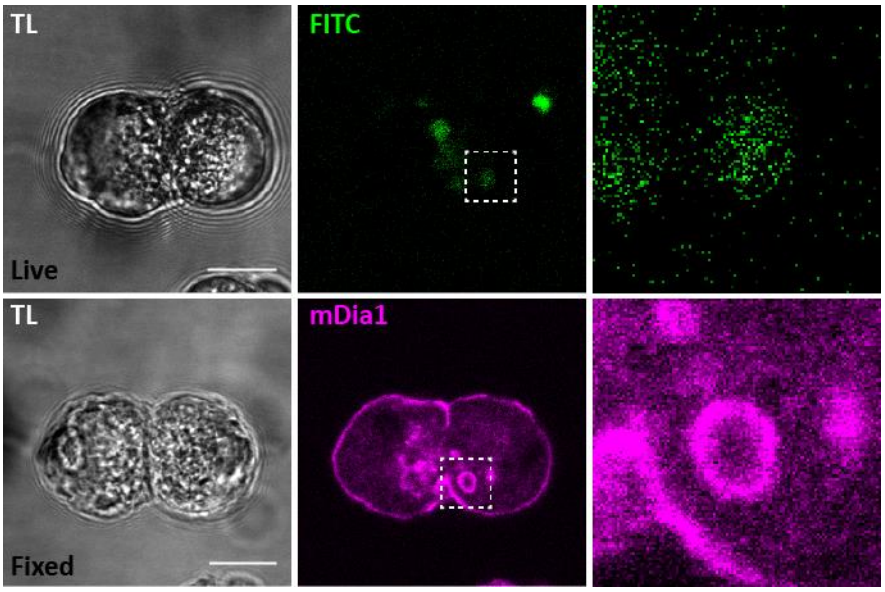

Figure 4.11 Endocytic vacuoles and correlative immunofluorescence for mDia1. PACs were stimulated with 10 nM CCK for 30 min at 34.5°C in presence of FITC dextran (green) and imaged live on gridded dishes. They were then fixed for 10 min in 4% PFA at RT and immunofluorescence staining for mDia1 (magenta) was performed as described in Section 2.9. A correlative image of the same cell live and fixed is shown, with an EV correlated to an mDia1-positive organelle shown in an expanded scale. Scale bars = 10 µm.

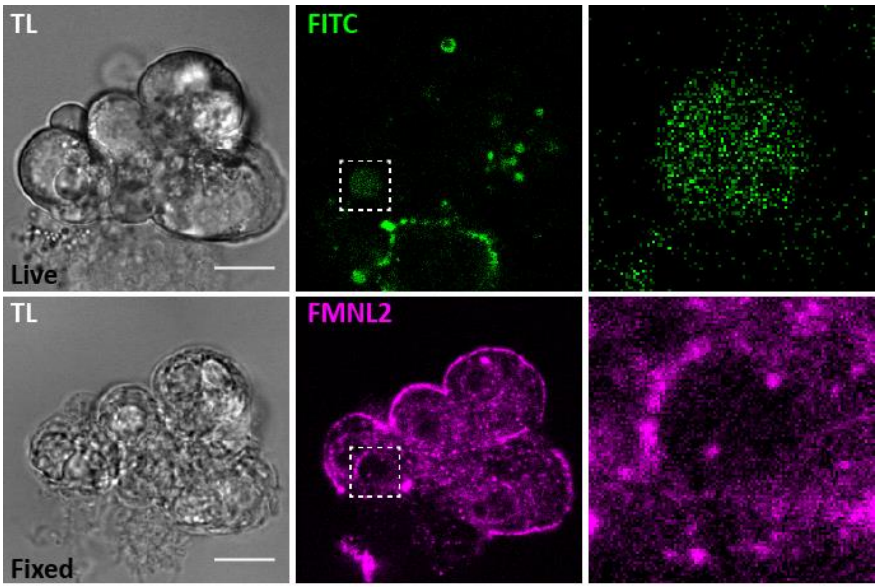

Figure 4.12 Endocytic vacuoles and correlative immunofluorescence for FMNL2. PACs were stimulated with 10 nM CCK for 30 min at 34.5°C in presence of FITC dextran (green) and imaged live on gridded dishes. They were then fixed for 10 min in 4% PFA at RT and immunofluorescence staining for FMNNL2 (magenta) was performed as described in Section 2.9. A correlative image of the same cell live and fixed is shown, with an EV correlated to an FMNL2-positive organelle shown in an expanded scale. Scale bars = 10 µm.

The Arp2/3 complex inhibitors CK-666 and CK-869 (Nolen *et al.*, 2009) caused a significant reduction in both the total number of EVs and the percentage of actin-coated EVs (Figure 4.13). These results suggest that the Arp2/3 complex is implicated in actin-coating of EVs. Correlative immunofluorescence experiments for P34-ARC/ARPC2 (referred to as P34), a subunit of the Arp2/3 complex, were thus performed. PACs stimulated with 10 nM CCK in presence of FITC dextran were imaged live to find EVs. The cells were then fixed and processed for immunofluorescence staining as described in Section 2.9, and the same cells were identified on the grid. 5 P34-coated organelles were correlated to EVs, in n=43 cells from N=2 mice. P34 staining appeared to localise mainly at the apical membrane (Figure 4.14).

Next, the potential interaction of EVs with N-WASP and WASH1, two NPFs activating the Arp2/3 complex and implicated in endocytic pathways (Merrifield *et al.*, 2004; Buckley *et al.*, 2016), was investigated. Correlative immunofluorescence experiments for these proteins were performed as described above. 3 N-WASP-positive organelles were correlated to EVs, in n=22 cells from N=2 mice. N-WASP staining appeared to localise mainly at the apical membrane (Figure 4.15). 3 WASH1-positive organelles were correlated to EVs, in n=32 cells from N=2 mice. WASH1 staining appeared to localise mainly at the apical membrane (Figure 4.16).

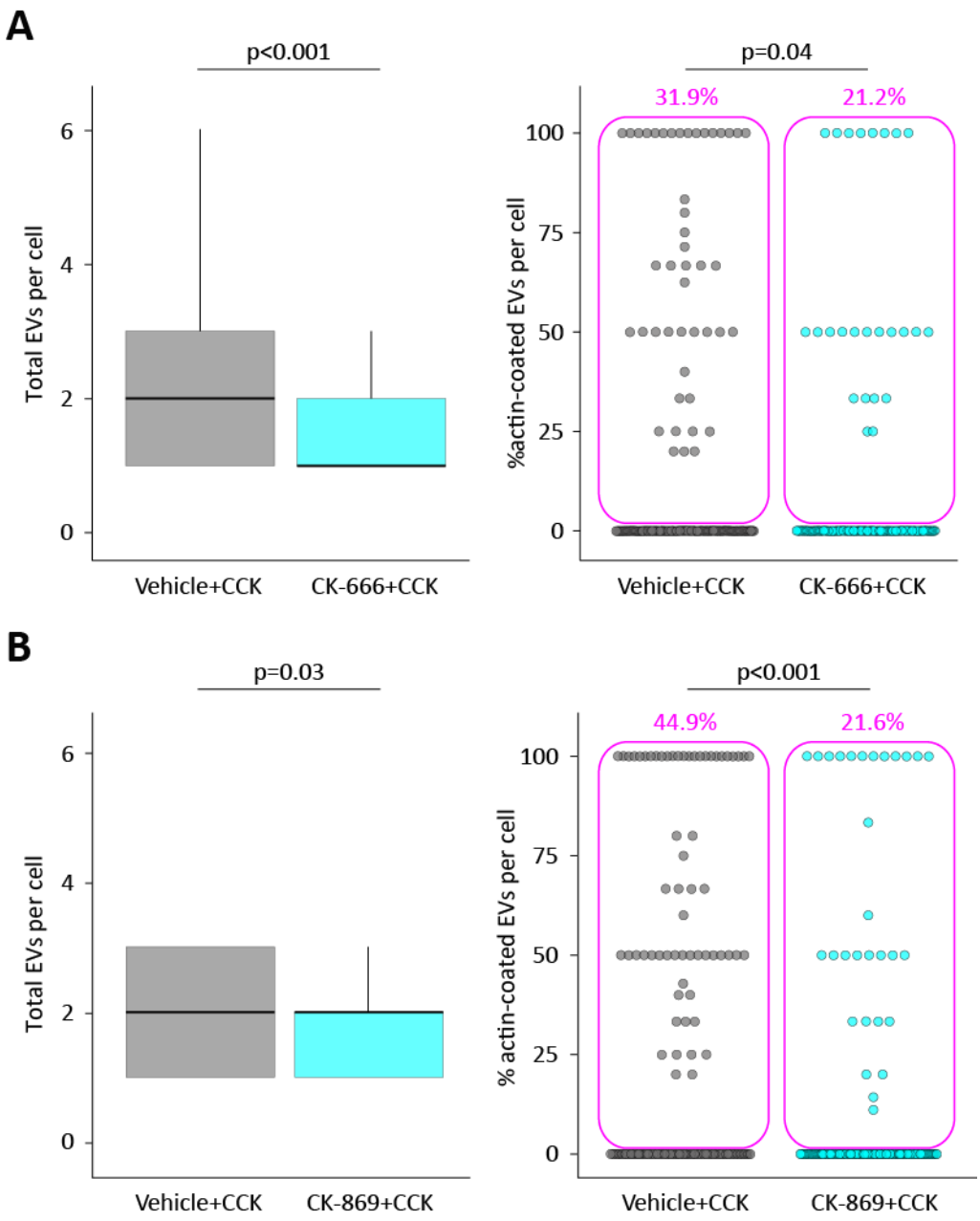

Figure 4.13 Arp2/3 complex inhibitors reduce the formation of endocytic vacuoles and the actin-coating. The box and whisker plots (left) show total number of EVs per cell, the dot plots (right) show percentage of actin-coated EVs per cell. In the dot plots, magenta boxes highlight cells with percentage of actin-coated EVs above 0, the percentage of such cells is indicated above. **A)** SiR-Actin stained PACs were stimulated with 10 nM CCK for 30 min, after 60 min pre-incubation and in continuous presence of 0.5% DMSO (Vehicle, n=141) or 500 µM CK-666 (n=118); N=3 for both conditions. **B)** SiR-Actin stained PACs were stimulated with 10 nM CCK for 30 min, after 60 min pre-incubation and in continuous presence of 0.5% DMSO (Vehicle, n=138) or 250 µM CK-869 (n=139); N=3 for both conditions. Data were compared by Wilcoxon-Mann-Whitney test.

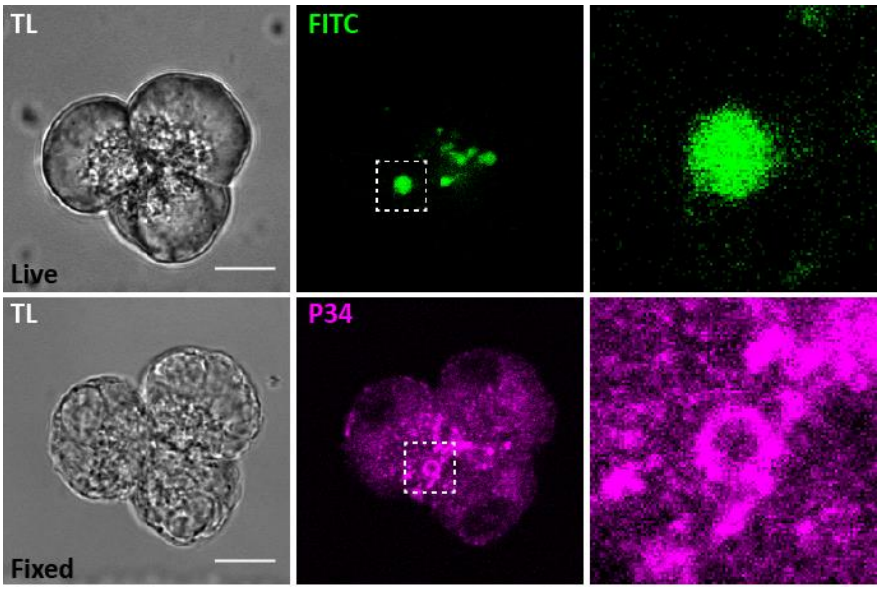

Figure 4.14 Endocytic vacuoles and correlative immunofluorescence for Arp2/3 complex. PACs were stimulated with 10 nM CCK for 30 min at 34.5°C in presence of FITC dextran (green) and imaged live on gridded dishes. They were then fixed for 10 min in 4% PFA at RT and immunofluorescence staining for P34 subunit of the Arp2/3 complex (magenta) was performed as described in Section 2.9. A correlative image of the same cell live and fixed is shown, with an EV correlated to a P34-positive organelle shown in an expanded scale. Scale bars = 10 µm.

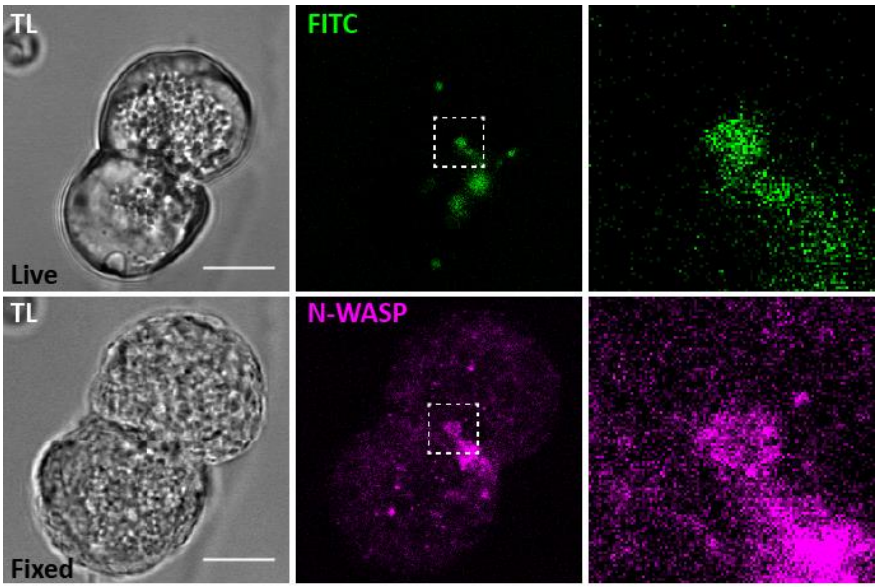

Figure 4.15 Endocytic vacuoles and correlative immunofluorescence for N-WASP. PACs were stimulated with 10 nM CCK for 30 min at 34.5°C in presence of FITC dextran (green) and imaged live on gridded dishes. They were then fixed for 10 min in 4% PFA at RT and immunofluorescence staining for N-WASP (magenta) was performed as described in Section 2.9. A correlative image of the same cell live and fixed is shown, with an EV correlated to an N-WASP-positive organelle shown in an expanded scale. Scale bars = 10 µm.

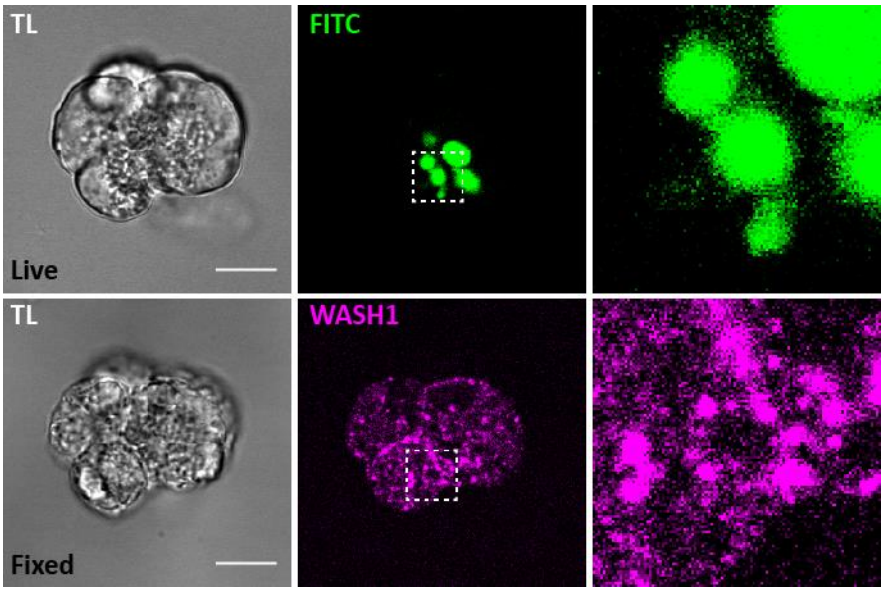

Figure 4.16 Endocytic vacuoles and correlative immunofluorescence for WASH1. PACs were stimulated with 10 nM CCK for 30 min at 34.5°C in presence of FITC dextran (green) and imaged live on gridded dishes. They were then fixed for 10 min in 4% PFA at RT and immunofluorescence staining for WASH1 (magenta) was performed as described in Section 2.9. A correlative image of the same cell live and fixed is shown, with an EV correlated to a WASH1-positive organelle shown in an expanded scale. Scale bars = 10 µm.

Having found that F-actin polymerisation required for coating of EVs is mediated by formins and Arp2/3 complex, the project sought to characterise the upstream regulators of these nucleators. Formins are activated by Rho GTPases (Tominaga *et al.*, 2000). The Rho inhibitor rhosin (Shang *et al.*, 2012) caused a significant reduction in the percentage of actin-coated EVs, without affecting the total number of EVs (Figure 4.17). The effect of Rho inhibition is comparable with the effect observed when inhibiting formins (**Figure 4.10**), consistent with the role of Rho in regulating actin dynamics via formins.

Rho also regulates actin dynamics via ROCK (Sit & Manser, 2011). The ROCK inhibitors Y27632 and GSK429286 did not affect the total number of EVs, but caused a significant reduction in the percentage of actin-coated EVs (Figure 4.18). ROCK controls actomyosin contractility; hence these results are consistent with the effect of the myosin II inhibitor blebbistatin reported earlier (**Figure 4.9**). Collectively these results indicate that Rho, through ROCK and formins, regulates the F-actin dynamics required for coating of EVs.

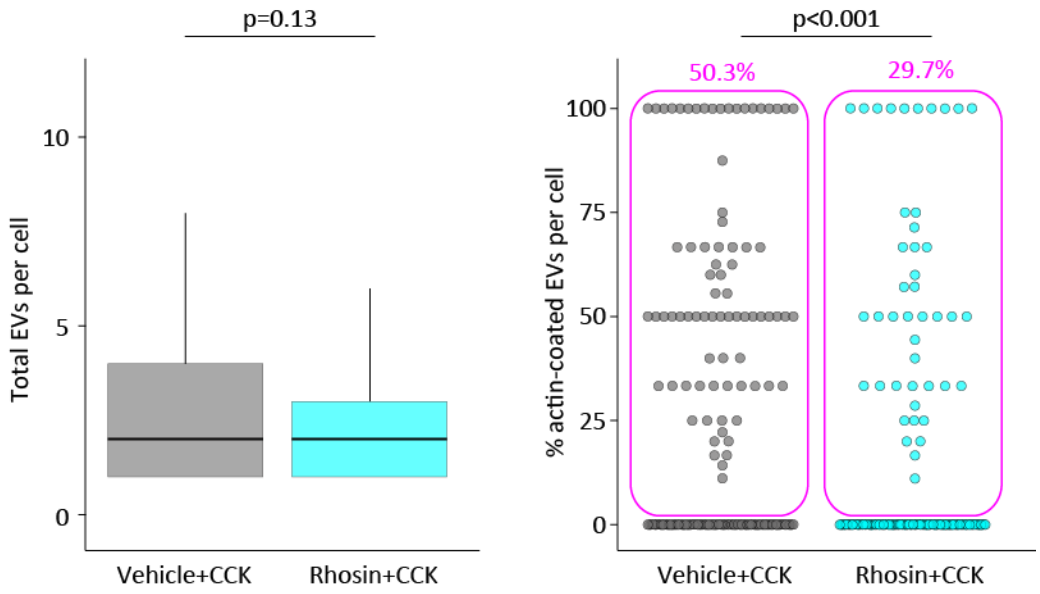

Figure 4.17 Rho inhibitor rhosin reduces the actin-coating of endocytic vacuoles. The box and whisker plot (left) shows total number of EVs per cell, the dot plot (right) shows percentage of actin-coated EVs per cell. In the dot plot, magenta boxes highlight cells with percentage of actin-coated EVs above 0, the percentage of such cells is indicated above. SiR-Actin stained PACs were stimulated with 10 nM CCK for 30 min, after 60 min pre-incubation and in continuous presence of 0.05% DMSO (Vehicle, n=155) or 30 µM rhosin (n=148); N=3 for both conditions. Data were compared by Wilcoxon-Mann-Whitney test.

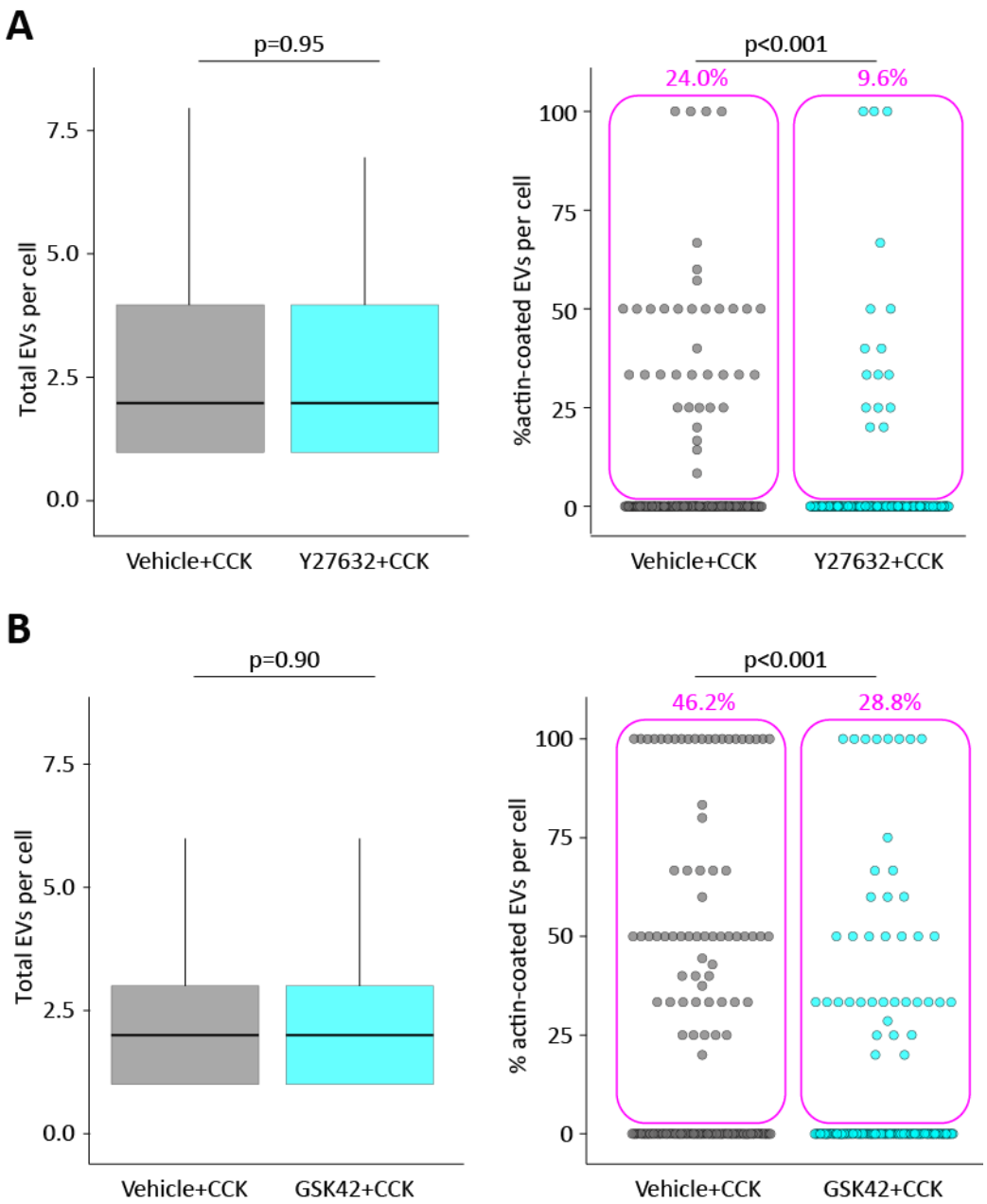

Figure 4.18 ROCK inhibitors reduce the actin-coating of endocytic vacuoles. The box and whisker plots (left) show total number of EVs per cell, the dot plots (right) show percentage of actin-coated EVs per cell. In the dot plots, magenta boxes highlight cells with percentage of actin-coated EVs above 0, the percentage of such cells is indicated above. **A)** SiR-Actin stained PACs were stimulated with 10 nM CCK for 30 min, after 60 min pre-incubation and in continuous presence of 0.1% DMSO (Vehicle, n=154) or 50 µM Y27632 (n=167); N=3 for both conditions. **B)** SiR-Actin stained PACs were stimulated with 10 nM CCK for 30 min, after 60 min pre-incubation and in continuous presence of 0.1% DMSO (Vehicle, n=145) or 10 µM GSK429286 (GSK42, n=139); N=3 for both conditions. Data were compared by Wilcoxon-Mann-Whitney test.

NPFs responsible for Arp2/3 complex activation are regulated by Rac1 and Cdc42 GTPases (Sit & Manser, 2011). Firstly, a Rac1/Cdc42 dual inhibitor, Aza1, which has no effect on Rho (Zins *et al.*, 2013), was tested. Aza1 caused a significant reduction in both the total number of EVs and the percentage of actin-coated EVs (Figure 4.19). Next the specific involvement of Rac1 and/or Cdc42 was probed. Rac1 inhibitor II had no effect on the total number of EVs or the percentage of actin-coated EVs (Figure 4.20). Conversely, the Cdc42 inhibitor ML141 (Hong *et al.*, 2013) significantly reduced the percentage of actin-coated EVs, not affecting the total number of EVs (Figure 4.21). Based on these results, it was concluded that F-actin dynamics involved in interaction with EVs are regulated by Rho and Cdc42, but not by Rac1.

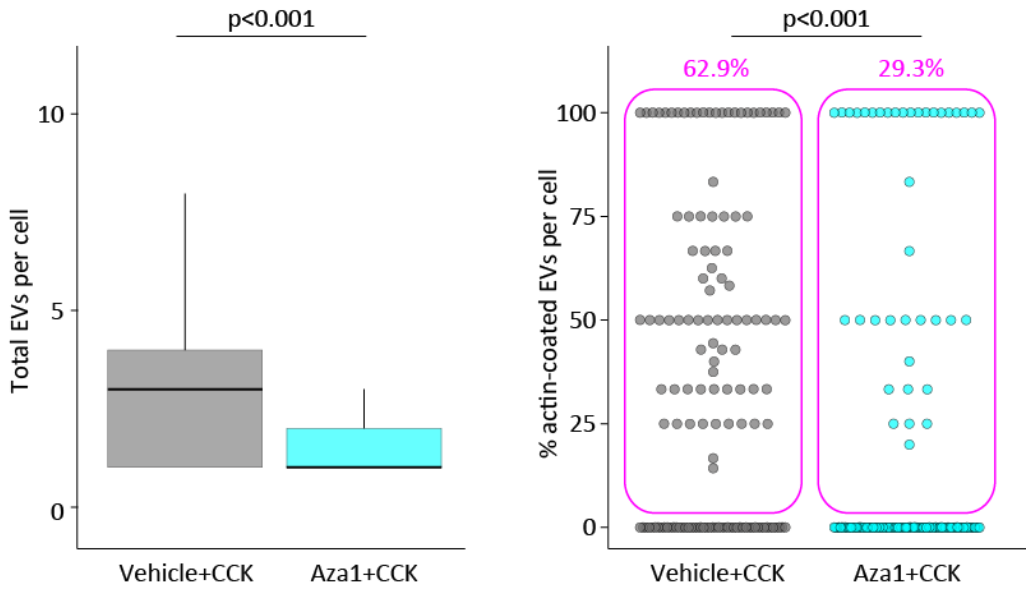

Figure 4.19 Rac1/Cdc42 dual inhibitor Aza1 reduces the actin-coating of endocytic vacuoles. The box and whisker plot (left) shows total number of EVs per cell, the dot plot (right) shows percentage of actin-coated EVs per cell. In the dot plot, magenta boxes highlight cells with percentage of actin-coated EVs above 0, the percentage of such cells is indicated above. SiR-Actin stained PACs were stimulated with 10 nM CCK for 30 min, after 60 min pre-incubation and in continuous presence of 1% DMSO (Vehicle, n=132) or 60 µM Aza1 (n=133); N=3 for both conditions. Data were compared by Wilcoxon-Mann-Whitney test.

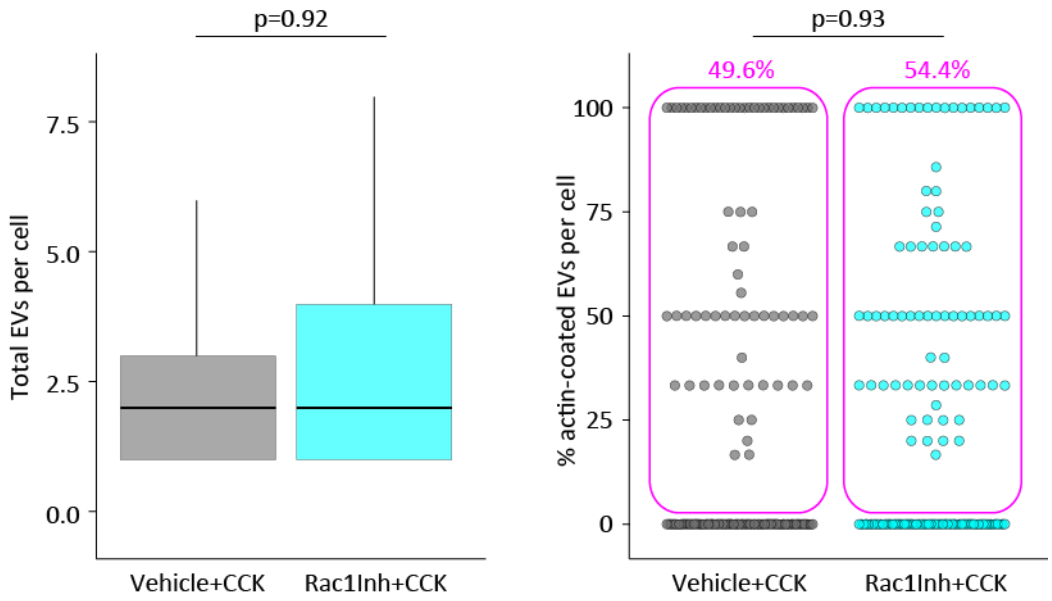

Figure 4.20 Rac1 inhibitor II does not affect the actin-coating of endocytic vacuoles. The box and whisker plot (left) shows total number of EVs per cell, the dot plot (right) shows percentage of actin-coated EVs per cell. In the dot plot, magenta boxes highlight cells with percentage of actin-coated EVs above 0, the percentage of such cells is indicated above. SiR-Actin stained PACs were stimulated with 10 nM CCK for 30 min, after 30 min pre-incubation and in continuous presence of 1% DMSO (Vehicle, n=141) or 100 µM Rac1 inhibitor II (Rac1Inh, n=136); N=3 for both conditions. Data were compared by Wilcoxon-Mann-Whitney test.

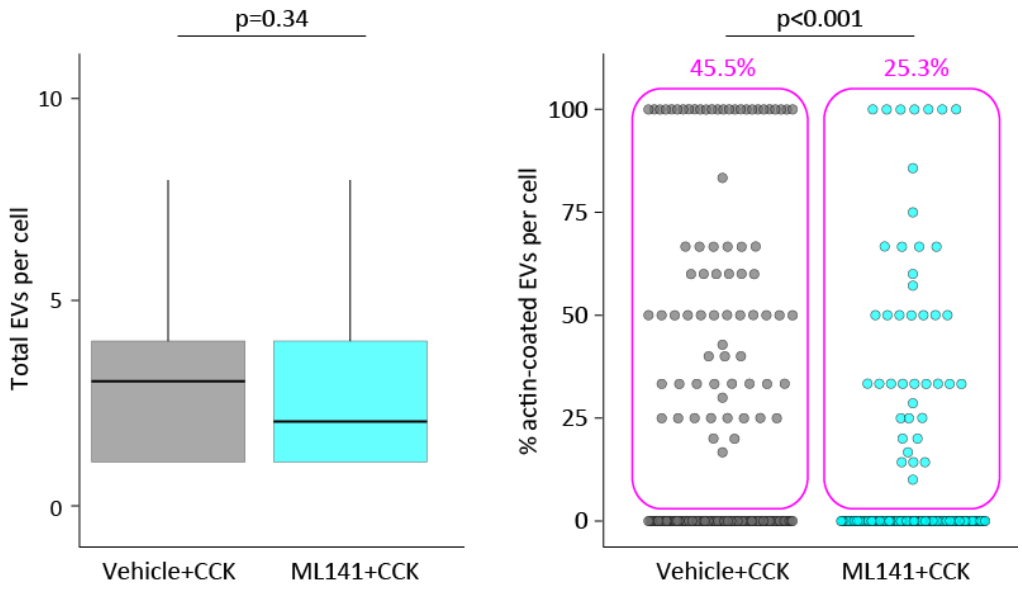

Figure 4.21 Cdc42 inhibitor ML141 reduces the actin-coating of endocytic vacuoles. The box and whisker plot (left) shows total number of EVs per cell, the dot plot (right) shows percentage of actin-coated EVs per cell. In the dot plot, magenta boxes highlight cells with percentage of actin-coated EVs above 0, the percentage of such cells is indicated above. SiR-Actin stained PACs were stimulated with 10 nM CCK for 30 min, after 30 min pre-incubation and in continuous presence of 0.1% DMSO (Vehicle, n=165) or 10 µM ML141 (n=166); N=3 for both conditions. Data were compared by Wilcoxon-Mann-Whitney test.

4.2.3 Phosphoinositides and actin-coating of endocytic vacuoles

PI conversion is essential for membrane dynamics. Class I PI(3)Ks produce PI(3)P, the defining PI in endocytic compartments (Schink *et al.*, 2016). Moreover, class I PI(3)Ks are activated by Rac1 and Cdc42 (Fritsch *et al.*, 2013). The PI(3)K inhibitors LY294002 and wortmannin caused significant reductions in the percentage of actin-coated EVs (**Figure 4.22**). These results indicate that PI(3)K activity is required for actin-coating of EVs. Whilst LY294002 slightly, although not significantly, increased the total number of EVs (**Figure 4.22** A), wortmannin reduced it significantly (**Figure 4.22** B). These results are consistent with similar observations in the results reported in Chapter 3.

PIKfyve converts PI(3)P to PI(3,5)P_2, the defining PI for late endosomes (LE) and lysosomes (Kim *et al.*, 2014). It has been reported that PI(3,5)P_2 affected F-actin stability on LE by competing with the actin-binding protein cortactin (Hong *et al.*, 2015). The PIKfyve inhibitor YM201636 caused a significant reduction in the percentage of actin-coated EVs, without affecting the total number of EVs (**Figure 4.23**). These results suggest that PIKfyve activity is required for actin-coating of EVs.

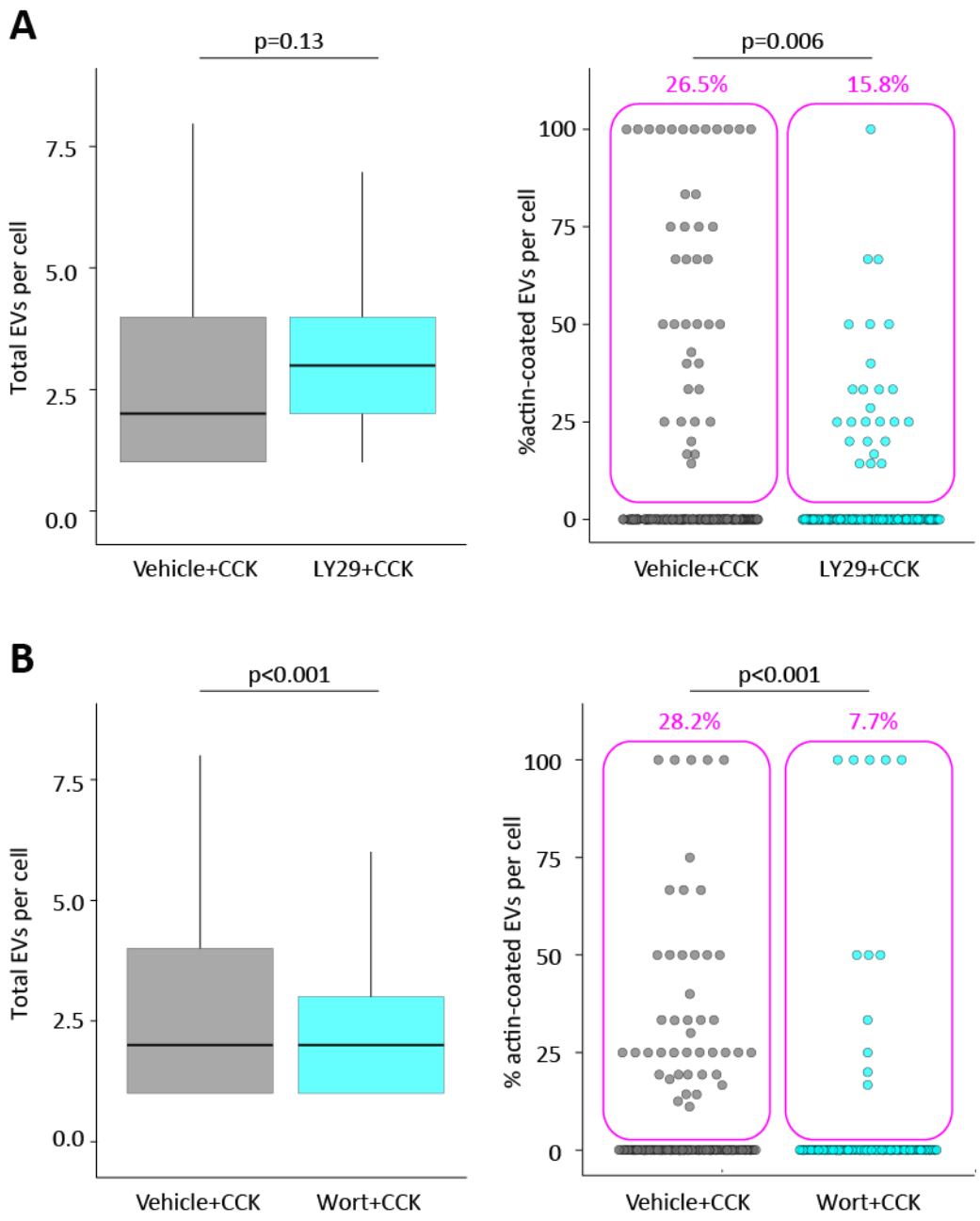

Figure 4.22 PI(3)K inhibitors reduce the actin-coating of endocytic vacuoles. The box and whisker plots (left) show total number of EVs per cell, the dot plots (right) show percentage of actin-coated EVs per cell. In the dot plots, magenta boxes highlight cells with percentage of actin-coated EVs above 0, the percentage of such cells is indicated above. **A)** SiR-Actin stained PACs were stimulated with 10 nM CCK for 30 min, after 45 min pre-incubation and in continuous presence of 0.1% DMSO (Vehicle, n=155) or 20 µM LY294002 (LY29, n=158); N=3 for both conditions. **B)** SiR-Actin stained PACs were stimulated with 10 nM CCK for 30 min, after 30 min pre-incubation and in continuous presence of 0.1% DMSO (Vehicle, n=156) or 10 µM wortmannin (Wort, n=156); N=3 for both conditions. Data were compared by Wilcoxon-Mann-Whitney test.

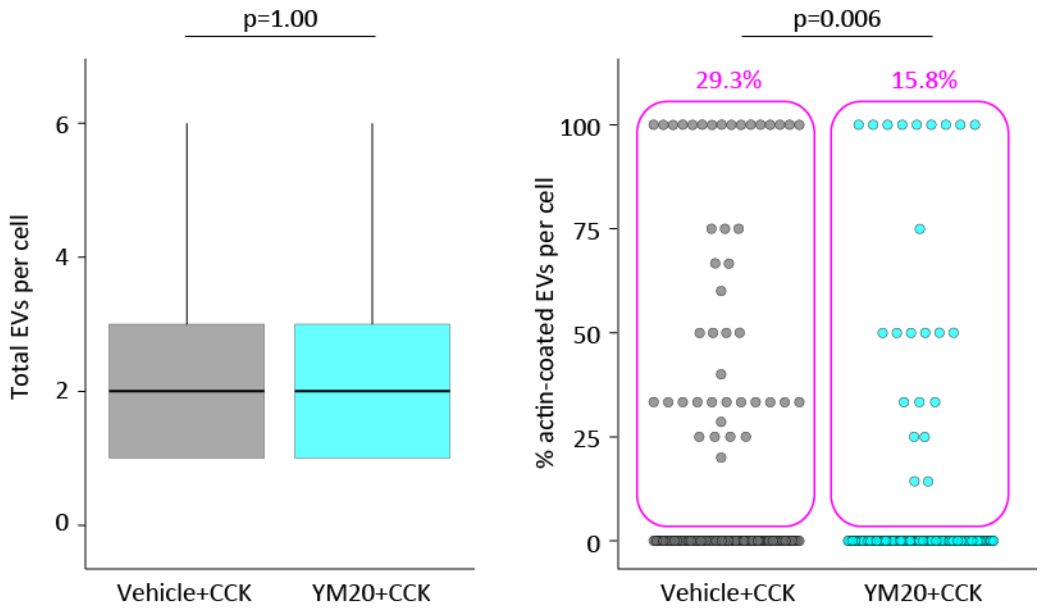

Figure 4.23 PIKfyve inhibitor YM201636 reduces the actin-coating of endocytic vacuoles. The box and whisker plot (left) shows total number of EVs per cell, the dot plot (right) shows percentage of actin-coated EVs per cell. In the dot plot, magenta boxes highlight cells with percentage of actin-coated EVs above 0, the percentage of such cells is indicated above. SiR-Actin stained PACs were stimulated with 10 nM CCK for 30 min, after 60 min pre-incubation and in continuous presence of 0.1% DMSO (Vehicle, n=150) or 100 nM YM201636 (YM20, n=146); N=3 for both conditions. Data were compared by Wilcoxon-Mann-Whitney test.

4.3 Discussion

In this chapter the interaction between EVs and F-actin has been examined. 28-39% of cells present EVs coated by F-actin following stimulation by physiological or supramaximal CCK concentrations. Approximately 13% of cells present EVs coated by F-actin following stimulation by TLC-S. This process depends on actin polymerisation, as it was inhibited by latrunculin A. As such, pharmacological investigation has been carried out (**Figure 4.24**). This process also involves actomyosin contractility, as it was reduced by myosin II inhibitor blebbistatin. The actin-coating of EVs was reduced, although not completely, by formin inhibitor SMIFH2 and by Arp2/3 complex inhibitors CK-666 and CK-869. Accordingly, partial co-localisation of EVs with formin mDia1 and with an Arp2/3 complex subunit occurred, and partial co-localisation with NPFs N-WASP and WASH1. Actin-coating of EVs was reduced, although not completely, by the Rho inhibitor rhosin, ROCK inhibitors Y27632 and GSK429286 and Cdc42 inhibitor ML141. Conversely, this phenomenon was not affected by Rac1 inhibition. Additionally, actin-coating of EVs was reduced by PI(3)K inhibitors LY294002 and wortmannin, and by PIKfyve inhibitor YM201636.

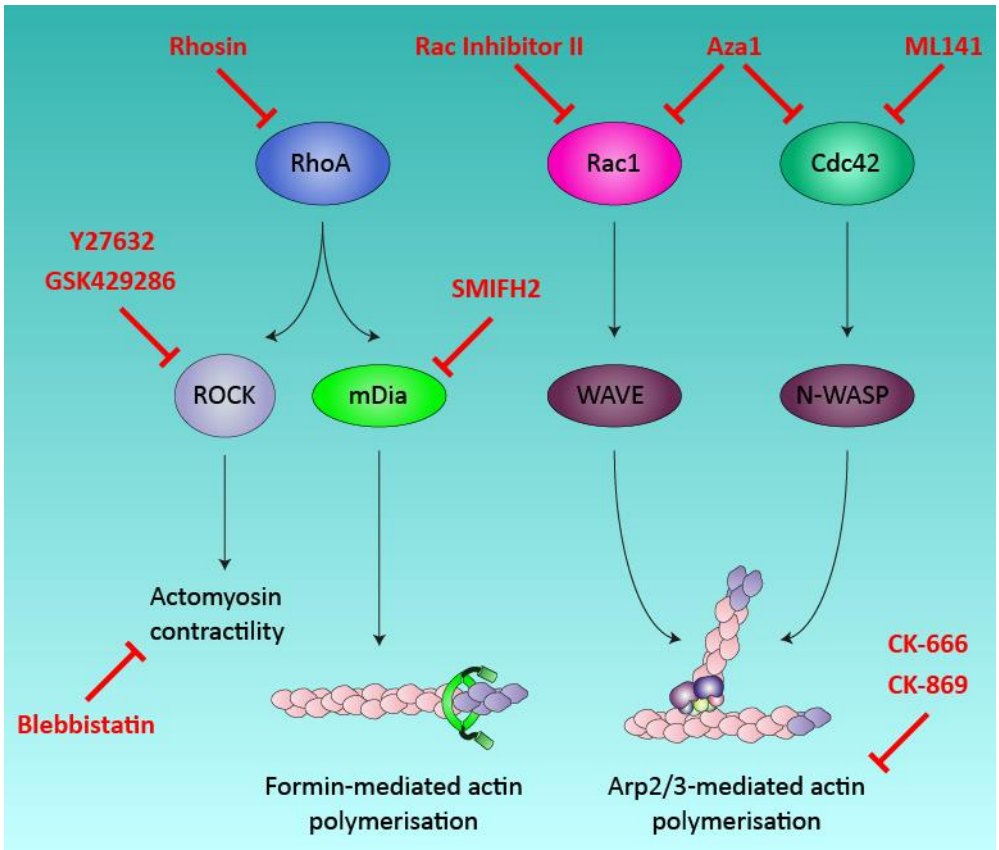

Figure 4.24 Pharmacological characterisation of actin polymerisation and nucleation. The schematic depicts a summary of the regulators of F-actin dynamics and the inhibitors utilised in this study.

It is crucial to consider the strengths and limitations of probes used for staining F-actin in live cells (Melak *et al.*, 2017). This is because F-actin is extremely dynamic, and one should be aware of potential artefacts when overexpressing exogenous actin or staining endogenous actin with compounds that bind to it. In the experiments presented in this chapter, I have utilised the adenoviral vector *LifeAct-tagRFP*. LifeAct is a 17 amino acid peptide which binds F-actin (Riedl *et al.*, 2008). Although overexpressed, LifeAct-RFP will thus only stain endogenous F-actin (as opposed to overexpressing actin reporter constructs such as GFP-actin). Based on its mode of interaction, LifeAct is not expected to affect F-actin dynamics (Riedl *et al.*, 2008). Nonetheless, adenoviral transfection of PACs sometimes represents a challenge and suffers from variable expression efficiency. Hence, I turned to the cell permeable indicator SiR-Actin. Being based on jasplakinolide, SiR-Actin requires caution when utilised in the study of actin dynamics (Lukinavicius *et al.*, 2014). I therefore verified that the concentration of SiR-Actin (1 µM) used for labelling would not affect the phenomenon I was studying: actin-coating of EVs and total number of EVs were not affected by 1 µM jasplakinolide. I thus feel that SiR-Actin represents a suitable tool for staining F-actin in this type of experiments.

In PACs, actin remodelling is essential for exocytosis (Muallem *et al.*, 1995), and several studies have shown that disrupting actin dynamics affects secretion. Actin stabilisation (with phalloidin or 3 µM jasplakinolide) inhibited secretagogue-induced amylase release (Muallem *et al.*, 1995; Valentijn *et al.*, 2000; Bi *et al.*, 2005). Conversely, 1 µM jasplakinolide increased CCK-induced amylase release (Bi *et al.*, 2005). Inhibiting actin polymerisation (with latrunculin A or cytochalasin D) reduced

secretagogue-induced amylase release (Valentijn *et al.*, 1999b; Bi *et al.*, 2005; Bi & Williams, 2005). Although latrunculin A or latrunculin B had no effect on ZG fusion to the plasma membrane, they appeared to reduce the latency of fusion pore opening (Nemoto *et al.*, 2004; Larina *et al.*, 2007). Based on these findings, the authors speculated that F-actin might stabilise the fused ZGs and facilitate content release. In fact, after fusion to the plasma membrane, actin-coating occurs on a proportion of ZGs (Valentijn *et al.*, 2000; Turvey & Thorn, 2004; Jang *et al.*, 2012). Actin-coating of ZGs was inhibited by latrunculin A and latrunculin B (Nemoto *et al.*, 2004; Jang *et al.*, 2012). Interestingly, latrunculin A and cytochalasin D induced the formation of large vacuoles, which were not coated by F-actin (Valentijn *et al.*, 1999b; Nemoto *et al.*, 2004). The identity of these organelles was not explored, so it is not clear if they are EVs. The work presented in this chapter shows that F-actin coats a proportion of EVs, and, consistently, this phenomenon is inhibited by latrunculin A.

Supramaximal secretagogue concentrations provoke drastic changes in the actin cytoskeleton, which are linked to the appearance of basolateral blebs (Burnham & Williams, 1982; O'Konski & Pandol, 1990). Inhibiting actin polymerisation with cytochalasin D or latrunculins prevents blebbing (Burnham & Williams, 1982; Bi *et al.*, 2005). Bleb formation is also associated to actomyosin contractility (Torgerson & McNiven, 1998) and to cortactin activity (Singh & McNiven, 2008). There was no difference in the percentage of actin-coated EVs induced by 10 pM or 10 nM CCK, and it was thus concluded that this phenomenon is not disrupted by supramaximal stimulation. The myosin II inhibitor blebbistatin reduced the percentage of actin-coated EVs. This suggests that actomyosin contractility is involved in this process, and

it is consistent with the evidence that supramaximal stimulation triggers myosin II activation (Torgerson & McNiven, 1998). The role of myosins in actination of ZGs is less clear. In fact, blebbistatin had no effect on actin-coating of fused ZGs (Bhat & Thorn, 2009), while the myosin inhibitor 2,3-butanedione monoxime resulted in accumulation of actin-coated ZGs (Valentijn *et al.*, 2000). 2,3-butanedione monoxime also suppressed secretagogue-induced secretion (Valentijn *et al.*, 2000), whilst blebbistatin had no effect on secretion (Bhat & Thorn, 2009). In the experiments reported in this chapter, blebbistatin had no effect on the total number of EVs. Actomyosin contractility is regulated by ROCK. Consistently, ROCK inhibitors had the same effect as blebbistatin (i.e. reducing actin-coated EVs not affecting total number of EVs).

Actin-coating of EVs was reduced by formin inhibitor SMIFH2 and by the Arp2/3 complex inhibitors CK-666 and CK-869. Both formins and Arp2/3 have been implicated in endocytic pathways (Merrifield *et al.*, 2004; Fernandez-Borja *et al.*, 2005). In PACs, the formin mDia1 generates actin bundles from the apical membrane (Geron *et al.*, 2013). While the actin bundles are sensitive to latrunculin A, actin-coating of ZGs is resistant. In my experiments, I also observed actin bundles; however, the actin-coating of EVs was reduced, although not completely, by latrunculin A. Geron *et al* used a lower concentration (1 µM) of latrunculin A and a shorter treatment (10 min) than used in the experiments presented in this chapter (10 µM, 30 min), which might explain the different result. In my experiments I also noticed that latrunculin A had a strong effect on depleting basolateral actin, whereas

the apical actin was more resistant. Similar observations had been reported before (Bi & Williams, 2005).

It was reported that actin-coated ZGs co-localise with the Arp2/3 complex and N-WASP (Geron *et al.*, 2013). The Arp2/3 complex and N-WASP are implicated in several endocytic processes (Castellano *et al.*, 2001; Merrifield *et al.*, 2004; Hoon *et al.*, 2012). The experiments described in this chapter indicated partial co-localisation of EVs with the P34 subunit of the Arp2/3 complex and N-WASP. When I attempted to explore the role of N-WASP with its inhibitor wiskostatin, I found that a low concentration (10 µM) triggered an inexplicable increase in both the total number of EVs and the percentage of actin-coated EVs. A higher (recommended) concentration (50 µM) provoked substantial cell death. To bypass the issues I encountered with wiskostatin, it would be interesting to explore this phenomenon in *N-WASP* KO mice.

WASH is another NPF activating the Arp2/3 complex (Campellone & Welch, 2010). WASH is recruited at phagosomes and macropinosomes, where it is involved in recycling surface proteins, the V-ATPase and lysosomal hydrolases (Carnell *et al.*, 2011; King *et al.*, 2013; Park *et al.*, 2013; Buckley *et al.*, 2016). The experiments described in this chapter indicated potential co-localisation of WASH1 with EVs. A recent study reported that WASH recruitment at endosomes was dependent on hepatocyte growth factor-regulated tyrosine kinase substrate (HRS) (MacDonald *et al.*, 2018). HRS is a component of the endosomal sorting complex required for transport (ESCRT). ESCRTs are thoroughly involved in endocytic processes, facilitating transport from endosomes to vacuoles and lysosomes through multivesicular bodies (Williams & Urbe, 2007), and assisting vesicle budding (Henne *et al.*, 2011). Exploring

the potential role of ESCRT in the EV dynamics might represent an interesting research line for the development of the project.

Arp2/3 complex, N-WASP and WASH1 immunofluorescence staining localised mainly at the apical membrane, whereas formins mDia1 and FMNL2 localised strongly along the basolateral membrane. Interestingly, apical localisation of N-WASP was also reported in polarised epithelial cells Caco2 (Kovacs *et al.*, 2011). The authors found that N-WASP was involved in an Arp2/3-independent process of F-actin stabilisation and incorporation into rings at adherens junctions. N-WASP has also been implicated in mutant KRas-dependent pancreatic carcinogenesis (Lubeseder-Martellato *et al.*, 2017). The authors reported that oncogenic KRas triggered fluid-phase endocytosis and they found that this was dependent on N-WASP expression. This study highlights the link between fluid-phase endocytosis and N-WASP upregulation, two early events in acinar cell transdifferentiation during pancreatic carcinogenesis.

RhoA, Rac1 and Cdc42 are known regulators of actin dynamics in endocytic pathways (Castellano *et al.*, 2001; Wallar *et al.*, 2007; Swanson, 2008; Hoon *et al.*, 2012). The experiments described in this chapter showed that Rho, ROCK or Cdc42 inhibition reduced the actin-coating of EVs. Conversely, Rac1 inhibition had no effect on this phenomenon. RhoA activates Dia-related formins (Tominaga *et al.*, 2000) and ROCK, whereas Cdc42 and Rac1 trigger activation of N-WASP and WAVE, which then activate the Arp2/3 complex (Campellone & Welch, 2010). Thus, finding that Rho or Cdc42 inhibition reduced the actin-coating of EVs is consistent with formin or Arp2/3 inhibition also affecting this phenomenon.

In PACs, RhoA and Rac1 are known mediators of CCK-stimulated exocytosis: CCK induces activation and apical translocation of RhoA and Rac1, and dominant negative Rho and Rac inhibit CCK-induced amylase release (Bi & Williams, 2005). The Rho inhibitor exoenzyme C3 also inhibited CCK-stimulated amylase release (Rosado *et al.*, 1998). Furthermore, exoenzyme C3 prevented actin-coating of ZGs (Nemoto *et al.*, 2004). In my experiments Rho inhibition reduced, although not significantly, the total number of EVs. Interestingly, the total number of EVs was also reduced by the dual inhibition of Rac1 and Cdc42, but not by Rac1 inhibition or Cdc42 inhibition alone. Significantly, all the inhibitors that caused a reduction in the percentage of actin-coated EVs did not have a complete effect. This suggests that more than one pathway is involved in this process. In this respect, a possible research development could be to simultaneously inhibit formins and Arp2/3 and, likewise, simultaneously inhibit RhoA, Rac1 and Cdc42.

F-actin was recently reported to interact with endosomal compartments located in the basal region of polarised epithelial cells MCF-10a (Samson *et al.*, 2017). The authors established that actin assembly and disassembly at these organelles was regulated by the multi-domain scaffold IQGAP. IQGAP acts by binding and stabilising Rac1 and Cdc42, and interacts with Arp2/3 complex and Dia1. In light of the similiarities between this process and the phenomenon observed in this study, it would be interesting to investigate the expression of IQGAP in PACs.

PI(3)K inhibition with LY294002 or wortmannin reduced the percentage of actin-coated EVs. Class I PI(3)K are involved in PI conversion in endocytosis, and are regulated by Rac1 and Cdc42 (Fritsch *et al.*, 2013). Finding that PI(3)K inhibition

affects actin-coating of EVs is thus consistent with Cdc42 inhibition having the same effect. PIKfyve inhibition by YM201636 also reduced the percentage of actin-coated EVs. Conversely, another work reported that PIKfyve inhibition stabilised LE-associated actin filaments (Hong *et al.*, 2015). This was a consequence of PI(3,5)P_2 depletion, which allowed cortactin binding and cortactin-mediated stabilisation of branched F-actin. It has not yet been determined whether the actin-coated EVs present PI(3,5)P_2. The different result might also be explained by the biphasic effect of YM201636 discussed in Chapter 3: low concentration of inhibitor prevents PI to PI(5)P conversion, whereas higher doses prevent PI(3)P to PI(3,5)P_2 conversion (Vicinanza *et al.*, 2015).

Class I PIP(5)Ks are also implicated in endocytic processes, and they are activated by RhoA, Rac1 and Cdc42 (Weernink *et al.*, 2004). Moreover, PIP(5)Ks facilitate actin polymerisation at membrane-bound vesicles via WASP and Arp2/3 (Rozelle *et al.*, 2000). PIP(5)Ks thus represent a logical target to link Rho GTPase signalling and actin nucleators in the interaction of F-actin and EVs. The product of PIP(5)K, PI(4,5)P_2, is known to activate dynamin (Zheng *et al.*, 1996). Dynamin and cortactin are involved in multiple endocytic processes, in particular CME and macropinocytosis (Sauvonnet *et al.*, 2005; Zhu *et al.*, 2005). In PACs, cortactin is implicated in supramaximal stimulation-induced membrane blebbing (Singh & McNiven, 2008), whilst dynamin is recruited at the Golgi apparatus following secretagogue stimulation (Dahan *et al.*, 2005). There is thus evidence that stimulation triggers dynamin and cortactin recruitment in PACs. In the future, this project could explore the role of dynamin and cortactin in the interaction of F-actin with EVs.

PI recruitment at endosomal compartments is associated with Rab proteins (Schink *et al.*, 2016). Rab proteins have essential roles in membrane trafficking (Stenmark, 2009), and Rab exchange occurs during maturation of EE (expressing Rab5) to LE (expressing Rab7) (Schink *et al.*, 2016). It was found that ZGs acquired F-actin and thereafter lost Rab3D (Valentijn *et al.*, 2000). Investigating the co-localisation of the actin-coated EVs with Rab proteins might shed light on the role of F-actin in the maturation of EVs along the endocytic pathway.

A recent study from our laboratory revealed that the actin coat on EVs can be homogeneous, fenestrated, or partial (Chvanov *et al.*, 2018). At this stage it is not known how F-actin is removed from EVs. To this end, it would be interesting to explore the potential role of actin binding proteins which facilitate depolymerisation, such as coronin, actin depolymerising protein (ADF)/cofilin, or the calcium-regulated protein gelsolin (Yin & Stossel, 1979; Bamburg *et al.*, 1980; Bamburg, 1999; Mikati *et al.*, 2015). In the same study we reported that CCK induced the rupture of a proportion of EVs (Chvanov *et al.*, 2018). These rupture events coincided with escape of membrane impermeable fluorescent indicators from the membrane enclosed EV into the cytosol. Notably, it was observed that leakage of EV content appeared to occur through fenestrations in the actin-coating. We thus enquired whether the actin coat might have a protective role from rupture of these organelles. Chvanov *et al* showed that 1 µM jasplakinolide reduced the CCK-induced increase in EV rupture. This finding suggests that stabilising the F-actin reinforces EVs. Chvanov *et al* also reported that EVs can undergo secondary exocytosis, which occurs at both basolateral and apical membranes (Chvanov *et al.*, 2018). In light of the role of F-

actin in exocytosis, it appears logical that F-actin will also be involved in secondary exocytosis of EVs.

In summary, the findings presented in this chapter indicate that EVs are coated by F-actin in a process dependent on formins and Arp2/3 complex. Accordingly, it is regulated by RhoA and Cdc42 GTPases. Future work should attempt to unveil the functional role of this phenomenon – in light of EV trafficking/maturation, rupture, secondary exocytosis. The next chapter will address the potential interaction of this process with the LC3 coating of EVs described in Chapter 3.

5 Investigating the relationship between actination, autophagy and pH of endocytic vacuoles

5.1 Introduction

This chapter will investigate the relationship between actination, autophagy and pH of EVs. Chapter 3 reported that some EVs are coated by LC3 by a non-canonical autophagy mechanism. Chapter 4 reported that some EVs are coated by F-actin. This part of the study will explore the reciprocal role of these processes in the maturation of EVs and the pH properties of these organelles.

The actin cytoskeleton is implicated in both starvation-induced autophagy in mammalian cells and selective autophagy in yeast. Actin and actin-binding proteins are required at several stages of the autophagic flux (Coutts & La Thangue, 2016; Kast & Dominguez, 2017). The most reported function of actin is at the autophagosome formation stage. As described in Section 1.5, autophagy initiation consists of ULK1 and PI(3)K complex recruitment at ATG9-labelled membranes. In yeast, Arp2/3 mediated actin polymerisation is required for Atg9 trafficking in selective autophagy (Reggiori *et al.*, 2005; Monastyrska *et al.*, 2008). In both *Drosophila* and mammalian cells, ATG9 transport is dependent on myosin II regulation by ATG1 in starvation-induced autophagy (Tang *et al.*, 2011). F-actin might even help shape the nascent phagophore membrane. Indeed, a study reported CapZ recruitment and actin polymerisation along the inner membrane of the isolation membrane in starved cells (Mi *et al.*, 2015). The authors observed F-actin ring-like structures around LC3 puncta. Moreover, they detected LC3 co-localisation with cofilin and P41 subunit of the Arp2/3 complex. Two more studies reported Arp2/3 mediated F-actin nucleation in starvation-induced autophagy, dependent on JMY and WHAMM recruitment at nascent autophagosomes, respectively (Coutts & La Thangue, 2015; Kast *et al.*, 2015).

Upstream regulators of actin dynamics have also been implicated in autophagosome biogenesis: RhoA, via ROCK, as an activator, Rac1 as an inhibitor (Aguilera *et al.*, 2012; Gurkar *et al.*, 2013).

So far, the role of F-actin in non-canonical autophagy has not been directly investigated. Non-canonical autophagy occurs, among other processes, in a specialised form of phagocytosis known as LAP (Sanjuan *et al.*, 2007; Florey *et al.*, 2015). Actin is required for phagocytosis, and it is involved in autophagic degradation of *Salmonella typhimurium*, via the autophagy receptor TAX1BP1 and myosin VI (Tumbarello *et al.*, 2015). It is therefore conceivable that actin is also involved in non-canonical mechanisms of pathogen clearance. Moreover, non-canonical autophagy is associated with macropinocytosis (Florey *et al.*, 2011), another process known to depend on actin (Merrifield *et al.*, 1999). Notably, the actin NPF WASH plays an essential role in macropinocytosis, phagocytosis and autophagy in *Dictyostelium* (Carnell *et al.*, 2011; King *et al.*, 2013; Park *et al.*, 2013; Buckley *et al.*, 2016). At an early stage, WASH allows for recycling of surface proteins via the retromer sorting complex, followed by organelle acidification and digestion of cargo (Buckley *et al.*, 2016). Thereafter, WASH mediates actin-dependent V-ATPase recycling, allowing for organelle neutralisation (Carnell *et al.*, 2011). Finally, WASH and the retromer sorting complex are recycled prior organelle exocytosis (Park *et al.*, 2013; Buckley *et al.*, 2016). Additionally, WASH is required for lysosomal hydrolase recycling, the enzymes responsible for phagosome and autophagosome cargo degradation (King *et al.*, 2013). This provides a clear link between F-actin, endolysosomal and autophagic pathways.

The endolysosomal pathway is characterised by progressive organellar acidification, which is required for recycling, trafficking and hydrolase activity. Specific cellular compartments have specific pH. Early endosomes have pH 6.0-6.5, late endosomes have pH 5.0-5.5 and lysosomes have pH 4.5-5.0 (Casey *et al.*, 2010; Scott & Gruenberg, 2011). Acidification is facilitated by V-ATPase activity (Sun-Wada *et al.*, 2004). Nonetheless, other channels and transporters are implicated in regulating organellar ion composition. Proton pumping into the lumen via the V-ATPase is compensated by chloride influx via members of the chloride channel (CLC) family (Jentsch, 2007). pH modification also occurs throughout the exocytic pathway (Casey *et al.*, 2010). In PACs, ZG packaging from the TGN requires acidic pH and ZGs are considered an acidified compartment, however the pH of isolated ZG was measured to be mildly acidic: ~6.5 (Gasser *et al.*, 1988; Thevenod, 2002). EVs originating from post-exocytic ZGs are also acidic, with measured pH ~5.9 (Sherwood *et al.*, 2007).

This chapter aims to characterise the relationship between the actination and lipidation processes occurring on EVs. Moreover, it aims to determine the pH inside these subpopulations of EVs. First, it was asked whether LC3 and F-actin interact on EVs. To address this question, F-actin was stained in live cells isolated from GFP-LC3 mice, and cell impermeant indicators were used to label EVs. PACs were stimulated with CCK and monitored by live cell imaging to investigate the interaction between F-actin, LC3 and EVs. LC3-coating was pharmacologically prevented to explore the effect on actination; *vice versa*, actin polymerisation was pharmacologically disrupted to assess the effect on LC3-coating. Finally, ratiometric pH measurements inside EVs, actin-coated EVs and LC3-coated EVs were performed.

5.2 Results

5.2.1 Relationship between LC3 and actin on endocytic vacuoles

Chapter 3 and 4 reported that some EVs are coated by LC3 and some EVs are coated by F-actin. Next, it was enquired whether these processes would simultaneously occur on the same EVs. GFP-LC3 PACs were therefore stained with SiR-Actin and stimulated with 100 pM CCK in the presence of TRD. Total EVs, LC3-coated EVs, and actin-coated EVs were counted. 583 EVs were analysed, of which 47 were LC3-coated (representing 8.06% of the total) and 51 were actin-coated (representing 8.75% of the total), from n=196 cells and N=8 mice. No EVs coated by both LC3 and F-actin were found. **Figure 5.1** shows an example of LC3-coated, actin-negative EV. **Figure 5.2** shows an example of actin-coated, LC3-negative EV. It was concluded that F-actin and LC3 coating are not present simultaneously on EVs.

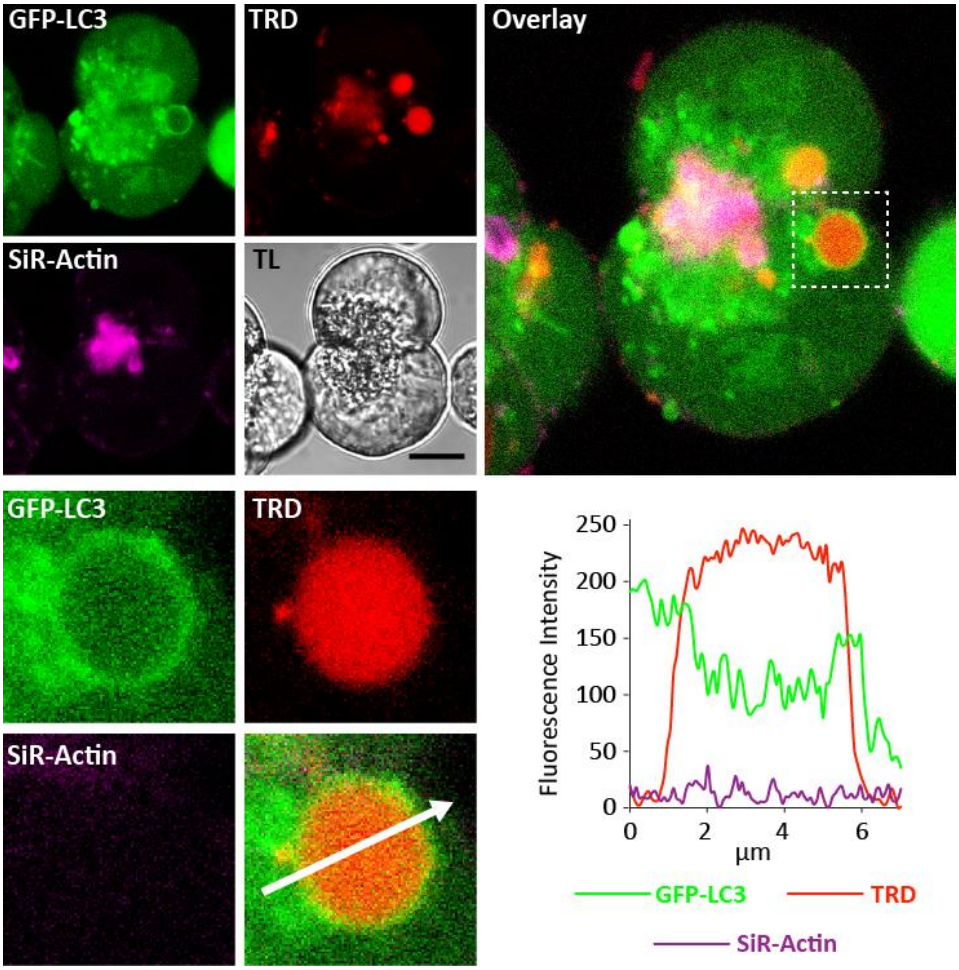

Figure 5.1 LC3-coated endocytic vacuoles are not coated by F-actin. Representative images of SiR-Actin (magenta) stained GFP-LC3 (green) PACs, incubated 30 min at 34.5°C in the presence of 100 pM CCK and TRD (red). Scale bar = 10 µm. A selected EV is highlighted by a dashed square and shown in an expanded scale in the lower panel. The fluorescence intensity profile along the arrow is plotted in the bottom right panel.

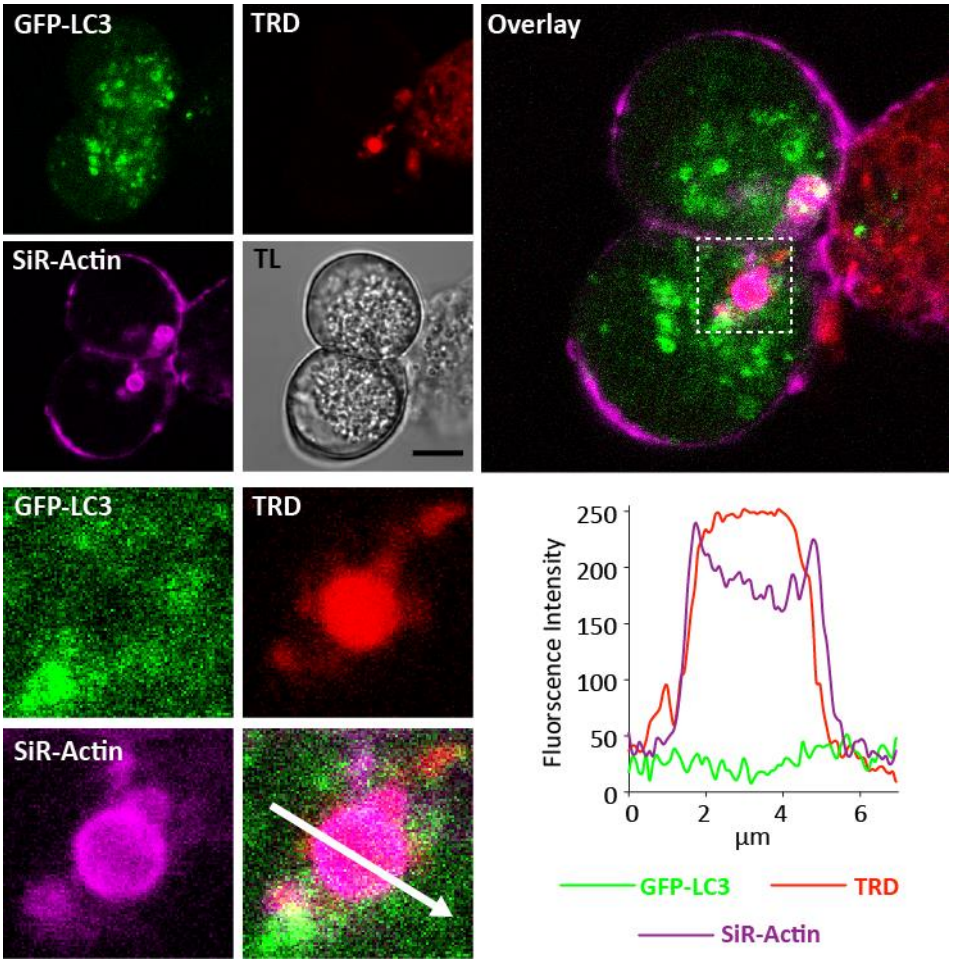

Figure 5.2 Actin-coated endocytic vacuoles are not coated by LC3. Representative images of SiR-Actin (magenta) stained GFP-LC3 (green) PACs, incubated 30 min at 34.5°C in the presence of 100 pM CCK and TRD (red). Scale bar = 10 µm. A selected EV is highlighted by dashed square and shown in expanded scale in the lower panel. The fluorescence intensity profile along the arrow is plotted in the bottom right panel.

Hypothesising that the actin and LC3 coating represent alternative, possibly sequential, processes, this study set to determine whether inhibiting one process would have an impact on the other. To this aim, I utilised inhibitors of LC3-coating and assessed the effect on actin-coating, and *vice versa*. The experiments reported in Chapter 3 showed that the V-ATPase inhibitor bafilomycin prevented LC3-coating of EVs. In SiR-Actin stained PACs stimulated with 10 nM CCK, bafilomycin had no effect on the actin-coating of EVs (**Figure 5.3**). The experiments reported in Chapter 4 showed that actin-depolymerising agent latrunculin A reduced the actin-coating of EVs. In GFP-LC3 PACs stimulated with 10 nM CCK, latrunculin B (structurally related to latrunculin A) significantly reduced the LC3-coating of EVs (**Figure 5.4**). These findings indicate that disrupting LC3-coating has no effect on actin-coating, whilst disrupting actin-coating affects LC3-coating. It was thus hypothesised that actin-coating would occur before LC3-coating.

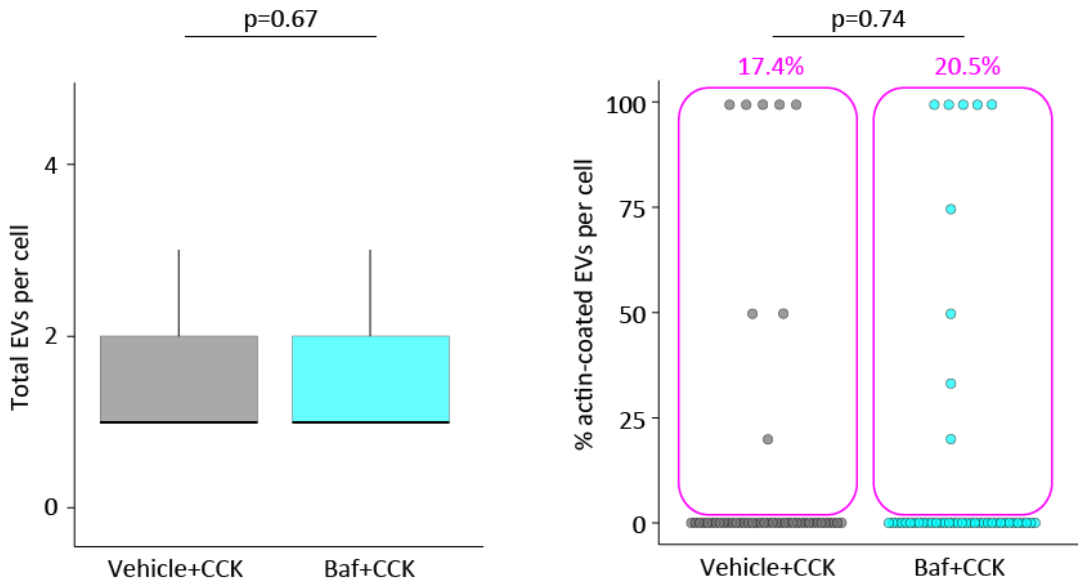

Figure 5.3 Bafilomycin does not affect the actin-coating of endocytic vacuoles. The box and whisker plot (left) shows total number of EVs per cell, the dot plot (right) shows percentage of actin-coated EVs per cell. In the dot plot, magenta boxes highlight cells with percentage of actin-coated EVs above 0, the percentage of such cells is indicated above. SiR-Actin stained PACs were stimulated with 10 nM CCK for 30 min, after 30 min pre-incubation and in continuous presence of 0.1% DMSO (Vehicle, n=46) or 100 nM bafilomycin (Baf, n=44); N=3 for both conditions. Data were compared by Wilcoxon-Mann-Whitney test.

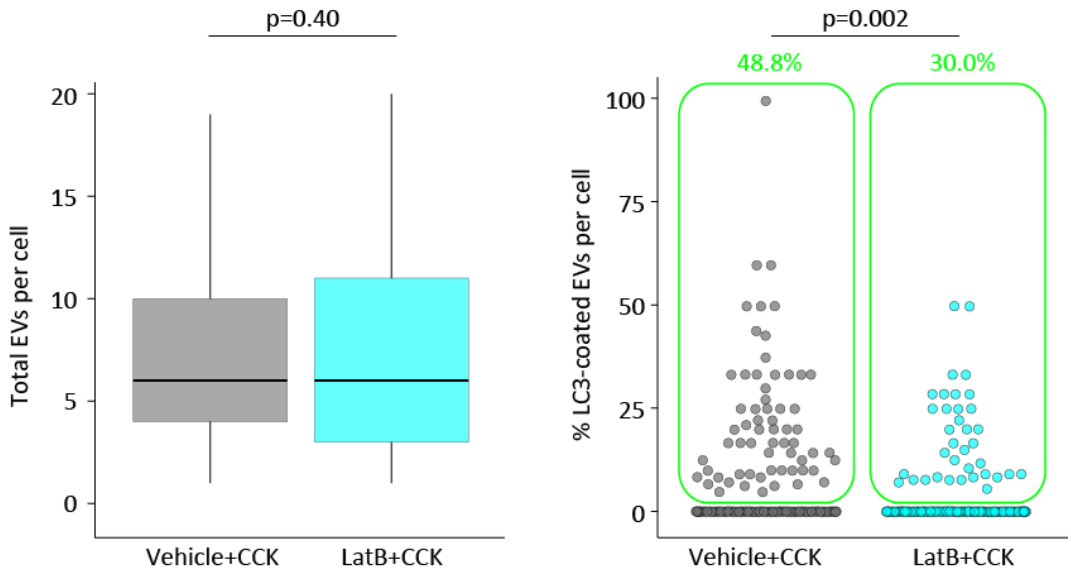

Figure 5.4 Latrunculin B reduces the LC3-coating of endocytic vacuoles. The box and whisker plot (left) shows total number of EVs per cell, the dot plot (right) shows percentage of LC3-coated EVs per cell. In the dot plot, green boxes highlight cells with percentage of LC3-coated EVs above 0, the percentage of such cells is indicated above. GFP-LC3 PACs were stimulated with 10 nM CCK for 30 min, after 30 min pre-incubation and in continuous presence of 0.1% DMSO (Vehicle, n=129) or 10 µM latrunculin B (Lat B, n=120); N=3 for both conditions. Data were compared by Wilcoxon-Mann-Whitney test.

5.2.2 pH of endocytic vacuoles

pH has an essential role in lysosomal function, and progressive acidification of organelles occurs throughout the endolysosomal pathway (Casey *et al.*, 2010; Scott & Gruenberg, 2011). Speculating that actin- and LC3-coating of EVs represent different maturation stages of these organelles, this study set out to characterise the pH of EVs, actin-coated EVs and LC3-coated EVs. Primarily, the protocol was optimised for measuring pH of all EVs (i.e. before adding an extra indicator for labelling F-actin or LC3). As described in Section 2.4.1, a pH-sensitive dextran, FITC (decreasing fluorescence intensity upon acidification), and a pH-insensitive dextran, TRD, were used. PACs were stimulated with 10 nM CCK in the presence of FITC dextran and TRD, and the fluorescence intensity ratio for the two indicators was measured in EVs. Calibration of the fluorescence intensity ratio was performed as described in Section 2.4.1 and 2.13. The EV pH was 5.4 ± 0.1 (**Figure 5.5**).

Next, the pH inside actin-coated and uncoated EVs was measured. Staining PACs with SiR-Actin enabled the use of the same combination of indicators described above. SiR-Actin stained PACs were stimulated with 10 nM CCK in presence of FITC dextran and TRD, and the fluorescence intensity ratio for the two indicators in EVs (distinguishing actin-coated and uncoated) was measured. Calibration of the fluorescence intensity ratio was performed as described in Section 2.4.1 and 2.13. The pH was 5.4 ± 0.2 in actin-coated EVs and 5.7 ± 0.1 in uncoated EVs, with no significant difference between the two (p=0.18) (**Figure 5.6**).

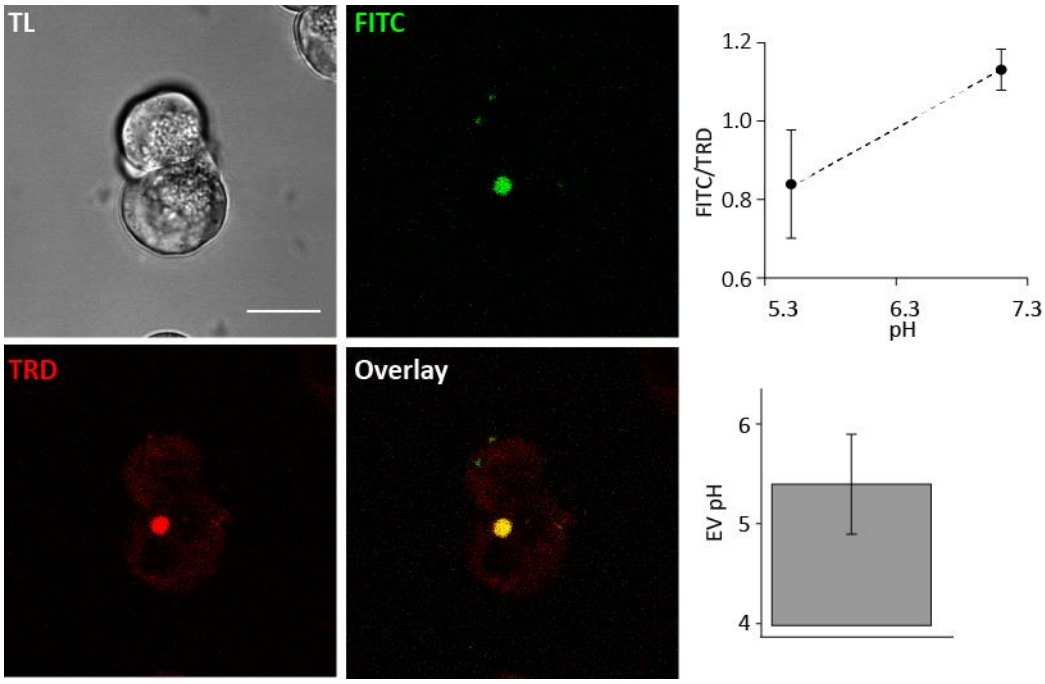

Figure 5.5 pH of endocytic vacuoles. PACs were stimulated with 10 nM CCK in presence of FITC dextran and TRD. A calibration curve was obtained as described in Section 2.4.1 and Section 2.13. The FITC/TRD ratios at pH 7.1 and 5.5 are statistically different ($p<0.001$ by paired t test, n=23 EVs). The bar graph represents mean ± SEM of EV pH (n=134 EVs, N=2 mice). Scale bar = 10 µm.

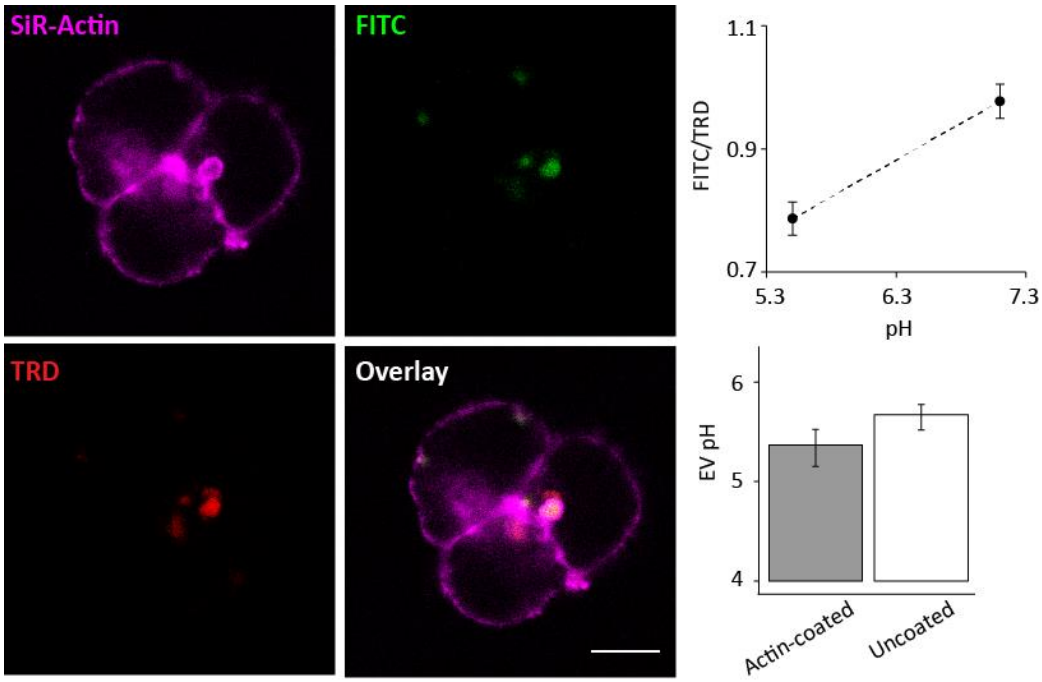

Figure 5.6 pH of actin-coated endocytic vacuoles. SiR-Actin stained PACs were stimulated with 10 nM CCK in presence of FITC dextran and TRD. Calibration curve was obtained as described in Section 2.4.1 and Section 2.13. The FITC/TRD ratios at pH 7.1 and 5.5 are statistically different ($p<0.001$ by paired t test, n=23 EVs). The bar graph represents mean ± SEM of EV pH (Actin-coated n=84 EVs, Uncoated n=168 EVs, N=4 mice). Scale bar = 10 µm.

Next, the pH inside LC3-coated and uncoated EVs was measured. The use of GFP-LC3 PACs required a different combination of cell impermeable indicators. As described in Section 2.4.1, a pH-sensitive dextran, pHrodo™ Red (increasing fluorescence intensity upon acidification) and a pH-insensitive dextran, Alexa Fluor™ 647, were used. GFP-LC3 PACs were stimulated with 10 nM CCK in presence of pHrodo™ Red dextran and Alexa Fluor™ 647 dextran, and the fluorescence intensity ratio for the two indicators in EVs (distinguishing LC3-coated and uncoated) was measured. Calibration of the fluorescence intensity ratio was performed as described in Section 2.4.1 and 2.13. The pH was 6.0 ± 0.6 in LC3-coated EVs and 5.5 ± 0.1 in uncoated EVs, with no significant difference between the two ($p=0.46$) (Figure 5.7). In order to optimise our optical systems, I utilised the same protocol on new samples, and carried out confocal microscopy using a Zeiss LSM 710. The pH was 5.9 ± 0.4 in LC3-coated EVs and 5.5 ± 0.1 in uncoated EVs, with no significant difference between the two ($p=0.31$) (Figure 5.8).

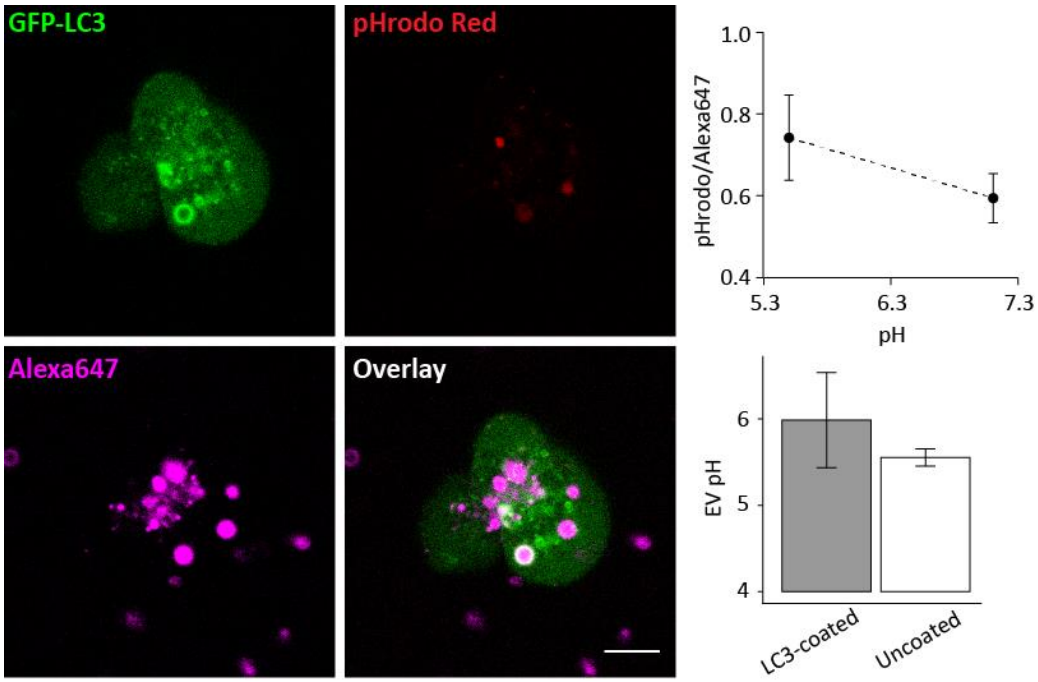

Figure 5.7 pH of LC3-coated endocytic vacuoles (imaging performed on Leica TCS SL). GFP-LC3 PACs were stimulated with 10 nM CCK in presence of pHrodo™ Red and Alexa Fluor™ 647 (Alexa647) dextrans. Confocal microscopy was carried out on Leica TCS SL. Calibration curve was obtained as described in Section 2.4.1 and Section 2.13. The pHrodo/Alexa647 ratios at pH 7.1 and 5.5 are statistically different ($p<0.001$ by paired t test, n=23 EVs). The bar graph represents mean ± SEM of EV pH (LC3-coated n=11 EVs, Uncoated n=228 EVs, N=5 mice). Scale bar = 10 µm.

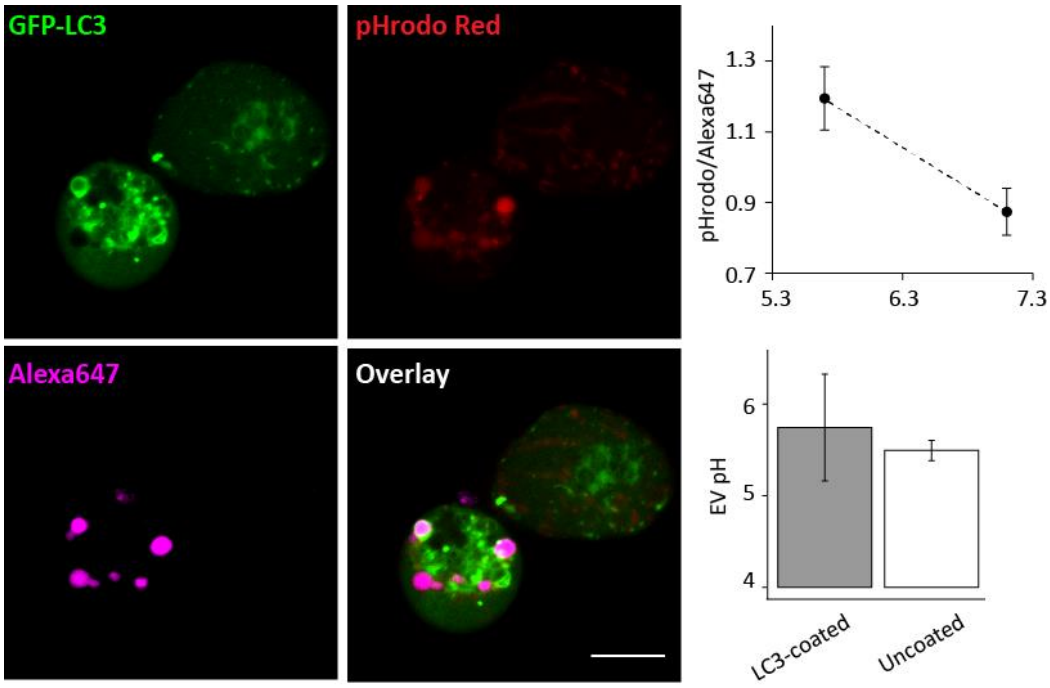

Figure 5.8 pH of LC3-coated endocytic vacuoles (imaging performed on Zeiss LSM 710). GFP-LC3 PACs were stimulated with 10 nM CCK in presence of pHrodo™ Red and Alexa Fluor™ 647 (Alexa647) dextrans. Confocal microscopy was carried out on Zeiss LSM 710. Calibration curve was obtained as described in Section 2.4.1 and Section 2.13. The pHrodo/Alexa647 ratios at pH 7.1 and 5.5 are statistically different ($p<0.001$ by paired t test, n=28 EVs). The bar graph represents mean ± SEM of EV pH (LC3-coated n=14 EVs, Uncoated n=199 EVs, N=4 mice). Scale bar = 10 µm.

5.3 Discussion

In this chapter the interaction between autophagy and actination of EVs has been examined. In CCK-stimulated PACs expressing GFP-LC3 and stained with SiR-actin, co-localisation of LC3 and F-actin on EVs was not found. Approximately 8% of EVs were LC3-coated, approximately 9% of the EVs were actin-coated, but no EVs presented both markers. Disrupting LC3-coating had no effect on the percentage of actin-coated EVs, whereas preventing actin polymerisation reduced the percentage of LC3-coated EVs. The pH inside the three subpopulations of EVs was measured, finding no significant difference in the (acidic) pH of uncoated EVs, actin-coated EVs, LC3-coated EVs.

8.06% of EVs were coated by LC3 and 8.75% of EVs were coated by F-actin, out of 583 total EVs. Based on this result, 4.11 (8.75%) out of the 47 LC3-coated EVs should have been actin-coated. Likewise, 4.11 (8.06%) out of the 51 actin-coated EVs should have been LC3-coated. Conversely, no EVs were positive for both markers. Hence, it was confidently concluded that F-actin and LC3 do not coexist on the same EVs.

Chapter 3 reported that bafilomycin completely prevented LC3 lipidation on EVs. The experiments presented in this chapter show that bafilomycin had no effect on the actin-coating of EVs. A previous study reported that bafilomycin caused actin puncta accumulation in starved cells where actin localised at isolation membranes (Mi *et al.*, 2015). *In vitro* experiments showed that the C subunit of the V-ATPase could stabilise and cross-link actin filaments forming bundles (Vitavska *et al.*, 2005). This result would suggest that inhibiting the V-ATPase could affect actin filaments. Indeed,

visible changes in F-actin were induced by inhibition of the V-ATPase in prostate cancer (Licon-Munoz *et al.*, 2017). Differently from Chapter 3, where it caused a moderate reduction, in this chapter bafilomycin did not affect the total number of EVs. In Chapter 3 PACs had been stimulated by 100 pM CCK, in this chapter PACs were stimulated by 10 nM CCK. This might explain the different result.

Latrunculin A and latrunculin B are structurally related and have the same mechanism of action. Latrunculin B is less potent but it is as broadly used in the actin research field (Spector *et al.*, 1989). I used concentrations of latrunculins comparable to other studies in the PAC field (Valentijn *et al.*, 2000; Nemoto *et al.*, 2004; Bi *et al.*, 2005; Bi & Williams, 2005; Larina *et al.*, 2007; Jang *et al.*, 2012; Geron *et al.*, 2013). Chapter 4 reported that latrunculin A inhibited the actin-coating of EVs. The experiments presented in this chapter show that latrunculin B inhibited the LC3-coating of EVs. A previous study reported that latrunculin B and cytochalasin B prevented the increase in LC3 puncta induced by starvation (Aguilera *et al.*, 2012). Conversely, another study reported that cytochalasin B did not alter the number, but affected the morphology, of LC3-positive autophagosomes (Mi *et al.*, 2015). These works investigated the role of actin polymerisation on classical autophagosome formation (i.e. in starvation-induced autophagy). Conversely, this thesis hypothesises that the LC3 coating of EVs represents a non-canonical autophagy mechanism; in this process F-actin might therefore play a different role. In degenerative astrocytes undergoing autophagic cell death, latrunculin A increased the size and number of autophagic vacuoles, whereas jasplakinolide had the opposite effect (Ryu *et al.*,

2011). Future experiments could also investigate the effect of jasplakinolide on LC3-coating of EVs.

Several studies reported that Arp2/3 complex inhibition by CK-666 and CK-869 impaired autophagosome formation (Coutts & La Thangue, 2015; Kast *et al.*, 2015; Mi *et al.*, 2015). The experiments presented in Chapter 4 showed that both Arp2/3 and formins were implicated in actin-coating of EVs. Thus, as a development of the project I could explore whether actin nucleators affect LC3-coating of EVs. Likewise, Rho GTPase signalling, in particular RhoA-ROCK and Rac1, have been implicated in autophagosome biogenesis (Aguilera *et al.*, 2012; Gurkar *et al.*, 2013; Mleczak *et al.*, 2013). The experiments presented in Chapter 4 showed that RhoA-ROCK and Cdc42 were implicated in actin-coating of EVs. Thus, in the future it would be interesting to enquire whether they also affect LC3-coating of EVs.

Interestingly, multiple evidence linked the role of actin polymerisation in autophagosome formation to PI(3)K complex activity, PI(3)P formation, and recruitment of FYVE domain proteins (Gurkar *et al.*, 2013; Kast *et al.*, 2015; Mi *et al.*, 2015). Indeed, the experiments presented in Chapter 4 showed that PI(3)K inhibitors LY294002 and wortmannin impaired the actin-coating of EVs. Nonetheless, as reported in Chapter 3, these inhibitors had no effect on the LC3-coating of EVs. This is likely due to the fact that the process investigated in this study is a non-canonical autophagy mechanism, and is as such PI(3)P-independent.

Multiple observations lead to speculate that the actin-coating occurs before the LC3-coating. First of all, since fused ZGs are coated by F-actin (Nemoto *et al.*, 2004; Turvey

& Thorn, 2004; Jang *et al.*, 2012), and EVs originate from post-exocytic ZGs, it seems logical that they retain the actin-coat. Secondly, the experiments presented in this chapter show that disrupting actin dynamics prevents LC3-coating, and not *vice versa*. Third, the experiments presented in Chapter 3 showed that a (small) proportion of LC3-coated EVs present lysosomal markers, and therefore they might represent a later maturation stage in the endocytic pathway. Yet, this point should be verified by assessing if, and how many, actin-coated EVs present lysosomal markers. Previous studies reported that actin co-localised with "early" autophagic markers (e.g. ATG14, Beclin1, DFCP1), thus suggesting that actin is present at a PI(3)K complex, pre-lysosomal stage (Aguilera *et al.*, 2012; Coutts & La Thangue, 2015; Kast *et al.*, 2015; Mi *et al.*, 2015). The best way to corroborate the sequence of the coating events is to perform time-lapse imaging to monitor the appearance/disappearance of the actin and LC3 coats. This is surely a desirable experiment, yet due to the rarity of these phenomena it might be low throughput. Moreover, as a result of the absence of overlap observed between actination and lipidation, it is difficult to predict the extent of the time gap between the disappearance of one and the appearance of the other. It is also a possibility that these events are not sequential and that they occur in parallel to different subsets of EVs. A higher throughput approach to test this hypothesis could be to compare the proportion of actinated and LC3-coated EVs at different times. If actination occurs before LC3 lipidation, the number of actin-coated EVs should decrease, and the number of LC3-coated EVs should increase, over time.

The experiments presented in this chapter show that the EV pH was 5.4 ± 0.1. This is slightly more acidic, but close to 5.9 ± 0.1 reported previously by our laboratory (Sherwood *et al.*, 2007). pH ~5.4 is comparable to LE (pH 5.0-5.5) (Casey *et al.*, 2010; Scott & Gruenberg, 2011). Chapter 3 reported that approximately 7% of LC3-coated EVs express the lysosomal marker LAMP1. It is therefore likely that these organelles are late-endosomal / pre-lysosomal compartments.

There was no difference in the pH inside actin-coated and uncoated EVs. Since bafilomycin did not affect the actin-coating of EVs, suggesting that acidity does not impact EV actination, this result is not surprising. Yet, F-actin is known to interact with the V-ATPase. It has been reported that F-actin couples the V0-V1 domains of the V-ATPase at the Golgi, thereby facilitating acidification (Serra-Peinado *et al.*, 2016). Interestingly, the PI(3)K inhibitors LY294002 and wortmannin triggered actin-binding to the B subunit of the V-ATPase in osteoclasts, again suggesting interaction between PIs, actin dynamics and V-ATPase (Chen *et al.*, 2004a).

There was no difference in the pH inside LC3-coated and uncoated EVs. This result is surprising, because the experiments presented in Chapter 3 showed that preventing acidification, with V-ATPase inhibitors or ionophores, inhibits LC3-coating of EVs. It was therefore expected that pH represented a discriminatory factor for LC3 lipidated and not LC3 lipidated EVs. Accordingly, in non-canonical autophagy LC3 appeared to coat acidic organelles (Florey *et al.*, 2015). Conversely, in the experiments presented in this chapter LC3-coated EVs appeared to be more alkaline than uncoated EVs, although the difference was only slight and not statistically significant.

GFP fluorescence quenches at acidic pH (Tsien, 1998). It is thus conceivable that I am missing a population of very acidic GFP-LC3-coated EVs. This could be verified with the tandem RFP-GFP-LC3 reporter (Klionsky *et al.*, 2016): if there was a population of LC3-coated EVs revealed by RFP but not by GFP, it could be concluded that acidic, LC3-coated EVs with quenched GFP exist.

The experiments presented in this chapter show that pH inside actin-coated EVs was 5.4 ± 0.2, pH inside LC3-coated EVs was 5.9 ± 0.3 (pooling together experiments carried out on two setups). The actin-coated EVs appear to be slightly more acidic than the LC3-coated EVs. However, this means comparing results from independent experiments, on cells isolated from different mouse strains and labelled with different indicators. The pH inside actin-coated EVs and LC3-coated EVs could not be investigated simultaneously. This would require separating excitation/emission spectra of four indicators: i.e. an LC3 reporter, an actin reporter, a pH-sensitive indicator, a pH-insensitive indicator. Unfortunately, I did not find a suitable combination of indicators to suit this purpose within the capabilities of our microscopes.

Endolysosomal compartments undergo progressive acidification (Casey *et al.*, 2010; Scott & Gruenberg, 2011). Overall, I have not found a large pH range to suggest different stages of EV maturation. Hypothesising that actination occurs before lipidation, it would have been expected LC3-coated EVs to be more acidic than actin-coated EVs. Nevertheless, F-actin is associated with recycling of the V-ATPase to allow for lysosomal neutralisation prior to exocytosis (Carnell *et al.*, 2011). It is

therefore conceivable that EVs that have lost the F-actin coat have also lost the V-ATPase, and are thus more alkaline.

Luminal pH determines recruitment of specific proteins at endosomes. For instance, the small GTPase Arf1 and COP proteins are recruited as a consequence of acidification (Aniento *et al.*, 1996; Gu & Gruenberg, 2000). There must thus be a pH sensor that transfers information of luminal pH to the cytosol. The a2 subunit of the V-ATPase has been proposed as a pH sensor (Marshansky, 2007). Indeed, dependent on acidification, the V-ATPase interacts with Arf6 and ARNO via the c and a2 subunits, respectively (Maranda *et al.*, 2001; Hurtado-Lorenzo *et al.*, 2006). It thus appears that the V-ATPase not only determines organellar pH, but also acts as messenger to attract binding proteins. Investigating this function of the V-ATPase, and monitoring pH-sensitive recruitment of proteins at the EVs, might help to better characterise the subpopulations of EVs.

It is known that classical autophagosomes move along microtubules (Kimura *et al.*, 2008; Kast & Dominguez, 2017). This thesis has not investigated the interaction of microtubules with EVs, and their potential role as a link between actinated and LC3-coated stages. In recycling endosomes, actin and microtubules are brought together by biogenesis of lysosome-related complex 1 (BLOC-1) (Delevoye *et al.*, 2016). Moreover, a study found that intact microtubules are required for autophagosome fusion to endosomes in starvation-induced autophagy (Kochl *et al.*, 2006). Hence, it would be interesting to prevent microtubule polymerisation with tubulin-binding compounds nocodazole and vinblastine and assess the effect on LC3-coated EVs.

In summary, the findings presented in this chapter indicate that actination and LC3-coating do not occur on the same EVs. Actin disruption affects LC3-coating, whereas preventing LC3-coating has no impact of actin-coating. It is thus proposed that actination - and loss of actin-coat - occurs before LC3-coating in the maturation of EVs. There were no differences in pH inside uncoated, actin-coated and LC3-coated EVs, so it appears that these processes are not associated with progressive acidification. Future work should try and determine which properties, if not pH, characterise these subpopulation of EVs and mark them for actination and LC3 lipidation. Future experiments should also attempt to elucidate the sequence and the physiological function of these events.

6 Concluding remarks

6.1 Summary and interpretation of the findings

EVs, formed as a consequence of ZG exocytosis, are the site of trypsinogen activation in cellular models of AP (Sherwood *et al.*, 2007). This work led to the discovery of two phenomena: the LC3 lipidation and the actination of EVs. Chapter 3 describes the LC3 lipidation on EVs and reports the unexpected observation that it is inhibited by bafilomycin. Given this major finding, it is likely that this phenomenon occurs via a non-canonical autophagy pathway. As such, experimental evidence reported in Chapter 3 demonstrates that the LC3 lipidation on EVs is independent from the ULK1 and PI(3)K complexes, but involves ATG5-ATG12-ATG16L1 machinery, corroborating the hypothesis of non-canonical autophagy. Accordingly, these organelles have a single, not double, membrane. Chapter 4 details the actination of EVs and demonstrates that this phenomenon requires a dynamic actin network, being inhibited by latrunculin A. Experimental evidence reported in Chapter 4 demonstrates that this process involves both the Arp2/3 complex and formins, and is regulated by Rho and Cdc42. Chapter 5 explores the interaction between LC3 lipidation and actination, and the pH properties of EVs. F-actin and LC3 do not co-localise on EVs, supporting the hypothesis that the processes of actination and LC3 lipidation occur separately. The intra-organellar pH does not differ in the subpopulations of EVs, suggesting that the targeting for these phenomena must depend on other properties of the organelles.

Figure 6.1 illustrates a putative evolution of the EVs. It is reasonable to suggest that actination occurs before LC3 lipidation. In fact, F-actin is already present on ZGs undergoing exocytosis (Ω-shapes) (Nemoto *et al.*, 2004; Turvey & Thorn, 2004; Jang

et al., 2012), and it is likely retained when EVs detach from post-exocytic structures or plasma membrane. Although the (non-canonical) LC3 lipidation on EVs does not require ULK1 and PI(3)K activation, it still involves assembly and targeting of the ATG5-ATG12-ATG16L1 complex at the organelles where LC3 is to be lipidated. Hence, this process conceivably requires more time than actination. We speculate that EVs are first actinated, then F-actin is removed, and at this point EVs undergo LC3 lipidation, which is likely responsible for targeting the content of these organelles for lysosomal degradation. Based on our observations, there is a phase where EVs have lost F-actin but not yet gained LC3. It is not known whether F-actin is removed in order to assist further exocytosis and endocytosis, to recycle membrane components from EVs thus making them targetable for LC3 lipidation, or for other purposes. Previous studies from our laboratory discovered that EVs are the site of intracellular trypsinogen activation (Sherwood *et al.*, 2007), can undergo rupture and leak their contents in the cytosol, and can undergo secondary exocytosis (Chvanov *et al.*, 2018). It is possible that rupture occurs in the time frame between actination and LC3 lipidation, when the actin coat is being dismantled and EVs are "unprotected". Based on this interpretation, both actination and LC3 lipidation are protective processes that stabilise EVs and target EV contents for degradation, protecting the cell against potential leakage of active trypsin from membrane enclosed EVs to the cytosol. Interestingly, LC3 lipidation and actination occur in both physiological and supramaximal stimulation. This suggests that these processes do occur physiologically and are not activated specifically as a response to pathological stimuli. It is conceivable that, in supramaximal stimulation, and in AP, these protective mechanisms are impaired or overwhelmed.

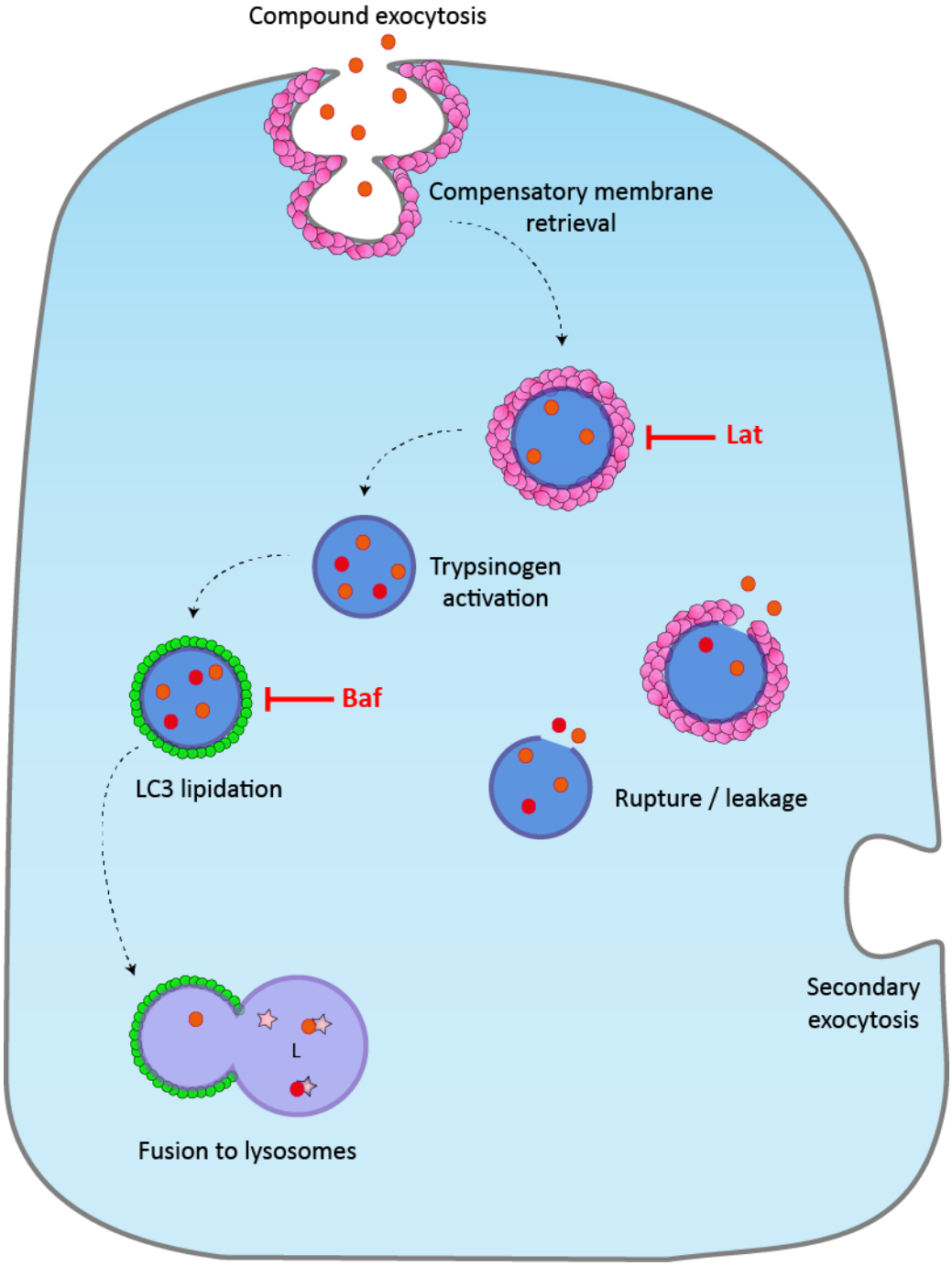

Figure 6.1 Formation and evolution of endocytic vacuoles in pancreatic acinar cells. The schematic depicts multiple phenomena occurring throughout the lifetime of EVs. Some of these phenomena have been previously reported (i.e. trypsinogen activation, rupture, secondary exocytosis), others have been described in this study (i.e. LC3 lipidation and actination). Actination is inhibited by latrunculin (Lat), LC3 lipidation is inhibited by bafilomycin (Baf). Orange dots indicate zymogens, red dots indicate active proteases.

6.2 Actin cytoskeleton and stabilisation of endocytic vacuoles

The formation of EVs from post-exocytic structures occurs via a still unidentified endocytic pathway. It is known that F-actin coats the ZGs fused to the plasma membrane (Ω-shapes) (Nemoto *et al.*, 2004; Turvey & Thorn, 2004; Jang *et al.*, 2012), and we propose that it is also directly responsible for completion of exocytosis and formation of EVs. The presence of actin-coating on Ω-shapes has been suggested to act as a force to facilitate content release and to stabilise the structure with open fusion pore (Nemoto *et al.*, 2001; Nemoto *et al.*, 2004; Larina *et al.*, 2007). On the EVs, the actin-coating might also act as a stabiliser. A recent study from our laboratory showed that EVs can leak their content in the cytosol through fenestrations in the F-actin coating, and F-actin stabilisation by jasplakinolide reduces the amount of leakage (Chvanov *et al.*, 2018). We therefore suggest that the actin coating accounts for EV stabilisation preventing them from rupture.

Actin coating of EVs is regulated by both formins and Arp2/3 complex, suggesting that both filament elongation and branching are required for interaction with EVs. The ring-like actin-coat on PAC EVs is pretty unique in comparison to other cell types where F-actin plays a role in endocytic (Parton *et al.*, 1994; Castellano *et al.*, 2001; Lee & Knecht, 2002; Swanson, 2008) or trafficking (Merrifield *et al.*, 1999) events. In endocytosis, phagocytosis and macropinocytosis, F-actin is present at membrane invaginations or protrusions, but it is not retained after the endosome/phagosome/macropinosome is internalised (Apodaca, 2001; Girao *et al.*, 2008). Likewise, endosomes move along actin filaments but are not coated by them (Merrifield *et al.*, 1999; Gasman *et al.*, 2003; Fernandez-Borja *et al.*, 2005; Wallar *et*

al., 2007). On PAC EVs, the actin-coat is retained after detachment from the plasma membrane. In other cell types, similar structures are associated to specific conditions. F-actin can form ring-like structures around phagosomes, as a temporary phenomenon termed actin flashing which delays fusion to lysosomes in cargo overloaded macrophages (Liebl & Griffiths, 2009). A similar, periphagosomal F-actin accumulation is triggered by *Leishmania donovani promastigotes* to inhibit phagosomal maturation (Lodge & Descoteaux, 2005; Moradin & Descoteaux, 2012). Whether the actin coat on PAC EVs has a similar role in delaying maturation/lysosomal fusion is not known and this generates a topic for further investigations. In *Dictyostelium*, it is WASH, rather than F-actin, to form ring-like structures coating phagosomes and macropinosomes (Carnell *et al.*, 2011; King *et al.*, 2013; Park *et al.*, 2013; Buckley *et al.*, 2016). This process is involved in recycling surface proteins before degradation, or recycling V-ATPase and lysosomal hydrolases before exocytosis. It is conceivable that the removal of the actin coat from EVs is also associated with recycling of membrane components; this process might, for instance, facilitate EV recognition by the LC3 lipidation machinery.

6.3 Non-canonical LC3 lipidation on endocytic vacuoles

Autophagy is a general term defining processes that target different types of cargo for lysosomal degradation. Whilst canonical autophagy is generally associated with the engulfment of cytosolic material, non-canonical pathways often deal with cargo of extracellular origin. Non-canonical autophagy occurs in immune cells for pathogen clearance (LAP) (Sanjuan *et al.*, 2007) or for antigen presentation (Ma *et al.*, 2012) and in epithelial cells during entosis and macropinocytosis (Florey *et al.*, 2011; Florey *et al.*, 2015). Non-canonical autophagy bypasses the ULK1 complex and, in some cases, the PI(3)K complex of the canonical pathway, and is therefore a quicker process for LC3 targeting and association to membranes. In PACs, EVs are formed from post-exocytic structures following release of zymogens in the acinar lumen. It is conceivable (and likely) that some EVs retain/incorporate zymogens. This could be one way of delivery of trypsinogen to EVs, where it can be activated (Sherwood *et al.*, 2007). Moreover, EVs can undergo rupture and leak their content in the cytosol (Chvanov *et al.*, 2018). Targeting and clearing these organelles before this occurs is therefore essential to prevent cell damage. This will require a fast response by the cell, and is thus likely to rely on non-canonical autophagy. In this study, it appears that both canonical and non-canonical autophagy are induced by CCK stimulation. The former is sensitive to bafilomycin, which potentiates LC3 puncta accumulation. The latter is also, but differently, sensitive to bafilomycin, which prevents LC3 lipidation on EVs. We thus speculate that both canonical and non-canonical autophagy are activated, but have different functions and possibly dynamics. The faster, non-canonical component has the role to target EV content for degradation.

6.4 Relevance to acute pancreatitis

EVs are the site of intracellular trypsinogen activation and can leak their content in the cytosol. These processes underpin the early pathophysiology of AP at the acinar cell level. The non-canonical LC3 lipidation of EVs might represent a protective mechanism to target EV content for lysosomal degradation. It would be interesting to induce experimental AP in E230 mice, specifically lacking non-canonical autophagy. In this work, the LC3 lipidation was significantly reduced in these animals. We could hypothesise that, if the LC3 lipidation is indeed protective, acinar cell damage in experimental AP will be exacerbated in the E230 mice.

Extensive investigation of the role of autophagy in experimental pancreatitis has been carried out. Previous studies have focused on late stages of autophagy, targeting LC3 conjugation machineries (ATG5 or ATG7) and lysosomal function (LAMP2 or cathepsins). It is important to note that these stages are common to canonical and non-canonical pathways. Inhibition of autophagy (*Atg5* KO or siRNA) reduces trypsinogen activation in experimental AP (Hashimoto *et al.*, 2008; Mareninova *et al.*, 2009). These results would suggest that autophagy somehow facilitates trypsinogen activation. Nevertheless, the common view in the field is that experimental AP impairs autophagic flux, in particular at lysosomal degradation stages (Gukovsky *et al.*, 2012; Gukovskaya *et al.*, 2017). Indeed, mouse models with defective autophagy (*Lamp2*, *Atg5* or *Atg7* KO) develop spontaneous AP (Mareninova *et al.*, 2015), CP (Diakopoulos *et al.*, 2015), or AP then resulting in CP (Zhou *et al.*, 2017), respectively. Thus, it is possible that autophagy (in our case, non-canonical autophagy of EVs) is protective, but in AP it loses its degradative capability. In this

thesis, focus has been placed on specifically addressing the targeting of EVs for LC3 lipidation. The lysosomal degradation of their cargo represents a further important question which will aid in the understanding of the role of these organelles in AP.

Several works report that impaired processing and sorting of lysosomal hydrolases is associated with trypsinogen activation, following co-localisation of cathepsins and zymogens (Saluja *et al.*, 1997; Van Acker *et al.*, 2002). A recent study showed that trypsin activity determined leakage of cathepsins B in the cytosol, where it triggered necrosis and apoptosis (Talukdar *et al.*, 2016). Conversely, our group found that nor trypsin nor cathepsin inhibition affected the leakage of contents from EVs (Chvanov *et al.*, 2018). This suggests that the fragility of our EVs is not associated with activity of these enzymes and might be associated with a different process, possibly loss of the F-actin coating.

It is also important to remember that *in vivo*, AP pathophysiology is also influenced by damage of PDCs (Hegyi *et al.*, 2011) and PSCs (Gryshchenko *et al.*, 2018) and by induction of the inflammatory response. Trypsinogen activation occurs in infiltrating macrophages, demonstrating that extra-acinar events contribute to disease (Aghdassi *et al.*, 2018; Sendler *et al.*, 2018). This thesis focused on isolated PACs but it is conceivable that the relevance of these phenomena is different *in vivo*.

6.5 Future perspectives

The relevance of this study lays in monitoring EV processing in live cells. The project has focused on characterising the properties of individual EVs, by performing immunofluorescence staining, electron microscopy and pH measurements of selected EVs. These experiments provide exciting data, but have their limitations. In the future, the study would benefit from biochemical approaches, for example to monitor the time course of LC3 lipidation (canonical and non-canonical) throughout stimulation. Immunoprecipitation techniques might help elucidate the proteins interacting with LC3 lipidation machinery and actin polymerising factors. Performing proteomic studies on isolated EVs might help characterise their membrane composition and possibly reveal the markers that mediate targeting for LC3 lipidation. Additionally, identifying the channels and transporters might shed light on the pH and osmotic properties throughout different developmental stages of EVs. Furthermore, it might be interesting to perform electrophysiology studies on isolated EVs to biophysically characterise their ion channels and transporters.

Autophagy (both canonical and non-canonical) are trending topics. Autophagic pathways occur in different cell types, in both physiological and pathological conditions. There is much to be discovered on the mechanistic features of these pathways. Determining the cargo of these organelles and monitoring its degradation constitutes a logical development to elucidate the function of the LC3 lipidation of EVs. Moreover, the fact that non-canonical autophagy is activated in an epithelial cell type as a mechanism of selective targeting of potentially harmful organelles is likely to be translatable to other cell types. It would be interesting to elucidate if this

phenomenon is common to other exocrine secretory epithelia, such as the salivary glands.

There is evidence that F-actin is implicated in exocytosis and compensatory membrane retrieval in lacrimal and salivary acinar cells (Segawa & Yamashina, 1989; Tojyo *et al.*, 1989; Okumura *et al.*, 1990; da Costa *et al.*, 2002; Masedunskas *et al.*, 2011). EVs are documented in submandibular acinar cells (Tapp, 1968). Interestingly, the treatment of parotid acinar cells with cytochalasin D determined the appearance of rhodamine-labelled cytosolic actin rings (Tojyo *et al.*, 1989). These structures resemble the ring-like appearance of the actin coat on PAC EVs. Hence, investigating interaction of F-actin and EVs in other exocrine glands represents a promising research line.

This study reports interesting phenomena but it is possibly limited to the conditions tested: CCK or TLC-S stimulation of murine PACs. For a translational perspective, it would be interesting to test other inducers of AP such as FAEEs. It would also be interesting to explore these phenomena in human PACs.

The EVs are unique organelles in the sense that they are almost exclusive to exocrine secretory cells. Nevertheless, I have found that they interact with (non-canonical) autophagy machinery and actin cytoskeleton, similarly to phagosomes, macropinosomes and entotic vacuoles. I hope that the findings reported in this study will prompt further investigations of the general principles of these processes.

Bibliography

Aghdassi AA, John DS, Sendler M, Weiss FU, Reinheckel T, Mayerle J & Lerch MM. (2018). Cathepsin D regulates cathepsin B activation and disease severity predominantly in inflammatory cells during experimental pancreatitis. *J Biol Chem* **293,** 1018-1029.

Aguilera MO, Beron W & Colombo MI. (2012). The actin cytoskeleton participates in the early events of autophagosome formation upon starvation induced autophagy. *Autophagy* **8,** 1590-1603.

Aniento F, Gu F, Parton RG & Gruenberg J. (1996). An endosomal beta COP is involved in the pH-dependent formation of transport vesicles destined for late endosomes. *J Cell Biol* **133,** 29-41.

Antonucci L, Fagman JB, Kim JY, Todoric J, Gukovsky I, Mackey M, . . . Karin M. (2015). Basal autophagy maintains pancreatic acinar cell homeostasis and protein synthesis and prevents ER stress. *Proc Natl Acad Sci U S A* **112,** E6166-6174.

Apodaca G. (2001). Endocytic traffic in polarized epithelial cells: role of the actin and microtubule cytoskeleton. *Traffic* **2,** 149-159.

Araki N, Johnson MT & Swanson JA. (1996). A role for phosphoinositide 3-kinase in the completion of macropinocytosis and phagocytosis by macrophages. *J Cell Biol* **135,** 1249-1260.

Auer M, Hausott B & Klimaschewski L. (2011). Rho GTPases as regulators of morphological neuroplasticity. *Ann Anat* **193,** 259-266.

Axe EL, Walker SA, Manifava M, Chandra P, Roderick HL, Habermann A, . . . Ktistakis NT. (2008). Autophagosome formation from membrane compartments enriched in phosphatidylinositol 3-phosphate and dynamically connected to the endoplasmic reticulum. *J Cell Biol* **182,** 685-701.

Bachem MG, Schneider E, Gross H, Weidenbach H, Schmid RM, Menke A, . . . Adler G. (1998). Identification, culture, and characterization of pancreatic stellate cells in rats and humans. *Gastroenterology* **115,** 421-432.

Baggaley EM, Elliott AC & Bruce JI. (2008). Oxidant-induced inhibition of the plasma membrane Ca2+-ATPase in pancreatic acinar cells: role of the mitochondria. *Am J Physiol Cell Physiol* **295,** C1247-1260.

Bamburg JR. (1999). Proteins of the ADF/cofilin family: essential regulators of actin dynamics. *Annu Rev Cell Dev Biol* **15,** 185-230.

Bamburg JR, Harris HE & Weeds AG. (1980). Partial purification and characterization of an actin depolymerizing factor from brain. *FEBS Lett* **121,** 178-182.

Banks PA, Freeman ML & Practice Parameters Committee of the American College of G. (2006). Practice guidelines in acute pancreatitis. *Am J Gastroenterol* **101,** 2379-2400.

Barrow SL, Voronina SG, da Silva Xavier G, Chvanov MA, Longbottom RE, Gerasimenko OV, . . . Tepikin AV. (2008). ATP depletion inhibits Ca2+ release, influx and extrusion in pancreatic acinar cells but not pathological Ca2+ responses induced by bile. *Pflugers Arch* **455,** 1025-1039.

Bayliss WM & Starling EH. (1902). The mechanism of pancreatic secretion. *J Physiol* **28,** 325-353.

Behrendorff N, Dolai S, Hong W, Gaisano HY & Thorn P. (2011). Vesicle-associated membrane protein 8 (VAMP8) is a SNARE (soluble N-ethylmaleimide-sensitive factor attachment protein receptor) selectively required for sequential granule-to-granule fusion. *J Biol Chem* **286,** 29627-29634.

Bel S, Pendse M, Wang Y, Li Y, Ruhn KA, Hassell B, . . . Hooper LV. (2017). Paneth cells secrete lysozyme via secretory autophagy during bacterial infection of the intestine. *Science* **357,** 1047-1052.

Bendayan M, Roth J, Perrelet A & Orci L. (1980). Quantitative immunocytochemical localization of pancreatic secretory proteins in subcellular compartments of the rat acinar cell. *J Histochem Cytochem* **28,** 149-160.

Berg TO, Fengsrud M, Stromhaug PE, Berg T & Seglen PO. (1998). Isolation and characterization of rat liver amphisomes. Evidence for fusion of autophagosomes with both early and late endosomes. *J Biol Chem* **273,** 21883-21892.

Bezprozvanny I, Watras J & Ehrlich BE. (1991). Bell-shaped calcium-response curves of Ins(1,4,5)P3- and calcium-gated channels from endoplasmic reticulum of cerebellum. *Nature* **351,** 751-754.

Bhat P & Thorn P. (2009). Myosin 2 maintains an open exocytic fusion pore in secretory epithelial cells. *Mol Biol Cell* **20,** 1795-1803.

Bi Y, Page SL & Williams JA. (2005). Rho and Rac promote acinar morphological changes, actin reorganization, and amylase secretion. *Am J Physiol Gastrointest Liver Physiol* **289,** G561-570.

Bi Y & Williams JA. (2005). A role for Rho and Rac in secretagogue-induced amylase release by pancreatic acini. *Am J Physiol Cell Physiol* **289,** C22-32.

Biczo G, Vegh ET, Shalbueva N, Mareninova OA, Elperin J, Lotshaw E, . . . Gukovskaya AS. (2018). Mitochondrial Dysfunction, Through Impaired Autophagy, Leads to Endoplasmic Reticulum Stress, Deregulated Lipid Metabolism, and Pancreatitis in Animal Models. *Gastroenterology* **154,** 689-703.

Bieger W, Martin-Achard A, Bassler M & Kern HF. (1976a). Studies on intracellular transport of secretory proteins in the rat exocrine pancreas. IV. Stimulation by in vivo infusion of caerulein. *Cell Tissue Res* **165,** 435-453.

Bieger W, Seybold J & Kern HF. (1976b). Studies on intracellular transport of secretory proteins in the rat exocrine pancreas. V. Kinetic studies on accelerated transport following caerulein infusion in vivo. *Cell Tissue Res* **170,** 203-219.

Blinman TA, Gukovsky I, Mouria M, Zaninovic V, Livingston E, Pandol SJ & Gukovskaya AS. (2000). Activation of pancreatic acinar cells on isolation from tissue: cytokine upregulation via p38 MAP kinase. *Am J Physiol Cell Physiol* **279,** C1993-2003.

Bolender RP. (1974). Stereological analysis of the guinea pig pancreas. I. Analytical model and quantitative description of nonstimulated pancreatic exocrine cells. *J Cell Biol* **61,** 269-287.

Bootman MD, Chehab T, Bultynck G, Parys JB & Rietdorf K. (2018). The regulation of autophagy by calcium signals: Do we have a consensus? *Cell Calcium* **70,** 32-46.

Bos JL, Rehmann H & Wittinghofer A. (2007). GEFs and GAPs: critical elements in the control of small G proteins. *Cell* **129,** 865-877.

Bouras EP, Misukonis MA & Liddle RA. (1992). Role of calcium in monitor peptide-stimulated cholecystokinin release from perifused intestinal cells. *Am J Physiol* **262,** G791-796.

Boyle KB & Randow F. (2015). Rubicon swaps autophagy for LAP. *Nat Cell Biol* **17,** 843-845.

Brooks CR, Yeung MY, Brooks YS, Chen H, Ichimura T, Henderson JM & Bonventre JV. (2015). KIM-1-/TIM-1-mediated phagocytosis links ATG5-/ULK1-dependent clearance of apoptotic cells to antigen presentation. *EMBO J* **34,** 2441-2464.

Bruce JI & Elliott AC. (2007). Oxidant-impaired intracellular Ca2+ signaling in pancreatic acinar cells: role of the plasma membrane Ca2+-ATPase. *Am J Physiol Cell Physiol* **293,** C938-950.

Bubb MR, Spector I, Beyer BB & Fosen KM. (2000). Effects of jasplakinolide on the kinetics of actin polymerization. An explanation for certain in vivo observations. *J Biol Chem* **275,** 5163-5170.

Buckley CM, Gopaldass N, Bosmani C, Johnston SA, Soldati T, Insall RH & King JS. (2016). WASH drives early recycling from macropinosomes and phagosomes to maintain surface phagocytic receptors. *Proc Natl Acad Sci U S A* **113,** E5906-E5915.

Burnham DB & Williams JA. (1982). Effects of high concentrations of secretagogues on the morphology and secretory activity of the pancreas: a role for microfilaments. *Cell Tissue Res* **222,** 201-212.

Campellone KG & Welch MD. (2010). A nucleator arms race: cellular control of actin assembly. *Nat Rev Mol Cell Biol* **11,** 237-251.

Campos-Toimil M, Bagrij T, Edwardson JM & Thomas P. (2002). Two modes of secretion in pancreatic acinar cells: involvement of phosphatidylinositol 3-kinase and regulation by capacitative Ca(2+) entry. *Curr Biol* **12,** 211-215.

Cancela JM, Churchill GC & Galione A. (1999). Coordination of agonist-induced Ca2+-signalling patterns by NAADP in pancreatic acinar cells. *Nature* **398,** 74-76.

Cancela JM, Gerasimenko OV, Gerasimenko JV, Tepikin AV & Petersen OH. (2000). Two different but converging messenger pathways to intracellular Ca(2+) release: the roles of nicotinic acid adenine dinucleotide phosphate, cyclic ADP-ribose and inositol trisphosphate. *EMBO J* **19,** 2549-2557.

Carnell M, Zech T, Calaminus SD, Ura S, Hagedorn M, Johnston SA, . . . Insall RH. (2011). Actin polymerization driven by WASH causes V-ATPase retrieval and vesicle neutralization before exocytosis. *J Cell Biol* **193,** 831-839.

Casey JR, Grinstein S & Orlowski J. (2010). Sensors and regulators of intracellular pH. *Nat Rev Mol Cell Biol* **11,** 50-61.

Cassidy LD, Young AR, Perez-Mancera PA, Nimmervoll B, Jaulim A, Chen HC, . . . Narita M. (2018). A novel Atg5-shRNA mouse model enables temporal control of Autophagy in vivo. *Autophagy***,** 1-11.

Castellano F, Chavrier P & Caron E. (2001). Actin dynamics during phagocytosis. *Semin Immunol* **13,** 347-355.

Chandrasekar I, Goeckeler ZM, Turney SG, Wang P, Wysolmerski RB, Adelstein RS & Bridgman PC. (2014). Nonmuscle myosin II is a critical regulator of clathrin-mediated endocytosis. *Traffic* **15,** 418-432.

Chen SH, Bubb MR, Yarmola EG, Zuo J, Jiang J, Lee BS, . . . Holliday LS. (2004a). Vacuolar H+-ATPase binding to microfilaments: regulation in response to phosphatidylinositol 3-kinase activity and detailed characterization of the actin-binding site in subunit B. *J Biol Chem* **279,** 7988-7998.

Chen X, Edwards JA, Logsdon CD, Ernst SA & Williams JA. (2002). Dominant negative Rab3D inhibits amylase release from mouse pancreatic acini. *J Biol Chem* **277,** 18002-18009.

Chen X, Li C, Izumi T, Ernst SA, Andrews PC & Williams JA. (2004b). Rab27b localizes to zymogen granules and regulates pancreatic acinar exocytosis. *Biochem Biophys Res Commun* **323,** 1157-1162.

Chen X, Ulintz PJ, Simon ES, Williams JA & Andrews PC. (2008). Global topology analysis of pancreatic zymogen granule membrane proteins. *Mol Cell Proteomics* **7,** 2323-2336.

Chen X, Walker AK, Strahler JR, Simon ES, Tomanicek-Volk SL, Nelson BB, . . . Andrews PC. (2006). Organellar proteomics: analysis of pancreatic zymogen granule membranes. *Mol Cell Proteomics* **5,** 306-312.

Chen Y & Klionsky DJ. (2011). The regulation of autophagy - unanswered questions. *J Cell Sci* **124,** 161-170.

Chhabra ES & Higgs HN. (2007). The many faces of actin: matching assembly factors with cellular structures. *Nat Cell Biol* **9,** 1110-1121.

Christophe J. (1994). Pancreatic tumoral cell line AR42J: an amphicrine model. *Am J Physiol* **266,** G963-971.

Chvanov M, De Faveri F, Moore D, Sherwood MW, Awais M, Voronina S, . . . Tepikin AV. (2018). Intracellular rupture, exocytosis and actin interaction of endocytic vacuoles in pancreatic acinar cells: initiating events in acute pancreatitis. *J Physiol* **596,** 2547-2564.

Compton LM, Ikonomov OC, Sbrissa D, Garg P & Shisheva A. (2016). Active vacuolar H+ ATPase and functional cycle of Rab5 are required for the vacuolation defect triggered by PtdIns(3,5)P2 loss under PIKfyve or Vps34 deficiency. *Am J Physiol Cell Physiol* **311,** C366-377.

Cosen-Binker LI, Binker MG, Wang CC, Hong W & Gaisano HY. (2008). VAMP8 is the v-SNARE that mediates basolateral exocytosis in a mouse model of alcoholic pancreatitis. *J Clin Invest* **118,** 2535-2551.

Coutts AS & La Thangue NB. (2015). Actin nucleation by WH2 domains at the autophagosome. *Nat Commun* **6,** 7888.

Coutts AS & La Thangue NB. (2016). Regulation of actin nucleation and autophagosome formation. *Cell Mol Life Sci* **73,** 3249-3263.

Criddle DN, Booth DM, Mukherjee R, McLaughlin E, Green GM, Sutton R, . . . Reeve JR, Jr. (2009). Cholecystokinin-58 and cholecystokinin-8 exhibit similar actions on calcium signaling, zymogen secretion, and cell fate in murine pancreatic acinar cells. *Am J Physiol Gastrointest Liver Physiol* **297,** G1085-1092.

Criddle DN, Murphy J, Fistetto G, Barrow S, Tepikin AV, Neoptolemos JP, . . . Petersen OH. (2006). Fatty acid ethyl esters cause pancreatic calcium toxicity via inositol trisphosphate receptors and loss of ATP synthesis. *Gastroenterology* **130,** 781-793.

Criddle DN, Raraty MG, Neoptolemos JP, Tepikin AV, Petersen OH & Sutton R. (2004). Ethanol toxicity in pancreatic acinar cells: mediation by nonoxidative fatty acid metabolites. *Proc Natl Acad Sci U S A* **101,** 10738-10743.

Croise P, Estay-Ahumada C, Gasman S & Ory S. (2014). Rho GTPases, phosphoinositides, and actin: a tripartite framework for efficient vesicular trafficking. *Small GTPases* **5,** e29469.

da Costa SR, Andersson S, Arber F, Okamoto C & Hamm-Alvarez S. (2002). Cytoskeletal participation in stimulated secretion and compensatory apical plasma membrane retrieval in lacrimal gland acinar cells. *Adv Exp Med Biol* **506,** 199-205.

Dahan S, Anderson KL, Weller S, Krueger E & McNiven MA. (2005). Agonist-induced vesiculation of the Golgi apparatus in pancreatic acinar cells. *Gastroenterology* **129,** 2032-2046.

Dartsch H, Kleene R & Kern HF. (1998). In vitro condensation-sorting of enzyme proteins isolated from rat pancreatic acinar cells. *Eur J Cell Biol* **75,** 211-222.

De Lisle RC & Williams JA. (1987). Zymogen granule acidity is not required for stimulated pancreatic protein secretion. *Am J Physiol* **253,** G711-719.

Delevoye C, Heiligenstein X, Ripoll L, Gilles-Marsens F, Dennis MK, Linares RA, . . . Raposo G. (2016). BLOC-1 Brings Together the Actin and Microtubule Cytoskeletons to Generate Recycling Endosomes. *Curr Biol* **26,** 1-13.

Derivery E, Sousa C, Gautier JJ, Lombard B, Loew D & Gautreau A. (2009). The Arp2/3 activator WASH controls the fission of endosomes through a large multiprotein complex. *Dev Cell* **17,** 712-723.

Deschodt-Lanckman M, Robberecht P, De Neef P, Lammens M & Christophe J. (1976). In vitro action of bombesin and bombesin-like peptides on amylase secretion, calcium efflux, and adenylate cyclase activity in the rat pancreas: a comparison with other secretagogues. *J Clin Invest* **58,** 891-898.

Diakopoulos KN, Lesina M, Wormann S, Song L, Aichler M, Schild L, . . . Algul H. (2015). Impaired autophagy induces chronic atrophic pancreatitis in mice via sex- and nutrition-dependent processes. *Gastroenterology* **148,** 626-638 e617.

Dolai S, Liang T, Lam PPL, Fernandez NA, Chidambaram S & Gaisano HY. (2012). Effects of ethanol metabolites on exocytosis of pancreatic acinar cells in rats. *Gastroenterology* **143,** 832-843 e837.

Dolai S, Liang T, Orabi AI, Holmyard D, Xie L, Greitzer-Antes D, . . . Gaisano HY. (2018). Pancreatitis-Induced Depletion of Syntaxin 2 Promotes Autophagy and Increases Basolateral Exocytosis. *Gastroenterology* **154,** 1805-1821 e1805.

Dolensek J, Rupnik MS & Stozer A. (2015). Structural similarities and differences between the human and the mouse pancreas. *Islets* **7,** e1024405.

Dooley HC, Razi M, Polson HE, Girardin SE, Wilson MI & Tooze SA. (2014). WIPI2 links LC3 conjugation with PI3P, autophagosome formation, and pathogen clearance by recruiting Atg12-5-16L1. *Mol Cell* **55,** 238-252.

Draber P, Sulimenko V & Draberova E. (2012). Cytoskeleton in mast cell signaling. *Front Immunol* **3,** 130.

Dufresne M, Seva C & Fourmy D. (2006). Cholecystokinin and gastrin receptors. *Physiol Rev* **86,** 805-847.

Durrbach A, Louvard D & Coudrier E. (1996). Actin filaments facilitate two steps of endocytosis. *J Cell Sci* **109 (Pt 2),** 457-465.

Echarri A & Del Pozo MA. (2015). Caveolae - mechanosensitive membrane invaginations linked to actin filaments. *J Cell Sci* **128,** 2747-2758.

Eskelinen EL & Kovacs AL. (2011). Double membranes vs. lipid bilayers, and their significance for correct identification of macroautophagic structures. *Autophagy* **7,** 931-932.

Falcon B, Noad J, McMahon H, Randow F & Goedert M. (2018). Galectin-8-mediated selective autophagy protects against seeded tau aggregation. *J Biol Chem* **293,** 2438-2451.

Falkowski MA, Thomas DD & Groblewski GE. (2010). Complexin 2 modulates vesicle-associated membrane protein (VAMP) 2-regulated zymogen granule exocytosis in pancreatic acini. *J Biol Chem* **285,** 35558-35566.

Falkowski MA, Thomas DD, Messenger SW, Martin TF & Groblewski GE. (2011). Expression, localization, and functional role for synaptotagmins in pancreatic acinar cells. *Am J Physiol Gastrointest Liver Physiol* **301,** G306-316.

Feil R, Brocard J, Mascrez B, LeMeur M, Metzger D & Chambon P. (1996). Ligand-activated site-specific recombination in mice. *Proc Natl Acad Sci U S A* **93,** 10887-10890.

Feng Y, He D, Yao Z & Klionsky DJ. (2014). The machinery of macroautophagy. *Cell Res* **24,** 24-41.

Ferguson SM, Raimondi A, Paradise S, Shen H, Mesaki K, Ferguson A, . . . De Camilli P. (2009). Coordinated actions of actin and BAR proteins upstream of dynamin at endocytic clathrin-coated pits. *Dev Cell* **17,** 811-822.

Fernandez-Borja M, Janssen L, Verwoerd D, Hordijk P & Neefjes J. (2005). RhoB regulates endosome transport by promoting actin assembly on endosomal membranes through Dia1. *J Cell Sci* **118,** 2661-2670.

Fischer L, Gukovskaya AS, Penninger JM, Mareninova OA, Friess H, Gukovsky I & Pandol SJ. (2007). Phosphatidylinositol 3-kinase facilitates bile acid-induced Ca(2+) responses in pancreatic acinar cells. *Am J Physiol Gastrointest Liver Physiol* **292,** G875-886.

Fischer L, Gukovskaya AS, Young SH, Gukovsky I, Lugea A, Buechler P, . . . Pandol SJ. (2004). Phosphatidylinositol 3-kinase regulates Ca2+ signaling in pancreatic acinar cells through inhibition of sarco(endo)plasmic reticulum Ca2+-ATPase. *Am J Physiol Gastrointest Liver Physiol* **287,** G1200-1212.

Fitzsimmons TJ, Gukovsky I, McRoberts JA, Rodriguez E, Lai FA & Pandol SJ. (2000). Multiple isoforms of the ryanodine receptor are expressed in rat pancreatic acinar cells. *Biochem J* **351,** 265-271.

Fletcher K, Ulferts R, Jacquin E, Veith T, Gammoh N, Arasteh JM, . . . Florey O. (2018). The WD40 domain of ATG16L1 is required for its non-canonical role in lipidation of LC3 at single membranes. *EMBO J*.

Florey O, Gammoh N, Kim SE, Jiang X & Overholtzer M. (2015). V-ATPase and osmotic imbalances activate endolysosomal LC3 lipidation. *Autophagy* **11,** 88-99.

Florey O, Kim SE, Sandoval CP, Haynes CM & Overholtzer M. (2011). Autophagy machinery mediates macroendocytic processing and entotic cell death by targeting single membranes. *Nat Cell Biol* **13,** 1335-1343.

Florey O & Overholtzer M. (2012). Autophagy proteins in macroendocytic engulfment. *Trends Cell Biol* **22,** 374-380.

Freedman SD & Scheele GA. (1993). Regulated secretory proteins in the exocrine pancreas aggregate under conditions that mimic the trans-Golgi network. *Biochem Biophys Res Commun* **197,** 992-999.

Fritsch R, de Krijger I, Fritsch K, George R, Reason B, Kumar MS, . . . Downward J. (2013). RAS and RHO families of GTPases directly regulate distinct phosphoinositide 3-kinase isoforms. *Cell* **153,** 1050-1063.

Fujino I, Yamada N, Miyawaki A, Hasegawa M, Furuichi T & Mikoshiba K. (1995). Differential expression of type 2 and type 3 inositol 1,4,5-trisphosphate receptor mRNAs in various mouse tissues: in situ hybridization study. *Cell Tissue Res* **280,** 201-210.

Fujita N, Itoh T, Omori H, Fukuda M, Noda T & Yoshimori T. (2008). The Atg16L complex specifies the site of LC3 lipidation for membrane biogenesis in autophagy. *Mol Biol Cell* **19,** 2092-2100.

Gaiser S, Daniluk J, Liu Y, Tsou L, Chu J, Lee W, . . . Ji B. (2011). Intracellular activation of trypsinogen in transgenic mice induces acute but not chronic pancreatitis. *Gut* **60,** 1379-1388.

Galluzzi L, Baehrecke EH, Ballabio A, Boya P, Bravo-San Pedro JM, Cecconi F, . . . Kroemer G. (2017). Molecular definitions of autophagy and related processes. *EMBO J* **36,** 1811-1836.

Gammoh N, Florey O, Overholtzer M & Jiang X. (2013). Interaction between FIP200 and ATG16L1 distinguishes ULK1 complex-dependent and -independent autophagy. *Nat Struct Mol Biol* **20,** 144-149.

Gao Y, Liu Y, Hong L, Yang Z, Cai X, Chen X, . . . Li M. (2016). Golgi-associated LC3 lipidation requires V-ATPase in noncanonical autophagy. *Cell Death Dis* **7,** e2330.

Gasman S, Kalaidzidis Y & Zerial M. (2003). RhoD regulates endosome dynamics through Diaphanous-related Formin and Src tyrosine kinase. *Nat Cell Biol* **5,** 195-204.

Gasser KW, DiDomenico J & Hopfer U. (1988). Potassium transport by pancreatic and parotid zymogen granule membranes. *Am J Physiol* **255,** C705-711.

Gautam D, Han SJ, Heard TS, Cui Y, Miller G, Bloodworth L & Wess J. (2005). Cholinergic stimulation of amylase secretion from pancreatic acinar cells studied with muscarinic acetylcholine receptor mutant mice. *J Pharmacol Exp Ther* **313,** 995-1002.

Geng J & Klionsky DJ. (2008). The Atg8 and Atg12 ubiquitin-like conjugation systems in macroautophagy. 'Protein modifications: beyond the usual suspects' review series. *EMBO Rep* **9,** 859-864.

Gerasimenko JV, Gryshchenko O, Ferdek PE, Stapleton E, Hebert TO, Bychkova S, . . . Petersen OH. (2013). Ca2+ release-activated Ca2+ channel blockade as a potential tool in antipancreatitis therapy. *Proc Natl Acad Sci U S A* **110,** 13186-13191.

Gerasimenko JV, Lur G, Sherwood MW, Ebisui E, Tepikin AV, Mikoshiba K, . . . Petersen OH. (2009). Pancreatic protease activation by alcohol metabolite depends on Ca2+ release via acid store IP3 receptors. *Proc Natl Acad Sci U S A* **106,** 10758-10763.

Gerasimenko JV, Peng S, Tsugorka T & Gerasimenko OV. (2018). Ca(2+) signalling underlying pancreatitis. *Cell Calcium* **70,** 95-101.

Gerasimenko JV, Sherwood M, Tepikin AV, Petersen OH & Gerasimenko OV. (2006). NAADP, cADPR and IP3 all release Ca2+ from the endoplasmic reticulum and an acidic store in the secretory granule area. *J Cell Sci* **119,** 226-238.

Geron E, Schejter ED & Shilo BZ. (2013). Directing exocrine secretory vesicles to the apical membrane by actin cables generated by the formin mDia1. *Proc Natl Acad Sci U S A* **110,** 10652-10657.

Girao H, Geli MI & Idrissi FZ. (2008). Actin in the endocytic pathway: from yeast to mammals. *FEBS Lett* **582,** 2112-2119.

Gluschko A, Herb M, Wiegmann K, Krut O, Neiss WF, Utermohlen O, . . . Schramm M. (2018). The beta2 Integrin Mac-1 Induces Protective LC3-Associated Phagocytosis of Listeria monocytogenes. *Cell Host Microbe* **23,** 324-337 e325.

Go VLW. (1993). *The Pancreas : biology, pathobiology, and disease*. Raven Press, New York.

Goley ED & Welch MD. (2006). The ARP2/3 complex: an actin nucleator comes of age. *Nat Rev Mol Cell Biol* **7,** 713-726.

Gordon PB & Seglen PO. (1988). Prelysosomal convergence of autophagic and endocytic pathways. *Biochem Biophys Res Commun* **151,** 40-47.

Gorelick FS, Shugrue CA, Kolodecik TR & Thrower EC. (2006). Vacuolar adenosine triphosphatase and pancreatic acinar cell function. *J Gastroenterol Hepatol* **21 Suppl 3,** S18-21.

Grasso D, Ropolo A, Lo Re A, Boggio V, Molejon MI, Iovanna JL, . . . Vaccaro MI. (2011). Zymophagy, a novel selective autophagy pathway mediated by VMP1-USP9x-p62, prevents pancreatic cell death. *J Biol Chem* **286,** 8308-8324.

Griffiths G & Simons K. (1986). The trans Golgi network: sorting at the exit site of the Golgi complex. *Science* **234,** 438-443.

Gryshchenko O, Gerasimenko JV, Gerasimenko OV & Petersen OH. (2016). Ca(2+) signals mediated by bradykinin type 2 receptors in normal pancreatic stellate cells can be inhibited by specific Ca(2+) channel blockade. *J Physiol* **594,** 281-293.

Gryshchenko O, Gerasimenko JV, Peng S, Gerasimenko OV & Petersen OH. (2018). Calcium signalling in the acinar environment of the exocrine pancreas: physiology and pathophysiology. *J Physiol* **596,** 2663-2678.

Gu F & Gruenberg J. (2000). ARF1 regulates pH-dependent COP functions in the early endocytic pathway. *J Biol Chem* **275,** 8154-8160.

Gukovskaya AS, Gukovsky I, Algul H & Habtezion A. (2017). Autophagy, Inflammation, and Immune Dysfunction in the Pathogenesis of Pancreatitis. *Gastroenterology* **153,** 1212-1226.

Gukovskaya AS, Gukovsky I, Zaninovic V, Song M, Sandoval D, Gukovsky S & Pandol SJ. (1997). Pancreatic acinar cells produce, release, and respond to tumor necrosis factor-alpha. Role in regulating cell death and pancreatitis. *J Clin Invest* **100,** 1853-1862.

Gukovsky I, Gukovskaya AS, Blinman TA, Zaninovic V & Pandol SJ. (1998). Early NF-kappaB activation is associated with hormone-induced pancreatitis. *Am J Physiol* **275,** G1402-1414.

Gukovsky I, Pandol SJ, Mareninova OA, Shalbueva N, Jia W & Gukovskaya AS. (2012). Impaired autophagy and organellar dysfunction in pancreatitis. *J Gastroenterol Hepatol* **27 Suppl 2,** 27-32.

Gurkar AU, Chu K, Raj L, Bouley R, Lee SH, Kim YB, . . . Lee SW. (2013). Identification of ROCK1 kinase as a critical regulator of Beclin1-mediated autophagy during metabolic stress. *Nat Commun* **4,** 2189.

Gutierrez MG, Munafo DB, Beron W & Colombo MI. (2004). Rab7 is required for the normal progression of the autophagic pathway in mammalian cells. *J Cell Sci* **117,** 2687-2697.

Haga RB & Ridley AJ. (2016). Rho GTPases: Regulation and roles in cancer cell biology. *Small GTPases* **7,** 207-221.

Halangk W, Lerch MM, Brandt-Nedelev B, Roth W, Ruthenbuerger M, Reinheckel T, . . . Deussing J. (2000). Role of cathepsin B in intracellular trypsinogen activation and the onset of acute pancreatitis. *J Clin Invest* **106,** 773-781.

Hanada T, Noda NN, Satomi Y, Ichimura Y, Fujioka Y, Takao T, . . . Ohsumi Y. (2007). The Atg12-Atg5 conjugate has a novel E3-like activity for protein lipidation in autophagy. *J Biol Chem* **282,** 37298-37302.

Hanna S & El-Sibai M. (2013). Signaling networks of Rho GTPases in cell motility. *Cell Signal* **25,** 1955-1961.

Hartwig JH, Bokoch GM, Carpenter CL, Janmey PA, Taylor LA, Toker A & Stossel TP. (1995). Thrombin receptor ligation and activated Rac uncap actin filament barbed ends through phosphoinositide synthesis in permeabilized human platelets. *Cell* **82,** 643-653.

Harvey WR. (1992). Physiology of V-ATPases. *J Exp Biol* **172,** 1-17.

Hashimoto D, Ohmuraya M, Hirota M, Yamamoto A, Suyama K, Ida S, . . . Yamamura K. (2008). Involvement of autophagy in trypsinogen activation within the pancreatic acinar cells. *J Cell Biol* **181,** 1065-1072.

Hasson T. (2003). Myosin VI: two distinct roles in endocytosis. *J Cell Sci* **116,** 3453-3461.

He H, Dang Y, Dai F, Guo Z, Wu J, She X, . . . Yu L. (2003). Post-translational modifications of three members of the human MAP1LC3 family and detection of a novel type of modification for MAP1LC3B. *J Biol Chem* **278,** 29278-29287.

Hegyi P, Pandol S, Venglovecz V & Rakonczay Z, Jr. (2011). The acinar-ductal tango in the pathogenesis of acute pancreatitis. *Gut* **60,** 544-552.

Henault J, Martinez J, Riggs JM, Tian J, Mehta P, Clarke L, . . . Sanjuan MA. (2012). Noncanonical autophagy is required for type I interferon secretion in response to DNA-immune complexes. *Immunity* **37,** 986-997.

Henne WM, Buchkovich NJ & Emr SD. (2011). The ESCRT pathway. *Dev Cell* **21,** 77-91.

Herzog V & Farquhar MG. (1977). Luminal membrane retrieved after exocytosis reaches most golgi cisternae in secretory cells. *Proc Natl Acad Sci U S A* **74,** 5073-5077.

Herzog V & Reggio H. (1980). Pathways of endocytosis from luminal plasma membrane in rat exocrine pancreas. *Eur J Cell Biol* **21,** 141-150.

Hofbauer B, Saluja AK, Lerch MM, Bhagat L, Bhatia M, Lee HS, . . . Steer ML. (1998). Intra-acinar cell activation of trypsinogen during caerulein-induced pancreatitis in rats. *Am J Physiol* **275,** G352-362.

Hollander F & Birnbaum D. (1952). The role of carbonic anhydrase in pancreatic secretion. *Trans N Y Acad Sci* **15,** 56-58.

Hong L, Kenney SR, Phillips GK, Simpson D, Schroeder CE, Noth J, . . . Wandinger-Ness A. (2013). Characterization of a Cdc42 protein inhibitor and its use as a molecular probe. *J Biol Chem* **288,** 8531-8543.

Hong NH, Qi A & Weaver AM. (2015). PI(3,5)P2 controls endosomal branched actin dynamics by regulating cortactin-actin interactions. *J Cell Biol* **210,** 753-769.

Hoon JL, Wong WK & Koh CG. (2012). Functions and regulation of circular dorsal ruffles. *Mol Cell Biol* **32,** 4246-4257.

Hou Y, Ernst SA, Lentz SI & Williams JA. (2016). Genetic deletion of Rab27B in pancreatic acinar cells affects granules size and has inhibitory effects on amylase secretion. *Biochem Biophys Res Commun* **471,** 610-615.

Hou Y, Ernst SA, Stuenkel EL, Lentz SI & Williams JA. (2015). Rab27A Is Present in Mouse Pancreatic Acinar Cells and Is Required for Digestive Enzyme Secretion. *PLoS One* **10,** e0125596.

Huang AY, Castle AM, Hinton BT & Castle JD. (2001). Resting (basal) secretion of proteins is provided by the minor regulated and constitutive-like pathways and not granule exocytosis in parotid acinar cells. *J Biol Chem* **276,** 22296-22306.

Huang J, Canadien V, Lam GY, Steinberg BE, Dinauer MC, Magalhaes MA, . . . Brumell JH. (2009). Activation of antibacterial autophagy by NADPH oxidases. *Proc Natl Acad Sci U S A* **106,** 6226-6231.

Huang LK & Wang MJJ. (1995). Image Thresholding by Minimizing the Measures of Fuzziness. *Pattern Recogn* **28,** 41-51.

Huang W, Booth DM, Cane MC, Chvanov M, Javed MA, Elliott VL, . . . Criddle DN. (2014). Fatty acid ethyl ester synthase inhibition ameliorates ethanol-induced Ca2+-dependent mitochondrial dysfunction and acute pancreatitis. *Gut* **63,** 1313-1324.

Huang W, Cane MC, Mukherjee R, Szatmary P, Zhang X, Elliott V, . . . Sutton R. (2017). Caffeine protects against experimental acute pancreatitis by inhibition of inositol 1,4,5-trisphosphate receptor-mediated Ca2+ release. *Gut* **66,** 301-313.

Hurtado-Lorenzo A, Skinner M, El Annan J, Futai M, Sun-Wada GH, Bourgoin S, . . . Marshansky V. (2006). V-ATPase interacts with ARNO and Arf6 in early endosomes and regulates the protein degradative pathway. *Nat Cell Biol* **8,** 124-136.

Ikeda Y & Fukuoka S. (2003). Phosphatidic acid production, required for cholecystokinin octapeptide-stimulated amylase secretion from pancreatic acinar AR42J cells, is regulated by a wortmannin-sensitive process. *Biochem Biophys Res Commun* **306,** 943-947.

Itakura E, Kishi-Itakura C & Mizushima N. (2012). The hairpin-type tail-anchored SNARE syntaxin 17 targets to autophagosomes for fusion with endosomes/lysosomes. *Cell* **151,** 1256-1269.

Jacquin E, Leclerc-Mercier S, Judon C, Blanchard E, Fraitag S & Florey O. (2017). Pharmacological modulators of autophagy activate a parallel noncanonical pathway driving unconventional LC3 lipidation. *Autophagy* **13,** 854-867.

Jaffe AB & Hall A. (2005). Rho GTPases: biochemistry and biology. *Annu Rev Cell Dev Biol* **21,** 247-269.

Jamieson JD & Palade GE. (1967). Intracellular transport of secretory proteins in the pancreatic exocrine cell. II. Transport to condensing vacuoles and zymogen granules. *J Cell Biol* **34,** 597-615.

Jamieson JD & Palade GE. (1971). Synthesis, intracellular transport, and discharge of secretory proteins in stimulated pancreatic exocrine cells. *J Cell Biol* **50,** 135-158.

Jang Y, Soekmadji C, Mitchell JM, Thomas WG & Thorn P. (2012). Real-time measurement of F-actin remodelling during exocytosis using Lifeact-EGFP transgenic animals. *PLoS One* **7,** e39815.

Javed MA, Wen L, Awais M, Latawiec D, Huang W, Chvanov M, . . . Sutton R. (2018). TRO40303 Ameliorates Alcohol-Induced Pancreatitis Through Reduction of Fatty Acid Ethyl Ester-Induced Mitochondrial Injury and Necrotic Cell Death. *Pancreas* **47,** 18-24.

Jentsch TJ. (2007). Chloride and the endosomal-lysosomal pathway: emerging roles of CLC chloride transporters. *J Physiol* **578,** 633-640.

Ji B, Bi Y, Simeone D, Mortensen RM & Logsdon CD. (2002). Human pancreatic acinar cells do not respond to cholecystokinin. *Pharmacol Toxicol* **91,** 327-332.

Jia J, Abudu YP, Claude-Taupin A, Gu Y, Kumar S, Choi SW, . . . Deretic V. (2018). Galectins Control mTOR in Response to Endomembrane Damage. *Mol Cell* **70,** 120-135 e128.

Jung N & Haucke V. (2007). Clathrin-mediated endocytosis at synapses. *Traffic* **8,** 1129-1136.

Kang R, Lotze MT, Zeh HJ, Billiar TR & Tang D. (2014). Cell death and DAMPs in acute pancreatitis. *Mol Med* **20,** 466-477.

Kasai H & Augustine GJ. (1990). Cytosolic Ca2+ gradients triggering unidirectional fluid secretion from exocrine pancreas. *Nature* **348,** 735-738.

Kasai H, Li YX & Miyashita Y. (1993). Subcellular distribution of Ca2+ release channels underlying Ca2+ waves and oscillations in exocrine pancreas. *Cell* **74,** 669-677.

Kast DJ & Dominguez R. (2017). The Cytoskeleton-Autophagy Connection. *Curr Biol* **27,** R318-R326.

Kast DJ, Zajac AL, Holzbaur EL, Ostap EM & Dominguez R. (2015). WHAMM Directs the Arp2/3 Complex to the ER for Autophagosome Biogenesis through an Actin Comet Tail Mechanism. *Curr Biol* **25,** 1791-1797.

Kern HF. (1993). Fine structure of the human exocrine pancreas. In *The pancreas: biology, pathobiology, and disease*, 2nd edn, pp. 9-19. Raven Press, New York.

Kim GH, Dayam RM, Prashar A, Terebiznik M & Botelho RJ. (2014). PIKfyve inhibition interferes with phagosome and endosome maturation in macrophages. *Traffic* **15,** 1143-1163.

Kim M, Nozu F, Kusama K & Imawari M. (2006). Cholecystokinin stimulates the recruitment of the Src-RhoA-phosphoinositide 3-kinase pathway by Vav-2 downstream of G(alpha13) in pancreatic acini. *Biochem Biophys Res Commun* **339,** 271-276.

Kim MS, Hong JH, Li Q, Shin DM, Abramowitz J, Birnbaumer L & Muallem S. (2009). Deletion of TRPC3 in mice reduces store-operated Ca2+ influx and the severity of acute pancreatitis. *Gastroenterology* **137,** 1509-1517.

Kim SW, Ehrman J, Ahn MR, Kondo J, Lopez AAM, Oh YS, . . . Lau KS. (2017). Shear stress induces noncanonical autophagy in intestinal epithelial monolayers. *Mol Biol Cell* **28,** 3043-3056.

Kimura S, Noda T & Yoshimori T. (2008). Dynein-dependent movement of autophagosomes mediates efficient encounters with lysosomes. *Cell Struct Funct* **33,** 109-122.

King JS, Gueho A, Hagedorn M, Gopaldass N, Leuba F, Soldati T & Insall RH. (2013). WASH is required for lysosomal recycling and efficient autophagic and phagocytic digestion. *Mol Biol Cell* **24,** 2714-2726.

Kiselyov KK, Ahuja M, Rybalchenko V, Patel S & Muallem S. (2012). The intracellular Ca(2)(+) channels of membrane traffic. *Channels (Austin)* **6,** 344-351.

Kissing S, Hermsen C, Repnik U, Nesset CK, von Bargen K, Griffiths G, . . . Saftig P. (2015). Vacuolar ATPase in phagosome-lysosome fusion. *J Biol Chem* **290,** 14166-14180.

Klionsky DJ, Abdelmohsen K, Abe A, Abedin MJ, Abeliovich H, Acevedo Arozena A, . . . Zughaier SM. (2016). Guidelines for the use and interpretation of assays for monitoring autophagy (3rd edition). *Autophagy* **12,** 1-222.

Kochl R, Hu XW, Chan EY & Tooze SA. (2006). Microtubules facilitate autophagosome formation and fusion of autophagosomes with endosomes. *Traffic* **7,** 129-145.

Kolodecik T, Gorelick F & Thrower E. (2009). Genetic and Pharmacologic Manipulation of Vacuolar Atpase; Effects on Zymogen Activation in Pancreatic Acini. *Open Access Anim Physiol* **2009,** 1-11.

Konturek SJ, Dubiel J & Gabrys B. (1969). Effect of acid infusion into various levels of the intestine on gastric and pancreatic secretion in the cat. *Gut* **10,** 749-753.

Korc M. (1993). Normal function of the endocrine pancreas. In *The pancreas: biology, pathobiology, and disease*, 2nd edn, pp. 751-758. Raven Press, New York.

Koukourakis MI, Kalamida D, Giatromanolaki A, Zois CE, Sivridis E, Pouliliou S, . . . Harris AL. (2015). Autophagosome Proteins LC3A, LC3B and LC3C Have Distinct Subcellular Distribution Kinetics and Expression in Cancer Cell Lines. *PLoS One* **10,** e0137675.

Kovacs EM, Verma S, Ali RG, Ratheesh A, Hamilton NA, Akhmanova A & Yap AS. (2011). N-WASP regulates the epithelial junctional actin cytoskeleton through a non-canonical post-nucleation pathway. *Nat Cell Biol* **13,** 934-943.

Kraehenbuhl JP, Racine L & Jamieson JD. (1977). Immunocytochemical localization of secretory proteins in bovine pancreatic exocrine cells. *J Cell Biol* **72,** 406-423.

Krishna S, Palm W, Lee Y, Yang W, Bandyopadhyay U, Xu H, . . . Overholtzer M. (2016). PIKfyve Regulates Vacuole Maturation and Nutrient Recovery following Engulfment. *Dev Cell* **38,** 536-547.

Kubler E & Riezman H. (1993). Actin and fimbrin are required for the internalization step of endocytosis in yeast. *EMBO J* **12,** 2855-2862.

Kudchodkar SB & Levine B. (2009). Viruses and autophagy. *Rev Med Virol* **19,** 359-378.

Lahiri V & Klionsky DJ. (2018). CCPG1 is a noncanonical autophagy cargo receptor essential for reticulophagy and pancreatic ER proteostasis. *Autophagy* **14,** 1107-1109.

Lampel M & Kern HF. (1977). Acute interstitial pancreatitis in the rat induced by excessive doses of a pancreatic secretagogue. *Virchows Arch A Pathol Anat Histol* **373,** 97-117.

Larina O, Bhat P, Pickett JA, Launikonis BS, Shah A, Kruger WA, . . . Thorn P. (2007). Dynamic regulation of the large exocytotic fusion pore in pancreatic acinar cells. *Mol Biol Cell* **18,** 3502-3511.

Laukkarinen JM, Van Acker GJ, Weiss ER, Steer ML & Perides G. (2007). A mouse model of acute biliary pancreatitis induced by retrograde pancreatic duct infusion of Na-taurocholate. *Gut* **56,** 1590-1598.

Leach SD, Modlin IM, Scheele GA & Gorelick FS. (1991). Intracellular activation of digestive zymogens in rat pancreatic acini. Stimulation by high doses of cholecystokinin. *J Clin Invest* **87,** 362-366.

Leblond FA, Viau G, Laine J & Lebel D. (1993). Reconstitution in vitro of the pH-dependent aggregation of pancreatic zymogens en route to the secretory granule: implication of GP-2. *Biochem J* **291 (Pt 1),** 289-296.

Lee E & Knecht DA. (2002). Visualization of actin dynamics during macropinocytosis and exocytosis. *Traffic* **3,** 186-192.

Lennemann NJ & Coyne CB. (2015). Catch me if you can: the link between autophagy and viruses. *PLoS Pathog* **11,** e1004685.

Liang T, Dolai S, Xie L, Winter E, Orabi AI, Karimian N, . . . Gaisano HY. (2017). Ex vivo human pancreatic slice preparations offer a valuable model for studying pancreatic exocrine biology. *J Biol Chem* **292,** 5957-5969.

Licon-Munoz Y, Michel V, Fordyce CA & Parra KJ. (2017). F-actin reorganization by V-ATPase inhibition in prostate cancer. *Biol Open* **6,** 1734-1744.

Liddle RA. (1995). Regulation of cholecystokinin secretion by intraluminal releasing factors. *Am J Physiol* **269,** G319-327.

Liddle RA. (1997). Cholecystokinin cells. *Annu Rev Physiol* **59,** 221-242.

Liddle RA, Misukonis MA, Pacy L & Balber AE. (1992). Cholecystokinin cells purified by fluorescence-activated cell sorting respond to monitor peptide with an increase in intracellular calcium. *Proc Natl Acad Sci U S A* **89,** 5147-5151.

Liebl D & Griffiths G. (2009). Transient assembly of F-actin by phagosomes delays phagosome fusion with lysosomes in cargo-overloaded macrophages. *J Cell Sci* **122,** 2935-2945.

Liou W, Geuze HJ, Geelen MJ & Slot JW. (1997). The autophagic and endocytic pathways converge at the nascent autophagic vacuoles. *J Cell Biol* **136,** 61-70.

Lodge R & Descoteaux A. (2005). Leishmania donovani promastigotes induce periphagosomal F-actin accumulation through retention of the GTPase Cdc42. *Cell Microbiol* **7,** 1647-1658.

Lombardi B, Estes LW & Longnecker DS. (1975). Acute hemorrhagic pancreatitis (massive necrosis) with fat necrosis induced in mice by DL-ethionine fed with a choline-deficient diet. *Am J Pathol* **79,** 465-480.

Lubeseder-Martellato C, Alexandrow K, Hidalgo-Sastre A, Heid I, Boos SL, Briel T, . . . Siveke JT. (2017). Oncogenic KRas-induced Increase in Fluid-phase Endocytosis is Dependent on N-WASP and is Required for the Formation of Pancreatic Preneoplastic Lesions. *EBioMedicine* **15,** 90-99.

Lukinavicius G, Reymond L, D'Este E, Masharina A, Gottfert F, Ta H, . . . Johnsson K. (2014). Fluorogenic probes for live-cell imaging of the cytoskeleton. *Nat Methods* **11,** 731-733.

Lur G, Haynes LP, Prior IA, Gerasimenko OV, Feske S, Petersen OH, . . . Tepikin AV. (2009). Ribosome-free terminals of rough ER allow formation of STIM1 puncta and segregation of STIM1 from IP(3) receptors. *Curr Biol* **19,** 1648-1653.

Luthen R, Owen RL, Sarbia M, Grendell JH & Niederau C. (1998). Premature trypsinogen activation during cerulein pancreatitis in rats occurs inside pancreatic acinar cells. *Pancreas* **17,** 38-43.

Ma J, Becker C, Lowell CA & Underhill DM. (2012). Dectin-1-triggered recruitment of light chain 3 protein to phagosomes facilitates major histocompatibility complex class II presentation of fungal-derived antigens. *J Biol Chem* **287,** 34149-34156.

MacDonald E, Brown L, Selvais A, Liu H, Waring T, Newman D, . . . Zech T. (2018). HRS-WASH axis governs actin-mediated endosomal recycling and cell invasion. *J Cell Biol* **217,** 2549-2564.

Maejima I, Takahashi A, Omori H, Kimura T, Takabatake Y, Saitoh T, . . . Yoshimori T. (2013). Autophagy sequesters damaged lysosomes to control lysosomal biogenesis and kidney injury. *EMBO J* **32,** 2336-2347.

Mankad P, James A, Siriwardena AK, Elliott AC & Bruce JI. (2012). Insulin protects pancreatic acinar cells from cytosolic calcium overload and inhibition of plasma membrane calcium pump. *J Biol Chem* **287,** 1823-1836.

Maranda B, Brown D, Bourgoin S, Casanova JE, Vinay P, Ausiello DA & Marshansky V. (2001). Intra-endosomal pH-sensitive recruitment of the Arf-nucleotide exchange factor ARNO and Arf6 from cytoplasm to proximal tubule endosomes. *J Biol Chem* **276,** 18540-18550.

Mareninova OA, Hermann K, French SW, O'Konski MS, Pandol SJ, Webster P, . . . Gukovskaya AS. (2009). Impaired autophagic flux mediates acinar cell vacuole formation and trypsinogen activation in rodent models of acute pancreatitis. *J Clin Invest* **119,** 3340-3355.

Mareninova OA, Sendler M, Malla SR, Yakubov I, French SW, Tokhtaeva E, . . . Gukovskaya AS. (2015). Lysosome associated membrane proteins maintain pancreatic acinar cell homeostasis: LAMP-2 deficient mice develop pancreatitis. *Cell Mol Gastroenterol Hepatol* **1,** 678-694.

Mari M, Tooze SA & Reggiori F. (2011). The puzzling origin of the autophagosomal membrane. *F1000 Biol Rep* **3,** 25.

Marshansky V. (2007). The V-ATPase a2-subunit as a putative endosomal pH-sensor. *Biochem Soc Trans* **35,** 1092-1099.

Martinez J, Almendinger J, Oberst A, Ness R, Dillon CP, Fitzgerald P, . . . Green DR. (2011). Microtubule-associated protein 1 light chain 3 alpha (LC3)-associated phagocytosis is required for the efficient clearance of dead cells. *Proc Natl Acad Sci U S A* **108,** 17396-17401.

Martinez J, Malireddi RK, Lu Q, Cunha LD, Pelletier S, Gingras S, . . . Green DR. (2015). Molecular characterization of LC3-associated phagocytosis reveals distinct roles for Rubicon, NOX2 and autophagy proteins. *Nat Cell Biol* **17,** 893-906.

Masamune A & Shimosegawa T. (2013). Pancreatic stellate cells--multi-functional cells in the pancreas. *Pancreatology* **13,** 102-105.

Masedunskas A, Sramkova M & Weigert R. (2011). Homeostasis of the apical plasma membrane during regulated exocytosis in the salivary glands of live rodents. *Bioarchitecture* **1,** 225-229.

Mauthe M, Orhon I, Rocchi C, Zhou X, Luhr M, Hijlkema KJ, . . . Reggiori F. (2018). Chloroquine inhibits autophagic flux by decreasing autophagosome-lysosome fusion. *Autophagy***,** 1-21.

Mauvezin C, Nagy P, Juhasz G & Neufeld TP. (2015). Autophagosome-lysosome fusion is independent of V-ATPase-mediated acidification. *Nat Commun* **6,** 7007.

May RC & Machesky LM. (2001). Phagocytosis and the actin cytoskeleton. *J Cell Sci* **114,** 1061-1077.

Meister T, Niehues R, Hahn D, Domschke W, Sendler M, Lerch MM & Schnekenburger J. (2010). Missorting of cathepsin B into the secretory compartment of CI-MPR/IGFII-deficient mice does not induce spontaneous trypsinogen activation but leads to enhanced trypsin activity during experimental pancreatitis--without affecting disease severity. *J Physiol Pharmacol* **61,** 565-575.

Melak M, Plessner M & Grosse R. (2017). Actin visualization at a glance. *J Cell Sci* **130,** 525-530.

Menteyne A, Burdakov A, Charpentier G, Petersen OH & Cancela JM. (2006). Generation of specific Ca(2+) signals from Ca(2+) stores and endocytosis by differential coupling to messengers. *Curr Biol* **16,** 1931-1937.

Merrifield CJ, Moss SE, Ballestrem C, Imhof BA, Giese G, Wunderlich I & Almers W. (1999). Endocytic vesicles move at the tips of actin tails in cultured mast cells. *Nat Cell Biol* **1,** 72-74.

Merrifield CJ, Qualmann B, Kessels MM & Almers W. (2004). Neural Wiskott Aldrich Syndrome Protein (N-WASP) and the Arp2/3 complex are recruited to sites of clathrin-mediated endocytosis in cultured fibroblasts. *Eur J Cell Biol* **83,** 13-18.

Messenger SW, Falkowski MA & Groblewski GE. (2014a). Ca(2)(+)-regulated secretory granule exocytosis in pancreatic and parotid acinar cells. *Cell Calcium* **55,** 369-375.

Messenger SW, Falkowski MA, Thomas DD, Jones EK, Hong W, Gaisano HY, . . . Groblewski GE. (2014b). Vesicle associated membrane protein 8 (VAMP8)-mediated zymogen granule exocytosis is dependent on endosomal trafficking via the constitutive-like secretory pathway. *J Biol Chem* **289,** 28040-28053.

Messenger SW, Jones EK, Holthaus CL, Thomas DDH, Cooley MM, Byrne JA, . . . Groblewski GE. (2017). Acute acinar pancreatitis blocks vesicle-associated membrane protein 8 (VAMP8)-dependent secretion, resulting in intracellular trypsin accumulation. *J Biol Chem* **292,** 7828-7839.

Messenger SW, Thomas DD, Cooley MM, Jones EK, Falkowski MA, August BK, . . . Groblewski GE. (2015). Early to Late Endosome Trafficking Controls Secretion and Zymogen Activation in Rodent and Human Pancreatic Acinar Cells. *Cell Mol Gastroenterol Hepatol* **1,** 695-709.

Messenger SW, Thomas DD, Falkowski MA, Byrne JA, Gorelick FS & Groblewski GE. (2013). Tumor protein D52 controls trafficking of an apical endolysosomal secretory pathway in pancreatic acinar cells. *Am J Physiol Gastrointest Liver Physiol* **305,** G439-452.

Meuth-Metzinger VL, Philouze-Rome V, Metzinger L, Gespach C & Guilloteau P. (2005). Differential activation of adenylate cyclase by secretin and VIP receptors in the calf pancreas. *Pancreas* **31,** 174-181.

Mi N, Chen Y, Wang S, Chen M, Zhao M, Yang G, . . . Yu L. (2015). CapZ regulates autophagosomal membrane shaping by promoting actin assembly inside the isolation membrane. *Nat Cell Biol* **17,** 1112-1123.

Mikati MA, Breitsprecher D, Jansen S, Reisler E & Goode BL. (2015). Coronin Enhances Actin Filament Severing by Recruiting Cofilin to Filament Sides and Altering F-Actin Conformation. *J Mol Biol* **427,** 3137-3147.

Mizushima N, Yamamoto A, Matsui M, Yoshimori T & Ohsumi Y. (2004). In vivo analysis of autophagy in response to nutrient starvation using transgenic mice expressing a fluorescent autophagosome marker. *Mol Biol Cell* **15,** 1101-1111.

Mizushima N, Yoshimori T & Ohsumi Y. (2011). The role of Atg proteins in autophagosome formation. *Annu Rev Cell Dev Biol* **27,** 107-132.

Mleczak A, Millar S, Tooze SA, Olson MF & Chan EY. (2013). Regulation of autophagosome formation by Rho kinase. *Cell Signal* **25,** 1-11.

Molejon MI, Ropolo A, Re AL, Boggio V & Vaccaro MI. (2013). The VMP1-Beclin 1 interaction regulates autophagy induction. *Sci Rep* **3,** 1055.

Monastyrska I, He C, Geng J, Hoppe AD, Li Z & Klionsky DJ. (2008). Arp2 links autophagic machinery with the actin cytoskeleton. *Mol Biol Cell* **19,** 1962-1975.

Monastyrska I, Rieter E, Klionsky DJ & Reggiori F. (2009). Multiple roles of the cytoskeleton in autophagy. *Biol Rev Camb Philos Soc* **84,** 431-448.

Mooren OL, Galletta BJ & Cooper JA. (2012). Roles for actin assembly in endocytosis. *Annu Rev Biochem* **81,** 661-686.

Moradin N & Descoteaux A. (2012). Leishmania promastigotes: building a safe niche within macrophages. *Front Cell Infect Microbiol* **2,** 121.

Moreau V, Galan JM, Devilliers G, Haguenauer-Tsapis R & Winsor B. (1997). The yeast actin-related protein Arp2p is required for the internalization step of endocytosis. *Mol Biol Cell* **8,** 1361-1375.

Muallem S, Kwiatkowska K, Xu X & Yin HL. (1995). Actin filament disassembly is a sufficient final trigger for exocytosis in nonexcitable cells. *J Cell Biol* **128,** 589-598.

Mukherjee R, Mareninova OA, Odinokova IV, Huang W, Murphy J, Chvanov M, . . . Unit NPBR. (2016). Mechanism of mitochondrial permeability transition pore induction and damage in the pancreas: inhibition prevents acute pancreatitis by protecting production of ATP. *Gut* **65,** 1333-1346.

Murphy JA, Criddle DN, Sherwood M, Chvanov M, Mukherjee R, McLaughlin E, . . . Sutton R. (2008). Direct activation of cytosolic Ca2+ signaling and enzyme secretion by cholecystokinin in human pancreatic acinar cells. *Gastroenterology* **135,** 632-641.

Naqvi SN, Zahn R, Mitchell DA, Stevenson BJ & Munn AL. (1998). The WASp homologue Las17p functions with the WIP homologue End5p/verprolin and is essential for endocytosis in yeast. *Curr Biol* **8,** 959-962.

Nemoto T, Kimura R, Ito K, Tachikawa A, Miyashita Y, Iino M & Kasai H. (2001). Sequential-replenishment mechanism of exocytosis in pancreatic acini. *Nat Cell Biol* **3,** 253-258.

Nemoto T, Kojima T, Oshima A, Bito H & Kasai H. (2004). Stabilization of exocytosis by dynamic F-actin coating of zymogen granules in pancreatic acini. *J Biol Chem* **279,** 37544-37550.

Nguyen N, Shteyn V & Melia TJ. (2017). Sensing Membrane Curvature in Macroautophagy. *J Mol Biol* **429,** 457-472.

Niederau C & Grendell JH. (1988). Intracellular vacuoles in experimental acute pancreatitis in rats and mice are an acidified compartment. *J Clin Invest* **81,** 229-236.

Nishida Y, Arakawa S, Fujitani K, Yamaguchi H, Mizuta T, Kanaseki T, . . . Shimizu S. (2009). Discovery of Atg5/Atg7-independent alternative macroautophagy. *Nature* **461,** 654-658.

Niso-Santano M, Malik SA, Pietrocola F, Bravo-San Pedro JM, Marino G, Cianfanelli V, . . . Kroemer G. (2015). Unsaturated fatty acids induce non-canonical autophagy. *EMBO J* **34,** 1025-1041.

Nolen BJ, Tomasevic N, Russell A, Pierce DW, Jia Z, McCormick CD, . . . Pollard TD. (2009). Characterization of two classes of small molecule inhibitors of Arp2/3 complex. *Nature* **460,** 1031-1034.

Nozu F, Owyang C & Tsunoda Y. (2000). Involvement of phosphoinositide 3-kinase and its association with pp60src in cholecystokinin-stimulated pancreatic acinar cells. *Eur J Cell Biol* **79,** 803-809.

O'Konski MS & Pandol SJ. (1990). Effects of caerulein on the apical cytoskeleton of the pancreatic acinar cell. *J Clin Invest* **86,** 1649-1657.

Ohmuraya M & Yamamura K. (2008). Autophagy and acute pancreatitis: a novel autophagy theory for trypsinogen activation. *Autophagy* **4,** 1060-1062.

Ohnishi H, Mine T, Shibata H, Ueda N, Tsuchida T & Fujita T. (1999). Involvement of Rab4 in regulated exocytosis of rat pancreatic acini. *Gastroenterology* **116,** 943-952.

Okumura K, Tojyo Y & Kanazawa M. (1990). Changes in microfilament distribution during amylase exocytosis in rat parotid salivary glands in vitro. *Arch Oral Biol* **35,** 677-679.

Orban PC, Chui D & Marth JD. (1992). Tissue- and site-specific DNA recombination in transgenic mice. *Proc Natl Acad Sci U S A* **89,** 6861-6865.

Orci L, Ravazzola M, Amherdt M, Perrelet A, Powell SK, Quinn DL & Moore HP. (1987a). The trans-most cisternae of the Golgi complex: a compartment for sorting of secretory and plasma membrane proteins. *Cell* **51,** 1039-1051.

Orci L, Ravazzola M & Anderson RG. (1987b). The condensing vacuole of exocrine cells is more acidic than the mature secretory vesicle. *Nature* **326,** 77-79.

Orsi A, Razi M, Dooley HC, Robinson D, Weston AE, Collinson LM & Tooze SA. (2012). Dynamic and transient interactions of Atg9 with autophagosomes, but not membrane integration, are required for autophagy. *Mol Biol Cell* **23,** 1860-1873.

Owyang C. (1996). Physiological mechanisms of cholecystokinin action on pancreatic secretion. *Am J Physiol* **271,** G1-7.

Pandol SJ. (2010). In *The Exocrine Pancreas*. San Rafael (CA).

Pandol SJ, Saluja AK, Imrie CW & Banks PA. (2007). Acute pancreatitis: bench to the bedside. *Gastroenterology* **132,** 1127-1151.

Pankiv S, Clausen TH, Lamark T, Brech A, Bruun JA, Outzen H, . . . Johansen T. (2007). p62/SQSTM1 binds directly to Atg8/LC3 to facilitate degradation of ubiquitinated protein aggregates by autophagy. *J Biol Chem* **282,** 24131-24145.

Park HS, Betzenhauser MJ, Won JH, Chen J & Yule DI. (2008). The type 2 inositol (1,4,5)-trisphosphate (InsP3) receptor determines the sensitivity of InsP3-induced Ca2+ release to ATP in pancreatic acinar cells. *J Biol Chem* **283,** 26081-26088.

Park L, Thomason PA, Zech T, King JS, Veltman DM, Carnell M, . . . Insall RH. (2013). Cyclical action of the WASH complex: FAM21 and capping protein drive WASH recycling, not initial recruitment. *Dev Cell* **24,** 169-181.

Park MK, Lomax RB, Tepikin AV & Petersen OH. (2001). Local uncaging of caged Ca(2+) reveals distribution of Ca(2+)-activated Cl(-) channels in pancreatic acinar cells. *Proc Natl Acad Sci U S A* **98,** 10948-10953.

Parton RG, Joggerst B & Simons K. (1994). Regulated internalization of caveolae. *J Cell Biol* **127,** 1199-1215.

Parzych KR & Klionsky DJ. (2014). An overview of autophagy: morphology, mechanism, and regulation. *Antioxid Redox Signal* **20,** 460-473.

Patel KK, Miyoshi H, Beatty WL, Head RD, Malvin NP, Cadwell K, . . . Stappenbeck TS. (2013). Autophagy proteins control goblet cell function by potentiating reactive oxygen species production. *EMBO J* **32,** 3130-3144.

Petersen OH & Tepikin AV. (2008). Polarized calcium signaling in exocrine gland cells. *Annu Rev Physiol* **70,** 273-299.

Petherick KJ, Conway OJ, Mpamhanga C, Osborne SA, Kamal A, Saxty B & Ganley IG. (2015). Pharmacological inhibition of ULK1 kinase blocks mammalian target of rapamycin (mTOR)-dependent autophagy. *J Biol Chem* **290,** 11376-11383.

Phillips PA, Yang L, Shulkes A, Vonlaufen A, Poljak A, Bustamante S, . . . Wilson JS. (2010). Pancreatic stellate cells produce acetylcholine and may play a role in pancreatic exocrine secretion. *Proc Natl Acad Sci U S A* **107,** 17397-17402.

Pickett JA, Campos-Toimil M, Thomas P & Edwardson JM. (2007). Identification of SNAREs that mediate zymogen granule exocytosis. *Biochem Biophys Res Commun* **359,** 599-603.

Pickett JA, Thorn P & Edwardson JM. (2005). The plasma membrane Q-SNARE syntaxin 2 enters the zymogen granule membrane during exocytosis in the pancreatic acinar cell. *J Biol Chem* **280,** 1506-1511.

Posor Y, Eichhorn-Grunig M & Haucke V. (2015). Phosphoinositides in endocytosis. *Biochim Biophys Acta* **1851,** 794-804.

Prudnikova TY, Rawat SJ & Chernoff J. (2015). Molecular pathways: targeting the kinase effectors of RHO-family GTPases. *Clin Cancer Res* **21,** 24-29.

Puri C, Renna M, Bento CF, Moreau K & Rubinsztein DC. (2013). Diverse autophagosome membrane sources coalesce in recycling endosomes. *Cell* **154,** 1285-1299.

Rahner C, Mitic LL & Anderson JM. (2001). Heterogeneity in expression and subcellular localization of claudins 2, 3, 4, and 5 in the rat liver, pancreas, and gut. *Gastroenterology* **120,** 411-422.

Raraty M, Ward J, Erdemli G, Vaillant C, Neoptolemos JP, Sutton R & Petersen OH. (2000). Calcium-dependent enzyme activation and vacuole formation in the apical granular region of pancreatic acinar cells. *Proc Natl Acad Sci U S A* **97,** 13126-13131.

Ravikumar B, Moreau K, Jahreiss L, Puri C & Rubinsztein DC. (2010). Plasma membrane contributes to the formation of pre-autophagosomal structures. *Nat Cell Biol* **12,** 747-757.

Reggiori F, Monastyrska I, Shintani T & Klionsky DJ. (2005). The actin cytoskeleton is required for selective types of autophagy, but not nonspecific autophagy, in the yeast Saccharomyces cerevisiae. *Mol Biol Cell* **16,** 5843-5856.

Riedel D, Antonin W, Fernandez-Chacon R, Alvarez de Toledo G, Jo T, Geppert M, . . . Jahn R. (2002). Rab3D is not required for exocrine exocytosis but for maintenance of normally sized secretory granules. *Mol Cell Biol* **22,** 6487-6497.

Riedl J, Crevenna AH, Kessenbrock K, Yu JH, Neukirchen D, Bista M, . . . Wedlich-Soldner R. (2008). Lifeact: a versatile marker to visualize F-actin. *Nat Methods* **5,** 605-607.

Rindler MJ, Xu CF, Gumper I, Smith NN & Neubert TA. (2007). Proteomic analysis of pancreatic zymogen granules: identification of new granule proteins. *J Proteome Res* **6,** 2978-2992.

Rizvi SA, Neidt EM, Cui J, Feiger Z, Skau CT, Gardel ML, . . . Kovar DR. (2009). Identification and characterization of a small molecule inhibitor of formin-mediated actin assembly. *Chem Biol* **16,** 1158-1168.

Rohatgi R, Ma L, Miki H, Lopez M, Kirchhausen T, Takenawa T & Kirschner MW. (1999). The interaction between N-WASP and the Arp2/3 complex links Cdc42-dependent signals to actin assembly. *Cell* **97,** 221-231.

Ronan B, Flamand O, Vescovi L, Dureuil C, Durand L, Fassy F, . . . Pasquier B. (2014). A highly potent and selective Vps34 inhibitor alters vesicle trafficking and autophagy. *Nat Chem Biol* **10,** 1013-1019.

Ropolo A, Grasso D, Pardo R, Sacchetti ML, Archange C, Lo Re A, . . . Vaccaro MI. (2007). The pancreatitis-induced vacuole membrane protein 1 triggers autophagy in mammalian cells. *J Biol Chem* **282,** 37124-37133.

Rosado JA, Salido GM, Jensen RT & Garcia LJ. (1998). Are tyrosine phosphorylation of p125(FAK) and paxillin or the small GTP binding protein, rho, needed for CCK-stimulated pancreatic amylase secretion? *Biochim Biophys Acta* **1404,** 412-426.

Rossman KL, Der CJ & Sondek J. (2005). GEF means go: turning on RHO GTPases with guanine nucleotide-exchange factors. *Nat Rev Mol Cell Biol* **6,** 167-180.

Rozelle AL, Machesky LM, Yamamoto M, Driessens MH, Insall RH, Roth MG, . . . Yin HL. (2000). Phosphatidylinositol 4,5-bisphosphate induces actin-based movement of raft-enriched vesicles through WASP-Arp2/3. *Curr Biol* **10,** 311-320.

Rubinsztein DC, Gestwicki JE, Murphy LO & Klionsky DJ. (2007). Potential therapeutic applications of autophagy. *Nat Rev Drug Discov* **6,** 304-312.

Ryu HJ, Kim JE, Yeo SI, Kim DW, Kwon OS, Choi SY & Kang TC. (2011). F-actin depolymerization accelerates clasmatodendrosis via activation of lysosome-derived autophagic astroglial death. *Brain Res Bull* **85,** 368-373.

Sabbatini ME, Bi Y, Ji B, Ernst SA & Williams JA. (2010). CCK activates RhoA and Rac1 differentially through Galpha13 and Galphaq in mouse pancreatic acini. *Am J Physiol Cell Physiol* **298,** C592-601.

Sabbatini ME, Chen X, Ernst SA & Williams JA. (2008). Rap1 activation plays a regulatory role in pancreatic amylase secretion. *J Biol Chem* **283,** 23884-23894.

Sabbatini ME & Williams JA. (2013). Cholecystokinin-mediated RhoGDI phosphorylation via PKCalpha promotes both RhoA and Rac1 signaling. *PLoS One* **8,** e66029.

Saluja AK, Donovan EA, Yamanaka K, Yamaguchi Y, Hofbauer B & Steer ML. (1997). Cerulein-induced in vitro activation of trypsinogen in rat pancreatic acini is mediated by cathepsin B. *Gastroenterology* **113,** 304-310.

Samad A, James A, Wong J, Mankad P, Whitehouse J, Patel W, . . . Bruce JI. (2014). Insulin protects pancreatic acinar cells from palmitoleic acid-induced cellular injury. *J Biol Chem* **289,** 23582-23595.

Samaniego R, Sanchez-Martin L, Estecha A & Sanchez-Mateos P. (2007). Rho/ROCK and myosin II control the polarized distribution of endocytic clathrin structures at the uropod of moving T lymphocytes. *J Cell Sci* **120,** 3534-3543.

Samson EB, Tsao DS, Zimak J, McLaughlin RT, Trenton NJ, Mace EM, . . . Diehl MR. (2017). The coordinating role of IQGAP1 in the regulation of local, endosome-specific actin networks. *Biol Open* **6,** 785-799.

Sanjuan MA, Dillon CP, Tait SW, Moshiach S, Dorsey F, Connell S, . . . Green DR. (2007). Toll-like receptor signalling in macrophages links the autophagy pathway to phagocytosis. *Nature* **450,** 1253-1257.

Sauer B & Henderson N. (1988). Site-specific DNA recombination in mammalian cells by the Cre recombinase of bacteriophage P1. *Proc Natl Acad Sci U S A* **85,** 5166-5170.

Sauvonnet N, Dujeancourt A & Dautry-Varsat A. (2005). Cortactin and dynamin are required for the clathrin-independent endocytosis of gammac cytokine receptor. *J Cell Biol* **168,** 155-163.

Sbrissa D, Ikonomov OC, Deeb R & Shisheva A. (2002). Phosphatidylinositol 5-phosphate biosynthesis is linked to PIKfyve and is involved in osmotic response pathway in mammalian cells. *J Biol Chem* **277,** 47276-47284.

Schaaf MB, Keulers TG, Vooijs MA & Rouschop KM. (2016). LC3/GABARAP family proteins: autophagy-(un)related functions. *FASEB J* **30,** 3961-3978.

Scheele GA, Palade GE & Tartakoff AM. (1978). Cell fractionation studies on the guinea pig pancreas. Redistribution of exocrine proteins during tissue homogenization. *J Cell Biol* **78,** 110-130.

Schink KO, Tan KW & Stenmark H. (2016). Phosphoinositides in Control of Membrane Dynamics. *Annu Rev Cell Dev Biol* **32,** 143-171.

Scott CC & Gruenberg J. (2011). Ion flux and the function of endosomes and lysosomes: pH is just the start: the flux of ions across endosomal membranes influences endosome function not only through regulation of the luminal pH. *Bioessays* **33,** 103-110.

Segawa A & Yamashina S. (1989). Roles of microfilaments in exocytosis: a new hypothesis. *Cell Struct Funct* **14,** 531-544.

Sendler M, Maertin S, John D, Persike M, Weiss FU, Kruger B, . . . Lerch MM. (2016). Cathepsin B Activity Initiates Apoptosis via Digestive Protease Activation in Pancreatic Acinar Cells and Experimental Pancreatitis. *J Biol Chem* **291,** 14717-14731.

Sendler M, Weiss FU, Golchert J, Homuth G, van den Brandt C, Mahajan UM, . . . Mayerle J. (2018). Cathepsin B-Mediated Activation of Trypsinogen in Endocytosing Macrophages Increases Severity of Pancreatitis in Mice. *Gastroenterology* **154,** 704-718 e710.

Senninger N, Moody FG, Coelho JC & Van Buren DH. (1986). The role of biliary obstruction in the pathogenesis of acute pancreatitis in the opossum. *Surgery* **99,** 688-693.

Serra-Peinado C, Sicart A, Llopis J & Egea G. (2016). Actin Filaments Are Involved in the Coupling of V0-V1 Domains of Vacuolar H+-ATPase at the Golgi Complex. *J Biol Chem* **291,** 7286-7299.

Sesso A, Assis JE, Kuwajima VY & Kachar B. (1980). Freeze-fracture and thin-section study of condensing vacuoles in rat pancreatic acinar cells. *Acta Anat (Basel)* **108,** 521-539.

Shang X, Marchioni F, Sipes N, Evelyn CR, Jerabek-Willemsen M, Duhr S, . . . Zheng Y. (2012). Rational design of small molecule inhibitors targeting RhoA subfamily Rho GTPases. *Chem Biol* **19,** 699-710.

Sherwood MW, Prior IA, Voronina SG, Barrow SL, Woodsmith JD, Gerasimenko OV, . . . Tepikin AV. (2007). Activation of trypsinogen in large endocytic vacuoles of pancreatic acinar cells. *Proc Natl Acad Sci U S A* **104,** 5674-5679.

Shoji-Kawata S & Levine B. (2009). Autophagy, antiviral immunity, and viral countermeasures. *Biochim Biophys Acta* **1793,** 1478-1484.

Singer MV & Niebergall-Roth E. (2009). Secretion from acinar cells of the exocrine pancreas: role of enteropancreatic reflexes and cholecystokinin. *Cell Biol Int* **33,** 1-9.

Singh P & Garg PK. (2016). Pathophysiological mechanisms in acute pancreatitis: Current understanding. *Indian J Gastroenterol* **35,** 153-166.

Singh VP & McNiven MA. (2008). Src-mediated cortactin phosphorylation regulates actin localization and injurious blebbing in acinar cells. *Mol Biol Cell* **19,** 2339-2347.

Singh VP, Saluja AK, Bhagat L, van Acker GJ, Song AM, Soltoff SP, . . . Steer ML. (2001). Phosphatidylinositol 3-kinase-dependent activation of trypsinogen modulates the severity of acute pancreatitis. *J Clin Invest* **108,** 1387-1395.

Sit ST & Manser E. (2011). Rho GTPases and their role in organizing the actin cytoskeleton. *J Cell Sci* **124,** 679-683.

Smith MD, Harley ME, Kemp AJ, Wills J, Lee M, Arends M, . . . Wilkinson S. (2018). CCPG1 Is a Non-canonical Autophagy Cargo Receptor Essential for ER-Phagy and Pancreatic ER Proteostasis. *Dev Cell* **44,** 217-232 e211.

Spannagel AW, Green GM, Guan D, Liddle RA, Faull K & Reeve JR, Jr. (1996). Purification and characterization of a luminal cholecystokinin-releasing factor from rat intestinal secretion. *Proc Natl Acad Sci U S A* **93,** 4415-4420.

Spector I, Shochet NR, Blasberger D & Kashman Y. (1989). Latrunculins--novel marine macrolides that disrupt microfilament organization and affect cell growth: I. Comparison with cytochalasin D. *Cell Motil Cytoskeleton* **13,** 127-144.

Stauffer PL, Zhao H, Luby-Phelps K, Moss RL, Star RA & Muallem S. (1993). Gap junction communication modulates [Ca2+]i oscillations and enzyme secretion in pancreatic acini. *J Biol Chem* **268,** 19769-19775.

Stenmark H. (2009). Rab GTPases as coordinators of vesicle traffic. *Nat Rev Mol Cell Biol* **10,** 513-525.

Straight AF, Cheung A, Limouze J, Chen I, Westwood NJ, Sellers JR & Mitchison TJ. (2003). Dissecting temporal and spatial control of cytokinesis with a myosin II Inhibitor. *Science* **299,** 1743-1747.

Straub SV, Giovannucci DR, Bruce JI & Yule DI. (2002). A role for phosphorylation of inositol 1,4,5-trisphosphate receptors in defining calcium signals induced by Peptide agonists in pancreatic acinar cells. *J Biol Chem* **277,** 31949-31956.

Straub SV, Giovannucci DR & Yule DI. (2000). Calcium wave propagation in pancreatic acinar cells: functional interaction of inositol 1,4,5-trisphosphate receptors, ryanodine receptors, and mitochondria. *J Gen Physiol* **116,** 547-560.

Stuenkel EL, Tsunoda Y & Williams JA. (1989). Secretagogue induced calcium mobilization in single pancreatic acinar cells. *Biochem Biophys Res Commun* **158,** 863-869.

Sun-Wada GH, Wada Y & Futai M. (2004). Diverse and essential roles of mammalian vacuolar-type proton pump ATPase: toward the physiological understanding of inside acidic compartments. *Biochim Biophys Acta* **1658,** 106-114.

Swanson JA. (2008). Shaping cups into phagosomes and macropinosomes. *Nat Rev Mol Cell Biol* **9,** 639-649.

Takahashi K, Mashima H, Miura K, Maeda D, Goto A, Goto T, . . . Ohnishi H. (2017). Disruption of Small GTPase Rab7 Exacerbates the Severity of Acute Pancreatitis in Experimental Mouse Models. *Sci Rep* **7,** 2817.

Takenawa T & Itoh T. (2001). Phosphoinositides, key molecules for regulation of actin cytoskeletal organization and membrane traffic from the plasma membrane. *Biochim Biophys Acta* **1533,** 190-206.

Talukdar R, Sareen A, Zhu H, Yuan Z, Dixit A, Cheema H, . . . Saluja AK. (2016). Release of Cathepsin B in Cytosol Causes Cell Death in Acute Pancreatitis. *Gastroenterology* **151,** 747-758 e745.

Tang HW, Wang YB, Wang SL, Wu MH, Lin SY & Chen GC. (2011). Atg1-mediated myosin II activation regulates autophagosome formation during starvation-induced autophagy. *EMBO J* **30,** 636-651.

Tani S, Itoh H, Okabayashi Y, Nakamura T, Fujii M, Fujisawa T, . . . Otsuki M. (1990). New model of acute necrotizing pancreatitis induced by excessive doses of arginine in rats. *Dig Dis Sci* **35,** 367-374.

Tanida I, Ueno T & Kominami E. (2004). Human light chain 3/MAP1LC3B is cleaved at its carboxyl-terminal Met121 to expose Gly120 for lipidation and targeting to autophagosomal membranes. *J Biol Chem* **279,** 47704-47710.

Tapp RL. (1968). The ultrastructure of watery vacuoles in the submandibular gland of the rat. *J R Microsc Soc* **88,** 1-11.

Tartakoff AM. (1983). Perturbation of vesicular traffic with the carboxylic ionophore monensin. *Cell* **32,** 1026-1028.

Tenner S, Baillie J, DeWitt J, Vege SS & American College of G. (2013). American College of Gastroenterology guideline: management of acute pancreatitis. *Am J Gastroenterol* **108,** 1400-1415; 1416.

Tepikin AV, Llopis J, Snitsarev VA, Gallacher DV & Petersen OH. (1994). The droplet technique: measurement of calcium extrusion from single isolated mammalian cells. *Pflugers Arch* **428,** 664-670.

Tepikin AV, Voronina SG, Gallacher DV & Petersen OH. (1992). Pulsatile Ca2+ extrusion from single pancreatic acinar cells during receptor-activated cytosolic Ca2+ spiking. *J Biol Chem* **267,** 14073-14076.

Thevenod F. (2002). Ion channels in secretory granules of the pancreas and their role in exocytosis and release of secretory proteins. *Am J Physiol Cell Physiol* **283,** C651-672.

Thorn P, Fogarty KE & Parker I. (2004). Zymogen granule exocytosis is characterized by long fusion pore openings and preservation of vesicle lipid identity. *Proc Natl Acad Sci U S A* **101,** 6774-6779.

Thorn P & Gaisano H. (2012). Molecular control of compound Exocytosis: A key role for VAMP8. *Commun Integr Biol* **5,** 61-63.

Thorn P, Lawrie AM, Smith PM, Gallacher DV & Petersen OH. (1993). Local and global cytosolic Ca2+ oscillations in exocrine cells evoked by agonists and inositol trisphosphate. *Cell* **74,** 661-668.

Toescu EC, Lawrie AM, Petersen OH & Gallacher DV. (1992). Spatial and temporal distribution of agonist-evoked cytoplasmic Ca2+ signals in exocrine acinar cells analysed by digital image microscopy. *EMBO J* **11,** 1623-1629.

Tojyo Y, Okumura K, Kanazawa M & Matsumoto Y. (1989). Effect of cytochalasin D on acinar cell structure and secretion in rat parotid salivary glands in vitro. *Arch Oral Biol* **34,** 847-855.

Tominaga T, Sahai E, Chardin P, McCormick F, Courtneidge SA & Alberts AS. (2000). Diaphanous-related formins bridge Rho GTPase and Src tyrosine kinase signaling. *Mol Cell* **5,** 13-25.

Tooze J, Hollinshead M, Ludwig T, Howell K, Hoflack B & Kern H. (1990). In exocrine pancreas, the basolateral endocytic pathway converges with the autophagic pathway immediately after the early endosome. *J Cell Biol* **111,** 329-345.

Torgerson RR & McNiven MA. (1998). The actin-myosin cytoskeleton mediates reversible agonist-induced membrane blebbing. *J Cell Sci* **111 (Pt 19),** 2911-2922.

Tsien RY. (1998). The green fluorescent protein. *Annu Rev Biochem* **67,** 509-544.

Tsuboyama K, Koyama-Honda I, Sakamaki Y, Koike M, Morishita H & Mizushima N. (2016). The ATG conjugation systems are important for degradation of the inner autophagosomal membrane. *Science* **354,** 1036-1041.

Tsujita K & Itoh T. (2015). Phosphoinositides in the regulation of actin cortex and cell migration. *Biochim Biophys Acta* **1851,** 824-831.

Tumbarello DA, Manna PT, Allen M, Bycroft M, Arden SD, Kendrick-Jones J & Buss F. (2015). The Autophagy Receptor TAX1BP1 and the Molecular Motor Myosin VI Are Required for Clearance of Salmonella Typhimurium by Autophagy. *PLoS Pathog* **11,** e1005174.

Turvey MR & Thorn P. (2004). Lysine-fixable dye tracing of exocytosis shows F-actin coating is a step that follows granule fusion in pancreatic acinar cells. *Pflugers Arch* **448,** 552-555.

Vaccaro MI. (2012). Zymophagy: selective autophagy of secretory granules. *Int J Cell Biol* **2012,** 396705.

Valentijn JA, Sengupta D, Gumkowski FD, Tang LH, Konieczko EM & Jamieson JD. (1996). Rab3D localizes to secretory granules in rat pancreatic acinar cells. *Eur J Cell Biol* **70,** 33-41.

Valentijn JA, Valentijn K, Pastore LM & Jamieson JD. (2000). Actin coating of secretory granules during regulated exocytosis correlates with the release of rab3D. *Proc Natl Acad Sci U S A* **97,** 1091-1095.

Valentijn K, Valentijn JA & Jamieson JD. (1999a). Role of actin in regulated exocytosis and compensatory membrane retrieval: insights from an old acquaintance. *Biochem Biophys Res Commun* **266,** 652-661.

Valentijn KM, Gumkowski FD & Jamieson JD. (1999b). The subapical actin cytoskeleton regulates secretion and membrane retrieval in pancreatic acinar cells. *J Cell Sci* **112 (Pt 1),** 81-96.

van Acker GJ, Perides G & Steer ML. (2006). Co-localization hypothesis: a mechanism for the intrapancreatic activation of digestive enzymes during the early phases of acute pancreatitis. *World J Gastroenterol* **12,** 1985-1990.

Van Acker GJ, Saluja AK, Bhagat L, Singh VP, Song AM & Steer ML. (2002). Cathepsin B inhibition prevents trypsinogen activation and reduces pancreatitis severity. *Am J Physiol Gastrointest Liver Physiol* **283,** G794-800.

Van Acker GJ, Weiss E, Steer ML & Perides G. (2007). Cause-effect relationships between zymogen activation and other early events in secretagogue-induced acute pancreatitis. *Am J Physiol Gastrointest Liver Physiol* **292,** G1738-1746.

Vicinanza M, Korolchuk VI, Ashkenazi A, Puri C, Menzies FM, Clarke JH & Rubinsztein DC. (2015). PI(5)P regulates autophagosome biogenesis. *Mol Cell* **57,** 219-234.

Vitavska O, Merzendorfer H & Wieczorek H. (2005). The V-ATPase subunit C binds to polymeric F-actin as well as to monomeric G-actin and induces cross-linking of actin filaments. *J Biol Chem* **280,** 1070-1076.

Voronina S, Collier D, Chvanov M, Middlehurst B, Beckett AJ, Prior IA, . . . Tepikin AV. (2015). The role of Ca2+ influx in endocytic vacuole formation in pancreatic acinar cells. *Biochem J* **465,** 405-412.

Voronina S, Longbottom R, Sutton R, Petersen OH & Tepikin A. (2002a). Bile acids induce calcium signals in mouse pancreatic acinar cells: implications for bile-induced pancreatic pathology. *J Physiol* **540,** 49-55.

Voronina S, Sukhomlin T, Johnson PR, Erdemli G, Petersen OH & Tepikin A. (2002b). Correlation of NADH and Ca2+ signals in mouse pancreatic acinar cells. *J Physiol* **539,** 41-52.

Voronina SG, Barrow SL, Simpson AW, Gerasimenko OV, da Silva Xavier G, Rutter GA, . . . Tepikin AV. (2010). Dynamic changes in cytosolic and mitochondrial ATP levels in pancreatic acinar cells. *Gastroenterology* **138,** 1976-1987.

Voronina SG, Sherwood MW, Gerasimenko OV, Petersen OH & Tepikin AV. (2007). Visualizing formation and dynamics of vacuoles in living cells using contrasting dextran-bound indicator: endocytic and nonendocytic vacuoles. *Am J Physiol Gastrointest Liver Physiol* **293,** G1333-1338.

Wallar BJ, Deward AD, Resau JH & Alberts AS. (2007). RhoB and the mammalian Diaphanous-related formin mDia2 in endosome trafficking. *Exp Cell Res* **313,** 560-571.

Wang Y, Arjonen A, Pouwels J, Ta H, Pausch P, Bange G, . . . Grosse R. (2015). Formin-like 2 Promotes beta1-Integrin Trafficking and Invasive Motility Downstream of PKCalpha. *Dev Cell* **34,** 475-483.

Waterford SD, Kolodecik TR, Thrower EC & Gorelick FS. (2005). Vacuolar ATPase regulates zymogen activation in pancreatic acini. *J Biol Chem* **280,** 5430-5434.

Weernink PA, Meletiadis K, Hommeltenberg S, Hinz M, Ishihara H, Schmidt M & Jakobs KH. (2004). Activation of type I phosphatidylinositol 4-phosphate 5-kinase isoforms by the Rho GTPases, RhoA, Rac1, and Cdc42. *J Biol Chem* **279,** 7840-7849.

Weidberg H, Shvets E, Shpilka T, Shimron F, Shinder V & Elazar Z. (2010). LC3 and GATE-16/GABARAP subfamilies are both essential yet act differently in autophagosome biogenesis. *EMBO J* **29,** 1792-1802.

Wen L, Voronina S, Javed MA, Awais M, Szatmary P, Latawiec D, . . . Sutton R. (2015). Inhibitors of ORAI1 Prevent Cytosolic Calcium-Associated Injury of Human Pancreatic Acinar Cells and Acute Pancreatitis in 3 Mouse Models. *Gastroenterology* **149,** 481-492 e487.

Whitcomb DC, Gorry MC, Preston RA, Furey W, Sossenheimer MJ, Ulrich CD, . . . Ehrlich GD. (1996). Hereditary pancreatitis is caused by a mutation in the cationic trypsinogen gene. *Nat Genet* **14,** 141-145.

Williams JA. (2001). Intracellular signaling mechanisms activated by cholecystokinin-regulating synthesis and secretion of digestive enzymes in pancreatic acinar cells. *Annu Rev Physiol* **63,** 77-97.

Williams JA. (2010). Regulation of acinar cell function in the pancreas. *Curr Opin Gastroenterol* **26,** 478-483.

Williams JA, Chen X & Sabbatini ME. (2009). Small G proteins as key regulators of pancreatic digestive enzyme secretion. *Am J Physiol Endocrinol Metab* **296,** E405-414.

Williams JA, Korc M & Dormer RL. (1978). Action of secretagogues on a new preparation of functionally intact, isolated pancreatic acini. *Am J Physiol* **235,** 517-524.

Williams RL & Urbe S. (2007). The emerging shape of the ESCRT machinery. *Nat Rev Mol Cell Biol* **8,** 355-368.

Wu H, Bhopale KK, Ansari GA & Kaphalia BS. (2008). Ethanol-induced cytotoxicity in rat pancreatic acinar AR42J cells: role of fatty acid ethyl esters. *Alcohol Alcohol* **43,** 1-8.

Wu J, Dang Y, Su W, Liu C, Ma H, Shan Y, . . . Yu L. (2006). Molecular cloning and characterization of rat LC3A and LC3B--two novel markers of autophagosome. *Biochem Biophys Res Commun* **339,** 437-442.

Yamasaki M, Masgrau R, Morgan AJ, Churchill GC, Patel S, Ashcroft SJ & Galione A. (2004). Organelle selection determines agonist-specific Ca2+ signals in pancreatic acinar and beta cells. *J Biol Chem* **279,** 7234-7240.

Yamasaki M, Thomas JM, Churchill GC, Garnham C, Lewis AM, Cancela JM, . . . Galione A. (2005). Role of NAADP and cADPR in the induction and maintenance of agonist-evoked Ca2+ spiking in mouse pancreatic acinar cells. *Curr Biol* **15,** 874-878.

Yin HL & Stossel TP. (1979). Control of cytoplasmic actin gel-sol transformation by gelsolin, a calcium-dependent regulatory protein. *Nature* **281,** 583-586.

Yoshii SR, Kuma A, Akashi T, Hara T, Yamamoto A, Kurikawa Y, . . . Mizushima N. (2016). Systemic Analysis of Atg5-Null Mice Rescued from Neonatal Lethality by Transgenic ATG5 Expression in Neurons. *Dev Cell* **39,** 116-130.

Yoshimori T, Yamamoto A, Moriyama Y, Futai M & Tashiro Y. (1991). Bafilomycin A1, a specific inhibitor of vacuolar-type H(+)-ATPase, inhibits acidification and protein degradation in lysosomes of cultured cells. *J Biol Chem* **266,** 17707-17712.

Yu G, Wan R, Hu Y, Ni J, Yin G, Xing M, . . . Hu G. (2014). Pancreatic acinar cells-derived cyclophilin A promotes pancreatic damage by activating NF-kappaB pathway in experimental pancreatitis. *Biochem Biophys Res Commun* **444,** 75-80.

Yu L, Chen Y & Tooze SA. (2018). Autophagy pathway: Cellular and molecular mechanisms. *Autophagy* **14,** 207-215.

Yule DI. (2015). Ca2+ Signaling in Pancreatic Acinar Cells. In *Pancreapedia: Exocrine Pancreas Knowledge Base*.

Yule DI, Ernst SA, Ohnishi H & Wojcikiewicz RJ. (1997). Evidence that zymogen granules are not a physiologically relevant calcium pool. Defining the distribution of inositol 1,4,5-trisphosphate receptors in pancreatic acinar cells. *J Biol Chem* **272,** 9093-9098.

Yule DI, Lawrie AM & Gallacher DV. (1991). Acetylcholine and cholecystokinin induce different patterns of oscillating calcium signals in pancreatic acinar cells. *Cell Calcium* **12,** 145-151.

Yule DI, Stuenkel E & Williams JA. (1996). Intercellular calcium waves in rat pancreatic acini: mechanism of transmission. *Am J Physiol* **271,** C1285-1294.

Zech T, Calaminus SD, Caswell P, Spence HJ, Carnell M, Insall RH, . . . Machesky LM. (2011). The Arp2/3 activator WASH regulates alpha5beta1-integrin-mediated invasive migration. *J Cell Sci* **124,** 3753-3759.

Zerial M & McBride H. (2001). Rab proteins as membrane organizers. *Nat Rev Mol Cell Biol* **2,** 107-117.

Zhang L, Zhang J, Shea K, Xu L, Tobin G, Knapton A, . . . Rouse R. (2014). Autophagy in pancreatic acinar cells in caerulein-treated mice: immunolocalization of related proteins and their potential as markers of pancreatitis. *Toxicol Pathol* **42,** 435-457.

Zheng J, Cahill SM, Lemmon MA, Fushman D, Schlessinger J & Cowburn D. (1996). Identification of the binding site for acidic phospholipids on the pH domain of dynamin: implications for stimulation of GTPase activity. *J Mol Biol* **255,** 14-21.

Zhou X, Xie L, Xia L, Bergmann F, Buchler MW, Kroemer G, . . . Fortunato F. (2017). RIP3 attenuates the pancreatic damage induced by deletion of ATG7. *Cell Death Dis* **8,** e2918.

Zhu J, Zhou K, Hao JJ, Liu J, Smith N & Zhan X. (2005). Regulation of cortactin/dynamin interaction by actin polymerization during the fission of clathrin-coated pits. *J Cell Sci* **118,** 807-817.

Zins K, Lucas T, Reichl P, Abraham D & Aharinejad S. (2013). A Rac1/Cdc42 GTPase-specific small molecule inhibitor suppresses growth of primary human prostate cancer xenografts and prolongs survival in mice. *PLoS One* **8,** e74924.

Zois CE, Giatromanolaki A, Sivridis E, Papaiakovou M, Kainulainen H & Koukourakis MI. (2011). "Autophagic flux" in normal mouse tissues: focus on endogenous LC3A processing. *Autophagy* **7,** 1371-1378.